PSERC

Risk of Cascading Outages

Final Project Report

Power Systems Engineering Research Center

A National Science Foundation
Industry/University Cooperative Research Center
since 1996

Power Systems Engineering Research Center

Risk of Cascading Outages

Final Project Report

Report Authors

James McCalley, Siddhartha Khaitan
Iowa State University

Ian Dobson, Kevin R. Wierzbicki, Janghoon Kim, Hui Ren
University of Wisconsin-Madison

PSERC Publication 08-04

February 2008

Information about this project

For information about this project contact:

Part A:
James D. McCalley
Iowa State University
Electrical and Computer Engineering Dept.
Ames, Iowa 50011
Phone: 515-294-4844
Fax: 515-294-4263
Email: jdm@iastate.edu

Part B:
Ian Dobson
University of Wisconsin-Madison
Electrical and Computer Engineering Dept.
Madison WI 53706
Phone 608-262-2661
Email: dobson@engr.wisc.edu

Power Systems Engineering Research Center

This is a project report from the Power Systems Engineering Research Center (PSERC). PSERC is a multi-university Center conducting research on challenges facing the electric power industry and educating the next generation of power engineers. More information about PSERC can be found at the Center's website: http://www.pserc.org.

For additional information, contact:

Power Systems Engineering Research Center
Arizona State University
577 Engineering Research Center
Box 878606
Tempe, AZ 85287-8606
Phone: 480-965-1643
FAX: 480-965-0745

Notice Concerning Copyright Material

Acknowledgements

This is the final report in two parts (A and B) for the Power Systems Engineering Research Center (PSERC) research project “Risk of Cascading Failure” (PSERC project S-26). We express our appreciation for the support provided by PSERC’s industrial members and by the National Science Foundation’s Industry/University Cooperative Research Center program. We gratefully acknowledge the inputs received from the industry experts - Anatoliy Meklin (PG&E), Floyd Galvan (Entergy), and Xiaoming Feng (ABB). Their insightful comments will also be very helpful in shaping the future course of work. We thank Benjamin Carreras of BACV Solutions, Oak Ridge, TN, for collaboration and contributions to section 3 in Part B. Ian Dobson, Janghoon Kim, and Hui Ren gratefully acknowledge support in part from NSF grants ECCS-0606003 and SES-0623985. Janghoon Kim gratefully acknowledges support in part from scholarships from the Korean Electric Power Corporation. Hui Ren gratefully acknowledges support in part from scholarships from the People's Republic of China and North China Electric Power University.

Executive Summary

Cascading outages in power systems are costly events that power system operators and planners actively seek to avoid. Such events can quickly result in power outages for millions of customers. Although it is unreasonable to claim that blackouts can be completely prevented, we can nonetheless reduce the frequency and impact of such high consequence events. Power operators can take actions if they have the right information provided by tools for monitoring and managing the risk of cascading outages. Such tools were developed in this research project by identifying contingencies that could initiate cascading outages and by determining operator actions to avoid the start of a cascade. Power system planners can also take actions if they have knowledge of the effects of transmission investments on the risk of cascading blackouts. In this project, system risk assessment tools were developed to estimate the overall risk of cascading transmission line overloads. The goal of this line of research on the risk of cascading outages is the creation of new tools that power system operators and planners can use to enhance system reliability.

Part A: Operational defense of power system cascading outages

A key to cascading outage defense is the level of situational awareness held by grid operators. Constraints in achieving operational defense are associated with the limited monitoring and data exchange capabilities beyond the control areas. Yet, modern power system operators are supervising one of the most complex systems of the society and are expected to take apt, correct and alert actions to ensure operational reliability and security of the power system. Under normal conditions they are able to sufficiently control the power system with sufficient automatic control support. Severe disturbances and complex unfolding of post-disturbance phenomena, including interdependent events, demand critical actions to be taken on the part of the operators, thus making operators even more dependent on decision support tools and automatic controls.

The market liberalization and push to operate the power system close to operational limits with less redundancy due to constraints placed by economical and environmental factors have made the operation more complex and exposed the power system to greater vulnerability to a disturbance, especially severe disturbances. In other industries (e.g., airline, nuclear, process control), control operators employ computational capabilities that help them predict system response and identify corrective actions. Power system operators should have a similar capability with online simulation tools.

To create an online simulator to help operators identify the potential for and actions to avoid cascades, we first developed a systematic way to identify power system initiating contingencies (including higher-order) for operational use. This methodology uses a B-matrix to represent the connectivity of functional groups (also called protection control groups). It is the first to give the formula in matrix form to evaluate the probabilities of fault plus stuck-breaker contingencies. The work extends the conventional contingency list by including a subset of high-order contingencies identified through topology processing.

The next design step was to select the desirable attributes of an online, mid-term simulator. Then, the simulator was designed to provide generalized, event-based, correc-

tive control and decision support for operators. This work is the first to propose the use of dynamic event tree (DET) as an operational defense plan for cascading events. The DET provides guidance for rapid operator response to high-risk *N-k* contingencies. The DET engine we designed would be seamlessly integrated with system real time information, such as topology and maintenance scheduling. Whenever the DET engine sees an overloading problem, it can suspend the on-going dynamic simulation process and do a static optimization to search for the redispatch to relieve the overloading.

The contingency selection and simulation capabilities were illustrated on two systems: a test system with six generators, and the IEEE RTS-96 with 33 generators. Comparisons with commercial grade simulators indicate the developed simulator is accurate and fast. A follow-on project is investigating parallelized deployment of the simulator on a supercomputer for additional speed enhancement.

Part B: Estimating failure propagation and the distribution of blackout size and evaluating the long-term risk of the N-1 criterion in an evolving power system

Blackouts become widespread by initial failures expanding in a diverse and intricate cascade of rare events. The ability to efficiently quantify cascading blackout risk from observed data and simulations could offer new ways to monitor power transmission system reliability, quantify the reliability benefit of proposed system improvements, and provide a useful method for finding and mitigating weaknesses in the power system. Established analytic methods of power system risk analysis can model the detail of some likely and foreseen combinations of failures and estimate their risk. This is very useful in finding and mitigating likely failures, but it does not address quantifying the overall risk of large cascading blackouts, in which there is combinatorial explosion of potential rare, unforeseen, and interacting events ranging from diverse power system physical effects through software failures to deficiencies in planning, operation, organization, and maintenance. Although the detailed analysis of the chain of events after a particular blackout is useful in suggesting specific weaknesses that can be rectified, it gives little guidance on the overall problem of whether society is rationally balancing the blackout risks with the costs of investing in increased reliability. Quantifying the overall blackout risk would allow this balancing by putting an approximate value on reliability.

Our methodology of cascading risk assessment is based on use of observed data or simulations to efficiently predict the probability distribution of blackout size. Blackout size is quantified in terms of line outages and amount interrupted load. We describe cascades using a bulk probabilistic model in which the initial failures propagate randomly according to a branching process. The branching process parameters can be statistically estimated from observed data or simulation. We review the current testing of these methods on simulations and observed data, and identify the next steps towards achieving verified and practical methods for quantifying cascading failure of electric power systems.

Cascading transmission line outages contribute to widespread blackouts. Power transmission engineers respond to the risk of cascading line outages by applying policies such as the *N-1* criterion and upgrading lines involved in recent blackouts. The transmission grid gradually evolves as these policies are applied to maintain reliability while the load grows. We suggest how to use simulations of the cascading line outages and the slow evolution of the transmission grid to assess the long-term effect of these policies on over-

all cascading blackout risk. The long-term effects of these policies on the distribution of cascading outages and the grid utilization are computed for the IEEE 118 bus test system.

Specific accomplishments from this work are listed below.

- We developed a statistical estimator to measure the extent to which transmission line outages propagate in cascading failures. This estimator has been tested on cascading line outage simulation data and initially tested on some industry line outage data.
- We extended the OPA (Oak Ridge National Laboratory, PSERC and University of Alaska) cascading line overload simulation to roughly estimate the long-term effect of the N-1 criterion on the distribution of sizes of cascading outages and the efficiency of network utilization.
- We made considerable progress in quantifying how well a branching process model approximates a probabilistic model of cascading failure. We have obtained useful bounds on the ratio and difference of the probabilities from these two models. This work helps to justify the use of branching processes as a high-level model to quantify cascading failure.
- We have, in collaboration with Professor Daniel Kirschen and Dr. Dusko Nedic of the University of Manchester, verified the criticality of blackout risk in an alternating current blackout model that represents many of the interactions that occur in cascading failure. A realistic case of a 1000 bus network was used and loading was gradually increased until a critical loading was found. At the critical loading there is a sharp rise (change of gradient) in the mean blackout size and a power law probability distribution of blackout size that indicates a phase change in the risk of large blackouts.

The objective of future work in a follow-on project in this line of research is to quantify the overall risk of cascading blackouts. We will further test and develop the high-level models and statistics to assess the overall risk of cascading outages from real and simulated cascading outage data.

Risk of Cascading Outages

Part A:

Operational Defense of Power System Cascading Outages

`

Part A Authors

James McCalley
Siddhartha Khaitan
Iowa State University

Information about Part A

For information about part A contact:

James D. McCalley
Iowa State University
Electrical and Computer Engineering Dept.
Ames, Iowa 50011
Phone: 515-294-4844
Fax: 515-294-4263
Email: jdm@iastate.edu

Power Systems Engineering Research Center

This is a project report from the Power Systems Engineering Research Center (PSERC). PSERC is a multi-university Center conducting research on challenges facing the electric power industry and educating the next generation of power engineers. More information about PSERC can be found at the Center's website: http://www.pserc.org.

For additional information, contact:

Power Systems Engineering Research Center
Arizona State University
577 Engineering Research Center
Box 878606
Tempe, AZ 85287-8606
Phone: 480-965-1643
FAX: 480-965-0745

Notice concerning copyright material

Table of Contents

Table of Contents (continued)

List of Tables

List of Figures

Table of Figures (continued)

1 Introduction

This chapter outlines the need for an extended term time domain simulator as an on-line cascading event tracking & avoidance decision support tool. At the outset, it discusses the blackout attributes, derived from a study of blackouts around the world over the past 40 years. This forms the foundation for the desirable simulator attributes. The chapter concludes with a summary of the simulator attributes.

A common perspective today is that a key to cascading outage defense is the level of situational awareness held by grid operators, and limitations are associated with the limited monitoring and data exchange capabilities beyond the control areas [1]. Yet, modern power system operators are supervising one of the most complex systems of the society and are expected to take apt, correct and alert actions to ensure operational reliability and security of the power system. Under normal conditions they are able to sufficiently control the power system with sufficient automatic control support. Severe disturbances and complex unfolding of post disturbance phenomena, including interdependent events, demand critical actions to be taken on the part of the operators which make them even more dependent on decision support and automatic controls at different levels [2, 3].

The market liberalization and push to operate the power system close to operational limits with less redundancy due to constraints placed by economical and environmental factors have made the operation more complex and exposed the power system to greater vulnerability to a disturbance, especially severe disturbances. There is indication in other industries (e.g., airline, nuclear, process control) that they employ a computational capability which provides operators with ways to predict system response and identify corrective actions. We think that power system operators should have a similar capability. The evolving power system demands ongoing and online operator training and capability enhancement tool to deal with any unforeseen initiating event/severe disturbance and unpredictable unfolding sequence of events.

On line dynamic simulation of power systems will have significant impact on their future design and operation. It will enhance power system security and reliability and hence customer satisfaction and utility profits, and will promote secure power grid expansion. To meet this challenging task of proper operator response and training, the attributes of an on-line mid-term simulator are proposed. This simulator will be used on-line to prepare the operators against extreme contingencies. It is expected to be a generalized event based corrective control/decision support for the operators. The next section describes blackout attributes, followed by desirable features of the on-line mid-term simulator we are developing.

1.1 Attributes of Blackout

We performed an extensive study of the blackouts around the world in the past 40 year (see www.ece.cmu.edu/cascadingfailures). A condensed version of this study is summarized in Fig. 1 and Fig. 2. We summarize our observations as follows:

- three of the 4 largest blackouts occurred in last 10 years
- the number of blackouts greater than 1000 MW doubles every 10 years

- 50% of them involved generation and 90% involved transmission
- 40% involved proper protection action
- 50% were slow (more than 3 minutes)
- 60% involved number of dependent events
- 50% had significant time between initiating and pre-collapse events

IMPACT

Location	Date	MW Lost	Duration	People affected	Approximate cost
US-NE	11/9/1965	20000	13 hours	30 million	
US-NE	7/13/1977	6000	22 hours	3 million	300 million
France	12/19/1978	30000	10 hours		
West Coast	12/22/1982	12350		5 million	
Sweden	12/27/1983	> 7000	5.5 hours	4.5 million	
Brazil	4/18/1984	15762			
Brazil	8/18/1985	7793			
Hydro Quebec	4/18/1988	18500			
US-West	1/17/1994	7500			
Brazil	12/13/1994	8630			
US-West	12/14/1994	9336		1.5 million	
Brazil	3/26/1996	5746			
US-West	7/2/1996	11743		1.5 million	
US-West	7/3/1996	1200		small number	
US-West	8/10/1996	30489		7.5 million	1 billion dollars
MAPP, NW Ontario	6/25/1998	950	19 hours	0.152 million	
San Francisco	12/8/1998	1200	8 hours	1 million	
Brazil	3/11/1999	25000	4 hours	75 million	
Brazil	5/16/1999	2000			
India	1/2/2001	12000	13 hours	220 million	107 million
Rome	6/26/2003	2150		7.3 million	
US-NE	8/14/2003	62000	1-2 days	50 million	4-6 billion
Denmark/Sweden	9/23/2003	6300	6.5 hours	5 million	
Italy	9/28/2003	27000	19.5 hours	57 million	
Croatia	12/1/2003	1270 mwh			2.5 million
Greece	7/12/2004	9000	3 hours	5 million	
Moscow/Russia	5/24-25/2005	2500	>6 hours	4 million	

Fig. 1: Blackout Impact

COLLAPSE TIME & NO. OF SUCCESSIVE EVENTS

Location	Date	Collapse time	#successive events
US-NE	11/9/1965	13 minutes	Many
US-NE	7/13/1977	1 hour	Many
France	12/19/1978	> 30 minutes	Many
West Coast	12/22/1982	few minutes	Many
Sweden	12/27/1983	> 1 minute	Many
Brazil	4/18/1984	> 10 minutes	Topology
Brazil	8/18/1985		Topology
Hydro Quebec	4/18/1988	< 1minute	Many
US-West	1/17/1994	1 minute	3
Brazil	12/13/1994		many
US-West	12/14/1994		substation topology
Brazil	3/26/1996		Topology
US-West	7/2/1996	36 seconds	Several
US-West	7/3/1996	> 1 minute	Prevented by fast op. action
US-West	8/10/1996	> 6 minutes	Many
MAPP, NW Ontario	6/25/1998	>44 minutes	substation topology
San Francisco	12/8/1998	16 seconds	many
Brazil	3/11/1999	30 seconds	substation topology
Brazil	5/16/1999		Topology
India	1/2/2001		
Rome	6/26/2003		
US-NE	8/14/2003	> 1 hour	Many
Denmark/Sweden	9/23/2003	7 minutes	Many
Italy	9/28/2003	27 minutes	Many
Croatia	12/1/2003	few seconds	many
Greece	7/12/2004	14 minutes	few
Moscow/Russia	5/24-25/2005	14 hours	Many

Fig. 2: Nature of Blackout

This study indicates that the nature of the blackouts with respect to time may be roughly classified as either fast (less than 3 minutes) or slow. And when they are slow, they always involve a cascading sequence. It is for the slow types that we propose a simulator as a decision support tool for the operators. There are four typical stages of such cascading sequences [4].

1. Initiating contingency;
2. Steady-state progression (slow succession);
    - System becomes stressed with heavy loading on lines, transformers, and generator;
    - Successive events occur, typically the trip of other components with fairly large inter-event time intervals.
3. Transient progression (fast succession);
    - System goes under-frequency and/or under-voltage;
    - Large number of components begins tripping quickly.
4. Uncontrolled islanding and blackout.

An important attribute of the events in stage two is that they are almost always dependent events in that their occurrence depends on the occurrence of one or more earlier events. It is recognized that the probability of occurrence of successive events increases dramatically following the occurrence of a contingency. The time interval between an initiating event and successive events varies greatly. For example, the time between a fault and an inadvertent relay trip can be less than a second. However, if a

fault followed by line clearing causes line overload and/or generator over-excitation, subsequent tripping may follow minutes or even hours later. The time interval may be long enough for an operator to initiate actions to mitigate the undesirable trend.

1.2 Simulator Attributes

The methodology discussed in Chapter 2 (see www.ece.cmu.edu/cascadingfailures) forms the foundation for continuous tracking of the system topology to generate high risk extended contingencies list for online security assessment. The proposed simulator should have the following features [5]:

- Intelligently select triggering events based on substation topology using switch-breaker data already existing in topology processor (chapter 2)
- Simulate conditions in the mid-term time frame (hours) very fast (chapter 3)
- Have detailed protective relaying and control system modeling (chapter 4)
- Provide decision support in the face of unfolding events (chapter 5)
- Provide "blackout avoidance" training tool for operators (chapter 5)
- Continuously identify catastrophic event sequences together with actions operators can take to mitigate them (chapter 5)
- Use current or forecasted conditions
- Store results for fast retrieval should an event occur

In keeping with the above a time domain simulator is the preferred analysis tool. However, it must be specialized to perform extended-term (several hours) of simulation ***very fast***, as suggested by the second bullet above. This means it must model both fast and slow dynamics and be capable of lengthening time steps when fast dynamics are inactive. In addition, it must have the necessary intelligence to recognize when failure conditions are encountered, retrieve earlier conditions, and determine appropriate actions; it must also have modeling capability for a wide range of protection devices. Fig. 3 illustrates a typical output from the proposed time domain simulator with desired capabilities of fast, long term, adaptive time step dynamic simulation of slow and fast dynamics and appropriate control action determination to arrest unfolding cascading event. The philosophy is to prepare and revise, track and defend.

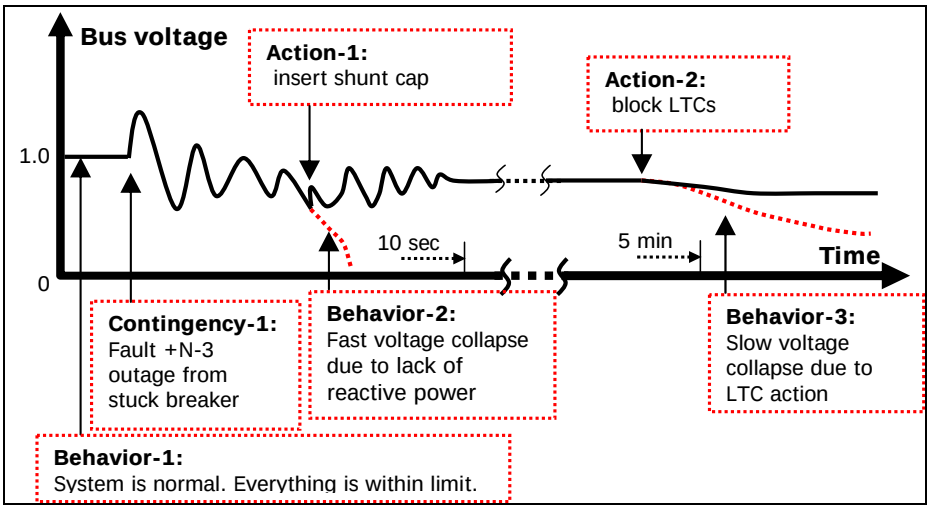

Fig. 3: Time domain simulator

Finally, in order to combine it with contingency identification and apply it online, it should be able to integrate with system real time information seamlessly, including switch-breaker data for automatic initiating event identification. Fig. 4 captures the proposed simulator's desired attributes in three dimensions of versatility namely:

- Simulation model complexity
- Computational characteristics
- Decision Set Priority

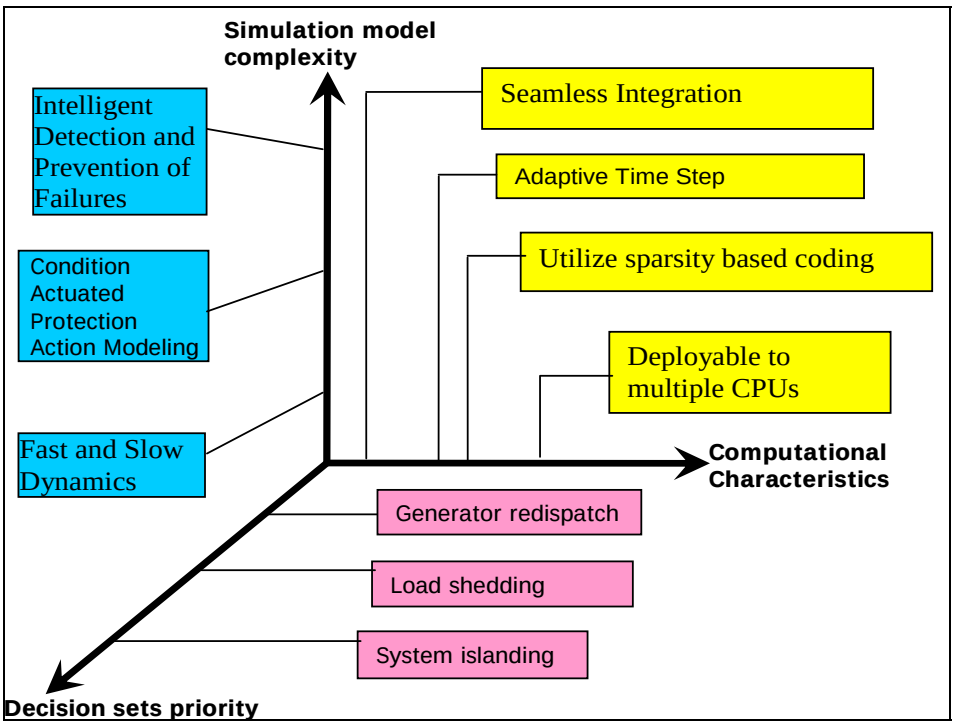

Fig. 4: Simulator attributes (in terms of Decision set priority, Computational characteristics, and simulation model complexity)

In this research, all the aspects of the proposed simulator's desired attributes have been addressed with the exception of its deploying to multiple CPUs, a task which we are pursuing in a follow up PSerc project.

1.3 Summary

In summary, the simulator should have the following capabilities:

- System Topology based Identification of High Risk N-k Contingencies (Chapter 2)
- Fast, long-term simulation capability (Chapter 3)
- Simulate both fast and slow dynamics with adaptive time step using implicit integration method (Chapter 3)
- Utilize sparsity-based coding (Chapter 3)
- Deployable to multiple CPUs (not considered in this work)
- Model fast dynamics, including generator, excitation, governor (Chapter 4)
- Model slow dynamics, including AGC, boiler, thermal loads (Chapter 4)
- Model condition-actuated protection action that trips element (Chapter 4)
- Model generator protection: field winding overexcitation, loss of field, loss of synchronism, overflux, overvoltage, underfrequency, and undervoltage (Chapter 4)
- Model transmission protection: impedance, overcurrent backup, out-of-step (not considered in this research)
- Contain intelligence to detect and prevent failures (Chapter 5)
- Be capable of saving & restarting from conditions at any time

2 N-k Contingency Selection

There is an increasing need to provide operators with enhanced on-line information regarding system security levels, what influences these levels, and what actions should be taken, or not taken, in order to most economically achieve an improved level. This section aims to address one aspect of this issue by providing a method to identify multiple component contingencies that represent high risk. The causes of cascading events in power systems are various [6]. One major contribution to cascading is high order initiating contingencies—removal of several power system components in a very short time, typically within seconds. Contingency set identification is an essential step in monitoring the power system security level [6]. Most literature [7, 8] on contingency selection emphasizes screening methods to select contingencies from a presumed $N-1$ contingency set plus a limited number of high order contingencies, ranking them using an appropriate severity index.

Some exceptions include [9 , 10 , 11] which studied the effect of multiple component contingencies caused by substation and protection failures. However, the literature on systematic selection of high order contingencies, called $N-k$ contingencies (where $k \geq 2$ is implicit), is limited. [12] and [13] proposed the on-line detection of hidden failure in protection device to prevent cascading failure. The proposed method needs exhaustive information on the logic of protection device installed in power system, which make it very difficult to be implemented. The difficulty of $N-k$ contingency selection lies in its combinatorial nature: the total number of distinct non-ordered (simultaneous) $N-k$ contingencies is $N!/[k!(N-k)]$. For a very modest size power system model with N=1000, there are 499,500 $N-2$ contingencies, 166,167,000 $N-3$ contingencies, over 41 billion $N-4$ contingencies, and so on.

One might argue that most of these contingencies are so low in probability that they do not warrant attention. However, $N-k$ contingencies do occur, and when they do, consequences can be very severe, and these very practical facts motivate the objective of this research, to identify high risk *N-k* contingencies for on-line security assessment. Such contingencies can then be added to the standard contingency list used by the energy management system (EMS) for transmission security assessment.

The purpose of this report is to illustrate the probability calculation for high-probability *N-k* contingencies. A systematic method to calculate the probabilities of *N-k* contingencies for online security assessment is presented. The developed methodology is illustrated through five substation configurations including single breaker-single bus, ring bus, double breaker-double bus, single-bus connected with bus tie, and breaker and a half. The difference between these five configurations lies in their robustness to N-k contingencies as illustrated in the probability calculation. The developed algorithms are implemented in Visual C++ and tested on a test system and IEEE-RTS 24 bus test system given in Appendix D and Appendix F. Some of the material in this report is drawn from [14].

2.1 System Topology and Primary Multiple Contingencies

Transmission substations are normally designed to ensure that a single fault results in at most the loss of a single circuit. However, the actual substation topology, at any given moment, may differ from the designed configuration, as the topological configuration of a substation, in terms of the connectivity of the elements through the switching devices (switches and breakers), may change. Variations in substation topology can occur as a result of operator action for purposes of facility maintenance and for purposes of mitigating undesirable operating conditions such as high circuit loading or out-of-limit voltages. To a lesser extent, topological variation may also occur as a result of forced outages.

Substation topological variation may, in some instances, result in situations where the operation of the protective systems, in response to the occurrence of a fault in the network, removes two or more elements when clearing the fault. Such topologies significantly increase the risk-level of the network, as it exposes the system to a multi-outage contingency as a result of a single fault, whose probability is equivalent to that of an *N*-1 contingency. As *N-k* contingencies are inherently more severe than *N*-1 contingencies, an *N-k* contingency having a probability of the same order of magnitude as an *N*-1 contingency may cause a very high amount of risk, since risk associated with a specific contingency is the expected value of the contingency consequence [15].

We will classify event probabilities by their *probability order* [16, 17, 18] which is best described by an example. If the probability of an event, say a fault at a particular location, occurring in the next hour, is 10^{-5}, then the probability of two independent faults occurring in the next time hour is 10^{-10}, and three independent faults 10^{-15}, and so on. We say, then, that any event (or event combination, independent or not) with probability having order of magnitude -5 is an *order* 1 event, any event with probability having order of magnitude -10 is an *order* 2 event, any event with probability having order of magnitude -15 is an *order* 3 event, and so on. A detailed discussion on probability precision based on rare event approximation and *probability orders* is given in Appendix A.

An operator may not be aware of increased *N-k* likelihood that results from switching actions. In this case, automated detection is critical. Even if the operator is aware of the increased likelihood, the question remains as to its severity and therefore its risk.

A search algorithm and the associated code have been developed to detect these situations and the pseudo code is given in Appendix B. The inputs required for the algorithm include the breaker-switch status data obtained from the SCADA system. As this data is also used for EMS topology processing, it is available in most control centers.

Another cause of *N-k* events is the failure of a breaker to open or protection failure to trip under a faulted condition. Such an event is of lower probability than that of an *N-1* outage, as it is comprised of a fault and a protection system failure. Because these are two independent events, it is of *order* 2. Yet, the severity, in terms of number of outaged elements, may be extreme, and therefore the risk may not be negligible. The graph-search algorithm given in Appendix B also detects this situation.

A systematic methodology for the probability calculation of inadvertent tripping or protection system misoperation leading to *N-k* events is also developed and illustrated through five substation topologies [19]. This is an *order* 2 or higher *order* contingency. The NERC Disturbance Analysis Working Group (DAWG) provides a database on large disturbances that have occurred in the bulk transmission systems in North America since 1984 [20]. The analysis of this information has resulted in a classification of three types among those related to protection failures: (1) inadvertent tripping, (2) protection relay fail to trip, and (3) breaker failure. A summary of the DAWG database in terms of this classification is given in Table 1. The approach developed in this work identifies the highest probability occurrence of these three different kinds of protection failure events.

Table 1: Summary on disturbances caused by protection system failures

Year	Inadvertent Tripping	Protection fails to trip	Breaker Failure	Total No. protection malfunction
1984	4	0	1	5
1985	2	0	5	7
1986	1	1	2	4
1987	2	0	0	2
1988	6	0	0	6
1989	6	0	0	6
1990	0	2	1	3
1991	3	1	1	5
1992	1	1	2	4
1993	1	0	3	4
1994	2	0	3	5
1995	5	1	1?	7
1996	2	0	1	3
1997	1	0	2	3
1998	0	0	0	0
1999	0	1	0	1
Total	36	7	22	65
Percentage	55%	11%	34%	100%

2.2 Topological Identification of Primary High-order Contingencies

In this section, detailed illustration of the three categories of high order contingencies caused by topology variation and component fault followed by one breaker failure or protection failure to trip are given in terms of a concise form to calculate the probability of these events by tracing the topology of system. A desirable contingency selection method should be able to identify, from topology data, high risk contingencies, that is, contingencies that have relatively high probability or high consequence or both. In addition to events with probability *order* 1, the method

proposed in this section strategically chooses a group of events that have a probability less than that of *order* 1 but greater than or equal to that of *order* 2. It is assumed that at most, only one breaker will suffer stuck failure, i.e., failure of two or more breakers to open when required poses negligible risk. This assumption is consistent with the rare event approximation, (Appendix A) as long as the occurrences of different failures are independent. An example is used to explain the approach.

2.2.1 Graph Representations of Power System Topology with Substation Model

Formally, a graph $G=(V,\ E)$ is defined by an ordered pair of finite sets V and E, where the elements in V are called the Vertices (also called nodes or points) and the elements in E are called edges (also called sides or arc) [21, 22]. Each element in E is a subset of V containing only two elements of V. For example

$$G=(V,\ E)=\left(\{V_1,\ V_2,\ V_3\},\ \{E_1=(V_1,\ V_2),\ \mathrm{E}_2=(V_1,\ V_3),\ \mathrm{E}_3=(V_2,\ V_3)\}\right)$$

defines the triangle graph in Fig. 5 with $\{V_1,\ V_2,\ V_3\}$ constituting its three vertices and $\{E_1=(V_1,\ V_2),\ \mathrm{E}_2=(V_1,\ V_3),\ \mathrm{E}_3=(V_2,\ V_3)\}$ constituting its three edges. Such graphs are used to represent the topology of power system components, i.e. generators, lines, transformers, bus section, breakers, switches, and loads.

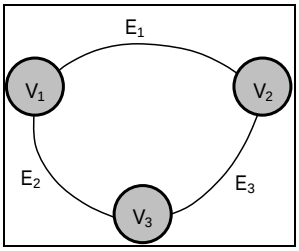

Fig. 5: A graph with three vertices and three edges

The one-line diagram in Fig. 6 shows part of a real power system with bus bar segment BS-7 out for maintenance. Every component is tagged with a unique ID. Each of the components other than a bus section connects two different bus sections. In reality not all non-bus-section components (line, breaker, capacitor, generator, and switches) are joined by two bus bars. In this case a bus section is inserted between two non-bus-section components. This ensures that the data format for the topology of the power system is the same as those in EMS. A bus section is connected by one or more other types of components. If we take all the breakers and open switches (which form a cut set) away from the diagram, the whole diagram is decomposed into seven isolated parts. Each of the isolated parts is contained within a dashed circle. The components contained in each dashed circle of form a *functional group* (Fig. 6) A functional group does not include any circuit breaker and open switch, which forms the interface between two different functional groups. Generally, there is only one interfacing component, a breaker or a switch, connecting two functional groups.

One convenient way to model the system is depicted in Fig. 7 (a). In this figure, the components are unanimously modeled as vertices. Each ellipse corresponds to a real

power system component. The edges only show how the component are connected but do not correspond to any real component. The functional groups are identified with dashed circles as in the one-line diagram in Fig. 6, and each one is assigned a label $FG-i$. The interfacing components between each functional group are indicated with a grey ellipse, i.e., components BR-1, BR-2, BR-3, SW-2, and SW-3.

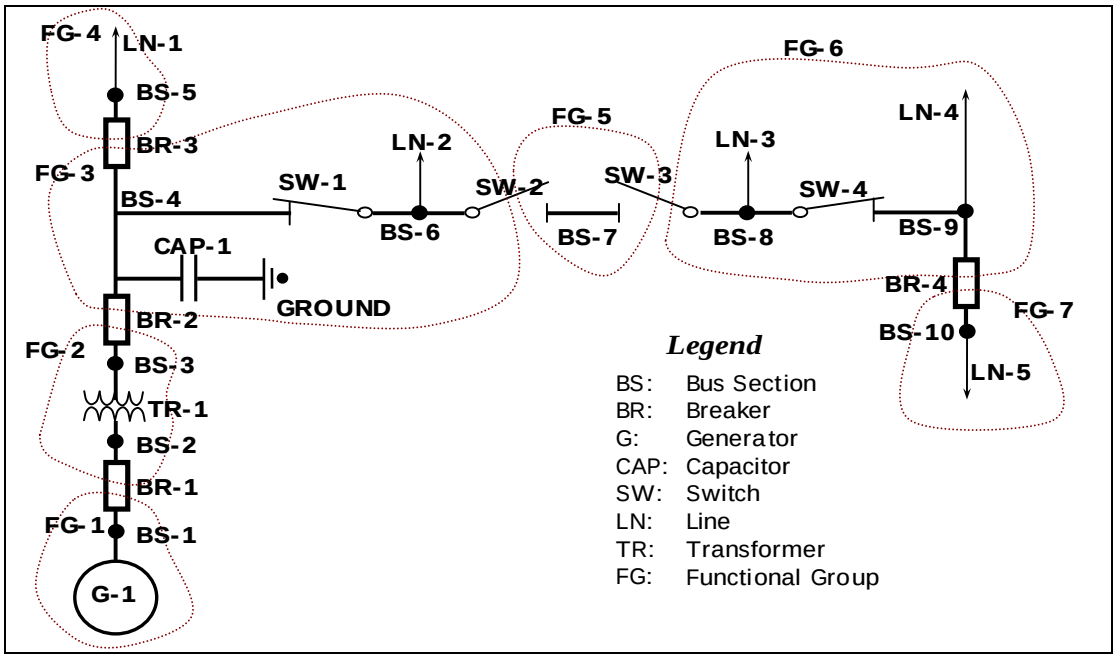

Fig. 6: One-line diagram of actual system illustrating functional groups

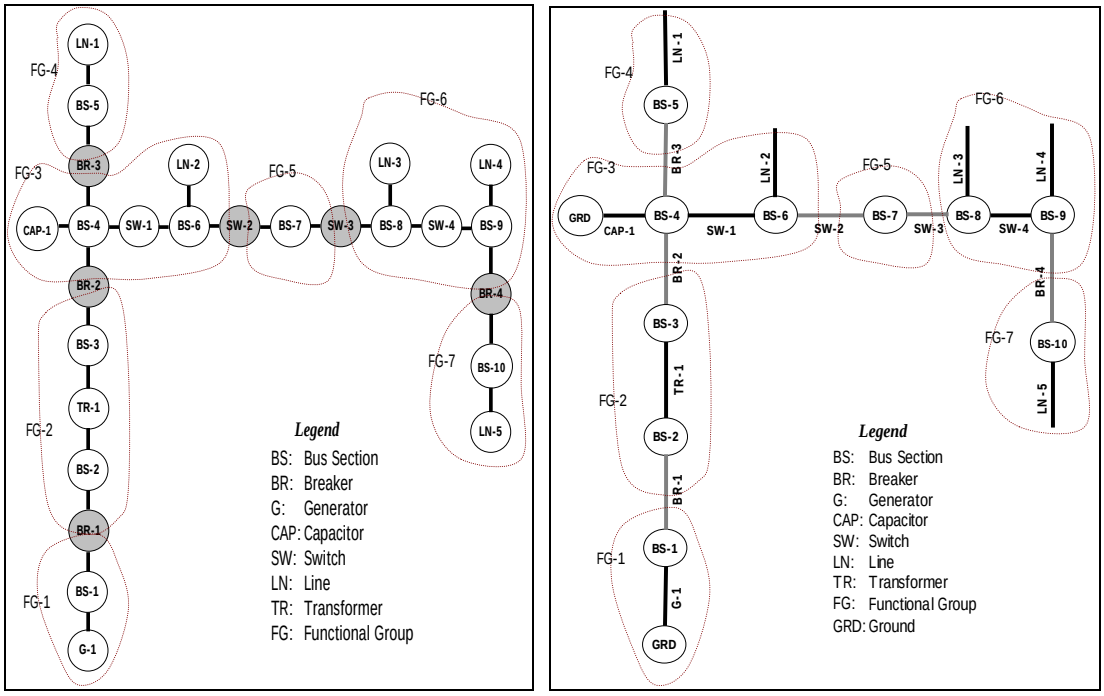

(a) **(b)**

Fig. 7: Graph representations of Fig. 6

The graph model used in some EMS is not as that in Fig. 7 (a), rather it models the topology as the graph shown in Fig. 7(b). This model is different in that both a vertex and an edge correspond to a real component. It treats all bus section components as vertices and all non bus-section components (line, breaker, capacitor, generator, and switches) as edges. Each vertex of the graph corresponds to a bus section component in the power system. The edges indicate how the bus sections are connected. Each edge corresponds to a non-bus section component (line, breaker, capacitor, generator, and switches). A bus section component may be connected by more than two edges, while each edge connects only two vertices. The functional groups are again identified with dashed circles, and each one is assigned a label $FG-i$. The interfacing components between each functional group are the same as in Fig. 7 (b), but they are modeled as edges instead of vertices. This graph is undirected which is different from the directed graph model in electrical circuit analysis and power flow. The graph for them is directed because they need a reference direction for electric current flow or power flow.

The expressions P_{FT}^{i}, P_{FL}^{i} and P_{PD}^{i} are three different reliability indices defined for power system components. P_{FT}^{i} is the probability that component has a ground fault contingency and P_{FL}^{i} means the probability that the component fails and has to be forced out from operation. Since fault contingency is only one of the different modes of failure, P_{FL}^{i} must be greater than or equal to P_{FT}^{i}. P_{PD}^{i} is called *per demand fail probability*, i.e. the conditional probability that the component fails to perform an action when the component is demanded to perform that action. Not all components require all three reliability indices. Both P_{FT}^{i} and P_{FL}^{i} are defined for non bus-section and non switching-components (line, capacitor and generator) because these components have many failure modes in addition to ground fault. Since these components are static devices that do not receive any command from control and perform any action, they do not have an P_{FD}^{i} index. Only P_{FL}^{i} is defined for bus sections since they are static and fault is virtually the only possible failure mode for them. Only P_{PD}^{i} is defined for switching components (breakers and switches) as they receive command from protection relay to connect or disconnect actions. Although it is possible for a switch component to have ground fault or other mode of failure, this probability is transferred to that of the two components the switch component connects by increasing the P_{FT}^{i} and P_{FL}^{i}. The value of P_{PD}^{i} depends on the switching status of the component. If the component is already in OPEN (or OFF) state, then P_{PD}^{i} is zero, otherwise, it is the conditional probability that the component fails to open when required.

The previous discussion is summarized in Table 2 and Table 3, for the specific sample system of Fig. 6. All the components treated as vertices are listed in Table 2, and all the components treated as edges are listed in Table 3. Each component is assigned a number I.D. in addition to the name I.D.

Table 2: List of vertex components of the power system diagram in Fig. 6

Name I.D.	BS-1	BS-2	BS-3	BS-4	BS-5	BS-6	BS-7	BS-8	BS-9	BS-10
Number	17	18	19	20	21	22	23	24	25	26
Fault Prob.	P_{FT}^{17}	P_{FT}^{18}	P_{FT}^{19}	P_{FT}^{20}	P_{FT}^{21}	P_{FT}^{22}	P_{FT}^{23}	P_{FT}^{24}	P_{FT}^{25}	P_{FT}^{26}

Table 3: List of edge components for the power system in Fig. 6

Name I.D.	No I.D.	Connected Bus Sections		Status	Probability		
		From	To		Fault	Fail	Per Demand
G-1	1	BS-1	Ground	Online	P_{FT}^{1}	P_{FL}^{1}	—
LN-1	2	BS-5	other system	Online	P_{FT}^{2}	P_{FL}^{2}	—
LN-2	3	BS-6	other system	Online	P_{FT}^{3}	P_{FL}^{3}	—
LN-3	4	BS-8	other system	Online	P_{FT}^{4}	P_{FL}^{4}	—
LN-4	5	BS-9	other system	Online	P_{FT}^{5}	P_{FL}^{5}	—
LN-5	6	BS-10	other system	Online	P_{FT}^{5}	P_{FL}^{5}	—
TR-1	7	BS-2	BS-3	Online	P_{FT}^{6}	P_{FL}^{6}	—
CAP-1	8	BS-4	Ground	Online	P_{FT}^{7}	P_{FL}^{7}	—
BR-1	9	BS-1	BS-2	On	0	0	P_{PD}^{9}
BR-2	10	BS-3	BS-4	On	0	0	P_{PD}^{10}
BR-3	11	BS-4	BS-5	On	0	0	P_{PD}^{11}
BR-4	12	BS-9	BS-10	On	0	0	P_{PD}^{12}
SW-1	13	BS-4	BS-6	On	0	0	P_{PD}^{13}
SW-2	14	BS-6	BS-7	Off	0	0	P_{PD}^{14}
SW-3	15	BS-7	BS-8	Off	0	0	P_{PD}^{15}
SW-4	16	BS-8	BS-9	On	0	0	P_{PD}^{16}

Since each functional group is tripped by protection relays as a whole entity, any fault or failure of a component within the group will cause the whole group to be tripped. The probability a functional group is tripped can be calculated as $\sum_{i \in S_i} P_{FL}^{i}$, where the elements of S_i are the indices of all the components in functional group i. The probability that a functional group is tripped due to fault can be calculated as $\sum_{i \in S_i} P_{FT}^{i}$ in the same way.

The equations for each individual group are summarized in the last two columns of Table 4. We assume the availability of the connection data for each power substation and the components within and between them, as summarized in the 3rd and 4th columns of Table 3. We perform a graph search using this information to identify the

functional groups. The results of this search for this example are provided in the first four columns of Table 4.

The fifth column of Table 4 provides the failure probabilities of the functional groups, which are the summation of the failure probabilities of the non-interfacing components comprising the functional group.

Table 4: List of functional groups and their failure probabilities

Functional Group FG-i	Interfacing Components (breaker or Open switch)	Per Demand Fail Prob. Of Interfacing Components	Non-interfacing Components S_i =	Fault/Failure Prob. Of Functional groups	
				Fault: $P_{FG_i}^{FT}$	Failure: $P_{FG_i}^{FL}$
FG-1	BR-1	P_{PD}^{9}	S_1 = {1,17}	$\sum_{i\in\{1,17\}} P_{FT}^{i}$	$\sum_{i\in\{1,17\}} P_{FL}^{i}$
FG-2	BR-1, BR-2	P_{PD}^{9}, P_{PD}^{10}	S_2 = {7,18,19}	$\sum_{i\in\{7,18,19\}} P_{FT}^{i}$	$\sum_{i\in\{7,18,19\}} P_{FL}^{i}$
FG-3	BR-2, BR-3, SW-2	P_{PD}^{10}, P_{PD}^{11}	S_3 = {8, 20, 13, 22, 3}	$\sum_{i\in\{8,\,20,\,13,\,22,\,3\}} P_{FT}^{i}$	$\sum_{i\in\{8,\,20,\,13,\,22,\,3\}} P_{FL}^{i}$
FG-4	BR-3	P_{PD}^{11}	S_4 = {2, 21}	$\sum_{i\in\{2,\,21\}} P_{FT}^{i}$	$\sum_{i\in\{2,\,21\}} P_{FL}^{i}$
FG-5	SW-2, SW-3	P_{PD}^{14}, P_{PD}^{15}	S_5 = {23}	$\sum_{i\in\{23\}} P_{FT}^{i}$	$\sum_{i\in\{23\}} P_{FL}^{i}$
FG-6	SW-3, BR-4	P_{PD}^{15}, P_{PD}^{12}	S_6 = {24, 4, 16, 25, 5}	$\sum_{i\in\{24,\,4,\,16,\,25,\,5\}} P_{FT}^{i}$	$\sum_{i\in\{24,\,4,\,16,\,25,\,5\}} P_{FL}^{i}$
FG-7	BR-4	P_{PD}^{12}	S_7 = {26, 6}	$\sum_{i\in\{26,\,6\}} P_{FT}^{i}$	$\sum_{i\in\{26,\,6\}} P_{FL}^{i}$

A careful observation of Fig. 7 shows that it can be reduced to the smaller graph in Fig. 8 if we take each functional group as a graph theoretic vertex, and any component (a breaker or an open switch) between two functional groups as an edge. If we define $(FG\text{-}i,\ FG\text{-}j)$ to be the component joining $FG\text{-}i$ and $FG\text{-}j$, the new graph can be expressed by $G=(X,\ E)$

where $X = \{FG\text{-}1,\ FG\text{-}2,\ FG\text{-}3,\ FG\text{-}4,\ FG\text{-}5,\ FG\text{-}7,\ FG\text{-}7\}$

and $E = \{(FG\text{-}1,\ FG\text{-}2),\ (FG\text{-}2,\ FG\text{-}3),\ (FG\text{-}3,\ FG\text{-}4),\ (FG\text{-}3,\ FG\text{-}5),\ (FG\text{-}5, FG\text{-}6),\ (FG\text{-}6,\ FG\text{-}7)\}$

$= \{BR\text{-}1,\ BR\text{-}2,\ BR\text{-}3,\ SW\text{-}2,\ SW\text{-}3,\ BR\text{-}4\}$

Fig. 8 shows the graph defined by $G=(X,\ E)$. Since the graph is an undirected graph, the pairs in E are defined as exchangeable, i.e. $(FG\text{-}i,\ FG\text{-}j)=(FG\text{-}j,\ FG\text{-}i)$.

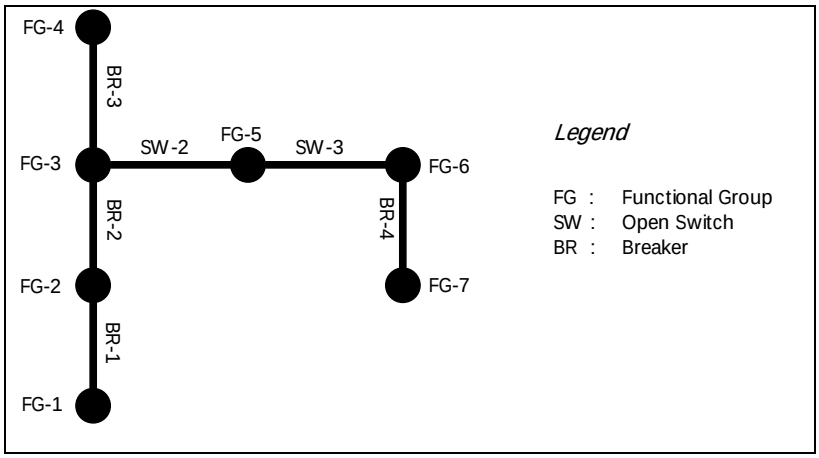

Fig. 8: Reduced functional group graph for Fig. 7

The results of the graph search also enable identification of the interconnections between functional groups, as summarized in Table 5. Each column in the table corresponds to a functional group, while each row corresponds to an interfacing component. There are two ones in each row, which indicate the interfacing component joint the two corresponding functional groups. The rest of the elements are all zeros. The array of elements in Table 3 can be represented via a matrix B in (1) where each row of B corresponds to an interfacing component, and each column corresponds to a functional group. This matrix is also called incidence matrix in graph theory [22].

Table 5: Connections for the interfacing components and the functional group (1- connected, 0- not connected)

—	FG-1	FG-2	FG-3	FG-4	FG-5	FG-6	FG-7
BR-1	1	1	0	0	0	0	0
BR-2	0	1	1	0	0	0	0
BR-3	0	0	1	1	0	0	0
SW-2	0	0	1	0	1	0	0
SW-3	0	0	0	0	1	1	0
BR-4	0	0	0	0	0	1	1

$$B = \begin{pmatrix} 1 & 1 & 0 & 0 & 0 & 0 & 0 \\ 0 & 1 & 1 & 0 & 0 & 0 & 0 \\ 0 & 0 & 1 & 1 & 0 & 0 & 0 \\ 0 & 0 & 1 & 0 & 1 & 0 & 0 \\ 0 & 0 & 0 & 0 & 1 & 1 & 0 \\ 0 & 0 & 0 & 0 & 0 & 1 & 1 \end{pmatrix} \quad (1)$$

If a component within either of the neighboring functional groups *FG-i* and *FG-j* has a fault and the breaker connecting *FG-i* and *FG-j* fails to open, generally, all the

components in the two neighboring functional groups will be taken out of service. The probability that the functional group G_i and G_j both fail during the time interval Δt can be expressed as:

$$P_{ij} = P_{PD}^{N_{ij}} \times \sum_{k \in S_i \cup S_j} P_{FT}^{k} = P_{PD}^{N_{ij}} \times \left[\sum_{k \in S_i} P_{FT}^{k} + \sum_{k \in S_j} P_{FT}^{k} \right]$$

$$= P_{PD}^{N_{ij}} \times \left(P_{FG_i}^{FT} + P_{FG_j}^{FT} \right) \tag{2}$$

where N_{ij} is the index of the interfacing component that joining functional group i and functional group j. Active failure rate (failure to open as required) of the interconnecting components between functional groups G_i and G_j (given by the failure rate of the interconnecting component), Δt is the next time interval considered, and P_k is the sum of the failure probabilities of all components in functional groups G_i and G_j. The last column of Table 3 provides the per demand failure probabilities of the interfacing components. We denote the vector of failure rates of interfacing component as

$$D = diag\left(P_{PD}^{9},\ P_{PD}^{10},\ P_{PD}^{11},\ P_{PD}^{14},\ P_{PD}^{15},\ P_{PD}^{12} \right) \tag{3}$$

where *diag* indicates a square matrix having diagonal elements equal to the argument of the *diag* function and zeros elsewhere. The index of each P_{PD}^{i} is the same as the index of the interfacing component. Then all the equations in form of (2) can be summarized in matrix form as:

$$\begin{pmatrix} P_{SBC_1} \\ P_{SBC_2} \\ P_{SBC_3} \\ P_{SBC_4} \\ P_{SBC_5} \\ P_{SBC_6} \end{pmatrix} = \begin{pmatrix} P_{12} \\ P_{23} \\ P_{34} \\ P_{35} \\ P_{56} \\ P_{67} \end{pmatrix} = \begin{pmatrix} P_{PD}^{9} & 0 & 0 & 0 & 0 & 0 \\ 0 & P_{PD}^{10} & 0 & 0 & 0 & 0 \\ 0 & 0 & P_{PD}^{11} & 0 & 0 & 0 \\ 0 & 0 & 0 & P_{PD}^{14} & 0 & 0 \\ 0 & 0 & 0 & 0 & P_{PD}^{15} & 0 \\ 0 & 0 & 0 & 0 & 0 & P_{PD}^{12} \end{pmatrix} \times$$

$$\times \begin{pmatrix} 1 & 1 & 0 & 0 & 0 & 0 & 0 \\ 0 & 1 & 1 & 0 & 0 & 0 & 0 \\ 0 & 0 & 1 & 1 & 0 & 0 & 0 \\ 0 & 0 & 1 & 0 & 1 & 0 & 0 \\ 0 & 0 & 0 & 0 & 1 & 1 & 0 \\ 0 & 0 & 0 & 0 & 0 & 1 & 1 \end{pmatrix} \times \begin{pmatrix} P_{FG_1}^{FT} \\ P_{FG_2}^{FT} \\ P_{FG_3}^{FT} \\ P_{FG_4}^{FT} \\ P_{FG_5}^{FT} \\ P_{FG_6}^{FT} \\ P_{FG_7}^{FT} \end{pmatrix} \tag{4}$$

or

$$P_{SBC} = D \times B \times P_{FG}^{FT} \tag{5}$$

where

$$
\begin{aligned}
P_{SBC} &= \left(P_{SBC_1}, \quad P_{SBC_2}, \quad P_{SBC_3}, \quad P_{SBC_4}, \quad P_{SBC_5}, \quad P_{SBC_6} \right)^T \\
&= \left(P_{12}, \quad P_{23}, \quad P_{34}, \quad P_{35}, \quad P_{56}, \quad P_{67} \right)^T \\
P_{FG}^{FT} &= \left(P_{FG_1}^{FT}, \quad P_{FG_2}^{FT}, \quad P_{FG_3}^{FT}, \quad P_{FG_4}^{FT}, \quad P_{FG_5}^{FT}, \quad P_{FG_6}^{FT}, \quad P_{FG_7}^{FT} \right)^T
\end{aligned}
\tag{6}
$$

D is given by (3),
B is given by (1),

As we mentioned previously, SW-2 and SW-3 are open, so it is not possible for the two switches to fail to open. Therefore we set P_{35} and P_{56} to zeroes. Now the above developed probability calculation method will be illustrated through five substation configurations discussed below.

2.3 Estimating the Reliability of Typical Substations

The five substation configurations discussed in this report are taken from [19]. All calculations assume that none of the substation components are in maintenance or out of service for any reason before a contingency. Furthermore, all the five configurations have four out-going or incoming connection points, so the apparent functions of them are the same *i.e.*, they are serving as a hub to join four branches. In terms of *N*-1 contingencies, the performances of all five configurations are the same. If any line has a fault and it is tripped correctly, all the three other lines will be still functional. *The difference between them lies in their robustness to high order contingencies*. Some substations are obviously more reliable than others for higher order contingencies, for example, the double-bus-double-breaker (DBDB) configuration is more reliable than the single-bus-single-breaker (SBSB) configuration in Fig. 9. A bus fault outage can defunct all the four lines from/to the SBSB station while the DBDB station can withstand such a disturbance without interrupting the service of any of the four lines. Usually, power system engineers study the reliability of substation using state diagrams with Markov or Monte Carlo methods [9, 10, 11] The full state diagram is not practical for a substation with many components. In this case, many simplifications have to be made so that the approach is feasible. The proposed approach provides a new way to study substation reliability, and the algorithm is not restricted by the number of components in a substation. The graphical functional group model described above is used to analyze the reliability of the five basic substations as shown in Fig. 9.

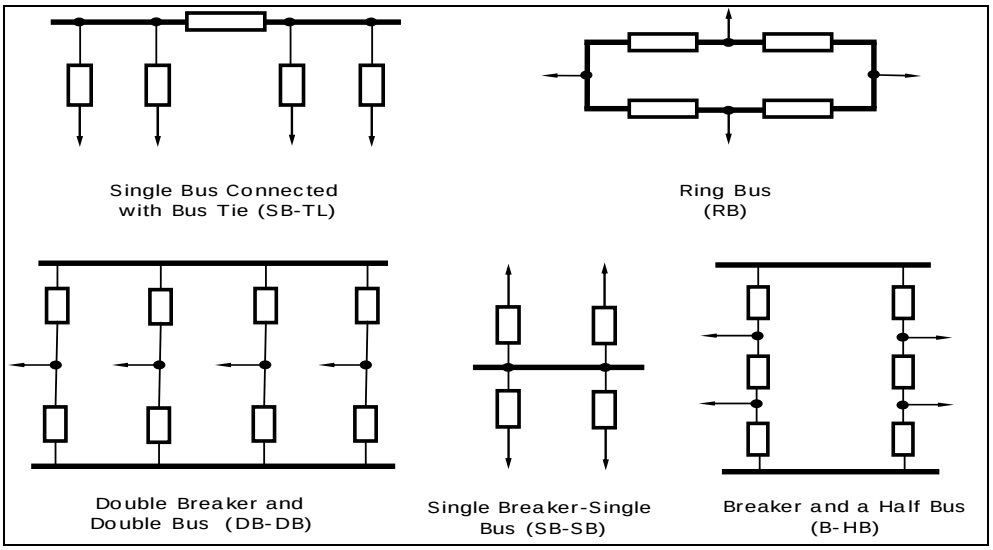

Fig. 9: Five typical substation configurations

Some of the notations used are defined below.

FSB_i: contingency caused by fault plus breaker i stuck;

p_{bs}^i: failure probability of bus section i. It is assumed to be zero for this discussion, i.e., $p_{bs}^i = 0$ for all i;

p_{sb}^i: conditional stuck probability (per demand failure rate) of breaker i. It is assumed to be the same (denoted as p_{sb}) for all breakers in the five substations;

D: diagonal matrix whose elements are P_{sb}^i's;

p_{lf}^i: fault probability of line i. It is assumed to be the same (denoted as p_l) for all transmission lines;

B: connection matrix of all function groups in a substation. Its elements are defined in (1);

$FG-i$: functional group i;

p_{FG}^i: fault probability of the i^{th} functional group;

P_{FG}: column vector representing the fault probabilities of all functional groups;

$p_{FSB-k}^{i,j}$: the aggregate probability of a group of contingencies caused by a fault within any of the two neighboring functional groups of breaker i and followed by the stuck failure of breaker i. The fault could happen on either side of the breaker. It could be a single line outage as well as a multiple line outage.

P_{FSB}: column vector made up of $p_{BR-k}^{i,j}$, the length of the vector is the same as the number of breaker in the study case;

2.3.1 Single Breaker and Single Bus (SB-SB)

This configuration is simple and straightforward. From Fig. 10, there are a total of five functional groups and 4 breakers, implying four stuck breaker contingencies. The *B*-matrix representing the connectivity of the four functional groups is also shown in Fig. 10. Clearly, with this single-bus-single-breaker substation diagram, any stuck breaker failure will cause the loss of all the four lines. The functional group fault probability, which is the summation of the fault probability of each component in the functional group, is calculated from (8), assuming the failure probability of the bus $p_{bf} = 0$.

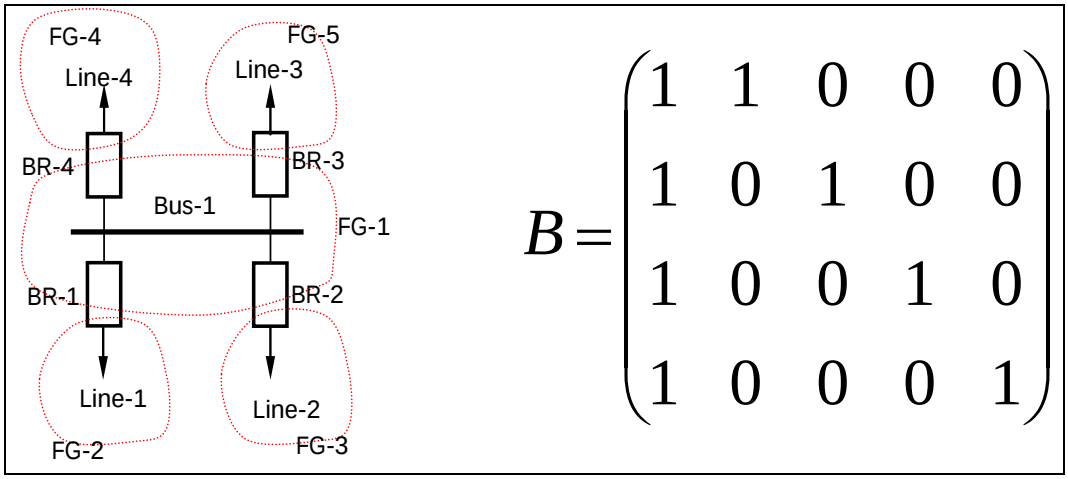

$$B = \begin{pmatrix} 1 & 1 & 0 & 0 & 0 \\ 1 & 0 & 1 & 0 & 0 \\ 1 & 0 & 0 & 1 & 0 \\ 1 & 0 & 0 & 0 & 1 \end{pmatrix}$$

Fig. 10: Single breaker single bus substation and its *B*-matrix.

$$P_{FSB} = \left(p_{FSB-1}, \quad p_{FSB-2}, \quad p_{FSB-3}, \quad p_{FSB-4} \right)^T \tag{7}$$

$$\begin{aligned} P_{FG} &= \left(p_{FG}^1, \quad p_{FG}^2, \quad p_{FG}^3, \quad p_{FG}^4, \quad p_{FG}^5 \right)^T \\ &= \left(p_{bf}, \quad p_{lf}, \quad p_{lf}, \quad p_{lf}, \quad p_{lf} \right)^T \end{aligned} \tag{8}$$

$$D = diag\left(p_{sb}^1, \quad p_{sb}^2, \quad p_{sb}^3, \quad p_{sb}^4, \right) = diag\left(p_{sb}, \quad p_{sb}, \quad p_{sb}, \quad p_{sb}, \right) \tag{9}$$

With *D*, *B*, P_{FG} known, the probabilities of all the stuck breaker contingencies can be calculated by

$$\begin{aligned} P_{FSB} &= D \times B \times P_{FG} \\ &= p_{sb} \times \left(p_b + p_l, \quad p_b + p_l, \quad p_b + p_l, \quad p_b + p_l \right)^T \end{aligned} \tag{10}$$

The total probability of having a fault plus stuck breaker contingency in the SB-SB substation is $\sum P_{FSB\text{-}i} = 4 \times p_{sb} \times p_{lf}$.

2.3.2 Ring Bus

This configuration is simple and straightforward too. From Fig. 11, there are a total of four functional groups and four breakers. The *B*-matrix representing the connectivity of the four functional groups is also shown in Fig. 11. With this ring bus configuration, any stuck breaker failure will outage at most two lines. The functional

group fault probability is calculated as from (12), assuming the failure probability of the bus $p_{bf} = 0$.

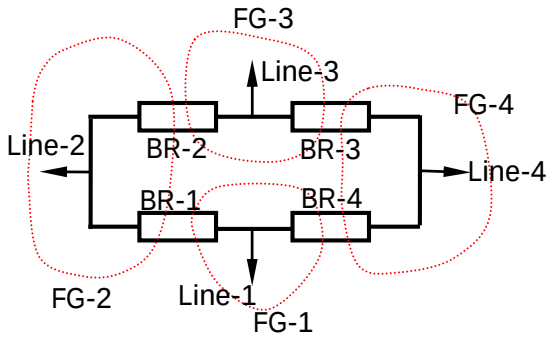

$$B = \begin{pmatrix} 1 & 1 & 0 & 0 \\ 0 & 1 & 1 & 0 \\ 0 & 0 & 1 & 1 \\ 1 & 0 & 0 & 1 \end{pmatrix}$$

Fig. 11: Ring bus substation and its *B*-matrix

$$P_{FSB} = \left(P_{FSB-1},\quad P_{FSB-2},\quad P_{FSB-3},\quad P_{FSB-4}\right)^T \tag{11}$$

$$\begin{aligned} P_{FG} &= \left(P_{FG}^1,\quad P_{FG}^2,\quad P_{FG}^3,\quad P_{FG}^4\right)^T \\ &= \left(p_l,\quad p_l,\quad p_l,\quad p_l,\right)^T \end{aligned} \tag{12}$$

$$D = diag\left(P_{sb}^1,\quad P_{sb}^2,\quad P_{sb}^3,\quad P_{sb}^4,\right) = diag\left(p_{sb},\quad p_{sb},\quad p_{sb},\quad p_{sb},\right) \tag{13}$$

With *D, B, P*$_{FG}$ known, the probabilities of all the stuck breaker contingencies can be calculated by

$$\begin{aligned} P_{FSB} &= D \times B \times P_{FG} \\ &= p_{sb} \times \left(2p_l,\quad 2p_l,\quad 2p_l,\quad 2p_l\right)^T \end{aligned} \tag{14}$$

The total probability of having a fault plus stuck breaker contingency for the ring bus station is $\sum P_{FSB\text{-}i} = 8 \times p_{sb} \times p_{lf}$.

2.3.3 Single Bus Connected with Tie Breaker (SB-TL)

This configuration SB-TL in Fig. 12 is adapted from SB-SB by splitting the bus and adding a tie-breaker between the two buses. When breakers 1-4 get stuck, only two lines will be lost at most. Note we assume Bus-1 and Bus-2 will never have a fault (p_{sb}=0), so it does not matter whether Breaker-5 gets stuck or not. The *B*-matrix representing the connectivity of the four functional groups is also shown in Fig. 12. The functional group fault probability is calculated as from (16), assuming the failure probability of the bus $p_{bf} = 0$.

$$P_{FSB} = \left(p_{FSB-1},\quad p_{FSB-2},\quad p_{FSB-3},\quad p_{FSB-4},\quad p_{FSB-5}\right)^T \tag{15}$$

$$\begin{aligned} P_{FG} &= (p_{FG}^1,\ p_{FG}^2,\ p_{FG}^3,\ p_{FG}^4,\ p_{FG}^5,\ p_{FG}^6) \\ &= (p_{l,}\ p_{l,}\ p_{l,}\ p_{l,}\ 0,\ 0)^T \end{aligned} \tag{16}$$

$$D = diag\left(p_{sb}^1,\quad p_{sb}^2,\quad p_{sb}^3,\quad p_{sb}^4,\quad p_{sb}^5\right) = diag\left(p_{sb},\quad p_{sb},\quad p_{sb},\quad p_{sb},\quad p_{sb}\right) \tag{17}$$

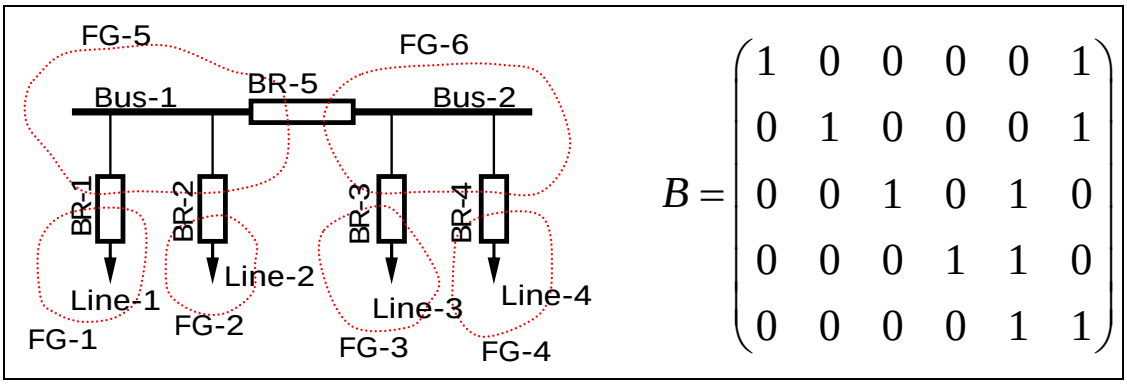

$$B=\begin{pmatrix}1&0&0&0&0&1\\0&1&0&0&0&1\\0&0&1&0&1&0\\0&0&0&1&1&0\\0&0&0&0&1&1\end{pmatrix}$$

Fig. 12: Single bus connected with tie-breaker and it's *B*-matrix

With *D*, *B*, and P_{FG} known, the probabilities of all the stuck breaker contingencies can be calculated by

$$P_{FSB}=D\times B\times P_{FG}=p_{sb}\times\left(p_l,\quad p_l,\quad p_l,\quad p_l,\quad 0\right)^T \tag{18}$$

The total probability of having a fault plus stuck breaker contingency for the SB-TL substation is $\sum P_{FSB\text{-}i}=4\times p_{sb}\times p_{lf}$.

2.3.4 Double Breaker and Double Bus (DB-DB)

The configuration of DB-DB is shown in Fig. 13, and there are a total of six functional groups and eight breakers, much more than other types of substations. The *B*-matrix representing the connectivity of the four functional groups is also shown in Fig. 13. With this DB-DB configuration, any stuck breaker failure would outage at most one line. The functional group fault probabilities are calculated from (20), assuming the failure probability of bus $p_{bf}=0$.

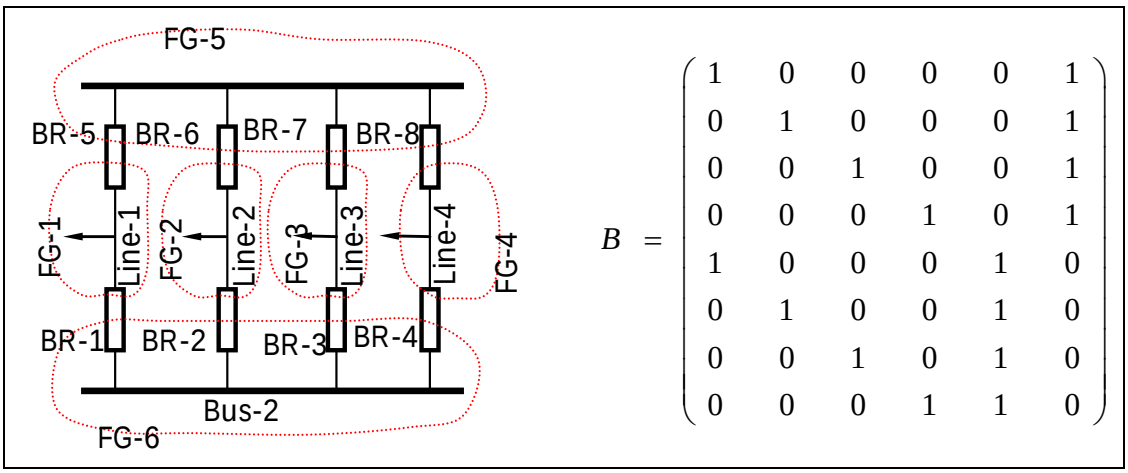

$$B=\begin{pmatrix}1&0&0&0&0&1\\0&1&0&0&0&1\\0&0&1&0&0&1\\0&0&0&1&0&1\\1&0&0&0&1&0\\0&1&0&0&1&0\\0&0&1&0&1&0\\0&0&0&1&1&0\end{pmatrix}$$

Fig. 13: Double breaker and double bus and it's *B*-matrix

$$P_{FSB}=\left(p_{FSB-1},\quad p_{FSB-2},\quad p_{FSB-3},\quad p_{FSB-4},\quad p_{FSB-5},\quad p_{FSB-6},\quad p_{FSB-7},\quad p_{FSB-8}\right)^T \tag{19}$$

$$P_{FG} = \left(p_{FG}^1, \quad p_{FG}^2, \quad p_{FG}^3, \quad p_{FG}^4, \quad p_{FG}^5, \quad p_{FG}^6 \right)^T$$
$$= \left(p_l, \quad p_l, \quad p_l, \quad p_l, \quad 0, \quad 0 \right)^T \tag{20}$$

$$D = (p_{sb}^1, p_{sb}^2, p_{sb}^3, p_{sb}^4, p_{sb}^5, p_{sb}^6, p_{sb}^7, p_{sb}^8) = (p_{sb}, p_{sb}, p_{sb}, p_{sb}, p_{sb}, p_{sb}, p_{sb}, p_{sb}) \tag{21}$$

With D, B, P_{FG} known, the probabilities of all the stuck breaker contingencies can be calculated by

$$P_{FSB} = D \times B \times P_{FG}$$
$$= p_{sb} \times \left(p_{lf}, \quad p_{lf}, \quad p_{lf}, \quad p_{lf}, \quad p_{lf}, \quad p_{lf}, \quad p_{lf}, \quad p_{lf} \right)^T \tag{22}$$

The total probability of having a fault plus stuck breaker contingency for DB-DB substation is $\sum P_{FSB\text{-}i} = 8 \times p_{sb} \times p_{lf}$. Among all fault plus stuck breaker contingencies, none of them involves more than one line.

2.3.5 Breaker and a Half Bus (B-HB)

The configuration of B-HB is shown in Fig. 14, having a total of six functional groups and six breakers. The *B*-matrix representing the connectivity of the four functional groups is also shown in Fig. 14. With this B-HB configuration, any stuck breaker failure will outage at most two lines. The functional group fault probabilities are calculated as from (24), assuming the failure probability of the bus $p_{bf} = 0$.

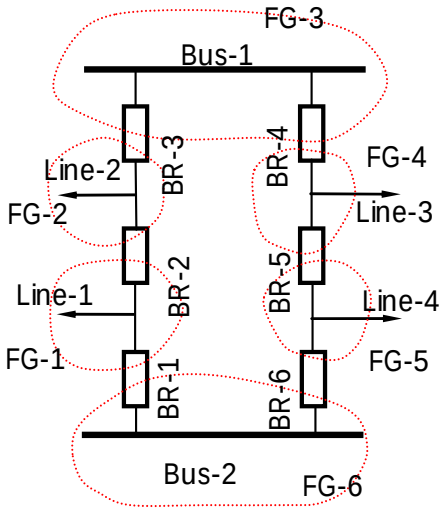

$$B = \begin{pmatrix} 1 & 0 & 0 & 0 & 0 & 1 \\ 1 & 1 & 0 & 0 & 0 & 0 \\ 0 & 1 & 1 & 0 & 0 & 0 \\ 0 & 0 & 1 & 1 & 0 & 0 \\ 0 & 0 & 0 & 1 & 1 & 0 \\ 0 & 0 & 0 & 0 & 1 & 1 \end{pmatrix}$$

Fig. 14: Breaker and a half bus and it's *B*-matrix

$$P_{FSB} = (p_{FSB-1}, p_{FSB-2}, p_{FSB-3}, p_{FSB-4}, p_{FSB-5}, p_{FSB-6}) \tag{23}$$

$$P_{FG} = (p_{FG}^1, p_{FG}^2, p_{FG}^3, p_{FG}^4, p_{FG}^5, p_{FG}^6)$$
$$= (p_l, \ p_l, \ 0, \ p_l, \ p_l, 0)^T \tag{24}$$

$$D = (p_{sb}^1, p_{sb}^2, p_{sb}^3, p_{sb}^4, p_{sb}^5, p_{sb}^6) = (p_{sb}, p_{sb}, p_{sb}, p_{sb}, p_{sb}, p_{sb}) \tag{25}$$

With D, B, P_{FG} known, the probabilities of all the stuck breaker contingencies can be calculated by

$$\begin{aligned} P_{FSB} &= D \times B \times P_{FG} \\ &= p_{sb} \times \left(p_{lb}, \quad 2p_{lb}, \quad p_{lb}, \quad p_{lb}, \quad 2p_{lb}, \quad p_{lb} \right)^T \end{aligned} \tag{26}$$

A stuck breaker 2 or a stuck breaker 5 will cause the removal of two lines while any other breaker stuck will cause the outage of only one line. The probability of having a fault plus stuck breaker contingency is $\sum P_{FSB\text{-}i} = 8 \times p_{sb} \times p_{lf}$. Among all fault plus stuck breaker contingencies, only a stuck breaker 2 or a stuck breaker 5 could involve more than one line.

2.4 High-order Contingencies due to inadvertent tripping

Inadvertent tripping after an initial fault or failure often leads to higher order contingencies. Inadvertent tripping generally occurs in the vicinity of the initial fault. Inadvertent tripping contingency forms the major part (about 55%) of the large system disturbances due to protection related cascading as given in Table 1. From practical experience it is seen that CT saturation causes misoperation of differential relays during external faults and delayed operation during internal faults. Inadvertent tripping often occurs at off-nominal frequency and due to outdated settings, human errors or overlapping zones of protection. The Northeast blackout on November 9, 1965, resulted in the loss of over 20,000 MW of load and affected 30 million people. It was a result of a faulty relay setting resulting in the tripping of one of five heavily loaded 230-kV transmission lines and the system cascaded in 2.5 seconds. On December 14, 1995, a fault occurred on a 345 kV line in southern Idaho, which tripped correctly, followed by an incorrect trip of a parallel line and a third line tripped on overloading. System instability resulted in the formation of four islands, with system frequency dropping to 58.75 Hz and 3,000 MW of load curtailed by under frequency load shedding. The blackout of West Coast on July 2, 1996 resulted in the loss of 11,850 MW of load and affected 2 million. Again it was a result of incorrect tripping of a parallel line after the initial contingency of a line sagging into a tree and resulted in the formation of five islands. In all the above cascading events inadvertent tripping played an important role. Table 6 summarizes a US utility experience with inadvertent tripping, and Table 7 summarizes the survey result conducted by Working Group I17 Transmission System Relay Performance Comparison on misoperation.

Table 6: A US Utility experience with misoperation

Utility: **Time Period:** Jan. - Dec. 2004

Voltage:	Dependability			Security		System Restoration	Total Misoperations
138 kV	Failure to Trip	Failure to Interrupt	Slow Trip	Unnecessary Trip During Fault	Unnecessary Trip Other Than Fault	Failure to Reclose	
Relay System	2	0	19	18	5	7	51
Circuit Breaker	1	1	0	0	3	2	7
Total Protective System	3	1	19	18	8	9	58
Percent Incorrect Operation Relay System	0.5%	0.0%	4.7%	4.5%	1.2%	1.7%	12.7%
Percent Incorrect Operation Circuit Breaker	0.3%	0.3%	0.0%	0.0%	0.8%	0.5%	1.8%
Percent Incorrect Operation Protective System	0.7%	0.2%	4.7%	4.5%	2.0%	2.2%	14.4%

138 kV
Relay K = 5
Breaker K = 0
Total Operations: 397

Table 7: Survey of US Utilities on Relay misoperation

% INCORRECT OPERATIONS, YEAR 2003

Company	Total Events	K Factor	Relay Misoperations		Voltage	Failure to Trip	Failure to Interrupt	Slow Trip	Unnecessary Trip During Fault	Unnecessary Trip Other Than Fault	Failure to Reclose	Total Misoperations
A					Above 400							
B												
C	3	0	1			0.0%	0.0%	0.0%	0.0%	33.3%	0.0%	33.3%
D												
E												
F												
H												
I												
A	23	0	4		301 - 400	0.0%	0.0%	0.0%	8.7%	8.7%	0.0%	17.4%
B	136	2	20			0.7%	0.0%	1.4%	5.1%	2.2%	5.1%	14.5%
C	22	1	13			0.0%	0.0%	0.0%	13.0%	39.1%	4.3%	56.5%
D												
E	16	4	7			0.0%	0.0%	0.0%	0.0%	0.0%	35.0%	35.0%
F	1	0	0			0.0%	0.0%	0.0%	0.0%	0.0%	0.0%	0.0%
H												
I	9	0	3			0.0%	0.0%	0.0%	0.0%	0.0%	33.3%	33.3%
A					201 - 300							
B												
C	9	1	2			0.0%	0.0%	0.0%	0.0%	20.0%	0.0%	20.0%
D												
E	1	0	0			0.0%	0.0%	0.0%	0.0%	0.0%	0.0%	0.0%
F												
H												
I												
A	72	0	22		101 - 200	1.4%	0.0%	1.4%	19.4%	8.3%	0.0%	30.6%
B	303	9	46			0.0%	0.0%	2.9%	6.7%	0.6%	4.5%	14.7%
C	128	0	29			0.0%	0.0%	0.0%	7.8%	7.0%	7.8%	22.7%
D												
E	115	3	23			0.8%	0.0%	0.0%	14.4%	4.2%	0.0%	19.5%
F	15	1	10			0.0%	0.0%	0.0%	50.0%	12.5%	0.0%	62.5%
H												
I	10	6	11			6.3%	0.0%	0.0%	18.8%	6.3%	37.5%	68.8%
A	105	0	7		51 - 100	1.0%	0.0%	0.0%	4.8%	0.0%	1.0%	6.7%
B	697	1	12			0.0%	0.0%	0.0%	1.1%	0.0%	0.6%	1.7%
C	397	1	24			0.3%	0.0%	0.0%	2.8%	0.8%	2.3%	6.0%
D												
E	291	5	30			0.7%	0.0%	0.3%	6.4%	1.0%	1.7%	10.1%
F												
H												
I	47	0	6			0.0%	0.0%	2.1%	4.3%	4.3%	2.1%	12.8%

It is assumed that only line or functional group connected to the initial contingent functional group or line will suffer inadvertent tripping. This assumption for the derivation of Inadvertent Tripping Contingency is based on the zones of protection in the real system. If there is more than one functional group that can suffer inadvertent tripping than it is assumed that they are disjoint or in other words only one of them can suffer inadvertent tripping at a time. We have no information of more than one simultaneous inadvertent tripping from the open literature. However without extra effort one can extend the equations developed below to take that into account in case the situation demands. A systematic methodology for the probability calculation of inadvertent tripping is developed and illustrated through the five substation topologies discussed above.

The total probability of an inadvertent tripping contingency (ITC) k involving line i and line j can be calculated by

$$\begin{aligned} P_{ITC_k} &= \Pr(\textit{line } j \textit{ trips} \mid \textit{line } i \textit{ trips}) + \Pr(\textit{line } i \textit{ trips} \mid \textit{line } j \textit{ trips}) \\ &= \Pr(\textit{line } j \textit{ trips} \cap \textit{line } i \textit{ trips}) / \Pr(\textit{line } i \textit{ trips}) \\ &+ \Pr(\textit{line } i \textit{ trips} \cap \textit{line } j \textit{ trips}) / \Pr(\textit{line } j \textit{ trips}) \\ &= \Pr(\textit{line } j \textit{ trips} \cap \textit{line } i \textit{ trips}) * \\ &\quad \left[(\Pr(\textit{line } i \textit{ trips}) + \Pr(\textit{line } j \textit{ trips})) / (\Pr(\textit{line } i \textit{ trips}) * \Pr(\textit{line } j \textit{ trips}))\right] \end{aligned} \tag{27}$$

assuming that the probability of failure/fault to be same for each line. Let

p_{lf}^{i} : fault probability of line i. It is assumed to be the same (denoted as p_l) for all transmission lines;

Therefore,

$$\begin{aligned} P_{ITC_k} &= \Pr(\textit{line } j \textit{ trips} \cap \textit{line } i \textit{ trips})[(2 * p_l)/(p_l^2)] \\ &= \Pr(\textit{line } j \textit{ trips} \cap \textit{line } i \textit{ trips}) * 2 * (1/p_l) \end{aligned} \tag{28}$$

The result generalizes in terms of the functional group concept discussed earlier. Let us consider two functional groups represented by FG-*i* and FG-*j*. The probability that a functional group FG-*i* is tripped due to failure of a component can be calculated as $\sum_{i \in S_i} P_{FL}^{j}$, where the elements of S_i are the indices of all the components in functional group i. The probability that a functional group is tripped due to fault can be calculated as $\sum_{i \in S_i} P_{FT}^{j}$ in the same way.

The probability of an ITC k due to failure that involved FG-i and FG-j can be calculated by

$$P_{ITC_k} = \Pr(FG-j\,trips \mid FG-i\,trips) + \Pr(FG-i\,trips \mid FG-j\,trips)$$

where

$$\begin{aligned}
\Pr(FG-j\,trips \mid FG-i\,trips) &= \Pr(FG-j\,trips \cap FG-i\,trips)/\Pr(FG-i\,trips) \\
P_{ITC_k} &= \Pr(FG-j\,trips \cap FG-i\,trips)/\Pr(FG-i\,trips) \\
&\quad + \Pr(FG-i\,trips \cap Fg-j\,trips)/\Pr(FG-j\,trips) \\
&= \Pr(FG-j\,trips \cap FG-i\,trips)* \\
&\quad \left[(\Pr(FG-i\,trips) + \Pr(FG-j\,trips))/(\Pr(FG-i\,trips)*\Pr(FG-j\,trips)\right] \\
&= \Pr(FG-j\,trips \cap FG-i\,trips)\left[\sum_{i\in S_i} P_{FL}^i + \sum_{i\in S_i} P_{FL}^j\right] / \left[\left(\sum_{i\in S_i} P_{FL}^i\right)*\left(\sum_{i\in S_i} P_{FL}^j\right)\right]
\end{aligned} \tag{29}$$

Similarly the probability of an ITC k due to fault that involved FG-i and FG-j can be calculated by

$$P_{ITC_k} = \Pr(FG-j\,trips \cap FG-i\,trips)\left[\sum_{i\in S_i} P_{FT}^i + \sum_{i\in S_i} P_{FT}^j\right] / \left[\left(\sum_{i\in S_i} P_{FT}^i\right)*\left(\sum_{i\in S_i} P_{FT}^j\right)\right] \tag{30}$$

In the above case it was considered that there is a possibility of only one additional functional group suffering inadvertent tripping. When there are more functional groups which can trip inadvertently then one can similarly find an expression of the total probability by conditioning on each functional group sequentially and adding their probabilities. For example when the failure of one can initiate inadvertent tripping of either of the two then the expression for total ITC probability will look like

$$\begin{aligned}
P_{ITC_l} &= \Pr(FG-i\,trips\ or\ FG-j\,trips \mid FG-k\,trips) \\
&\quad + \Pr(FG-i\,trips\ or\ FG-k\,trips \mid FG-j\,trips) \\
&\quad + \Pr(FG-j\,trips\ or\ FG-k\,trips \mid FG-i\,trips)
\end{aligned} \tag{31}$$

2.4.1 Generalized form for Inadvertent Tripping Contingency

In this section a generalized method from the system topology to find the total probability of ITC after an initial contingency is developed. As it was discussed above, the power system can be represented as an undirected graph with functional groups as the vertices and the interfacing elements as the edges. The graph search algorithm developed enables identification of the interconnections between functional groups. The methodology will be illustrated with the example of the power system shown in Fig. 6 and the result generalized. For the power system shown in Fig. 6, the result of the graph search is summarized in Table 5. Each column in the table corresponds to a functional group, while each row corresponds to an interfacing component. There are two ones in each row, which indicate the interfacing component joining the two corresponding functional groups. The rest of the elements are all zeros. This is represented as the incidence matrix in (1) which is reproduced below

$$B = \begin{pmatrix} 1 & 1 & 0 & 0 & 0 & 0 & 0 \\ 0 & 1 & 1 & 0 & 0 & 0 & 0 \\ 0 & 0 & 1 & 1 & 0 & 0 & 0 \\ 0 & 0 & 1 & 0 & 1 & 0 & 0 \\ 0 & 0 & 0 & 0 & 1 & 1 & 0 \\ 0 & 0 & 0 & 0 & 0 & 1 & 1 \end{pmatrix} \tag{32}$$

The new matrix B^T in (33) is obtained by taking the transpose of the matrix B in (1)

$$B^T = \begin{pmatrix} 1 & 0 & 0 & 0 & 0 & 0 \\ 1 & 1 & 0 & 0 & 0 & 0 \\ 0 & 1 & 1 & 1 & 0 & 0 \\ 0 & 0 & 1 & 0 & 0 & 0 \\ 0 & 0 & 0 & 1 & 1 & 0 \\ 0 & 0 & 0 & 0 & 1 & 1 \\ 0 & 0 & 0 & 0 & 0 & 1 \end{pmatrix} \tag{33}$$

Each column in (33) corresponds to an interfacing component, while each row corresponds to a functional group.

$$X = \{FG\text{-}1,\ FG\text{-}2,\ FG\text{-}3,\ FG\text{-}4,\ FG\text{-}5,\ FG\text{-}6,\ FG\text{-}7\} \tag{34}$$

$$K = \bigcap P(B * diag(X)) \tag{35}$$

$$D = diag(K) \tag{36}$$

$$C(1) = (1\ 1\ 1 \ldots.) \tag{37}$$

where C(1) is the unit column matrix of order (1*7), $\bigcap P$ is the joint probability of failure of the functional groups in each row of the matrix $B * diag(X)$ which can be approximately calculated from the outage data base available in the utilities for past many years.

Then all the equations in (30) and (31) can be summarized in the matrix form as

$$P_{IFG}^{FT} = (1/P_{FG_1}^{FT}, 1/P_{FG_2}^{FT}, 1/P_{FG_3}^{FT}, 1/P_{FG_4}^{FT}, 1/P_{FG_5}^{FT}, 1/P_{FG_6}^{FT}, 1/P_{FG_7}^{FT})^T \tag{38}$$

$$P_{ITC} = [(B^T * D)^T * diag(P_{IFG}^{FT})]^T * C(1) \tag{39}$$

$$\text{where } P_{ITC} = \begin{pmatrix} P_{FG_1}^{ITC} \\ P_{FG_2}^{ITC} \\ P_{FG_3}^{ITC} \\ P_{FG_4}^{ITC} \\ P_{FG_5}^{ITC} \\ P_{FG_6}^{ITC} \\ P_{FG_7}^{ITC} \end{pmatrix} \tag{40}$$

and $P_{FG_1}^{ITC}$ is the total probability of ITC given the fault/ failure in functional group 1. It is assumed that $P_{FG_i}^{FT}$ is not identically equal to zero. In other words it is not a bus section. The case where FG_i is a bus section is discussed as a special case below.

Equation (39) is the general formula for any power system whose topology is known in terms of the switching elements and components of the functional group. So for the power system example in Fig. 6, the ITC probability for each functional group can be calculated as below.

$$\begin{pmatrix} P_{FG_1}^{ITC} \\ P_{FG_2}^{ITC} \\ P_{FG_3}^{ITC} \\ P_{FG_4}^{ITC} \\ P_{FG_5}^{ITC} \\ P_{FG_6}^{ITC} \\ P_{FG_7}^{ITC} \end{pmatrix} = [A * diag(P_{IFG}^{FT})]^T * C(1) \tag{41}$$

$$\text{where } A = \left[\begin{pmatrix} 1 & 0 & 0 & 0 & 0 & 0 \\ 1 & 1 & 0 & 0 & 0 & 0 \\ 0 & 1 & 1 & 1 & 0 & 0 \\ 0 & 0 & 1 & 0 & 0 & 0 \\ 0 & 0 & 0 & 1 & 1 & 0 \\ 0 & 0 & 0 & 0 & 1 & 1 \\ 0 & 0 & 0 & 0 & 0 & 1 \end{pmatrix} * \begin{pmatrix} P(FG_1 \cap FG_2) & 0 & 0 & 0 & 0 & 0 \\ 0 & P(FG_2 \cap FG_3) & 0 & 0 & 0 & 0 \\ 0 & 0 & P(FG_3 \cap FG_4) & 0 & 0 & 0 \\ 0 & 0 & 0 & P(FG_3 \cap FG_5) & 0 & 0 \\ 0 & 0 & 0 & 0 & P(FG_5 \cap FG_6) & 0 \\ 0 & 0 & 0 & 0 & 0 & P(FG_6 \cap FG_7) \end{pmatrix} \right]^T$$

In the same way the ITC can be found for any power system once the functional groups are identified. With the changing topology of the power system the functional groups can be identified in an updating mode and continuous tracking of increased ITC probability can be very useful in real time operations.

2.4.2 Special Case

When all the functional group(s) connected by the interfacing element(s) of the failed or faulted functional group contains/contain only bus sections as their components then all the functional groups connected to these bus sections will have equal probability to suffer inadvertent tripping. This special case is incorporated by modifying the matrix B. The modified matrix is obtained by subtracting the column corresponding to the faulted functional group from the sum of the columns of the functional groups connected to the faulted functional group through the interfacing elements of the faulted functional group. In the next step the columns corresponding to the functional groups connected to the faulted functional group are made zero. To find the ITC corresponding to this special case only the transpose of the column corresponding to the faulted functional group in the B^T matrix is needed. This gives the ITC probability of the functional group which is connected only to the bus section through all interfacing elements. From practical experience the probability of a fault in a bus section is once in a lifetime and is 'almost zero' compared to other components fault probability. Thus the probability of bus fault is assumed to be zero. Similarly the probability of simultaneous outage of two functional groups where one of the functional group is a bus section is zero. Hence the ITC probability for an initial contingency on a bus section is zero and is not calculated.

Although the equations above give a concise mathematical form to calculate the probability of inadvertent tripping contingencies, it depends on the availability of matrix B, which is not easy to obtain. In addition, the size of *B* is very large and sparsity technology has to be used to handle it efficiently. Other matrix operations in case of a functional group connected only to the bus sections through the interfacing elements are memory intensive. However, a computer algorithm is developed to search for functional groups, its components, the interfacing elements and to get the ITC without formulating the *B* matrix.

In the next section, the probability calculation for the typical substation topologies are illustrated directly from the topology and with the help of the formula developed. This will illustrate the effectiveness of the concise formula developed for a large system where it is not easy to enumerate all the different possibilities easily. A systematic method is indispensable for a large system.

2.5 Probability calculation illustration for the Typical Substation Topologies

2.5.1 Ring Bus

This configuration is simple and straightforward. From Fig. 15, there are a total of four functional groups and four breakers. In this simple configuration from the

topology it is evident that a fault on a single line can trigger inadvertent tripping on either of the two lines connected to the same bus through an electrical distance of one breaker. For illustration purposes it is assumed that the fault occurs on line 3 or FG-3 and is tripped correctly.

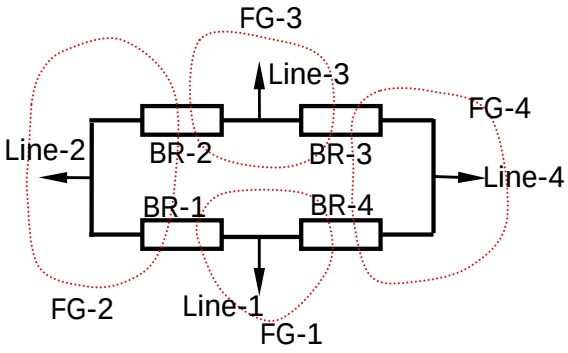

$$B = \begin{pmatrix} 1 & 1 & 0 & 0 \\ 0 & 1 & 1 & 0 \\ 0 & 0 & 1 & 1 \\ 1 & 0 & 0 & 1 \end{pmatrix}$$

Fig. 15: Ring bus station with *B*-matrix

Now one of the two functional groups FG-2 or FG-4 can trip inadvertently. The functional group fault probability is calculated as in (12), and assuming the failure probability of bus $p_{bf} \approx 0$. So the probability of ITC when FG-3 trips is

$$P_{ITC_1} = \Pr(FG-2 \ trips \ or \ FG-4 trips \,|\, FG-3 trips) \tag{42}$$

Since the inadvertent tripping of any of the functional groups is independent of each other and assuming they are disjoint the above expression becomes.

$$\begin{aligned} P_{ITC_1} &= \Pr(FG-2 \ trips \,|\, FG-3 \ trips) + \Pr(FG-4 trips \,|\, FG-3 \ trips) \\ &= [P(FG_2 \cap FG_3) + P(FG_3 \cap FG_4)]\left(1/P_{FG_3}^{FT}\right) \end{aligned} \tag{43}$$

The ITC probability calculations using equations (34)-(40) are also shown below.

$$P_{IFG}^{FT} = (1/P_{FG_1}^{FT}, 1/P_{FG_2}^{FT}, 1/P_{FG_3}^{FT}, 1/P_{FG_4}^{FT})^T \tag{44}$$

$$P_{ITC} = [(B^T * D)^T * diag(P_{IFG}^{FT})]^T * C(1) \tag{45}$$

$$\begin{pmatrix} P_{FG_1}^{ITC} \\ P_{FG_2}^{ITC} \\ P_{FG_3}^{ITC} \\ P_{FG_4}^{ITC} \end{pmatrix} = \left[\left\{ \begin{pmatrix} 1 & 0 & 0 & 1 \\ 1 & 1 & 0 & 0 \\ 0 & 1 & 1 & 0 \\ 0 & 0 & 1 & 1 \end{pmatrix} * \begin{pmatrix} P(FG_1 \cap FG_2) & 0 & 0 & 0 \\ 0 & P(FG_2 \cap FG_3) & 0 & 0 \\ 0 & 0 & P(FG_3 \cap FG_4) & 0 \\ 0 & 0 & 0 & P(FG_1 \cap FG_4) \end{pmatrix} \right\}^T * diag(P_{IFG}^{FT}) \right]^T * \begin{pmatrix} 1 \\ 1 \\ 1 \\ 1 \end{pmatrix}$$

$$\begin{pmatrix} P_{FG_1}^{ITC} \\ P_{FG_2}^{ITC} \\ P_{FG_3}^{ITC} \\ P_{FG_4}^{ITC} \end{pmatrix} = \begin{pmatrix} .. \\ .. \\ [P(FG_2 \cap FG_3) + P(FG_3 \cap FG_4)]\left(1/P_{FG_3}^{FT}\right) \\ .. \end{pmatrix} \tag{46}$$

which is same as obtained from the topology in (43).

2.5.2 Breaker and a Half Bus (B-HB)

The configuration of B-HB is shown in Fig. 16, having a total of six functional groups and six breakers. In this simple bus configuration a fault on a single line can trigger inadvertent tripping on only lines connected between the same pair of buses through an electrical distance of one breaker and on the same side. For illustration purposes it is assumed that the fault occurs on line 3 or FG-4.

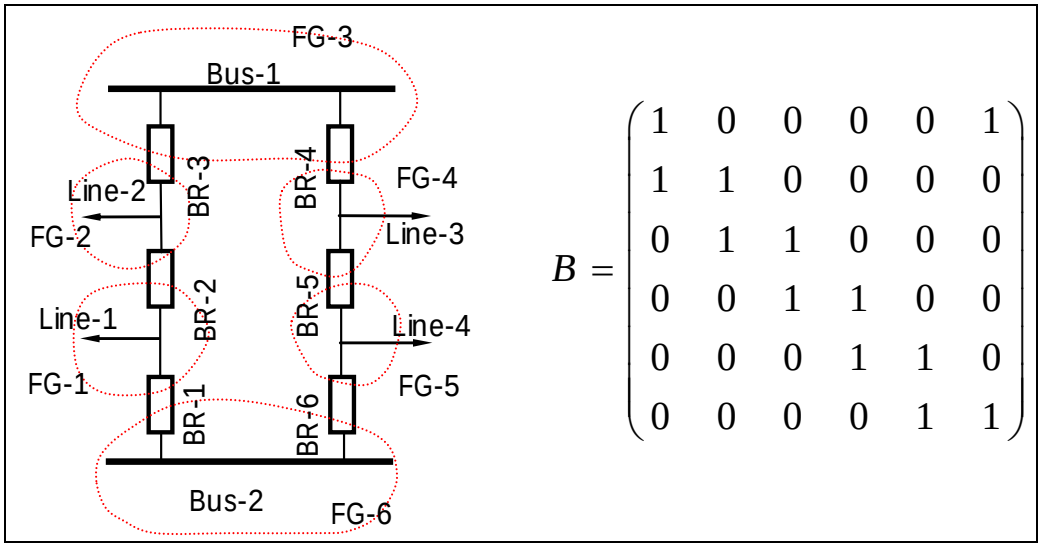

$$B = \begin{pmatrix} 1 & 0 & 0 & 0 & 0 & 1 \\ 1 & 1 & 0 & 0 & 0 & 0 \\ 0 & 1 & 1 & 0 & 0 & 0 \\ 0 & 0 & 1 & 1 & 0 & 0 \\ 0 & 0 & 0 & 1 & 1 & 0 \\ 0 & 0 & 0 & 0 & 1 & 1 \end{pmatrix}$$

Fig. 16: Breaker and a half bus

Now only FG-5 can trip inadvertently which is on the same side as FG-4 and between the same pair of buses. The functional group fault probabilities are calculated as from (24), assuming the failure probability of bus $p_{bf} \approx 0$. So the probability of ITC contingency when FG-4 trips

$$P_{ITC_2} = \Pr(FG-5\ trips \mid FG-4 trips) \tag{47}$$

$$= [P(FG_5 \cap FG_4)]\left(1/P_{FG_4}^{FT}\right)$$

Now from equations (34)-(40) the corresponding equations for a breaker and half are as follows

$$P_{IFG}^{FT} = (1/P_{FG_1}^{FT}, 1/P_{FG_2}^{FT}, 1/P_{FG_3}^{FT}, 1/P_{FG_4}^{FT}, 1/P_{FG_5}^{FT}, 1/P_{FG_6}^{FT})^T \tag{48}$$

where $P_{FG_3}^{FT}$ and $P_{FG_6}^{FT}$ are zero. But all the terms of the form $P(FG_j \cap FG_i) * \left(1/P_{FG_i}^{FT}\right)$ are zero where i = 3, 6 $j \neq i$.

$$P_{ITC} = [(B^T * D)^T * diag(P_{IFG}^{FT})]^T * C(1) \tag{49}$$

$$\begin{pmatrix} P_{FG_1}^{ITC} \\ P_{FG_2}^{ITC} \\ P_{FG_4}^{ITC} \\ P_{FG_6}^{ITC} \end{pmatrix} = \begin{pmatrix} .. \\ .. \\ [P(FG_5 \cap FG_4)]\left(1/P_{FG_4}^{FT}\right) \\ .. \end{pmatrix} \tag{50}$$

which is same as calculated from the topology. In the final expression the terms $P_{FG_3}^{ITC}$ and $P_{FG_6}^{ITC}$ are not included because they are bus sections and ITC corresponding to them is zero as explained earlier.

2.5.3 Single Bus Connected with Tie Breaker (SB-TB)

This configuration SB-TB in Fig. 17 is adapted from SB-SB by splitting the bus and adding a tie-breaker between the two buses. From the topology it is evident that a fault on a single line can trigger inadvertent tripping on only lines connected to the same bus through an electrical distance of one breaker and on the same side of the tie breaker. For illustration purposes it is assumed that the fault occurs on line 1 or FG-1.

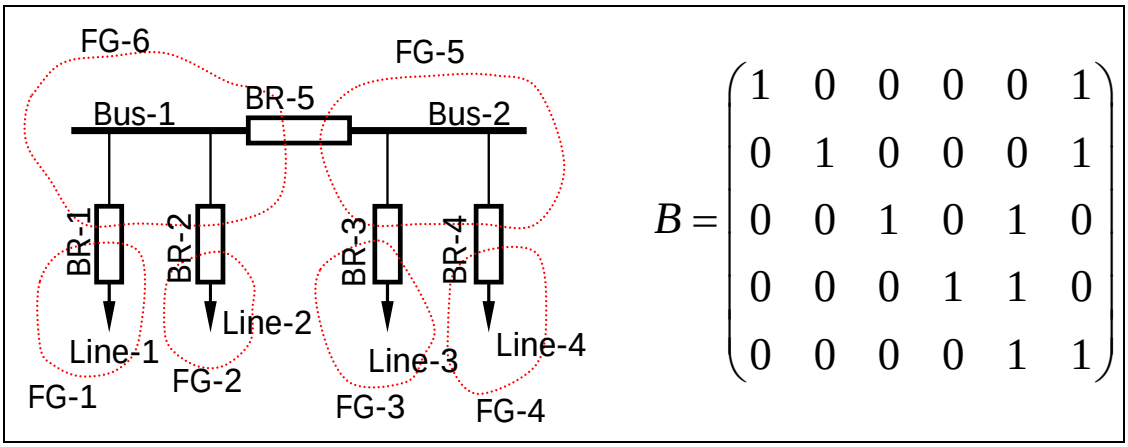

$$B = \begin{pmatrix} 1 & 0 & 0 & 0 & 0 & 1 \\ 0 & 1 & 0 & 0 & 0 & 1 \\ 0 & 0 & 1 & 0 & 1 & 0 \\ 0 & 0 & 0 & 1 & 1 & 0 \\ 0 & 0 & 0 & 0 & 1 & 1 \end{pmatrix}$$

Fig. 17: Single bus connected with tie-breaker and it's *B*-matrix

So now only FG-2 can trip inadvertently. The functional group fault probability is calculated as in (16), assuming the failure probability of the bus $p_{bf} \approx 0$. So the probability of ITC contingency when FG-1 trips is

$$P_{ITC_3} = \Pr(FG-2 \ trips | FG-1 trips) \tag{51}$$
$$= [P(FG_2 \cap FG_1)]\left(1/P_{FG_1}^{FT}\right)$$

Now from equations (34)-(40) the corresponding equations for this configuration are as follows

$$P_{IFG}^{FT} = (1/P_{FG_1}^{FT}, 1/P_{FG_2}^{FT}, 1/P_{FG_3}^{FT}, 1/P_{FG_4}^{FT}, 1/P_{FG_5}^{FT}, 1/P_{FG_6}^{FT})^T \tag{52}$$

where $P_{FG_5}^{FT}$ and $P_{FG_6}^{FT}$ are zero. But all the terms of the form $P(FG_j \cap FG_i) * \left(1/P_{FG_i}^{FT}\right)$ are zero where i = 5, 6 $j \neq i$.

$$P_{ITC} = [(B^T * D)^T * diag(P_{IFG}^{FT})]^T * C(1) \tag{53}$$

$$\begin{pmatrix} P_{FG_1}^{ITC} \\ P_{FG_2}^{ITC} \\ P_{FG_3}^{ITC} \\ P_{FG_4}^{ITC} \end{pmatrix} = \begin{pmatrix} [P(FG_2 \cap FG_1)]\left(1/P_{FG_1}^{FT}\right) \\ \vdots \\ \vdots \\ \vdots \end{pmatrix} \tag{54}$$

which is same as calculated from the topology. In the final expression the terms $P_{FG_5}^{ITC}$ and $P_{FG_6}^{ITC}$ are not included because they are bus sections and ITC corresponding to them is zero as explained earlier

2.5.4 Single Breaker and Single Bus (SB-SB)

In the simple configuration in Fig. 18, a fault on a single line can trigger inadvertent tripping on any one of the remaining three lines since all are connected to the same bus through an electrical distance of one breaker. For illustration purposes it is assumed that the fault occurs on line 3 or FG-3.

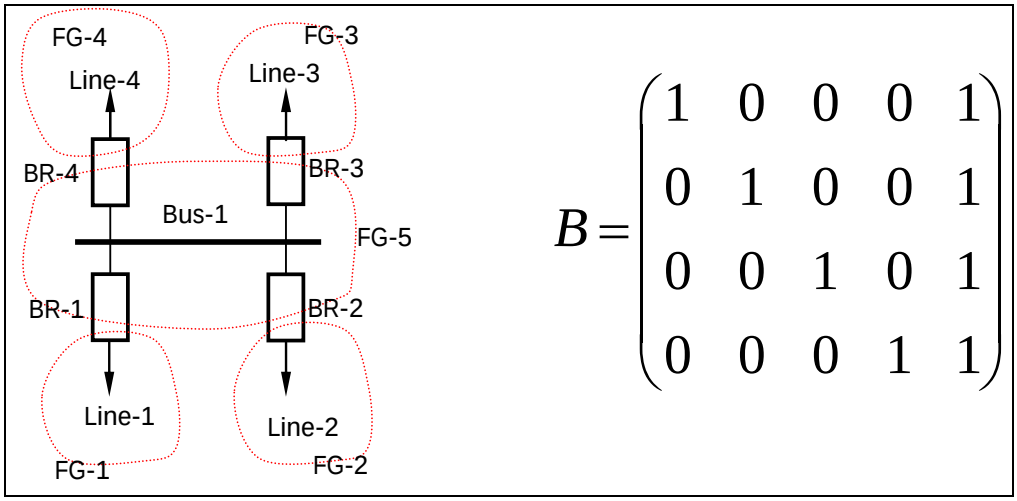

$$B = \begin{pmatrix} 1 & 0 & 0 & 0 & 1 \\ 0 & 1 & 0 & 0 & 1 \\ 0 & 0 & 1 & 0 & 1 \\ 0 & 0 & 0 & 1 & 1 \end{pmatrix}$$

Fig. 18: Single breaker single bus substation and it's *B*-matrix

Now one or more of the remaining functional groups can trip inadvertently. The functional group fault probability, which is the summation of the fault probability of each component in the functional group, is calculated from (8), assuming the failure probability of the bus p_{bf} ≈ 0. So the probability of ITC when FG-3 trips is

$$P_{ITC_4} = \Pr(FG-1 \ trips \, or \, FG-2 \ trips \ or \ FG-4 trips \,|\, FG-3 \, trips) \tag{55}$$

Since the inadvertent tripping of any of the functional groups is independent of each other and assuming they are disjoint the above expression becomes.

$$\begin{aligned} P_{ITC_4} = {} & \Pr(FG-1 \ trips \,|\, FG-3 trips) + \Pr(FG-2 \ trips \,|\, FG-3 \, trips) \\ & + \Pr(FG-4 trips \,|\, FG-3 \, trips) \end{aligned} \tag{56}$$

$$= [P(FG_1 \cap FG_3) + P(FG_2 \cap FG_3) + P(FG_4 \cap FG_3)]\left(1/P_{FG_3}^{FT}\right) \quad (57)$$

This configuration falls under the category of special case where the faulted functional group is connected only to a bus section. So to calculate its ITC probability through (34)-(40) the matrix B is modified as explained earlier. So in this case the B matrix for ITC probability of FG-3 becomes

$$B' = \begin{pmatrix} 1 & 0 & 1 & 0 & 0 \\ 0 & 1 & 1 & 0 & 0 \\ 0 & 0 & 0 & 0 & 0 \\ 0 & 0 & 1 & 1 & 0 \end{pmatrix} \quad (58)$$

$B^{T'} = \begin{pmatrix} 1 & 1 & 0 & 1 \end{pmatrix}$ row corresponding to FG-3 (59)

$$P_{IFG}^{FT} = (1/P_{FG_1}^{FT}, 1/P_{FG_2}^{FT}, 1/P_{FG_3}^{FT}, 1/P_{FG_4}^{FT}, 1/P_{FG_5}^{FT})^T \quad (60)$$

where $P_{FG_5}^{FT}$ **is** zero. But all the terms of the form $P(FG_j \cap FG_i) * \left(1/P_{FG_i}^{FT}\right)$ are zero where i = 5 and $j \neq i$.

$$P_{ITC} = [(B^T * D)^T * diag(P_{IFG}^{FT})]^T * C(1) \quad (61)$$

$$P_{FG_3}^{ITC} = [P(FG_1 \cap FG_3) + P(FG_2 \cap FG_3) + P(FG_4 \cap FG_3)]\left(1/P_{FG_3}^{FT}\right) \quad (62)$$

which is same as calculated from the topology. In this configuration all the non bus section functional groups are connected only to the bus section and ITC is calculated similarly for each of them.

2.5.5 Double Breaker and Double Bus (DB-DB)

The configuration of DB-DB is shown in Fig. 19, and there are a total of six functional groups and eight breakers, much more than other types of substations. In this configuration a fault on a single line can trigger inadvertent tripping on any one of the remaining three lines since all are connected to the same bus through an electrical distance of one breaker. For illustration purposes it is assumed that the fault occurs on line 1 or FG-1. The functional group fault probabilities are calculated from (20), assuming the failure probability of the bus $p_{bf} \neq 0$.

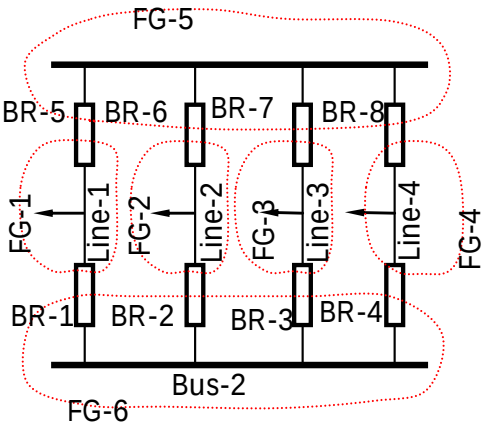

$$B = \begin{pmatrix} 1 & 0 & 0 & 0 & 0 & 1 \\ 0 & 1 & 0 & 0 & 0 & 1 \\ 0 & 0 & 1 & 0 & 0 & 1 \\ 0 & 0 & 0 & 1 & 0 & 1 \\ 1 & 0 & 0 & 0 & 1 & 0 \\ 0 & 1 & 0 & 0 & 1 & 0 \\ 0 & 0 & 1 & 0 & 1 & 0 \\ 0 & 0 & 0 & 1 & 1 & 0 \end{pmatrix}$$

Fig. 19: Double breaker and double bus and it's *B*-matrix

So the probability of ITC contingency when FG-1 trips is

$$P_{ITC_5} = \Pr(FG-2 \ trips \, or \, FG-3 \ trips \ or \ FG-4 \, trips \,|\, FG-1 \, trips) \tag{63}$$

Since the inadvertent tripping of any of the functional groups is independent of each other and assuming they are disjoint the above expression becomes.

$$\begin{aligned} P_{ITC_5} &= \Pr(FG-2 \ trips \,|\, FG-1 trips) + \Pr(FG-3 \ trips \,|\, FG-1 \, trips) \\ &\quad + \Pr(FG-4 trips \,|\, FG-1 \, trips) \end{aligned} \tag{64}$$

$$= [P(FG_1 \cap FG_2) + P(FG_1 \cap FG_3) + P(FG_1 \cap FG_4)]\left(1/P_{FG_1}^{FT}\right) \tag{65}$$

This configuration is similar to SB-SB in that the faulted functional groups are connected only to functional groups containing a bus section. So to calculate its ITC probability the matrix B is modified as explained earlier. So in this case the B matrix for ITC probability of FG-1 becomes

$$B' = \begin{pmatrix} 0 & 0 & 0 & 0 & 0 & 0 \\ 1 & 1 & 0 & 0 & 0 & 0 \\ 1 & 0 & 1 & 0 & 0 & 0 \\ 1 & 0 & 0 & 1 & 0 & 0 \\ 0 & 0 & 0 & 0 & 0 & 0 \\ 1 & 1 & 0 & 0 & 0 & 0 \\ 1 & 0 & 1 & 0 & 0 & 0 \\ 1 & 0 & 0 & 1 & 0 & 0 \end{pmatrix} \tag{66}$$

$$B^{T'} = (0\,1\,1\,1\,0\,1\,1\,1) \text{ row corresponding to FG-1} \tag{67}$$

$$P_{IFG}^{FT} = (1/P_{FG_1}^{FT}, 1/P_{FG_2}^{FT}, 1/P_{FG_3}^{FT}, 1/P_{FG_4}^{FT}, 1/P_{FG_5}^{FT}, 1/P_{FG_6}^{FT})^T \tag{68}$$

where $P_{FG_5}^{FT}$ and $P_{FG_6}^{FT}$ are zero. But all the terms of the form $P(FG_j \cap FG_i) * \left(1/P_{FG_i}^{FT}\right)$ are zero where i = 5, 6 and $j \neq i$.

$$P_{ITC} = [(B^T * D)^T * diag(P_{IFG}^{FT})]^T * C(1) \quad (69)$$

$$P_{FG_1}^{ITC} = 2*[P(FG_1 \cap FG_2) + P(FG_1 \cap FG_3) + P(FG_1 \cap FG_4)]\left(1/P_{FG_1}^{FT}\right) \quad (70)$$

This is twice as calculated from the topology. This makes sense because both the functional groups connected to the faulted functional group are in turn connected to same set of functional groups. And with large number of breakers, relays and overlapping zones of protection, along with advantages comes disadvantages of higher likelihood of misoperation or inadvertent tripping. So ITC probability after an initial contingency is higher than expected. Similarly the ITC probabilities for other non bus section functional groups are computed.

Table 8 gives a summary of the topological analysis results for higher order stuck breaker and inadvertent tripping contingencies. In Table 8, the smallest ITC probability ($P_{ITC_2} = k$) is much smaller than the smallest stuck breaker contingency probability ($4 \times p_{sb} \times p_{lb}$).

Table 8: The probability of high-order contingency for different substations

Type	Prob. (Fault plus Stuck breaker)	Prob. (Fault plus ITC)	number of breakers	Fault plus stuck breaker Contingency set
SB-SB	$4 \times p_{sb} \times p_{lb}$	$P_{ITC_4} = 3*k$	*4*	*FG_1 and FG_5 , FG_2 and FG_5, FG_3 and FG_5 , FG_4 and FG_5*
Ring Bus	$8 \times p_{sb} \times p_{lb}$	$P_{ITC_1} = 2*k$	*4*	*FG1 and FG2, FG2 and FG3, FG3 and FG4, FG4 and FG1*
SB-TL	$4 \times p_{sb} \times p_{lb}$	$P_{ITC_3} = k$	*5*	*FG1 and FG5, FG2 and FG5, FG5 and FG6, FG3 and FG6, FG4 and FG6*
DB-DB	$8 \times p_{sb} \times p_{lb}$	$P_{ITC_5} = 3*k$	*8*	*FG1 and FG5, FG2 and FG5, FG3 and FG5, FG4 and FG5, FG1 and FG6, FG2 and FG6, FG3 and FG6, FG4 and FG6*
B-HB	$8 \times p_{sb} \times p_{lb}$	$P_{ITC_2} = k$	*6*	*FG1 and FG2, FG2 and FG3, FG3 and FG4, FG4 and FG5, FG5 and FG6, FG6 and FG1*

2.6 Test System

The developed methodology is implemented in Visual C++ computer language. The approach is tested on a test system given in Appendix D with 12 substations, 6 generators, 10 transformers, 119 bus section nodes and 39 line nodes. The test system data are given in Table 17 and Table 18 (APPENDIX E), and the result for the test system is summarized below in Table 9. The algorithm is also tested on IEEE-RTS 24 bus test system given in Appendix F. The results for the IEEE-RTS system are summarized in Table 10. In both the cases the full run of the program takes less than a second.

Table 9: Result of N-k contingency selection algorithm on Test System

Type	Functional Group	Stuck Breaker	Inadvertent Tripping
Number	71	126	125

Table 10: Result of N-k contingency selection algorithm on IEEE-RTS 24 Bus Test System

Type	Functional Group	Stuck Breaker	Inadvertent Tripping
Number	117	126	196

In both the above cases the results found by the program are the same as those found by inspection. Thus, the developed methodology is powerful yet simple to implement and has immense value in on-line tracking of the system's exposure to vulnerability via changes in the system topology.

The topology of the power system is continuously changing and hence the approach can be used in an updating mode, taking into consideration the changes in the status of the switches and breakers which would normally result in the formation of one or more new functional groups or merging into smaller number of functional groups. This updating mode makes the process very computationally efficient.

2.7 Summary

This chapter documents systematic method for computing probability *order* of different contingencies as a function of the switch-breaker data commonly available within the EMS. In many decision problems, knowledge of the "*probability order*" of the significant events is sufficient to distinguish between alternatives because probability order is a reasonable measure of event's probability. Rare event approximations (Appendix A) underpin the selection of high order contingencies for online security assessment. This makes sense because the probability of a compound event is dominated by the lowest order terms.

Five substation configurations, including single-bus connected with bus tie, ring bus, double breaker-double bus, single breaker-single bus, and breaker and a half are used in the illustrations of the probability calculation approach developed for *N-k* ($k \geq 2$ implied) contingencies, and the results are summarized in Table 8.

The methodology developed for probability calculation is simple and needs no extra information other that switch-breaker data which is available in most control centers. The approach can be used in an updating mode with the changes in the topology of the system, taking into consideration changes in the status of the switches and breakers which normally results in formation of one or more new functional groups or merging into smaller number of functional groups. Thus continuous tracking of system topology generates the higher order contingencies based on probability *order* for online security assessment.

3 Numerical Methods

The long-term dynamic simulation of a power system is of interest in this research because it enables the evaluation and analysis of events which may lead to cascading outages. However, in order for such simulation to be of value in an operational context, it must be able to perform simulations very fast. This chapter is motivated by the desire to make algorithmic improvements to power system time domain simulation methods that will enhance computational efficiency.

Power system response to disturbances is decided not only by fast dynamics of its machines, but also by the action of slow processes, such as tap changers and the load dynamics. They often cause voltage problems and/or thermal loading problems after an extended period. Over the decades there has been intense intellectual labor and resulting technological advancement in speed of computers and numerical algorithms. The availability of these sophisticated numerical integration algorithms with variable time steps has made large simulation time steps possible. Commercial programs such as EUROSTAG, GE's EXSTAB, and Powertech's TSAT have successfully implemented the so called "A-stable" implicit method of performing numerical integration [23].

In general, there are two broad categories of numerical methods - the explicit and the implicit. In the explicit methods, the next step calculation uses only the solution information known; whereas the implicit methods use the unknown solution information of next-step(s). Iterative methods, such as Newton method are needed to solve the implicit non-linear equations. One attractive feature of implicit methods lies in the fact that they allow very large time steps. Reference [24] reports the usage of 20 seconds in EXSTAB and [23] reports the usage of 10 seconds time step in EUROSTAG without the loss of numerical stability.

Although some companies have implemented on-line transient instability analysis for detection of early-swing problems, we are aware of no company that has implemented long-term simulation capability for on-line purposes. Reasons for this are (a) perceived need and (b) technological capability. We have addressed the operational need for such simulation capability in Chapter 1, with underlying rationale being it will provide ability to prepare for multi-element (N-k) events that can result in severe impact. In this chapter, we address one aspect of the technological capability issue, and that is algorithmic speed. Given the complexity of the interconnected power grid, it is difficult to gain significant scaling in computational speed without exploiting the structure and the nature of the differential equations governing the power system. In this research we employ advanced numerical algorithms which take advantage of the power system governing equations.

This chapter is organized as follows. Section 3.1 presents in summary form the differential-algebraic equations (DAE which will be derived in Chapter 4), and we discuss their nature and uniqueness. Section 3.2 discusses potential targets for enhancing computational efficiency. Section 3.3 focuses on the algorithmic targets of enhancing computational efficiency, including application of unsymmetric multifrontal methods to the linear system solution step of the implicit integration procedure. The frontal and multifrontal methods and the advantages of multifrontal methods are

identified. Section 3.4 illustrates the method on a test system, and Section 3.5 provides a quantitative comparison of the multifrontal methods with the Gaussian elimination.

3.1 Formulation of Dynamic Algebraic Equations

Chapter 4 discusses in detail the individual power system component modeling and problem formulation for dynamic simulation studies. For the sake of completion, we preempt the derivations here, and present the resulting differential algebraic equations (DAE) developed in Chapter 4. The equations developed are for all the generations including the exciter, the governor, and the AGC models. The two axis model for the generator is used in the present study. For generators, the notation used is the same as in [25]. The limiter for each variable is implemented in program logic, and is not shown in the equations. The set of differential equations are as follows

$$\frac{\partial \delta}{\partial t} = \omega - 1 \tag{71}$$

$$\frac{\partial \omega}{\partial t} = \left[\left(Y \times P_r \right) - Ds\left(\omega - 1 \right) - \left(E_d^{'} I_d + E_q^{'} I_q - \left(X_q^{'} - X_d^{'} \right) I_q I_d \right) \right] \Big/ T_j \tag{72}$$

$$\frac{\partial E_d^{'}}{\partial t} = \left[-E_d^{'} - \left(X_q - X_q^{'} \right) I_q \right] \Big/ T_{q0}^{'} \tag{73}$$

$$\frac{\partial E_q^{'}}{\partial t} = \left[EDF - E_q^{'} + \left(X_d - X_d^{'} \right) I_d \right] \Big/ T_{d0}^{'} \tag{74}$$

$$\frac{\partial Y}{\partial t} = \left[Y - Y_0 \right] / T_{CH} \tag{75}$$

$$\frac{\partial Y_0}{\partial t} = -R \times K_G \times Y_0 + K_G \left[\left(\omega_r - \omega \right) + R\left(L_{ref\,0}^{g} - \delta_c / T_g \right) \right] \Big/ T_{CH} \tag{76}$$

$$\frac{\partial \Delta E_f}{\partial t} = \left[-\Delta E_f + E_q^{'} + K_a \left(V_{ref} - V_t \right) I_d \right] \Big/ T_e \tag{77}$$

The set of algebraic equations are as follows, where *i* is the index of the generator, and *j* is the index of the generator bus.

$$\begin{pmatrix} V_q^i \\ V_d^i \end{pmatrix} - \begin{pmatrix} E_q^{'i} \\ E_d^{'i} \end{pmatrix} + \begin{pmatrix} r^i & -X_d^i \\ X_d^i & r^i \end{pmatrix} \begin{pmatrix} I_q^i \\ I_d^i \end{pmatrix} = 0 \tag{78}$$

for each generator;

$$\begin{pmatrix} V_x^j \\ V_y^j \end{pmatrix} - \begin{pmatrix} \cos\delta^j, & -\sin\delta^j \\ \sin\delta^j, & \cos\delta^j \end{pmatrix} \begin{pmatrix} V_q^j \\ V_d^j \end{pmatrix} = 0 \tag{79}$$

for each generator bus;

$$\begin{pmatrix} I_x^j \\ I_y^j \end{pmatrix} - \begin{pmatrix} \cos\delta^j, & -\sin\delta^j \\ \sin\delta^j, & \cos\delta^j \end{pmatrix} \begin{pmatrix} I_q^j \\ I_d^j \end{pmatrix} = 0 \tag{80}$$

for each generator bus;

$$Y_{bus} \times \begin{pmatrix} V_x^1 \\ V_y^1 \\ \vdots \\ V_x^n \\ V_y^n \end{pmatrix} - \begin{pmatrix} I_x^1 \\ I_y^1 \\ \vdots \\ I_x^n \\ I_y^n \end{pmatrix} = 0 \tag{81}$$

for the whole linear impedance network with n voltage bus (Y_{bus} is the system admittance matrix);

$$\begin{pmatrix} P^i \\ Q^i \end{pmatrix} - \begin{pmatrix} V_x^i & V_y^i \\ V_y^i & -V_x^i \end{pmatrix} \begin{pmatrix} I_x^i \\ I_y^i \end{pmatrix} = 0 \tag{82}$$

for each load bus with constant P and Q. The loads in our test system are modeled as constant active and reactive power injection.

Equations (78) to (80) are for each individual generator. Equations (81) and (82) are for the whole network and each voltage bus respectively. The differential algebraic equation (DAE) developed in (71) through (82) can be summarized as

$$\frac{dx}{dt} = f(x, y) \tag{83}$$

$$0 = g(x, y) \tag{84}$$

where

x is a vector of state variables in (71)~(77)
(13) is the group of equations in (71)~(77)
y is a vector of the additional variables in (78)~(82)
(14) is the group of equations in (78)~(82).

The DAE have been called singular, implicit, differential-algebraic, descriptor, generalized state space, noncanonic, noncausal, degenerate, semistate, constrained, reduced order model, and nonstandard systems depending on the area of application it emerged from.

At this point, we would like to discuss the reasons to consider the equations (83)-(84) in this form, rather than trying to convert it as an ODE to solve. Just like in the present formulation, the formulation of many physical systems takes the form of a DAE depicting a collection of relationships between variables of interest and some of their derivatives. These variables usually have a physical significance. Attempting to covert the DAE to an ODE may result in the loss of their direct meanings and physical significance. Also in many cases it may be time consuming or impossible to obtain an explicit ODE model.

Often parameters are associated with applications like power systems. Changing parameter values can alter the relationships between variables, and may require different explicit models with solution manifolds of different dimensions. If we can solve the DAE directly, then it becomes easier to study the effect of modeling changes and parametric variations. It also facilitates the interfacing of modeling software with

the design software. The change to explicit form can destroy sparsity and prevent the exploitation of system structure, which is one of the major area we take advantage of in this research. All the above advantages and numerical reasons have led to significant research in the development of algorithms for solving DAE. None of the currently available numeric techniques support working with all DAE. Some additional conditions, either on the structure of the DAE and /or the numerical method, need to be satisfied for each case.

In the literature [26], there has been a significant effort to develop A-stable, accurate, and fast numerical integration methods with variable time steps. Although the different numerical integration schemes differ in their convergence, order, stability, and other properties, they do not necessarily offer considerable improvement in computational efficiency. In the next section, we discuss the solution strategy for the integration of DAE which are well suited for power systems.

3.2 Solution Strategy

One of the aims of this research is to obtain high speed to simulate extended time domain simulation for the purpose of online monitoring, tracking, and devising correcting action strategies for mitigating the frequency and impact of high consequence events. Most of the current methods for solving the power system dynamic simulation problems are developed for use on conventional sequential machines. This leads to the natural conclusion that there are two viable options to reduce the wall-clock time to solve a computationally intensive problem like power system time domain simulation. These are i) advanced hardware technology in terms of speed, memory, I/O, architecture and so on, and ii) more efficient algorithm. Although the emphasis is generally on the hardware, nevertheless efficient algorithms can offer great advantage in achieving the desired speed. There exists a symbiotic relationship between the two. We focus on the efficient algorithms to achieve high computational gain.

We can safely divide our simulator software into three parts, namely 1) a user interface 2) DAE solver kernel and 3) the output assembler. The maximum time amounting to almost 90%-95% of the total time is spent on the DAE solver. Any DAE solver requires three categories of numerical analysis techniques:

- Numerical Integration schemes
- Solution of non linear equations
- Solution of linear equations

In the following subsections we discuss the implementation of these numerical techniques.

3.3 Integration Scheme for DAE

As seen in the previous section, the power system is modeled, in summary by a set of thousands of differential and algebraic equations. These have inherent nonlinearities in them and the resulting DAE is highly stiff in nature. Switching events, contingencies, forced outages introduce significant discontinuities in the system variables. The numerical scheme must converge quickly, give desired accuracy, be reliable and stable. The implicit integration scheme called Theta method [27] satisfies

all the above requirements and is used in our simulator. It does not have the infamous *Hyper Stability* problem [23], which means that an algorithm will falsely report stability when the physical system is actually unstable. Theta Method is an example of a general approach to designing algorithms in which geometric intuition is replaced by Taylor series expansion. Invariably the implicit function theorem is also used in the design and analysis of the scheme. This method is also known as the weighted method.

Consider $$\frac{dx}{dt} = f(t, y) \tag{85}$$

The theta method can be expressed in the general form as

$$y_{n+1} = y_n + h[\theta f(t_{n+1}, y_{n+1}) + (1-\theta) f(t_n, y_n)] \quad n = 0,1,... \tag{86}$$

where h_n is the time step of integration at time n, n =0,1,2..

$\theta = 0$; Explicit Euler

$\theta = 1$; Implicit Euler

$\theta = ½$; Trapezoidal

The $\theta = 1$ case is very practical. At $\theta = 1$, it is called the ``Backward Euler'' or ``Implicit Euler'' scheme. It is a simple yet robust method for solving stiff ODEs. The difference between the exact solution and the above approximation at $t = t_n$ is

$$\left(\theta - \frac{1}{2}\right) h^2 y^n(t_n) + \left(\frac{1}{2}\theta - \frac{1}{3}\right) h^3 y'''(t_n) + \theta\left(h^4\right) \tag{87}$$

Hence, the method is order 2 for $\theta = ½$ which corresponds to Trapezoidal integration method, and otherwise it is of order 1. The concept of order is based on assumption that error is concentrated on the leading order of the Taylor series expansion (on real computers, h is small, but finite). For example at $\theta = ⅔$, $O\left(h^3\right)$ are removed while retaining $O\left(h^2\right)$. Hence, for different types of $f(t, y)$ one can tune θ to control whether $O\left(h^3\right)$ and higher order terms, or $O\left(h^2\right)$ and higher order terms contribute to the overall error when h is finite. It may be possible to choose θ that generates a more optimal or smaller error.

One can show easily that for $h > 0$ and sufficiently small,

$$\begin{aligned} e_{n+1} &= e_n + \theta h\left[f\left(t_n, y(t_n) + e_n\right) - f\left(t_n, y(t_n)\right)\right] \\ &\quad + (1-\theta) h\left[f\left(t_{n+1}, y(t_{n+1}) + e_{n+1}\right) - f\left(t_{n+1}, y(t_{n+1})\right)\right] \\ &= \begin{cases} -\frac{1}{12} h^3 y'''(t_n) + O(h^4) & \theta = \frac{1}{2} \\ +(\theta - \frac{1}{2}) h^2 y''(t_n) + O(h^3) & \theta \neq \frac{1}{2} \end{cases} \end{aligned} \tag{88}$$

Similarly, using the implicit function theorem

$$e_{n+1} = \begin{cases} -\frac{1}{12} h^3 y'''(t_n) + O(h^4) & \theta = \frac{1}{2} \\ +(\theta - \frac{1}{2}) h^2 y''(t_n) + O(h^3) & \theta \neq \frac{1}{2} \end{cases} \tag{89}$$

where $e_n =$ error at n^{th} iteration

Both the Euler and Trapezoidal integration scheme fit the equation of the above form. The choice of the Theta method is preferred over the Trapezoidal rule as it

avoids the numerical oscillations following the occurrence of switching events, where such oscillations can occur when using the Trapezoidal rule [28].
Discretizing (83) and (84) using Theta-method, we find

$$\left[x_{n+1} - x_n - h\theta \dot{x}_n\right] - (1-\theta) hf\left(x_{n+1}, y_{n+1}\right) = 0 \tag{90}$$

$$g\left(x_{n+1}, y_{n+1}\right) = 0 \tag{91}$$

Note that in (90) and (91), only x_{n+1} and y_{n+1} are unknown variables and the rest are all known. Equations (90) and (91) constitute one set of nonlinear algebraic equations of the form

$$F\left(x_{n+1}, y_{n+1}\right) = 0 \tag{92}$$

The DAE equations now are transformed into a set of purely algebraic equations, which can be solved efficiently by the established Newton-Raphson method. We choose $\theta = 0.47$ for the work reported, as suggested in [23].

3.3.1 Nonlinear Equation Solution

The set of nonlinear equations in (92), are solved at each time step using the Newton-Raphson method where, at the i^{th} iteration, the unknowns are updated as follows:

$$x_{n+1}^{(i)} = x_{n+1}^{i-1} - \gamma \Delta x \tag{93}$$

$$y_{n+1}^{(i)} = x_{n+1}^{i-1} - \gamma \Delta y \tag{94}$$

where Δx and Δy are obtained by solving the set of linear equations:

$$J\begin{bmatrix}\Delta x \\ \Delta y\end{bmatrix} = \begin{bmatrix}R_x \\ R_y\end{bmatrix} \tag{95}$$

which can be represented by

$$Ax = b \tag{96}$$

where:
A=J=Jacobian matrix
R_x=differential equation residual per (80)
R_y=differential equation residual per (81)
$x_{n+1}^{(i)}$, $y_{n+1}^{(i)}$ = state variables and additional variables at the i^{th} iteration
γ=deceleration factor

$$b = \begin{bmatrix}R_x \\ R_y\end{bmatrix}$$

The Newton iterations are stopped when the residual vectors are “smaller” than pre-specified tolerances based on norm and rate of convergence. The computation of the correction vector $\left[\Delta x, \Delta y\right]^T$ requires the solution of the set of linear equations given by (96) which is discussed in the next section.

3.3.2 Linear equation Solver

As seen in the previous section the core of any iterative solver like Newton-Raphson is the solution of a system of equations represented by (96). In case of the power system, the Jacobian matrix *A* is highly sparse and the fill-in is very low. This is taken advantage of in the current research to gain high computational efficiency by employing a multifrontal based sparse linear solver. Multifrontal methods have been used earlier in the power system studies in the solution of sparse linear systems arising in the power flow studies. However the matrices in power flow studies have symmetric zero pattern and non zero diagonal elements. On serial platforms the multifrontal methods were used for power flow in references [29] and [30]. Reference [29] implements an older version of multifrontal methods and since then there has been lot of research in the area of multifrontal methods and we have much more advanced algorithms for ordering to reduce fill-in, many new features, higher speed and performance [31, 32, 33, 34, 35]. In reference [30], the main focus of the paper is to promote the FPGA technology for hardware implementation of sparse linear solver as compared to the software solution for multifrontal solver UMFPACK [31]. However from the open literature we have no information of any precedence of the application of multifrontal methods in time domain simulation of power system where the Jacobian is highly unsymmetric and unsymmetric zero pattern.

Steady state and dynamic simulation tools are an integral part in the design, optimization, and operation of large interconnected power system. Advances in numerical methods, sophisticated algorithms for exploiting sparsity and high performance computational resources have made real time tracking of cascading events a conceivable and achievable goal for the power industry.

In the solution of the DAE arising out of the dynamic modeling of the power system, the most vital and computationally intensive steps are the Jacobian building and the solution of the sparse system of linear equations. However the purpose of Jacobian is to provide adequate convergence and as long as it is achieved, one can use the same partial derivatives [23]. Thus the key computational step amounting to 80%-90% of the machine cycle is the solution of the sparse linear system of equations.

In the solution of the linear equations, the Jacobian matrices do not have any of the desirable structural or numerical properties such as symmetry, positive definiteness, diagonal dominance, and bandedness, which are generally associated with sparse matrices, to exploit in developing efficient algorithms for linear direct solvers. In general, the algorithms for sparse matrices are more complicated than for dense matrices. The complexity is mainly attributed to the need to efficiently handle the fill-in in the factor matrices. A typical sparse solver consists of four distinct steps as opposed to two in the dense case:

1. The ordering step minimizes the fill-in, and exploits special structures, such as block triangular form.
2. An analysis step or symbolic factorization determines the nonzero structures of the factors, and creates suitable data structures for the factors.
3. Numerical factorization computes the factor matrices.
4. The solve step performs forward and/or backward substitutions.

This research offers a new dimension into the solution technique of sparse linear systems arising in the power system dynamic simulation through the implementation of multifrontal methods. Multifrontal methods are a generalization of the frontal methods developed primarily for finite element problems [36] for symmetric positive definite system which were extended to unsymmetric systems [37]. These methods were then applied to general class of problems in reference [38]. In the next section, we discuss the fundamentals of the frontal and the multifrontal methods.

3.3.3 Frontal method

Frontal methods were originally developed for solving banded matrices from finite element problems [36]. The motivation was to limit computation on small matrices to solve problems on machines with small core memories. Presently frontal codes are widely used in finite element problem because very efficient dense matrix kernels, particularly Level 3 Basic Linear Algebra Subprograms (BLAS) [39], can be designed over a wide range of platforms. A frontal matrix is a small dense submatrix that holds one or more pivot rows and their corresponding pivot columns.

The frontal elimination scheme can be summarized as follows:

1. Assemble a row into the frontal matrix.
2. Determine if any columns are fully summed in the frontal matrix. A column is fully summed if it has all of its nonzero elements in the frontal matrix.
3. If there are fully summed columns, then perform partial pivoting in those columns, eliminating the pivot rows and columns and doing an outer-product update on the remaining part of the frontal matrix.
4. Repeat until all the columns have been eliminated and matrix factorization is complete.

The basic idea in frontal methods is to restrict elimination operations to a frontal matrix, on which dense matrix operations are performed using Level 3 BLAS. In frontal scheme, the factorization proceeds as a sequence of partial factorization on frontal matrices, which can be represented as:

$$F = \begin{bmatrix} F_{11} & F_{12} \\ F_{21} & F_{22} \end{bmatrix} \tag{97}$$

Pivots can be chosen from the matrix F_{11} since there are no other entries in these rows and columns in the overall matrix. Subsequently, F_{11} is factorized, multipliers are stored over F_{12}, and the Schur complement $F_{22} - F_{12}^T F_{11}^{-1} F_{12}$ is formed, using full matrix kernels. At the next stage, further entries from the original matrix are assembled with this Schur complement to form another frontal matrix. For example, consider the 6 by 6 matrix shown in Fig. 20(a). The non-zero entries in the matrix are represented by dots. The frontal method to factorize the matrix proceeds as follows:

In this example, the process begins by assembling row 1 into an empty frontal matrix shown in Fig. 20(b). At this point, none of the variables are fully summed. Subsequently, we assemble row 2 to get the matrix in Fig. 20(c). Now variable 4 is fully summed, and hence, column 4 can be eliminated. To eliminate a column, a pivot needs to be selected in that column. Let it be selected from row 2.

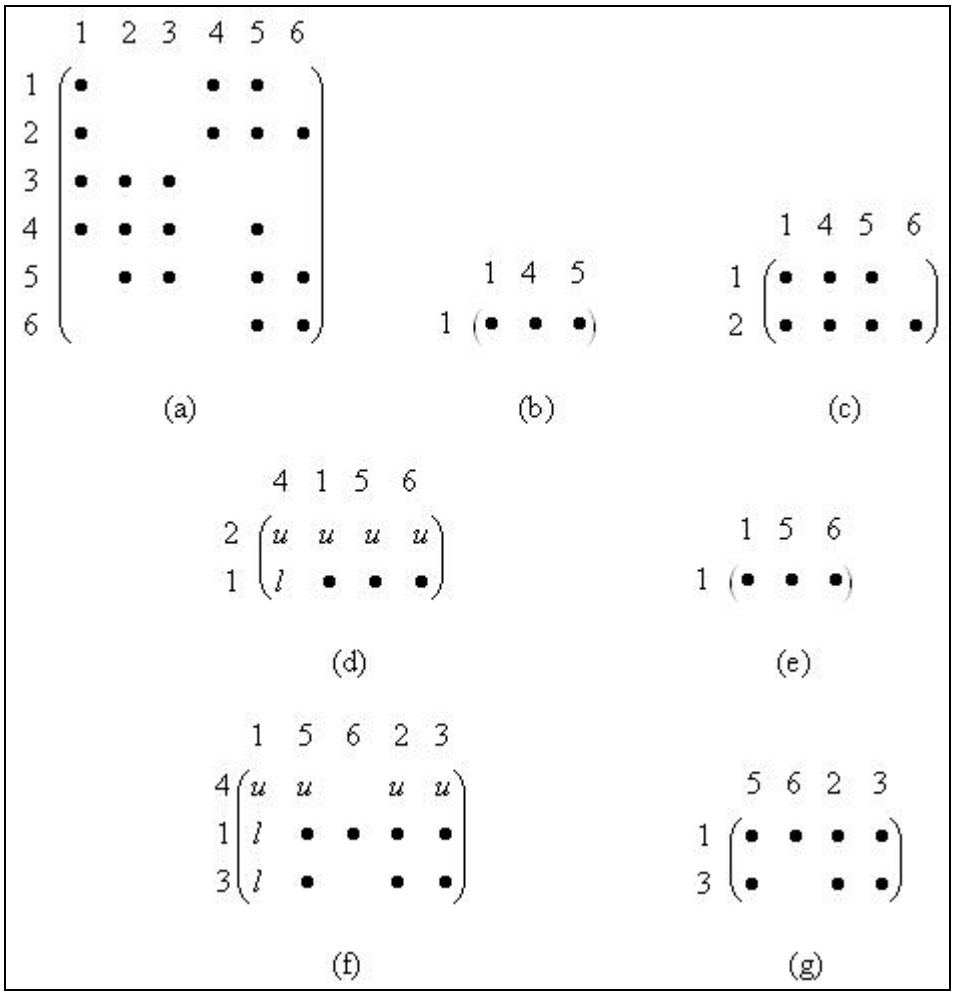

Fig. 20: Example for frontal method

Rearranging the matrix to bring the pivot element (2, 4) to the top left position, we get the matrix in Fig. 20(d). Here, *u* indicates an element of the upper triangular matrix, and *l* denotes an element of the lower triangular matrix. After elimination, the updated frontal matrix would be as shown in Fig. 20(e). In this way, we proceed with assembling rows. Again, when rows 3 and 4 are assembled, variable 1 is fully summed, and hence the column 1 can be eliminated. Choosing the pivot element to be (4, 1), the matrix with pivot element moved to top left corner is shown in Fig. 20(f), and the updated frontal matrix after elimination is shown in Fig. 20(g). In this way, the frontal method continues until matrix factorization is complete.

In the frontal method, the pivot order of the columns is dependent on the row ordering, and the pivot order of the rows can vary only within certain constraints. A row can become pivotal any time between the time it is entered into the frontal matrix and the end of the factorization. Rows are entered into the frontal matrix in a predefined order. The pivot column ordering depends solely on the initial preordering of the rows. Frontal matrix sizes, and thus the computational performance, depend on row ordering. Thus, there arises a need for a good row ordering to keep the size of the matrix small. There is a vast literature addressing this issue [40].

Frontal methods [41, 42, 43, 44, 45, 46] have demonstrated great potential as a sparse linear equation solver. Although with frontal methods one can achieve large computational gain [47, 48, 49, 50], there are many unnecessary operations on the frontal matrices which are often large and sparse and thus it lowers the overall performance. If we view the factorization in terms of a computational tree where nodes correspond to factorizations of the form as in (97), and edges correspond to the transfer of the Schur complement data, then the computational tree of the method just described would be a chain. Data must be received from the child to complete computation at the parent node. Thus frontal methods offer little scope for parallelism other than that which can be obtained within the higher level BLAS.

These deficiencies can be at least partially overcome through allowing the use of more than one front called multifrontal method [51, 52, 53, 54]. This permits pivot orderings that are better at preserving sparsity and also gives more possibility for exploitation of parallelism through working simultaneously on different fronts

Thus, in our research we have proposed multifrontal methods as a viable solution methodology for large unsymmetric sparse matrices which are common in power system online dynamic simulation. The fundamentals of the multifrontal methods are discussed in the next section.

3.3.4 Multifrontal method

The multifrontal method, is a generalization of the frontal method, and was originally developed for symmetric systems [51]. Subsequently, unsymmetric multifrontal algorithm UMFPACK [31, 32, 33, 34, 35] was developed for general sparse unsymmetric matrices. The advent of multifrontal solvers has greatly increased the efficiency of direct solvers for sparse systems. They make full use of the high performance computer architecture by invoking the level 3 Basic Linear Algebra Subprograms (BLAS) library. Thus memory requirement is greatly reduced and the computing speed is greatly enhanced.

In this section, we give an overview of the multifrontal method for the solution of large sparse matrices. There is a vast literature on the subject. Beginning with its development in 1983 by Duff and Reid [51], it has undergone many developments at different stages of its formulation, and different algorithms perform best for different classes of matrices. Broadly speaking, one can categorize them into following classes: (1) symmetric positive definite matrices [55, 56, 57, 58]; (2) symmetric indefinite matrices [51, 59, 60]; (3) unsymmetric matrices with actual or implied symmetric nonzero pattern [53, 61, 62, 63, 64]; (4) unsymmetric matrices where the unsymmetric nonzero pattern is partially preserved [65]; (5) unsymmetric matrices where the unsymmetric nonzero pattern is fully preserved [31, 66, 67, 68, 69]; and (6) QR factorization of rectangular matrices [70, 71]. There are significant differences amongst the various approaches. In this report, we present the fundamentals of the multifrontal method for symmetric positive definite linear systems, which is easier to understand and forms the foundation for multifrontal approach to other classes of matrices.

The method reorganizes the overall factorization of a sparse matrix into a sequence of subtasks, each of which involves partial factorizations of smaller dense matrices.

Reference [58] forms the foundation for the concepts presented below on the theory of multifrontal methods.

Cholesky factorization of an n by n symmetric positive definite matrix is defined by

$$A = LL^T \tag{98}$$

Depending on the order in which the matrix entries are accessed and/or updated for factorization, the Cholesky factorization can be classified into row, column, or submatrix Cholesky schemes. In row Cholesky, each step computes a factor-row by solving a triangular system, whereas in column Cholesky, the factor matrix is computed column by column with updates from previous column followed by scaling. In submatrix-Cholesky scheme, as each factor column is formed, all its updates to the submatrix remaining to be factored are computed. Based on the above classification, multifrontal method performs Cholesky factorization by submatrices. However, the novel feature of the multifrontal method is that the update contributions from a factor column to the remaining submatrix are computed, but not applied directly to the matrix entries. They are aggregated with contributions from other factor columns before the actual updates are performed.

We will explain the main concepts of the multifrontal method through an example. Consider a sparse symmetric positive definite n by n matrix A and its Cholesky factor as shown Fig. 21. Each "•" represents an original nonzero in the matrix A, and "o" a fill in for the factor matrix L.

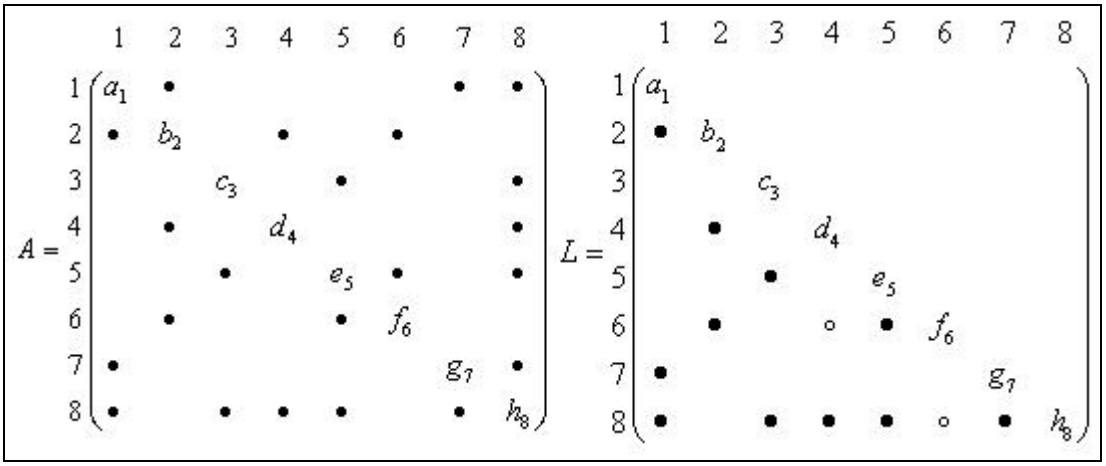

Fig. 21: Example symmetric positive definite matrix and it's Cholesky factor matrix

The elimination tree of the matrix A represented by $T(A)$ is defined to be the structure with n nodes $\{1,...,n\}$ such that node p is the parent of j if and only if

$$p = \min\{i > j \mid l_{ij} \neq 0\} \tag{99}$$

The elimination tree is a tree if A is irreducible, otherwise it will be a forest. For our purposes, we assume it to be tree. There are as many nodes in the tree as there are columns in the matrix or the Cholesky factor. In this example, we have eight nodes. From Fig. 21, we can see that for the fourth node d_4, the parent node is f_6 and for f_6 the parent node is h_8. Similarly for each node we can derive the parent node. Thus,

traversing the path for all the nodes, we get the elimination tree shown in Fig. 22 for the example in Fig. 21.

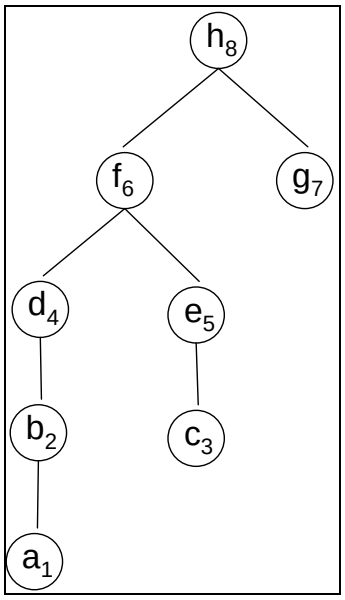

Fig. 22: Elimination tree for matrix *A*

The most fundamental elements in understanding the multifrontal method are the concepts of frontal matrix, subtree update matrix, and the update matrix. To explain these concepts, we will first introduce the concept of descendents of a node in the elimination tree.

The descendants of the node *j* in the elimination tree *T(A)* contains *j* and the set of nodes in the subtree rooted at the node *j*. The symbol *T*[*j*] is used to represent the set of descendents.

Theorem 1: If node *k* is a descendant of *j* in the elimination tree, then the structure of the vector $(l_{jk} \cdots, l_{jk})^T$ is contained in the structure of $(l_{jj} \cdots, l_{jk})^T$

Theorem 2: If $l_{jk} \neq 0$ 0 and $k < j$, then the node *k* is a descendant of *j* in the elimination tree.

For the above example the descendent of 1 is *T*[1] = {1}, descendents of 2 are *T*[2]={1,2}, descendent of 3 is *T*[3] = {3}, descendents of 4 are *T*[4] = {1,2,4} and of 6 are *T*[6] = {1,2,3,4,5,6}.

Subtree Update Matrix and Frontal Matrix: Let $(i_0, i_1, i_2 \cdots i_r)$ be nonzero row subscripts in the j[th] column of the Cholesky factor, and $i_0 = j$. Then, the subtree update matrix $\bar{U}_j$ at column *j* for the sparse matrix *A* is defined to be

$$\bar{U}_j = -\sum_{k \in T[j]-\{j\}} \begin{pmatrix} l_{j,k} \\ l_{i_1,k} \\ \vdots \\ l_{i_r,k} \end{pmatrix} \begin{pmatrix} l_{j,k} & l_{i_1,k} & \cdots & l_{i_r,k} \end{pmatrix} \tag{100}$$

and the Frontal Matrix F_j is defined to be

$$F_j = \begin{pmatrix} a_{j,j} & a_{j,i_1} & \cdots & a_{j,i_r} \\ a_{i_1,j} & & & \\ \vdots & & 0 & \\ a_{i_r,j} & & & \end{pmatrix} + \bar{U}_j \tag{101}$$

Both F_j and $\bar{U}_j$ have order r+1 which is equal to the number of nonzeros in the j^{th} column of the Cholesky factor which includes the diagonal element. From the definition of F_j it is clear that when F_j is computed, the first row/column of F_j has been completely updated. Therefore, one step of elimination on F_j gives the nonzero entries of the factor column L_{*j}. So F_j can be factorized as

$$F_j = \begin{pmatrix} l_{j,j} & 0 \\ l_{i_1,j} & \\ \vdots & I \\ l_{i_r,j} & \end{pmatrix} \begin{pmatrix} 1 & 0 \\ & \\ 0 & U_j \end{pmatrix} \begin{pmatrix} l_{j,j} & l_{i_1,j} & \cdots & l_{i_r,j} \\ & & & \\ 0 & & I & \end{pmatrix} \tag{102}$$

This gives the Update matrix U_j after one step elimination on F_j. The Update Matrix is a full matrix and is derived from equation to be

$$U_j = -\sum_{k \in T[j]} \begin{pmatrix} l_{i_1,k} \\ \vdots \\ l_{i_r,k} \end{pmatrix} \begin{pmatrix} l_{i_1,k} & \cdots & l_{i_r,k} \end{pmatrix} \tag{103}$$

It is clear from the definition of $\bar{U}_j$ and U_j, that $\bar{U}_j$ is used to form the j^{th} frontal matrix F; whereas U_j is generated from an elimination step with F_j. $\bar{U}_j$ has one more row/column than U_j.

We saw above that the descendent of 1 is $T[1] = \{1\}$, descendents of 2 are $T[2] = \{1,2\}$, descendent of 3 is $T[3] = \{3\}$, descendents of 4 are $T[4] = \{1,2,4\}$ and of 6 are $T[6] = \{1,2,3,4,5,6\}$. So, from the definition of subtree update matrix, we have $\bar{U}_1 = 0$ and therefore F_1 is

$$F_1 = \begin{pmatrix} a_{1,1} & a_{1,2} & a_{1,7} & a_{1,8} \\ a_{2,1} & 0 & 0 & 0 \\ a_{7,1} & 0 & 0 & 0 \\ a_{8,1} & 0 & 0 & 0 \end{pmatrix} + \bar{U}_1 = \begin{pmatrix} a_{1,1} & a_{1,2} & a_{1,7} & a_{1,8} \\ a_{2,1} & 0 & 0 & 0 \\ a_{7,1} & 0 & 0 & 0 \\ a_{8,1} & 0 & 0 & 0 \end{pmatrix} \tag{104}$$

$$\text{Therefore } U_1 = -\begin{pmatrix} l_{2,1}^2 & l_{2,1}l_{7,1} & l_{2,1}l_{8,1} \\ l_{7,1}l_{2,1} & l_{7,1}^2 & l_{7,1}l_{8,1} \\ l_{8,1}l_{2,1} & l_{8,1}l_{7,1} & l_{8,1}^2 \end{pmatrix} \tag{105}$$

Similarly, we can then calculate $\bar{U}_2$, and hence F_2 and the update matrix. The process continues till the entire matrix is factorized. The advantage with multifrontal method is that it is not sequential, rather it has a parallel hierarchy as visible from the elimination tree of the given example. Formation of the subtree update matrix begins on multiple fronts namely $\bar{U}_1$, $\bar{U}_3$ and $\bar{U}_7$. We can verify that for the above example the subtree update matrices $\bar{U}_1$ to $\bar{U}_4$ are as given below.

$$\begin{aligned}
\bar{U}_1 &= 0 \\
\bar{U}_2 &= -\begin{pmatrix} l_{2,1} \\ 0 \\ 0 \end{pmatrix}\begin{pmatrix} l_{2,1} & 0 & 0 \end{pmatrix} \\
\bar{U}_3 &= 0 \\
\bar{U}_4 &= -\begin{pmatrix} 0 \\ 0 \\ l_{8,1} \end{pmatrix}\begin{pmatrix} 0 & 0 & l_{8,1} \end{pmatrix} - \begin{pmatrix} l_{4,2} \\ l_{6,2} \\ 0 \end{pmatrix}\begin{pmatrix} l_{4,2} & l_{6,2} & 0 \end{pmatrix}
\end{aligned} \tag{106}$$

Matrix extend add operator: Let *R* be an *r* by *r* matrix with $r \le n$ and *S* be an *s* by *s* matrix with $s \le n$. Each row/column of *R* and *S* corresponds to a row/column of the given *n* by *n* matrix *A*. Let $i_1 \le i_2 \le \cdots i_r$ be the subscripts of *R* in *A*, and $j_1 \le j_2 \le \cdots j_s$ be those of *S*. Consider the union of the two subscript sets. Let $k_1, k_2, \cdots k_t$ be the resulting union. The matrix R can be extended to conform to the subscript set $(k_1, k_2, \cdots k_t)$, by introducing a number of zero rows and columns. In a similar way, the matrix *S* can be extended. Here, $R \Updownarrow S$ is defined to be the *t* by *t* matrix *T* formed by adding the two extended matrices of *R* and *S*. The matrix operator "$\Updownarrow$" is known as the matrix extend-add operator. For example, let

$$R = \begin{pmatrix} p & q \\ u & v \end{pmatrix}, \quad S = \begin{pmatrix} w & x \\ y & z \end{pmatrix} \text{ then} \tag{107}$$

$$R \Updownarrow S = \begin{pmatrix} p & q & 0 \\ u & v & 0 \\ 0 & 0 & 0 \end{pmatrix} + \begin{pmatrix} w & 0 & x \\ 0 & 0 & 0 \\ y & 0 & z \end{pmatrix} = \begin{pmatrix} p+w & q & x \\ u & v & 0 \\ y & 0 & z \end{pmatrix} \tag{108}$$

Now, in terms of the extend-add operator defined above, we can see that the relationship between the frontal matrices $\{F_j\}$ and the update matrices $\{U_j\}$ is

$$F_j = \begin{pmatrix} a_{j,j} & a_{j,i_1} & \cdots & a_{j,i_r} \\ a_{i_1,j} & & & \\ \vdots & & 0 & \\ a_{i_r,j} & & & \end{pmatrix} \Updownarrow U_{c_1} \Updownarrow \ldots \Updownarrow U_{c_s} \tag{109}$$

where $c_1, c_2, \cdots c_s$ are the children of the node *j* in the elimination tree. Thus $\bar{U}_j$ = $U_{c_1} \Updownarrow \ldots \Updownarrow U_{c_s}$, and $T[j]$-$\{j\}$ is the disjoint union of the nodes in the subtree $T[c_1]$,...,

$T[c_s]$. Duff and Reid [51] refer to the process of forming the j^{th} frontal matrix F_j from A_{*j} and the update matrices of its tree children as the frontal *matrix assembly* operation, and the tree structure on which the assembly operations are based is called the assembly tree.

We now summarize the essence of the multifrontal methods in the form of an algorithm for multifrontal Cholesky factorization in Fig. 23.

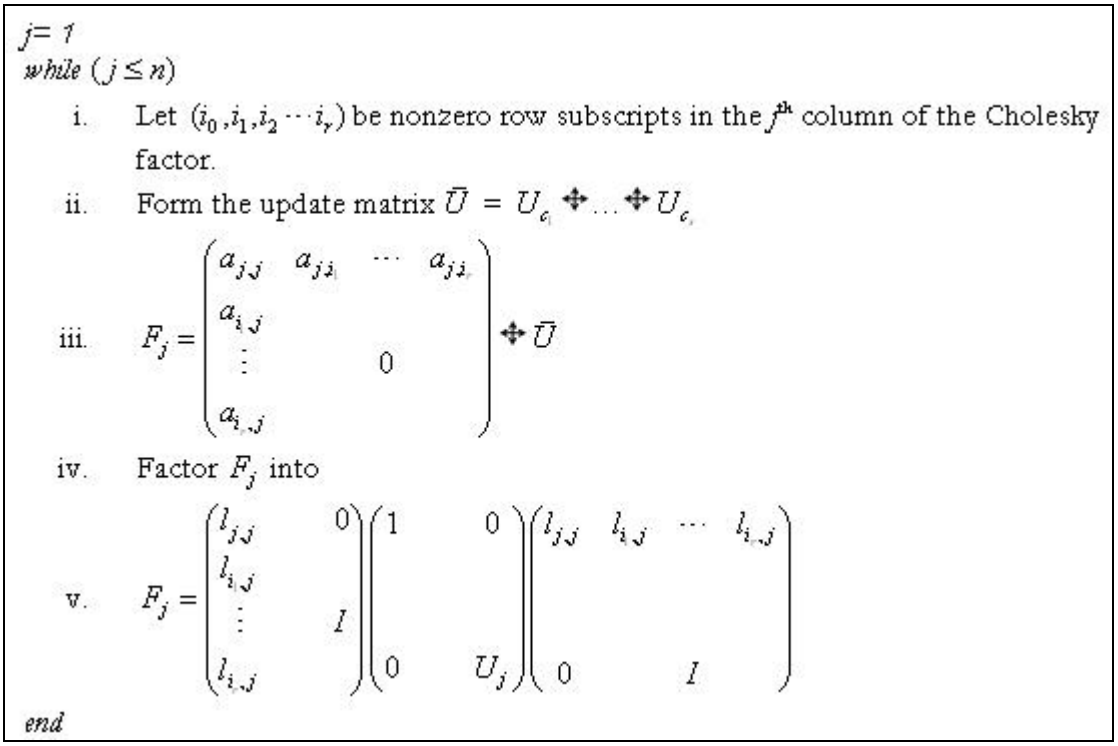

Fig. 23: Algorithm for multifrontal Cholesky factorization

In summary, the multifrontal method reorganizes the numerical computation, and the factorization is performed as a sequence of factorization on multiple fronts. In practice, structural pre-processing [58] is done to reduce the working storage requirements by restructuring the tree, and finding the optimal post-ordering of the tree. After the pre-processing, the computation of the Cholesky factor matrix by the multifrontal method is done as described in the above algorithm in Fig. 23.

As discussed earlier, there exist many approaches to apply the multifrontal method for different classes of matrices. Broadly, they can be classified into: (1) symmetric positive definite matrices; (2) symmetric indefinite matrices; (3) unsymmetric matrices with actual or implied symmetric nonzero pattern; (4) unsymmetric matrices where the unsymmetric nonzero pattern is partially preserved; (5) unsymmetric matrices where the unsymmetric nonzero pattern is fully preserved; and (6) QR factorization of rectangular matrices.

Below, we give the summary of the discussion on the differences in the multifrontal methods for the above classes of matrices presented in reference [33]. For approaches (1) to (4), the frontal matrices are related to one another by the elimination

tree of A, or the elimination tree of $A+A^T$ if A is unsymmetric. The elimination tree has n nodes, each node corresponding to one pivot row and column. A frontal matrix assembles the contribution blocks of each of its children in the assembly tree. The assembly step thus adds the contribution blocks of each child into the current frontal matrix. For symmetric positive definite matrices, all of the pivots originally assigned to a frontal matrix by the symbolic analysis phase are numerically factorized within that frontal matrix. For other matrices, some pivots might not be eliminated, and the contribution block may be larger than predicted. The un-eliminated pivot is delayed, and its elimination is attempted in the parent instead.

In the first three approaches, the frontal matrices are square. The frontal matrix may be rectangular, but the assembly tree is still used. The first four approaches precede the numerical factorization with a symmetric reordering of A or $A+A^T$, typically with a minimum degree or nested-dissection ordering as part of a symbolic analysis phase.

UMFPACK is based on the fifth approach. It does not use a pre-ordering or symbolic analysis phase. Rectangular frontal matrices are constructed during numerical factorization, using an approximate Markowitz ordering.. The frontal matrices are related to one another via a directed acyclic graph (DAG) rather than an elimination tree. The last approach, multifrontal QR factorization [70, 71], is based on the column elimination tree of A**.**

Now we illustrate with a simple example in Fig. 24, the working of the multifrontal method for the same unsymmetrical matrix in Fig. 20 for which the working of frontal method was illustrated earlier. The frontal matrices here are rectangular and not square.

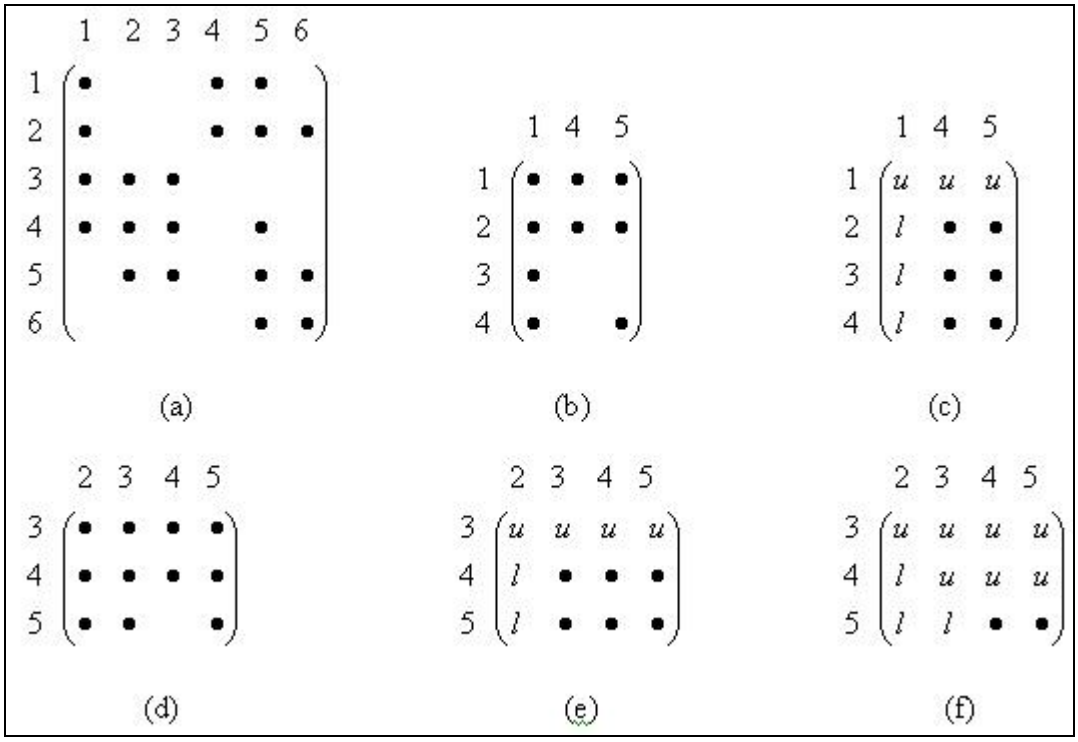

Fig. 24: Example for unsymmetric multifrontal method

Consider the unsymmetrical matrix shown in Fig. 24(a). An initial pivot element is chosen, say element (1, 1). The corresponding first frontal matrix with this pivot row and column and all contributions to them is shown in Fig. 24(b). Subsequently, a pivot operation is performed to eliminate variable 1, which gives the resultant frontal matrix with *u* (upper triangular matrix), *l* (lower triangular matrix), and the non-zero entries in the non-pivot rows and columns corresponding to the contribution block (represented by dots). Further, after the elimination of variable 1, another pivot is selected, say (3, 2). A new frontal matrix is then constructed with row 3 and column 2, with all contributions to them from both the original matrix and the contribution block of the previous frontal matrix. The resulting frontal matrix is shown in Fig. 24(c). After performing a pivot operation to eliminate variable 2, we get the matrix as shown in Fig. 24(d), but here another pivot operation on element (4, 3) can be performed to eliminate variable 3 as well, since all contributions to row 4 and column 3 can also be assembled into the same matrix. A pivot operation on element (4, 3) reduces the frontal matrix further as shown in Fig. 24(e). In this way, the frontal matrices are continued to be assembled, and pivot operations are performed on them until the matrix is completely factorized. Table 11 below lists the available direct solvers for serial machines [72]

Table 11: Sparse Direct Solvers

Code	Technique	Scope	Contact	Ref.
CHOLMOD	Left-looking	SPD	Davis	[73]
MA57	Multifrontal	Sym	HSL	[51]
MA41	Multifrontal	Sym-pat	HSL	[61]
MA42	Frontal	Unsym	HSL	[49]
MA67	Multifrontal	Sym	HSL	[74]
MA48	Right-looking	Unsym	HSL	[54]
Oblio	Left/right/Multifr.	sym, out-core	Dobrian	[75]
SPARSE	Right-looking	Unsym	Kundert	[76]
SPARSPAK	Left-looking	SPD, Unsym, QR	George et al.	[77]
SPOOLES	Left-looking	Sym, Sym-pat, QR	Ashcraft	[78]
SuperLLT	Left-looking	SPD	Ng	[79]
SuperLU	Left-looking	Unsym	Li	[80]
UMFPACK	Multifrontal	Unsym	Davis	[81]

Abbreviations used in the table:
SPD : symmetric and positive definite
Sym : symmetric and may be indefinite
Sym-pat: symmetric non zero pattern but unsymmetric values
Unsym: unsymmetrical

In the present study, UMFPACK 4.4 [34] is used as the engine for the solution of equations (80) and (81) by multifrontal direct method. UMFPACK consists of a set of ANSI/ISO C routines for solving unsymmetric sparse linear systems using unsymmetric multifrontal method. It requires the unsymmetric, sparse matrix to be input in a sparse triplet (compressed sparse column) format. UMFPACK 4.4 consists of four steps for solving the linear system. In the first step, it reorders the rows and columns such that the factors suffer little fill, or that the matrix has special structure,

such as block-triangular form. In the second, it performs symbolic factorization, computing the upper bounds on the non zeros in *L* and *U*, the floating point operations required, and the memory usage of the factorization routine. It is an analysis step to determine the nonzero structures of the factors, and to create suitable data structures for the factors. In the third step, numerical factorization is carried out to compute the *LU* factors. Finally, it solves the linear system using the computed *LU* factors by performing the forward and back substitutions.

Different pre-ordering strategies are used to make the solver more memory efficient. It finds both a row and column pivot ordering as the matrix is factorized. No preordering or partial preordering is used. At the start of the factorization, no frontal matrix exists. It starts a new frontal matrix with a global Markowitz-style pivot search. It combines a column ordering strategy with a right-looking unsymmetric-pattern multifrontal numerical factorization. All pivots with zero Markowitz cost are eliminated first and placed in the *LU* factors. In the analysis phase it selects one of three ordering and pivoting strategies namely unsymmetric, 2-by-2, or symmetric. For symmetric matrices with non zero elements in the diagonal, the symmetric strategy is used to compute a column ordering using approximate minimum degree (AMD). No modification of the column ordering is made during the numerical factorization. A nonzero diagonal entry is selected as a suitable pivot if, in magnitude it is at least *a* times the largest entry in its column. Otherwise, an off-diagonal pivot is selected with magnitude at least *b* times the largest entry in its column. The parameters *a* and *b* are controllable with default values of 0.001 and 0.1, respectively. Thus, strong preference is given to pivoting on diagonal entries. For symmetric indefinite problems with zero entries in the diagonal, the 2 by 2 strategy is selected wherein a row permutation is done, that puts nonzero entries onto the diagonal. Then, the symmetric strategy is applied to the permuted matrix.

It is possible that the built-in ordering schemes may not be the best for the target applications, and one may use an external ordering scheme for better performance. The multifrontal method for the solving sparse systems of linear equations offers a significant performance advantage over more conventional factorization schemes by permitting efficient utilization of parallelism and memory hierarchy. The main concern of the present study is the quantitative comparison of the performance of Newton's method coupled with the multifrontal solver and one with the Gaussian elimination.

3.3.5 Time Step

Reference [23] provides an excellent discussion on the variable time step strategy chosen for the Theta method. In this research also we use the variable time step scheme. However, the criteria used for time step adjustment are more stringent than in reference [23]. The maximum time step used in our simulator is 40 seconds unlike 20 seconds in reference [23]. The minimum time step is 0.0002. The increase in time step depends on both the local truncation error and the number of iterations it takes to converge to the solution for each time step. If the iteration error is less than the tolerance, and the number of iterations it takes to converge to solution is less than a predefined number for 5 consecutive time steps, then the time step is doubled. However, if the number of iterations is more than the maximum number of iterations, or the iteration error is greater than the maximum tolerance, then the integration is

repeated with time step reduced to half. On the other hand, if the number of iterations is more than a predefined number of iterations which is 6 in this case, and the iteration error is within the tolerance, then the time step is reduced for the solution of the next time step. Reduction in time step is also by a factor of 2 but is fixed at minimum. Failure to reduce the time step for ascertained number of times will result in stopping the integration.

3.3.6 Jacobian Building

The task of Jacobian building for every iteration within an integration time step is a formidable task in terms of computational resources required. The demand on time increases with the increase in size of the power system. Thus, we use the same Jacobian matrix as long as the convergence is acceptable and fast. Since the terms of the Jacobian involve time step, there is a direct relation between the variation in time step, system condition, and frequency of Jacobian building. Interested readers can see reference [23] for more elaborate discussion on considerations on Jacobian matrix computation. Effective strategy to rebuild Jacobian has resulted in considerable time saving for each simulation. The results are presented in the next section.

3.4 Test System

The proposed method is tested on two systems i) IEEE RTS-96 with 33 generators, and ii) Test system with 6 generators, 21 bus, 21 lines, 9 transformers and 3 tie lines as shown in the Appendix F and Appendix D respectively.

3.5 Performance Comparison

The system is simulated for 3600 seconds on a Pentium 4, 2.8 GHz, and 1 GB RAM. The system is simulated with an initial contingency which belongs to the set of contingencies containing functional group contingency, stuck breaker contingency or inadvertent trip contingency. A 20% load ramping from 900 seconds to 2700 seconds is also implemented.

Table 12 shows the performance comparison for the multifrontal method with the full Gaussian elimination algorithm on the 6 generator test system for 6 different critical initiating contingencies on the system. Column 1 shows the contingency number, columns 2 and 3 show the simulation time in seconds with the Gaussian and the multifrontal algorithms respectively. Column 4 shows the speed up achieved using the multifrontal method, which varies between 3.75 times to 7 times. For practical purposes we show the time saving per contingency in columns 5 and 6. For this system there are a total of around 300 contingencies. We can see from columns 7 and 8 that using the multifrontal method saves around 16 to 22 hours for this small test system.

Table 12: 6-generator Test System

Contin-gency number	Gaussian	Multifrontal	Speed up (Col2/Col3)	Difference in time (saving)			
				per contingency		For 300 similar contingencies	
				seconds	minutes	minutes	hours
1	321.505	46.138	6.9683341	275.367	4.58945	1376.84	22.94725
2	261.394	56.816	4.6007111	204.578	3.4096333	1022.89	17.04817
3	232.613	44.08	5.2770644	188.533	3.1422167	942.665	15.71108
4	247.113	65.624	3.7655888	181.489	3.0248167	907.445	15.12408
5	287.003	51.826	5.5378189	235.177	3.9196167	1175.89	19.59808
6	260.988	69.622	3.7486427	191.366	3.1894333	956.83	15.94717

The Fig. 25 below compares graphically the speed of the multifrontal method to that of the Gaussian algorithm.

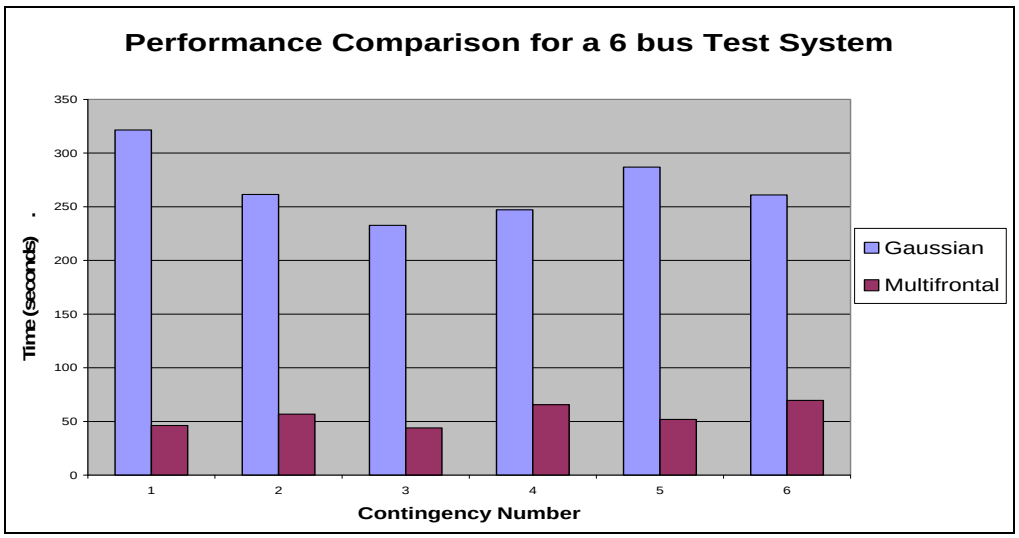

Fig. 25: Performance Comparison for a 6 generator system

Table 13 shows the performance comparison for the multifrontal method with the full Gaussian elimination algorithm on the 32 generator test system for 3 different critical initiating contingencies on the system. Column 1 shows the contingency number, column 2 and 3 shows the simulation time in seconds with the Gaussian and the multifrontal algorithms respectively. Column 4 shows the speed up achieved using the multifrontal method, which varies between 4 times to 6.4 times. For practical purposes we show the time saving per contingency in column 5 and 6. For this system to analyze 300 contingencies as in the previous case, we can see from column 7 and 8 that using multifrontal method saves around 67 to 100 hours for this test system. Fig. 26 below shows graphically the speed up of the multifrontal method over the Gaussian algorithm for the 32 generator case.

Table 13: 32-generator Test System

Contingency Number	Gaussian	Multifrontal	Speed Up	Difference in time (saving)			
				Per contingency		For 300 similar contingencies	
				Seconds	minutes	minutes	Hours
1	1420.789	222.807	6.37677	1197.982	19.966367	5989.91	99.83183
2	1419.301	356.227	3.98426	1063.074	17.7179	5315.37	88.5895
3	1047.513	242.878	4.3129184	804.635	13.410583	4023.18	67.05292

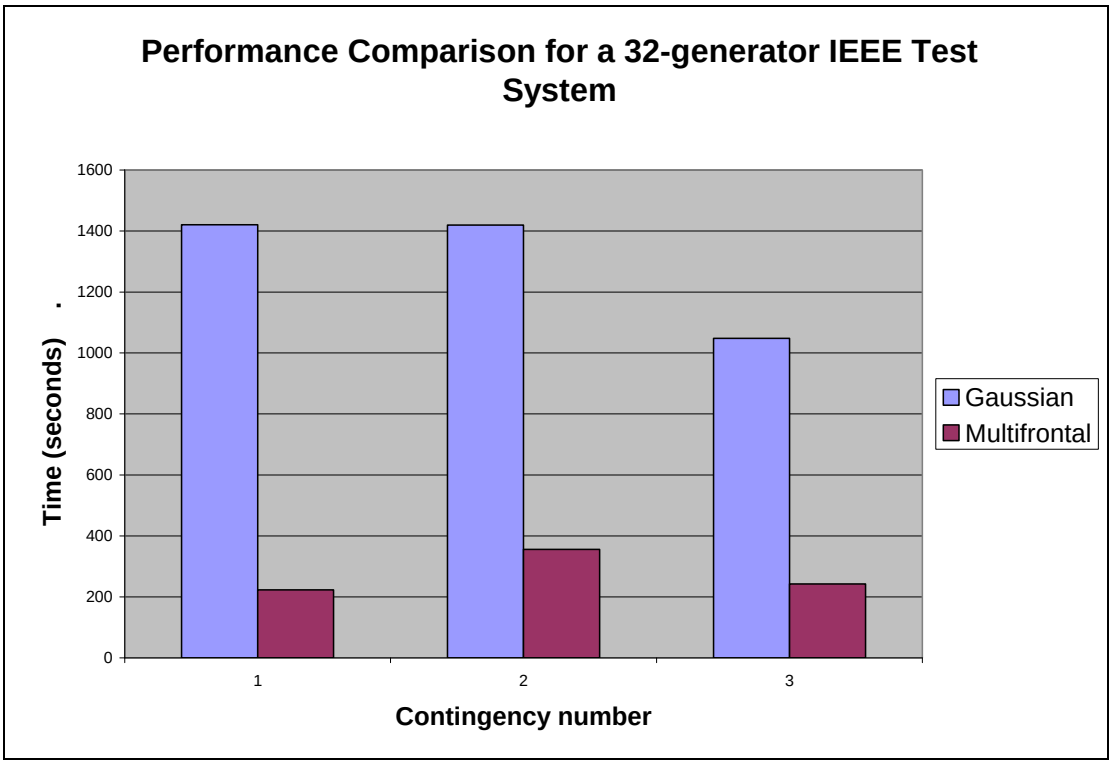

Fig. 26: Performance Comparison for a 32-generator test system

We can see that we the size of the system the amount of time saving has increased drastically even though the speed is practically same due to the overhead associated with the multifrontal methods. However with the further increase in system by orders of magnitude the speed up also would increase by orders of magnitude and the time saving would be huge. We projected the simulation time for a 500 and 5000 bus system under similar conditions of load. It would save more than 2 months of time just for 300 contingencies. Actually the system would have large number of contingencies. The time saving would be enormous. Thus the multifrontal methods are highly appealing in the research effort for online mid-time domain simulation.

4 Modeling and Protection

This chapter describes the modeling of the power system components and generator protection adopted for this research. At the outset the chapter describes the component modeling and the formulation of the differential algebraic equations governing the system. Following this the results of an in depth study of cascading events over the past 40 years focusing on generator protection under abnormal conditions are synoptically presented, highlighting the importance of generation protection during the unfolding of such uncontrolled high consequence scenarios. After the historical perspective a detailed description of generator protection modeling used in this research is given. The chapter is followed by the results and discussion of the implementation of the above described component modeling and generator protection on a test system.

4.1 Component Modeling and Formulation of Dynamic Algebraic Equations

4.1.1 Exciter Model

In this research a simple PI controller is used for generator terminal-voltage control. The block diagram of the exciter is shown below in Fig. 27.

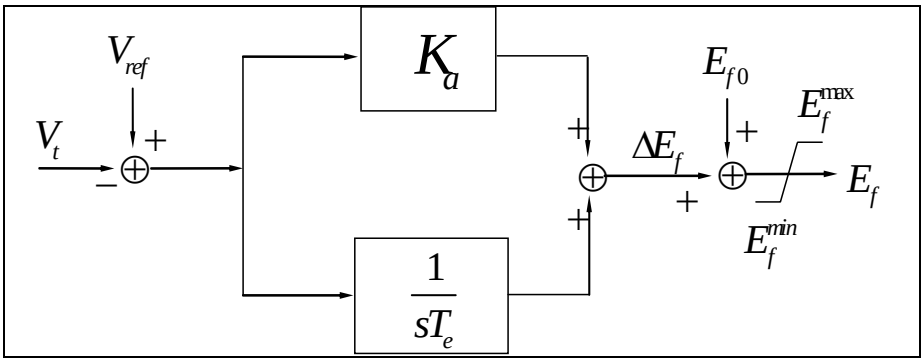

Fig. 27: Block diagram of exciter

4.1.2 Governor Model

The governors are all modeled as a speed integrator with droop ratio *R* as in Fig. 28. T_{CH} is the time constant for hydro-mechanically server, which is modeled as an inertia link. The output of the governor is *Y*, which is the mechanical power input to electric machine. L^g_{ref} is the output of Automatic Generation Control (AGC), which is illustrated in Fig. 29. It is actually the summation of the gate reference $L^g_{ref\,0}$ and the AGC adjustment signal. Here it is assumed that every generator participates in the global frequency adjustment.

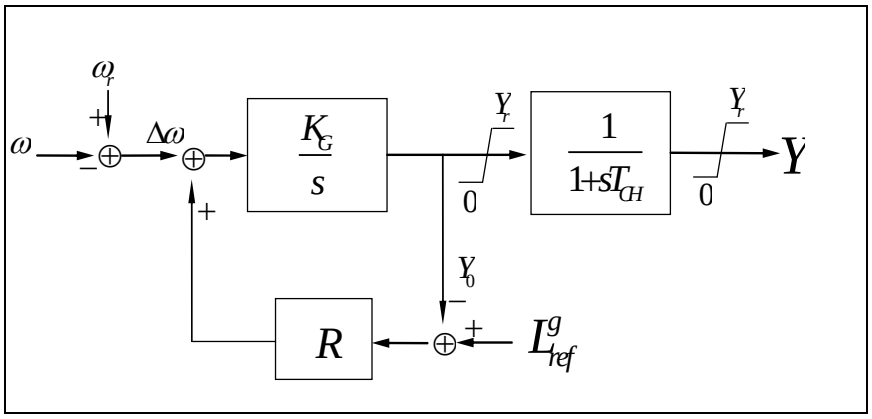

Fig. 28: Governor

4.1.3 AGC Model

Fig. 29 illustrates the AGC model used in this research. The aim of the AGC is to regulate the system frequency to the reference frequency ω_g^{ref} . Any deviation from this value will be sensed by the AGC. The inverse of the time constant in each of the integrators in Fig. 29 is proportional to the size of the unit, for which the output signal is intended. This underlying philosophy is that a larger generator contributes more to regulate the frequency than a smaller generator.

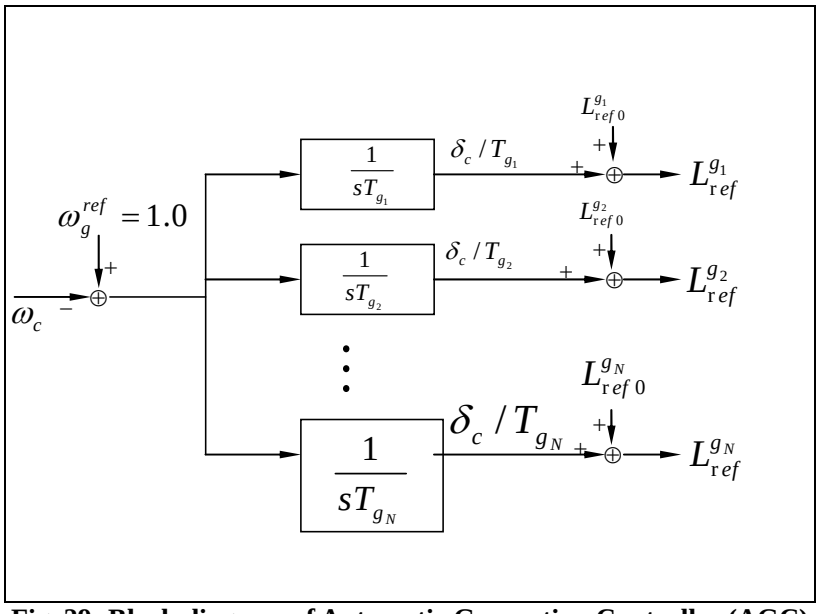

Fig. 29: Block diagram of Automatic Generation Controller (AGC)

4.1.4 Over-excitation Limiter Model

A summed-type over-excitation limiter (OEL) model shown in

Fig. 30 is used in this research. The regulating part of the OEL is a pure integrator. It simulates the heat build-up in the exciter. A wind-up limiter is added to the integrator to limit the output of OEL to exciter. The direct output of OEL is not limited because it is a reflection of winding temperature rather than a concrete element that has a physical limit.

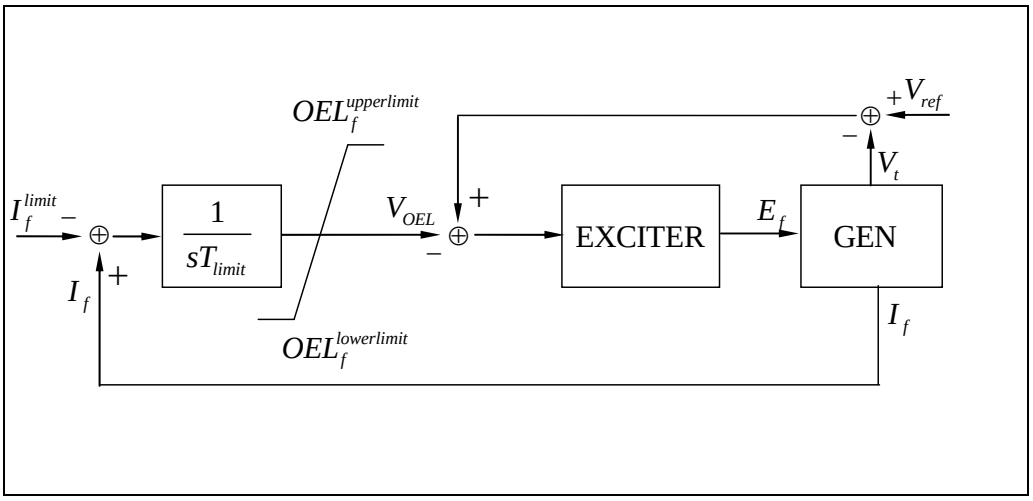

Fig. 30: Over-exciter limiter

4.1.5 Load Model

The loads are modeled as constant active and reactive power injection.

4.1.6 Formulation of Dynamic Algebraic Equations

The equations developed are for all the generations including the exciter, the governor and the AGC models. The two axis model for the generator is used in the present study. For generators, the meanings of the notation are the same as in [25]. The notation for exciter, governor, and the AGC are same as shown in Fig. 27-Fig. 30. The limiter for each variable is implemented as logic in program and is not shown in the above equations.

The set of differential equations are as follows

$$\frac{\partial \delta}{\partial t} = \omega - 1 \tag{110}$$

$$\frac{\partial \omega}{\partial t} = \left[\left(Y \times P_r \right) - Ds\left(\omega - 1 \right) - \left(E_d^{'} I_d + E_q^{'} I_q - \left(X_q^{'} - X_d^{'} \right) I_q I_d \right) \right] \Big/ T_j \tag{111}$$

$$\frac{\partial E_d^{'}}{\partial t} = \left[-E_d^{'} - \left(X_q - X_q^{'} \right) I_q \right] \Big/ T_{q0}^{'} \tag{112}$$

$$\frac{\partial E_q^{'}}{\partial t} = \left[EDF - E_q^{'} + \left(X_d - X_d^{'} \right) I_d \right] \Big/ T_{d0}^{'} \tag{113}$$

$$\frac{\partial Y}{\partial t} = \left[Y - Y_0 \right] / T_{CH} \tag{114}$$

$$\frac{\partial Y_0}{\partial t} = -R \times K_G \times Y_0 + K_G \left[\left(\omega_r - \omega \right) + R\left(L^g_{ref\,0} - \delta_c / T_g \right) \right] / T_{CH} \tag{115}$$

$$\frac{\partial \Delta E_f}{\partial t} = \left[-\Delta E_f + E_q^{'} + K_a \left(V_{ref} - V_t \right) I_d \right] / T_e \tag{116}$$

The set of algebraic equations are as follows, where *i* is the i^{th} generator and *j* means the j^{th} generator bus.

$$\begin{pmatrix} V_q^i \\ V_d^i \end{pmatrix} - \begin{pmatrix} E_q^{'i} \\ E_d^{'i} \end{pmatrix} + \begin{pmatrix} r^i & -X_d^i \\ X_d^i & r^i \end{pmatrix} \begin{pmatrix} I_q^i \\ I_d^i \end{pmatrix} = 0 \tag{117}$$

for each generator;

$$\begin{pmatrix} V_x^j \\ V_y^j \end{pmatrix} - \begin{pmatrix} \cos\delta^j, & -\sin\delta^j \\ \sin\delta^j, & \cos\delta^j \end{pmatrix} \begin{pmatrix} V_q^j \\ V_d^j \end{pmatrix} = 0 \tag{118}$$

for each generator bus;

$$\begin{pmatrix} I_x^j \\ I_y^j \end{pmatrix} - \begin{pmatrix} \cos\delta^j, & -\sin\delta^j \\ \sin\delta^j, & \cos\delta^j \end{pmatrix} \begin{pmatrix} I_q^j \\ I_d^j \end{pmatrix} = 0 \tag{119}$$

for each generator bus;

$$Y_{bus} \times \begin{pmatrix} V_x^1 \\ V_y^1 \\ \vdots \\ V_x^n \\ V_y^n \end{pmatrix} - \begin{pmatrix} I_x^1 \\ I_y^1 \\ \vdots \\ I_x^n \\ I_y^n \end{pmatrix} = 0 \tag{120}$$

for the whole linear impedance network with *n* voltage bus (Y_{bus} is the system admittance matrix);

$$\begin{pmatrix} P^i \\ Q^i \end{pmatrix} - \begin{pmatrix} V_x^i & V_y^i \\ V_y^i & -V_x^i \end{pmatrix} \begin{pmatrix} I_x^i \\ I_y^i \end{pmatrix} = 0 \tag{121}$$

for each load bus with constant P and Q.

The loads in our test system are modeled as constant active and reactive power injection.

Equations (117) to (119) are for each individual generator. Equations (120) and (121) are for the whole network and each voltage bus respectively

A general power system dynamic algebraic equation (DAE) groups for equations in (110) through (121) can be summarized as

$$\frac{dx}{dt} = f\left(x, y\right) \tag{122}$$

$$0 = g(x, y) \tag{123}$$

where

x is a vector of state variables in (110)~(116)

(122) is the group of equations in (110)~(116)

y is a vector of the variables in (117)~(121) excluding those in x in (123) is the group of equations in (117)~(121)

4.2 Generator Protection

4.2.1 Importance of Generator Protection

Power systems are constantly subjected to the transient disturbances due to system component faults, switching of major loads, occasional lightening flashover, intentional sabotage, human errors and unintentional protective relay operation and so on. During this transient period from one steady state to the next the performance of the generator excitation system and the turbine control system play an important role in ensuring system stability. However, the coordination between these and the other control mechanisms with system protection is of prime importance to avert a cascading event [82]. Of particular importance in this long term simulation study is the role of generator protection especially under abnormal conditions. Along with coordinating with the system to avoid misoperation, the protective relays must protect the generating plant damage which would otherwise seriously hamper restoration and cause huge economic loss.

In many of the past blackouts the operation of the generator protective relays stands out as one of the very critical events in the sequence of events leading to those catastrophic scenarios. Many times the unexpected relay operation has been due to the lack of coordination between the control and protection function of the generator with that of the system [83]. This research effort reports conclusively the importance of generator protection modeling in dynamic simulation studies to trace the system trajectory following a transient disturbance to the system. This study is also important in planning out control strategies to interrupt the unfolding of a cascading event.

4.3 Historical Evidence/Perspective

This section presents a historical perspective, over the past 40 years, of the role of generator protection under abnormal conditions in the unfolding of the cascading events. The purpose of this section is not to describe any of these catastrophic events in detail which would be voluminous, rather in this section an attempt is made to report the critical protective relay operations for generator protection leading to these blackouts. The purpose of this study is to substantiate the importance of generator protection modeling in the dynamic simulation study of the power system.

4.3.1 Northeast Blackout November 9-10, 1965

This information was obtained from [83, 84, 85, 86, 87, 88]. An out of step condition developed due to continued acceleration of The PASNY and Ontario Hydro generators at Niagara Falls, and caused two 345 kV lines between Rochester and Syracuse to be opened by distance relay action; all parallel underlying lower voltage lines were also

tripped. Four seconds after the initial line trip, five out of the sixteen PASNY-Massena generators tripped and the system islanded into 5 areas as shown in Fig. 31.

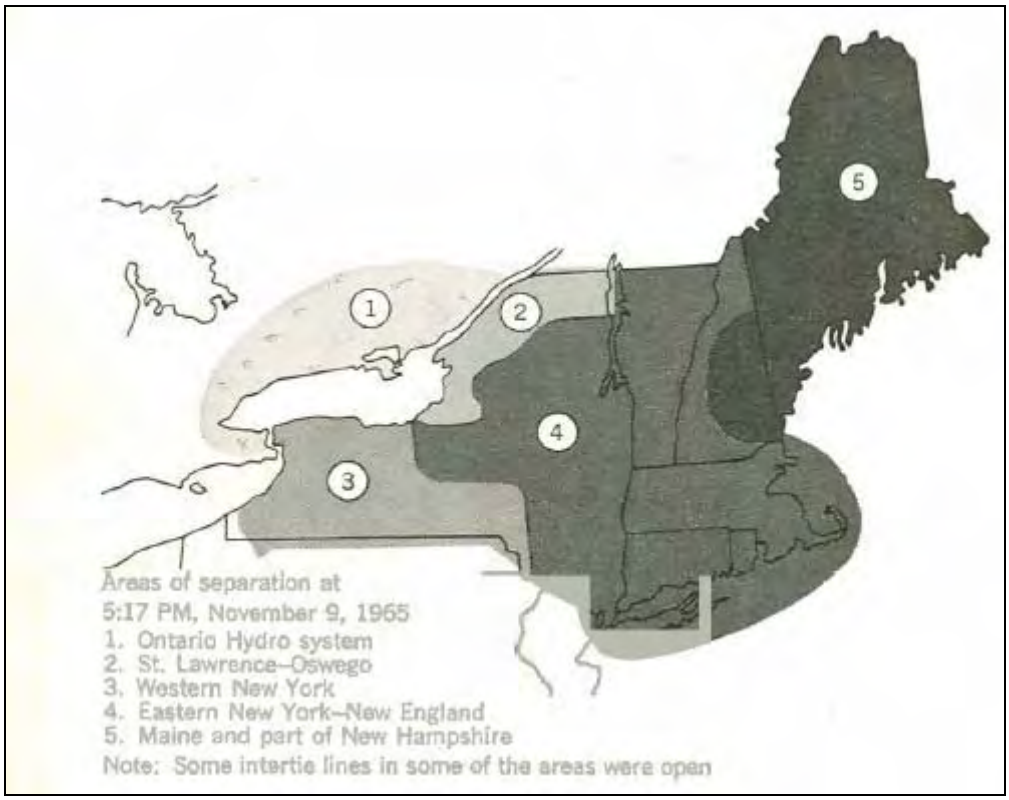

Fig. 31: System islanding into 5 areas [83]

In area 3 an *overfrequency* condition developed due to large generation excess and thus all steam power plants were tripped by *overspeed protection*. This was followed in quick succession by simultaneous tripping of 10 generators at Beck due to excessive governor operation and tripping five PASNY-Niagara pumping-generating units by *overspeed* protection. Thus an underfrequency condition ensued and the whole area blacked out. Similarly in area 4 there was complete blackout since all the generators tripped within 11 minutes due to *undervoltage* and *underfrequency protection*.

4.3.2 June 5, 1967, PJM Disturbance

About 26 generators were automatically tripped during this disturbance—12 by loss-of-field relaying, six due to abnormal current or voltage, four by turbine protection, and four by other protective devices [82].

4.3.3 North American Northeast Blackouts of 1977

This information was obtained from [83, 89, 90, 91]. After a sequence of line trips and a generator trip, the loss of a generator, Ravenswood #3 unit, due to the *loss of field* relay operation was very critical because it was responding to sharp voltage fluctuations accompanying load shedding. This caused sharp frequency drop up to 54 Hz and Arthur

Kills #3 unit tripped due to *underfrequency protection*. This was followed by immediate tripping of remaining generators in the islanded Con Edison system.

4.3.4 French Blackout December 19, 1978

The sequential tripping of a 400 kV line and three 225 kV lines due to overcurrent protection followed by the tripping of a hydro unit of Revin power plant due to generator *overcurrent protection* led to this blackout [82].

4.3.5 Tennessee Disturbance August 22, 1987

Voltage controlled/restrained overcurrent and distance relays on generators tripped [82]. This started a cascading effect that eventually tripped all source lines into TVA's South Jackson, Milan, and Covington substations [92].

4.3.6 The Tokyo Blackout 1987

After the initial tripping of lines and transformers due to improper operation of zone 4 impedance relay, the loss of the load caused a frequency spike and due to overfrequency generator protection the units Kashima #6 and Kawasaki #6 tripped and Kashima #4 was manually stopped [82, 92].

4.3.7 PECO Disturbance February 21, 1995

During the second fault, the Limerick 1 and 2 generators were tripped by ground overcurrent relays connected to their step-up transformers [82].

4.3.8 Western System July 2, 1996

This information was obtained from [4, 83, 93, 94]. At 1:25 P.M. on July 2, 1996, a huge disturbance occurred in WSCC system. A short circuit occurred on a 345 kV line between the Jim Bridger plant near Rock Springs and it was tripped successfully. This disturbance caused a parallel line to be tripped also. An SPS scheme was initiated after the tripping of the two lines, which shut down two generating units at the Jim Bridger plant. About 24 seconds after the fault, the outage cascaded through tripping of small generators near Boise plus tripping of the 230 kV line from Western Montana to SE Idaho. . The *undervoltage* and *inter-area oscillation* problem developed quickly throughout the system. This was further aggravated by false *tripping* of 3 units at McNary. Within a few seconds, five islands were formed and as a result. 2,500MW power was lost and 1,500,000 customers were affected.

4.3.9 Western System August 10, 1996

This information was obtained from [4, 95, 96]. Due to poor design of *overexcitation limiters* many generators tripped at inappropriate time. The most critical event was sequential tripping of 13 McNary generators due to the *generator field current protection* scheme which operated to trip the generators instead of limiting the field current. In the southern islands, many generators tripped undesirably following underfrequency load shedding. A total of 175 generating units were tripped and 5,700,000 customers were interrupted.

4.3.10 Chilean Blackout May 1997

The main cause identified for the voltage collapse in the Chilean Interconnection System was the overexcitation limits in the generating units at Colbun-Pehuenche [82].

4.3.11 North American Northeast Blackouts of August 14, 2003

Eastlake 5 unit tripped due to *overexcitation protection*. Machines in Detroit pulled out of step and lost synchronism. Among other factors overreaching impedance relays (zone 2 and zone 3) and a lack of coordination between *generation protection* and transmission protection systems led to this widespread blackout [1, 97].

4.3.12 Blackout in Southern Sweden and Eastern Denmark – September 23, 2003

This information was obtained from [98, 99, 100]. A nuclear plant at Oskarshamn tripped at 12:30 due to technical problems and the north south flow on the west side increased. Coincidently the switching device at Horred substation broke apart with another nuclear plant and two important north-south connections lost. Due to loss of transmission path to the west coast the east side became overloaded. Thus within seconds, the *underfrequency* and *undervoltage* generator and other grid protections reacted and resulted in a complete voltage collapse.

4.3.13 Italian Blackout September 28, 2003

One of the main lessons learnt after this severe disturbance was that a thorough and accurate testing of protecting devices and governors should be performed during the commissioning of the power system [101, 102, 103, 104].

4.3.14 Greece July 12, 2004

The critical event occurred at 12:37 when Unit 3 of Aliveri power station serving the weak area of Central Greece tripped *automatically* [105]. At 12:38 the remaining unit in Aliveri was *manually* tripped. At 12:39 voltage instability leading to collapse happened and the system was split in two by line protection devices and disconnected the generation from the separated Southern part. Thus the blackout spread into the area of Athens and Peloponnesus.

4.3.15 Australian Blackout Friday August 13, 2004

The initiating event was an internal fault in a transformer which triggered the tripping of three generators due to *generator differential protection* [83, 106]. Another independent generator tripped due to premature *negative phase sequence protection* as a result of a faulty timer circuit. Due to sudden generation loss the frequency dropped and Underfrequency load shedding along with generator trippings due to *underfrequency protection* and *automatic voltage regulator protection* followed.

4.3.16 Central-South System Collapse of the Peninsular Malaysia Grid System January 13, 2005

After the initial circuit trippings, the North East and the Central South sub system were left interconnected only through the four transformers at Port Klang [83]. The sub

systems began to pull apart as the generators in the North East went *out of step* with those in the Central South sub system. Soon they separated with each sub system having load and generation imbalances. In the Central sub system the frequency spiraled down due to generation deficiency and all the generators tripped. However it was not due to underfrequency protection. The system frequency fluctuations disrupted the fuel to air ratio of premix burners, resulting in a very lean mix of fuel and air that caused flame instability. Along with this there were other factors involved and finally the *turbine protections* acted to trip the turbines due to high vibration in the combustion chamber. The major disturbances in 1996, 1998, 2001 and 2005 on the TNB grid were due to either inadvertent tripping of the gas turbine based plants or undesirable performance of the gas turbine based units.

4.3.17 Blackout in the Swiss Railway Electricity Supply System June 22, 2005

After the initial event the SBB system was split into two parts, the Southern and the Northern [83]. The southern part had an excess of 200MW which led to frequency increase and thus the *overfrequency protection* tripped most of the generators were tripped within eight seconds and the whole area was blacked out. On the contrary the northern part was generation deficient and to maintain the stability the generation from Châtelard, Vernayaz and Etzel power plants and the import from Germany increased. However shortly after this the generators were tripped due to *overload* and the tie line from Germany was opened causing complete system shutdown.

4.3.18 UCTE Major Disturbance of 4 November, 2006

In the Western Subsystem load generation imbalance led to frequency decline to 49 Hz and *underfrequency* tripping of pump storage hydro units and large portion of wind and cogeneration units [83]. The North East Subsystem had huge excess of generation up to 10 GW and the frequency initially increased to 51.4 Hz. To the advantage, wind generations tripped due to *overfrequency protection* and the frequency recovered. But unfortunately soon some of the wind generators automatically reconnected as the frequency recovered, and the frequency once again began to increase.

4.4 Generator Protection Types and Strategies

In this research the main concern is the generator protective relay operation under severe disturbance conditions. In the previous section on the synoptic study of the past blackouts, the specific generator protections that operated and which were critical events in the unfolding of the cascading were identified in italics. Of all them we would focus on a subset which is most important and frequent in such critical scenarios. They are enumerated below and are followed by a detailed discussion of each of them. In this study the generator protection studied are as follows:

- Overexcitation
- Overcurrent
- Overvoltage
- Undervoltage
- Overfrequency
- Underfrequency

- Out of Step

In summary the generator protection must be coordinated with the allowed voltage and frequency regulating ranges. Thus the generator voltage protection is set outside a threshold of about ±10% of nominal voltage and the frequency related protection generally operates within ±5% of the nominal speed. The overcurrent protection is delayed with respect to the automatic voltage regulator and governor dynamics. Most of materials discussed below on the different generator protection under abnormal conditions come from references [82, 107, 108, 109, 110, 111, 112, 113, 114, 115, 116, 117, 118].

4.4.1 Overexcitation (Volt per Hertz protection) Device 24

Generators and transformers require an internal magnetic field to operate. The core of a transformer and the stator of a generator are designed to provide the magnetic flux necessary for rated load. Deviations in frequency, power factor and voltages outside the intended limits of generator and transformer operation cause thermal stress and insulation degradation. An overexcitation condition occurs when the generator or the transformer equipment is operated such that flux levels exceed the design values. These design limits are specified in terms of the ratio of the voltage to frequency (V/Hz) applied at the terminals of the equipment.

The core area and the magnetic properties of the core material define the excitation capability of a generator or transformer. The core is designed to support a flux density necessary for full load operation and to dissipate the heat associated with that excitation level.

Standards ANSI/IEEE C50.13 (generators); C57.12 (transformers); IEEE Std C50.12, 4.1.5; IEEE C50.13, 4.17; IEEE Std 67 do not specify V/Hz limits for transformer or generators directly, but the voltage limits specified for this equipment at rated frequency imply continuous V/Hz limits. For instance the standards require a generator to be capable of operation at rated kVA, frequency and power factor with terminal voltage variations of ± 5%. Continuous operating capabilities are indicated below:

- Generators: 1.05 p.u. (generator base);
- Transformers: 1.05 p.u. on transformer base at full load, 0.8 pf or 1.1 p.u. at no load at the secondary terminals of the transformer.

Transformers and generators can withstand overexcitation for a short time. Maximum allowable component temperature and the rate of temperature rise in these components determine the limits. However the limiting component vary with design, and this has prevented the standardization of on overexcitation withstand characteristic and it must be obtained from individual manufacturers.

1) Overexcitation and Overvoltage

A generator operating at no load with rated voltage and frequency would have one per unit flux and is said to be operating at one per unit excitation. Overexcitation would result from high voltage at rated frequency and from rated voltage with low frequency. Overexcitation condition is not the same as overvoltage condition where the dielectric breakdown is the concern. Overexcitation can occur without notice being a function of

voltage and frequency. Generators can be subjected to repeated overexcitation by inappropriate operating practices or operator error without a disruption to operations. The resulting thermal degradation of insulating material is cumulative. The transformer or generator that survives a serious overexcitation event or many small events may fail as a result of a moderate event or during normal service.

2) Causes of overexcitation

It usually occurs during periods of reduced frequency operation such as start up or shutdown under automatic voltage regulator control. CTGs with converter starting may be subjected to very low frequencies (such as 2 Hz) during starting. Another classic V/Hz damage scenario is the failure of the field breaker to open for shutdown. Failure within voltage regulator and associated circuits can cause damaging overexcitation to the synchronized generator and connected transformer. The loss of generator voltage signal to the regulator is an example.

Load rejection with the automatic voltage regulator in service and a capacitive load can cause overexcitation. The capacitive load could be shunt capacitor used for voltage control or VAR support or it could be the charging current for a high voltage transmission line. The V/Hz may exceed 125%.

Overexcitation Due to Overvoltage: When a power system island is formed during a major system disturbance, it may have excessive VARS in relationship to VAR load. These VAR sources are shunt capacitors, as well as VARS produced by generators within the island. Sudden power system disturbances can also unload transmission lines whose shunt capacitance can contribute to high VAR levels within the island. Ideally, control actions, such as tripping of shunt capacitor banks within the island, will reduce system voltage to within generator and transformer continuous capabilities. At power plants, automatic generator excitation control will reduce VAR output to control voltage within the island. If required, generators can operate underexcited and absorb VARS. The amount of VARS that the generator can absorb is limited by the generator underexcited capability, which is limited by stator end iron heating. Other considerations, such as steady-state stability limits and loss of excitation protection can also limit under excited generator operation. The minimum excitation limiter in the voltage regulator limits the VAR intake level. This is a settable control within the generator voltage regulator that needs to be properly adjusted, to coordinate with generator capability and steady state stability limitations. If during a major system disturbance, the generator excitation control is in manual, none of the generator control actions described above will take place and the generator VAR output will not be reduced to lower system voltage. If a significant number of generators within an island formed during a major disturbance are operating with their voltage regulator control in manual, it will greatly exacerbate high voltage problems with the island. If high voltage during a major system disturbance is not reduced to within generator and transformer capabilities, protection is provided to trip generators and their associated transformers.

Overexcitation Due to Underfrequency: A volts per hertz overexcitation condition can also occur due to low system frequency resulting from a major system disturbance. This,

however, is a less likely cause than high voltage. Its trip time is usually much slower than under frequency relaying.

3) Damage

When a transformer or a generator is operating within rated parameters, the flux in the core will be below the saturation flux density and it will confine itself to the core since the core permeability will be much higher than that of adjacent structures. Core heating will also be within design limits. Flux produced in excess of design limits will saturate the core and will spill into the surrounding air space and stray flux would be induced into non-laminated metallic structures around the core which are not designed to carry flux. Damage to a laminated core due to increased losses requires extreme overexcitation for a significant time. However eddy currents induced in non-laminated structures can cause severe component damage and quick thermal runaway.

In a generator the most damaging spill flux will appear at the ends of the stator core. Also, the excessive induced currents within the stator laminations can create voltage gradients between core laminations sufficient to break down the inter-laminar insulation. If it occurs the core will be permanently damaged, rendering it incapable of carrying even normal flux without arcing, increased heating and further deterioration. Stator core restacking is a very expensive procedure. Field current in the generator can also become excessive.

4) Protection

Protection for a generator or generator and connected transformer against overexcitation can be provided in several forms such as V/Hz relaying at the generator terminals, by V/Hz limiting circuitry within the automatic voltage regulator, or by relay sensing machine field current or voltage.

Field Monitoring Relays: Relays within the excitation system can provide limited overexcitation protection by monitoring field current or voltage. This relaying would be set slightly above the field current or field voltage necessary to produce rated generator output voltage at no load. Tripping would be through a timer with a few second delay. This relaying would be in service only when the generator is offline to provide overexcitation protection during startup and shutdown.

V/Hz Limiter: V/Hz limiter circuitry is within the automatic voltage regulator. It senses voltage and frequency at generator terminals and adjusts the generator field as required to prevent operation above a preset V/Hz value. Many limiter designs exist and it may be in service at all times or it may be in service only when the generator is offline. It functions only in the automatic control mode. Care should be taken while setting the limiter so that the short time overexcitation capability of the generator can be utilized during system disturbances. When the excitation control is out of service then V/Hz relaying is used to protect the station transformers and the generator.

V/Hz Relay Application (Device 24): If the prime mover and associated mechanical systems are capable of withstanding a load rejection, the V/Hz relaying should trip the

field and generator breakers. The prime mover need not be tripped. This will facilitate a rapid restart of the unit after the cause of the overexcitation is cleared. If the mechanical system cannot withstand the load rejection associated with the generator trip, a prime mover trip must be initiated. V/Hz relaying for the protection of the generator is applied at the generator terminals. They have either the definite time or inverse time characteristic. Either characteristic must be set to initiate tripping before damage occurs at the maximum level of overexcitation anticipated. The inverse time characteristic is preferred to allow maximum utilization of the short time capability of the generator. The definite time characteristic overprotects at low levels of overexcitation, thus jeopardizing unit availability during system disturbances.

Practical Consideration: The reset is intended to mimic the thermal characteristic of the protected generator or transformer. Assume that a given overexcitation condition will damage equipment in 60 seconds and therefore V/Hz relay is set to operate in 50 seconds. But the V/Hz limit violation is removed after 40 seconds and reappears after 10 seconds. If the relay is reset after the initial violation recedes, then upon recurrence of the event the equipment will be subjected to the overexcitation condition for full 50 seconds before tripping. This means the equipment is exposed for 90 seconds. This would cause damage to the equipment. Also the heat generated in the protected equipment will not dissipate in short time between events. Therefore the memory feature is required for the relay to reset at a rate comparable to the cooling rate of the protected equipment.

5) Settings

The system operating voltage range extends to the continuous V/Hz capability of generators and transformers. Thus the setting must be done in a way to guarantee that overexcitation protection will not actuate when the system is operating at the maximum continuous V/Hz capability of the equipment. To accomplish this, the settings must be above the applicable limit with sufficient margin to allow for relay and potential transformer errors. The setting should also include an appropriate safety margin. The resulting V/Hz settings can be substantially above the continuous V/Hz capability.

The delay for the overexcitation protection should allow for the maximum utilization of the short time capability of the protected equipment. Overexcitation can occur during a system disturbance because of field forcing, reduced system frequency or both. In this situation the output of every generator is very critical to system recovery. Protective relays that do not optimize the equipment capability reduce the reliability of the entire power system. The setting for the generator is straightforward. The V/Hz limit at the generator terminal is 105% regardless of the load condition. The initiation setting for the pickup of the relay should be set above 105%+margin (device error + PT error + safety margin). Short-time overexcitation withstand curves provided by manufacturers are often based on actual core limits. When such curves are applied at the equipment terminals, they represent a no load condition. The application of such curves under load may be optimistic. When using short time curves, the applicable conditions for the curves must be known.

Time delay settings: The V/Hz relay must be set with sufficient time delay to override system fault voltage transients and to allow the voltage regulator to restore normal

voltage following load rejection. These minimum delay conditions are normally met when the delay is set to maximize utilization of the short time overexcitation capability of the equipment. However the determination of anticipated maximum excitation level would require a dynamic study involving the generator, voltage regulator and governor, saturation characteristics of the generator and transmission parameters. In practice the maximum V/Hz condition at the generator terminals can be estimated from the generator's open circuit saturation curve. Generally the shape of the curve is such that the saturation of the stator will limit the terminal voltage to less than about 1.25 pu. Therefore at 1.25 pu the limiter if installed should act to reduce the excitation before relaying initiates a generator trip, otherwise the relay must initiate a trip before the short time withstand of the generator or connected transformer.

4.4.2 Overcurrent

The continuous output capability of a generator is expressed in kilovolt-amperes (kVA) available at the terminals at a specified frequency, voltage, and power factor. For hydrogen-cooled generators, the output rating is usually given at the maximum and several lesser hydrogen pressures. For CTGs, this capability is given at an inlet air temperature in the range of –20° C to 50° C. In general, generators may operate successfully at rated kVA, frequency, and power factor for a voltage variation of 5% above or below rated voltage.

Under emergency conditions, it is permissible to exceed the continuous output capability for a short time. In accordance with IEEE Std. C50.13, the armature winding short time thermal capability is given in Table 14.

Table 14: Overcurrent relay settings

Time (seconds)	10	30	60	120
Armature current (percent)	218	150	127	115

where 100% current is the rated current of the machine at maximum hydrogen pressure. In some instances, generator overload protection may be provided through the use of a torque controlled overcurrent relay that is coordinated with the IEEE C50.13 short time capability curve. This relay consists of an instantaneous overcurrent (IOC) unit and a time-overcurrent unit having an extremely inverse characteristic. The instantaneous unit is set to pick up at 115% of full-load current and is used to torque control the time-overcurrent unit. The instantaneous unit dropout should be 95% or higher of pickup setting.

The time-overcurrent unit is set to pick up at 75% to 100% of full-load current, and a time setting is chosen so that the relay operating time is 7.0 s at 218% of full-load current. With this approach, the relay is prevented from tripping for overloads below 115% of full-load current and yet provides tripping in a prescribed time for overloads above 115% of full-load current. The overcurrent relay settings should be provided to transmission system protection personnel for coordination purposes. An overload alarm may be desirable to give the operator an opportunity to reduce load in an orderly manner. This alarm should not give nuisance alarms for external faults and should coordinate with the generator overload protection if this protection is provided.

For air-cooled generators that may operate in a wide range of ambient temperatures, it is necessary to coordinate the IEEE C50.13 thermal capability and the relay setting with the increased capability of the turbine and the generator at reduced ambient temperature. Conversely, it may be difficult to protect the generator for its reduced capability when the ambient temperature is high.

4.4.3 Overvoltage

Voltage regulators control the generator excitation levels to ensure the terminal voltage is maintained at a level that is within the rated operating range of the generator. Voltages outside that range could result in damage to the generator or unacceptable power system conditions. Voltages may exceed rated levels during system disturbances, while the generator excitation system is limited by its internal controllers, or is operating in a manual control mode. Abnormal voltage protection for generators must coordinate with any external control systems regulating the system voltage that would help to restore normal voltage levels at the generator terminals.

Abnormally high voltages could cause excessive dielectric stress on the generator or unit transformer insulating materials and result in insulation failure. As discussed earlier overexcitation and overvoltage are related but not the same. Overvoltage condition may occur without necessarily exceeding the flux limits. For example in hydrogenerators an overspeed of 200% or more can occur upon load rejection leading to serious overvoltage condition especially if they are operating in manual excitation control mode.

Overvoltage protection is sometimes provided to protect the generator from excessive dielectric stress. In addition to coordinating with external system voltage control devices, generator overvoltage protection must also coordinate with internal excitation system voltage controllers. Such coordination is not difficult as long as the protection is set to pick up at a higher level than the maximum setting on the generator voltage reference control and the setting of the excitation system volts per hertz controller at a fundamental frequency (if this auxiliary control device is provided). Coordination with exciter controls for temporary excursions above the maximum controlled voltage level is easily achieved with even small time delays on the protection, because the control devices are normally quite fast (exerting control within less than 1 s).

A major cause of overvoltage is sudden loss of load. Power equipment involving iron (rotating generators, transformers) operate close to the knee of their saturation curves. Thus small overvoltages result in large increases in exciting current and cause major damage. Typical permissible overvoltage at no load is given in Table 15.

Table 15: Typical Overvoltage limits

Generator	
105%	Continuous
110%	30 minutes
115%	5 minutes
125%	2 minutes

Instantaneous overvoltage setting should be about 106%-110% of rated voltage to ensure prompt removal.

4.4.4 Undervoltage

Undervoltage conditions are not usually harmful to generators themselves, so direct undervoltage protection is not normally provided for them. However sustained operation of a generator with terminal voltage lower than 95% of its rated voltage may cause reduction in stability limits, import of excessive reactive power from the grid to which it is connected and can lead to malfunctioning of voltage sensitive devices and equipments. Also, overheating due to extended operation at low voltages may damage the auxiliary motors for turbine generator sets. Auxiliary supplies are therefore sometimes monitored by undervoltage relays that may trip the generator off line to protect the motors.

Auxiliary undervoltage tripping is usually applied at nuclear generating stations, where the protection of safety related auxiliary equipment is of paramount importance. The undervoltage relays are typically set close to 0.9 p.u. of normal operating voltage, with time delay to prevent tripping during successful clearing of external faults. However, this setting can cause tripping during system disturbances involving sustained undervoltage conditions.

4.4.5 Overfrequency

Off nominal frequency operation is a result of load generation mismatch. Turbine operation capabilities at abnormal frequency are usually more restrictive than generators and transformers. Operation of a turbine between 59.5 and 60.5 Hz (in a 60-Hz system) is considered within the unrestricted time operating frequency limits, whereas the operation above 60.5 Hz and below 59.5 Hz is regions of restricted time operating frequency limits. Continuous operation in this region under generator-loaded condition is not recommended.

Overfrequency is usually the result of a sudden reduction in load or unit full load rejection and, therefore, corresponds to light-load or no-load operation of a generator. Overfrequency operation is less of a concern than underfrequency operation. This is because normal frequency can be quickly restored by reduction in generation by operator or governor control action. Overfrequency increases ventilation and therefore the load carrying capability is increased without the danger of overheating. Also the flux density required for a given terminal voltage is reduced.

As an example overfrequency operation or overspeed operation is a concern for a hydro turbine. A hydro turbine typically has a huge mass and high kinetic energy of water in the penstock. A sudden loss of load on it accelerates the turbine- generator mass and results in an overspeed of up to 150%. On a hydro turbine, the input energy is a large mass of water traveling at significant speed. A rapid closure of the gate would result in water hammer with a pressure spike that would damage the penstock. Consequently, the minimum and maximum design pressures for the penstock limit the rate of gate movement. However, if a failure occurs within the gate or governor system, the hydro unit could attain a speed of 200% rated, incurring major damage.

4.4.6 Underfrequency

Frequency decay is a generally a result of a system disturbance caused by the loss of a large generation resulting in system separation and overloading. The generators may be subjected to prolonged periods of underfrequency operation which pose a serious threat

to the turbines and other auxiliaries along with the generator. Underfrequency operation reduces ventilation, increases overheating and reduces the load carrying capability of the generators.

The generators can operate up to 0.95 pu rated speed for prolonged periods without overexcitation if the output is reduced proportional to speed at rated terminal voltage. From 0.95 pu to 0.90 rated speed, both output voltage and current should be reduced in proportion to speed, thus reducing output capability by the square of the speed reduction [116].

The standards do not specify generator capability at reduced frequencies, but this information can be made available from the generator manufacturer. The reduction in output capability coupled with possible overloading of the generator during a system disturbance may result in thermal damage to the generator if its short time thermal capability is exceeded.

1) Underfrequency Turbine Capability

Generally the turbines are considered to be more restrictive than the generators they drive at reduced frequencies because of possible mechanical resonances in the many stages of turbine blades. These limitations usually apply to steam turbine generators. Combustion turbine generators (CTGs) in general have greater tolerance than steam units for underfrequency operation.

Combustion turbine generators: They can usually operate down to 57 or 58 Hz for extended periods of time. The specific underfrequency limit should however be consulted from the manufacturer for each CTG. However, CTGs are frequently limited by combustion instability and/or sharply reduced turbine output as frequency drops due to reduced airflow through the turbine. Loss of air flow will result in immediate unit trip following the detection of a change in axial rotor position, shaft and/or bearing vibration, loss of flame in the combustor(s), or excess temperature of the turbine. One manufacturer estimated a 17% loss in output at 55 Hz. In general, there are no restrictions on hydrogenerators. Combustion turbines (particularly under 200MW) have limited number of blade sizes and, therefore, have fewer resonant frequencies.

Steam turbine generators: Of all turbines steam turbines are most adversely affected by underfrequency operation. Damage due to blade resonance is of primary concern in the turbine blade design. Resonance occurs when the frequency of the vibratory stimuli and the natural frequency of a blade coincides or are close to each other. The steam flow path is not homogeneous due to physical irregularities in the flow path and this produces cyclical force to the blades. At resonance the cyclical forces increases the stress and the damage to the blades is accumulated and may appear as a crack of some parts in the assembly. Although these cracks especially in tie wire and blade cover may not be catastrophic in these areas but they can alter the blade tuning such that resonance could occur near rated speed.

Every turbine blade has numerous natural resonance modes, namely tangential, axial, and torsional. Each mode has a natural frequency that varies with the physical dimensions of the blade. Short blades in the high-pressure and intermediate pressure stages of the turbine can be designed to withstand a resonant condition. However the longer turbine blades associated with the low pressure turbine are prone to damage by prolonged

abnormal frequency operation. These blades are protected by tuning their natural resonant frequencies away from rated speed. These blades generally determine the turbine's vulnerability to under frequency operation.

Standards do not specify short time limits for over-or underfrequency operation. The manufacturer of the specific turbine must provide this data. Reference [117] lists the following limitations for one manufacture's turbines as:

- 1% change (59.4–60.6 Hz), no adverse effect on blade life
- 2% change (58.8–61.2 Hz), potential damage in about 90 minutes
- 3% change (58.2–61.8 Hz), potential damage in about 10–15 minutes
- 4% change (57.6–62.4 Hz), potential damage in about 1 minute

Reference [118] states that with a 5% frequency deviation, damage could occur within a few seconds. These withstand times are not typical. Limits vary dramatically among manufacturers, as can be seen in Fig. 32, which includes limitation curves from four manufacturers.

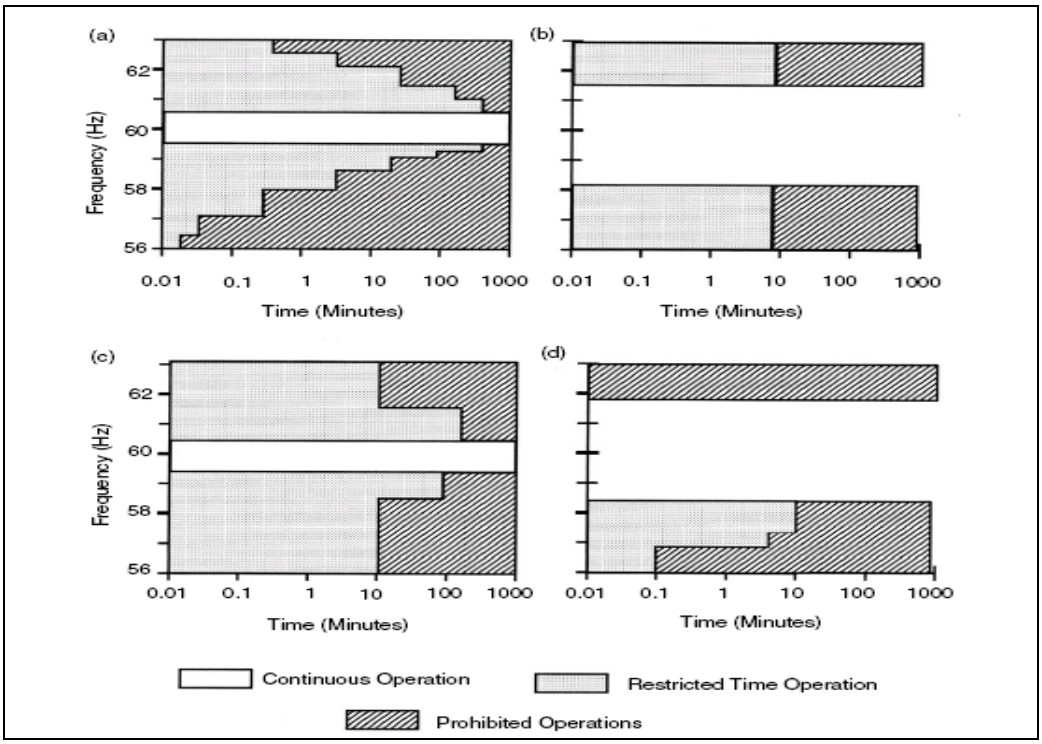

Fig. 32: Steam Turbine Partial or Full-Load Operating Limitations During Abnormal Frequency [115]

Time spent in a given frequency band and hence the fatigue damage is cumulative and is independent of the time accumulated in any other band. For each incident, the first ten cycles in a given frequency band are not accumulated since some time is required for mechanical resonance to be established in the turbine blades. The fatigue life is used up during abnormal underfrequency operation and a series of such events influence the total

fatigue life, as the first underfrequency event will weaken the turbine blades and reduce the number of cycles to failure for subsequent events.

2) Settings

The settings should be such as to coordinate with the automatic load shedding on the system and at the same time provides protection for each band of the manufacturer's withstand characteristics. It is also important to take into account the past history of the turbine with respect to the accumulated vibratory stresses in each band of underfrequency operation.

The first line of action against the underfrequency protection is automatic load shedding. This is continued until there is no mismatch between the load and the generation. It is designed based on the frequency decay and the rate of frequency decay. It is generally employed in steps. However due to the extreme complexity of the power system it is extremely difficult to reach an exact match between load and generation especially during cascading events when several islands are formed with different load and generation mismatch. Moreover this island formation may be different can conceived in the planning stage for the automatic load shedding. Finally the frequency decay is also oscillatory and non homogeneous. Thus second line of defense in the form of backup protection is essential and is discussed in the following paragraph.

The backup protection employs a multilevel underfrequency tripping scheme. A separate time delayed underfrequency function is required for each band on the manufacturer's limit curve. The scheme for timers used in this research is one of cumulative timers to store a history of the operating time in each protective band in a nonvolatile memory. This scheme takes full advantage of the underfrequency capability of the prime mover and is only available in microprocessor relays. The timers set near the maximum allowable time for the band they protect. This strategy aims at maximizing the availability of large units during system disturbances, thus enhancing the power system's ability to ride through such disturbances. Fig. 33 shows a six-level accumulated time scheme. Underfrequency trip settings are slightly above the start of each band, and timers are set slightly below the total allowable time for each band. When the cumulative operating time in a band for all previous underfrequency events plus the current event equals that band timer setting, the scheme will operate to trip the generator. The operation of this scheme indicates that the blades associated with the actuated band are at the end of their useful life. At a minimum, a complete inspection of the blades is indicated.

The first line of defense is preferred as long as the disturbance can be successfully handled by it.

The commonly used timer schemes do not have memory. They measure the duration of current frequency operation and then resets to zero. Also they keep on accumulating the time as long as the frequency remains below their actuation limit. This does not correspond to the actual behavior of the turbine. Hence it is a compromise protection scheme.

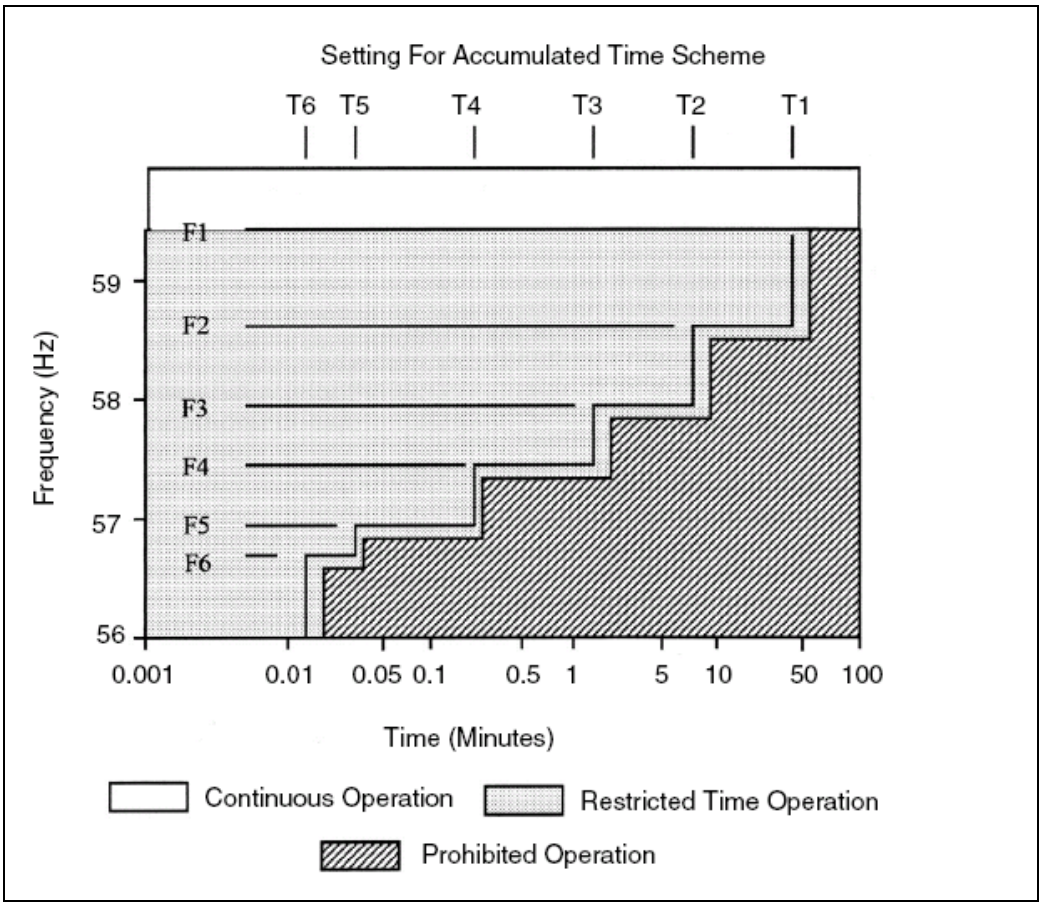

Fig. 33: Time accumulation based Timers [109]

4.4.7 Out of Step

The discussion on out of step is taken mainly from references [82] and [109]. Prior to the 1960s, electrical centers were normally found on the transmission system and out-of step protection was provided by line relaying without the need for trip generation. Over the years, the transmission system became stronger. Generator and GSU transformer impedances have increased because the improved cooling technology provided greater MVA capacity from physically smaller units. As a result, the electrical centers on many systems have moved into the GSU transformer and the generator itself, significantly increasing the stresses on both the components. These swings would not be detected by network protection, thus the need for out-of-step protection at the generator.

Out-of-step protection may also be required at the generator if the electrical center is located beyond the GSU on the transmission system, but the transmission relaying is slow or incapable of detecting the out-of-step condition. Also, the overcurrent relays used for generator protection do not provide reliable loss of synchronism detection. Although currents may be high enough to actuate an overcurrent relay, tripping will depend on the duration of the excess current, which is determined by the slip frequency. The operating time of an overcurrent relay will normally exceed the duration of the current pulse each slip cycle. If the condition persisted for many slip cycles, an electromechanical

overcurrent relay might “ratchet” closed and trip the generator. Solid-state and microprocessor relays with fast reset characteristics will not ratchet.

Differential relays will not detect an out-of-step condition because the infeed and outfeed currents within the differential zone are equal. Following a system disturbance, the generator rotor angle will oscillate as the generator attempts to find a new steady-state operating point. These rotor oscillations produce variations of stator voltage and current. The quotient of these varying quantities represents the dynamic system impedance during the transient as viewed from the generator terminal. The dynamic impedance is also referred to as the “swing impedance” or just “swing.” Distance relays applied at the generator as system backup protection will detect a swing if the swing impedance passes through the trip characteristic. The relay time delay and the speed at which the apparent system impedance crosses the relay characteristic will determine if tripping is initiated. Normally, the delay required for coordination with network relaying will prevent these schemes from operating during out-of-step events. Loss-of-field protection is an impedance-based relay scheme applied at the generator terminals to detect the failure of the generator field.

Fig. 34 shows the trip characteristic for one popular LOF configuration. The trip characteristic is set with a time delay. Because this scheme measures the impedance looking into the generator, it cannot detect swings that pass through the GSU transformer.

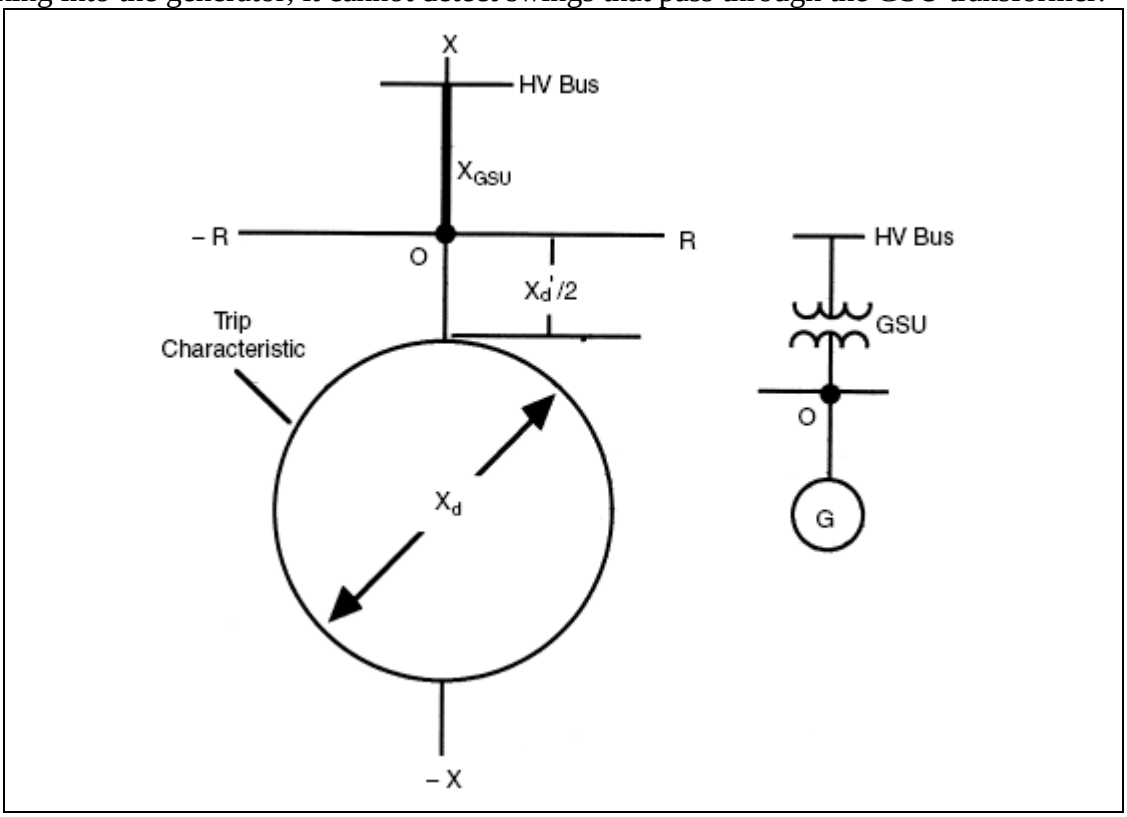

Fig. 34: Loss of field relay Characteristics

The offset of the characteristic also precludes detection of swings within the generator near the terminals. The trip characteristic will operate for slow-moving swings that linger within its characteristic in excess of the trip delay setting, typically 0.5 sec to 1.0 sec. The

bottom line is that the loss-of-field protection may operate for specific out-of-step conditions, but cannot provide standalone out-of-step protection.

Over the years, specialized detection schemes have been developed. Early out-of-step protection schemes counted the current pulsation each time a generator pole slipped (passed through 180 degree separation with system voltage). Tripping was initiated after a preset number of counts. Now it is recognized that the system impedance viewed from the generator terminals provides a method for the rapid detection of a loss of synchronism. Consequently, out-of-step detection schemes employ impedance-sensing elements and specialized logic to distinguish between a fault condition and a loss of synchronism. In order to apply this type of protection, it is necessary to understand how system impedance varies during a loss of synchronism.

When a generator loses synchronism, the resulting high peak currents and off-frequency operation can cause winding stresses, high rotor iron currents, pulsating torques, and mechanical resonances that are potentially damaging to the machine. To minimize damage, the generator should be tripped without delay, preferably on the first slip cycle. During an out-of-step condition, the apparent impedance, as viewed from the generator terminals, will vary as a function of system and generator voltages and the angular separation between them. The impedance locus will depend on the excitation system, machine loading, and initiating disturbance.

Normally, system transient studies should be performed to determine the system impedance swing against time for different scenarios. The relays are set so that they will not trip for any stable swing but will trip if the swing is unstable. The swing is more likely to be unstable when the generator is operating at unity or leading power factor with the automatic voltage regulator out of service. For unstable swings, the impedance loci for each generator should be determined with system configurations that give maximum and minimum system impedances and with voltage regulators in and out of service. With different generator loading conditions and system configurations, the transient response of the machines is determined for different fault conditions. Generally, systems are required to withstand close in three-phase fault on the high side of the step-up transformer and breaker failure conditions. Even with fast relaying and breaker operating times, this condition may sometimes result in generator loss of synchronism. Out-of-step protection on a generator is required when relatively a large generator can go unstable for reasonable system contingencies and the swing goes through the generator/transformer zone. Many new generating plants are combined cycle, with a combination of gas turbines and a steam turbine at the same location. The latter will normally be lower inertia and will tend to go out of step before the higher inertia units. Out-of-step protection applied on the steam unit can lead to faster recognition of out-of-step conditions and it is possible that, in some cases, tripping of the steam unit quickly will result in the gas turbines staying in synchronization with the system. It has also been suggested that a back-up distance relay, set to trip if the primary breaker does not clear the critical fault, can be used in some conditions to trip the steam turbine and keep the gas turbines on line.

While planning studies can identify what setting to apply to out-of-step relays, it should be recognized that these studies are usually based on limited anticipated scenarios (e.g., three phase faults, breaker failure, specific system configurations, and loading, etc.). Severe system disturbances often involve multiple events with depressed system

voltages, switching events, and system oscillations. In addition, under abnormal system conditions, such as underfrequency, the relay characteristics may vary from ideal. Under these circumstances, application of an out-of-step relay may cause the impedance to enter the relay tripping characteristic for some situations where the machine is not necessarily out of step, thus causing nuisance tripping and possibly worsening overall system conditions. Detailed studies of performance under severe multiple contingencies must balance the risk of undesirable tripping against the risk of damage to the machine. The tripping mode recommended (breaker trip, assuming the unit can respond to full load rejection) does allow the machine to be quickly reconnected. Reference [109] provides a detailed discussion on the swing characteristics and the settings consideration for the relay.

5 Results and Discussion

5.1 Validation of the Dynamic Simulation Tool

We test our dynamic simulation engine on the Ontario Hydro 4 bus test system (see Appendix A for details of the system). Since our program builds network model directly from EMS's one-line substation in addition to an initial converged power flow case, we added 18 breakers to the test system so that all the lines, generators, load and shunt can be isolated by opening the associated breakers. Other parameters of the system stay unchanged.

Before fault, the statuses of generators are listed in Table 16. These initial generator parameters are sufficient to decide all other variables like bus voltages and line flows. The exciter model we use is a standard ETMSP Type 30 as shown in Fig. 35. The scenario we simulated is a 3-phase ground fault at bus 5. The fault was cleared by itself after 0.01 second without any breaker operation. We use the ETMSP application as a benchmark to our program.

Table 16: Initial status of generator for Ontario test system

No	V-abs	V-angle	P	Q
1	1.03	2.928	790	77.57608
2	1.01	-7.906	790	188.01250
3	1.03	0.6634	690	69.85064
4	1.01	-8.78658	740	85.26508

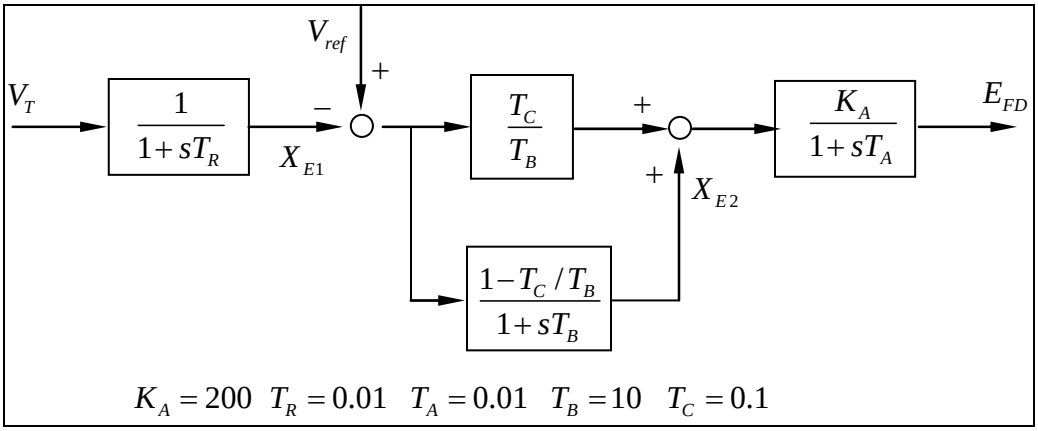

Fig. 35: ETMSP type 30 exciter for Ontario hydro 4-generator

The simulation results from the ETMSP application and our dynamic simulation engine are presented in Fig. 36 and Fig. 37 respectively. The two figures are almost identical. The minimal differences are probably introduced by different algorithm the two programs use. The ETMSP application uses fixed step Runge-Kutta algorithm for integral while our engine uses step-variable implicit integration algorithm.

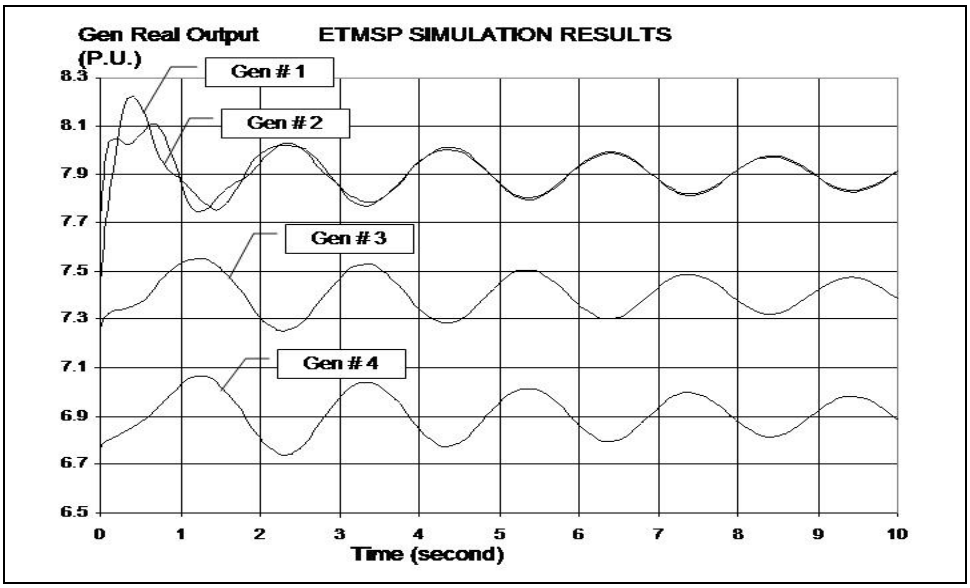

Fig. 36: Response of generator after a temporary fault at bus section 5 (ETMSP)

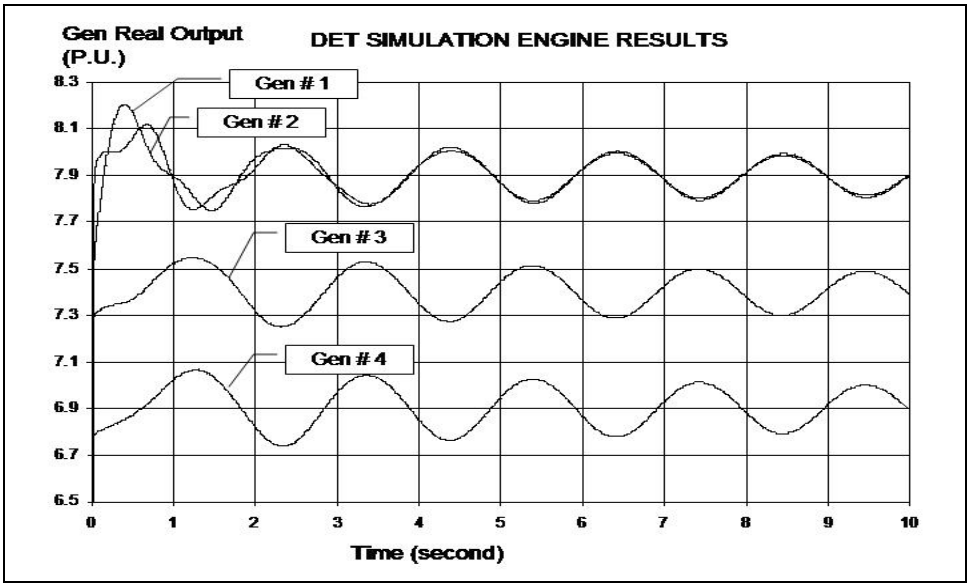

Fig. 37: Response of a generator after a temporary fault at bus section 5 (DET engine)

5.2 Decision Event Tree Generation

The test simulation uses the current system topology to generate an extended contingency list as the first tier of event nodes. An iterative programming technique and an LP optimizer are then employed to build a Decision Event Tree (DET) for each contingency as illustrated in Fig. 38. The branches B1, B3, and B5 represent the initial contingency, the system reconfiguration, and the emergency load shedding respectively, The branches B2 and B4 represent the "do-nothing" decision. The nodes (S_i's) in Fig. 38 represent the status/trajectory of the system after/before the actions (B_i's) are applied to the system.

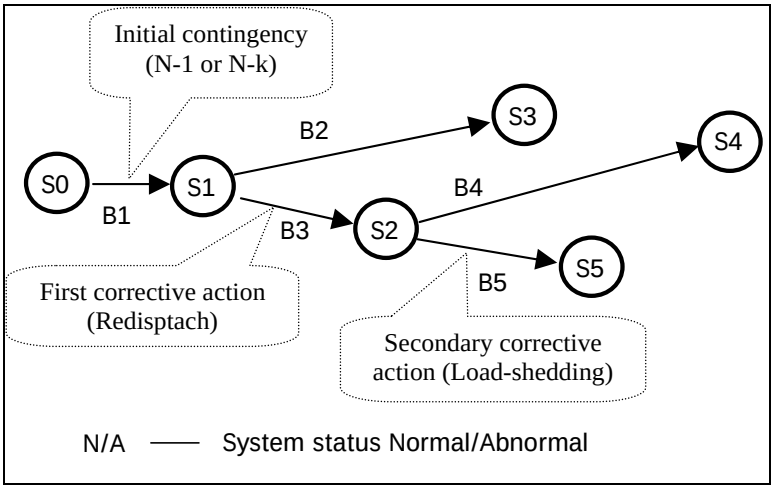

Fig. 38: Dynamic event tree template for DET test system

5.2.1 Test Scenario

We studied the possible cascading for a one-hour time interval during which the load ramped 20% from 900 seconds to 2700 seconds as shown in Fig. 39 for a scenario where the system is in a weakened condition due to the outage of a tie line. Line loadings are monitored, and the most effective redispatch & load curtailment actions are identified for overloaded lines.

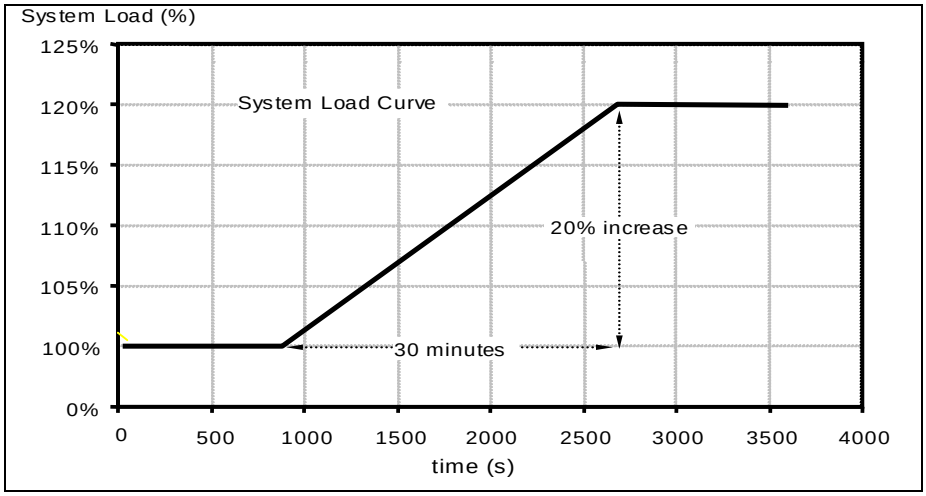

Fig. 39: System load ramp curve

5.2.2 Contingency Event Branch

We generated a comprehensive list of initiating contingencies for the selected scenario. Since we are going to do dynamic simulation (both long-term and transient in one application), we assume faults are cleared without any delay. This was done as a result of a programming limitation and is now being modified. However, this assumption does not seriously compromise our analysis since a close examination of all the NERC's record [20] of major power system disturbances find an initiating fault never causes the

immediate collapse of system; rather it is always a fault followed by an outage that causes a serious problem.

5.2.3 Decision Event Branch Set and Decision Identification

The decision set is the combination of all the redispatch of all the available generators and, if necessary, load curtailment. We assume any of the available generators can generate between zero MW to its maximum output. We use linear programming optimization to find the initiating redispatch and/or load curtailment to back off any line loading that exceeds a specified threshold. The formulation for this approach is provided in Appendix G. It is solved within the time domain simulation process only whenever it is necessary, i.e., when the flow on a line exceeds a defined percent its emergency loading. After we find the primary redispatch, we set the governor setting of each generator according to the redispatch and simulate the response of system to check if the redispatch is effective. Since the system total load increases between 900s and 2700s, decisions that are effective for now may fail after loading increases to certain level. In that case, we apply the secondary decision straightforward: direct load shedding, i.e. shed any increased load(s) that cause new problem.

5.3 Results Analysis

5.3.1 Without Generation Protection

In this section we present the simulation results without the generator protection in the simulator. The result of the DET engine computations for this scenario is a large repository of information that includes contingency specification, the response curves of all key variables for those contingencies and necessary actions. Of the 322 contingencies we analyzed, 10 resulted in fast (within 1 minute) instability and 312 of them resulted in stable, but unacceptable performance. Our implementation of the DET engine does not generate a corrective action for cases resulting in instability within 1 minute since this is not enough time to implement operator-initiated actions. Of the other 394 contingencies, all of them resulted in overloading problems that were corrected by proper generator and load reconfiguration as identified by our optimization approach. Fig. 40 illustrates a representative contingency via the one-hour trajectory of power flow on each line after the loss of the largest generator (G-101) in the upper area, which serves as B1, the initial contingency in the template DET in Fig. 38. We see that line L401 is the most loaded line for the entire system. Fig. 41 shows the time domain simulation results of the flow on Line L401 with and without the first and second actions (B3 and B5 in Fig. 38) applied. The effectiveness of the first redispatch only holds until time 1100s. After that, load increase causes the flow on that line to exceed 100% again. To prevent further loading, an emergency load-shedding scheme is identified and executed to prevent circuit loadings from exceeding their ratings. The initiating contingency and system trajectory with and without actions, as shown in Fig. 41, are mapped to the DET branches and nodes shown in Fig. 38.

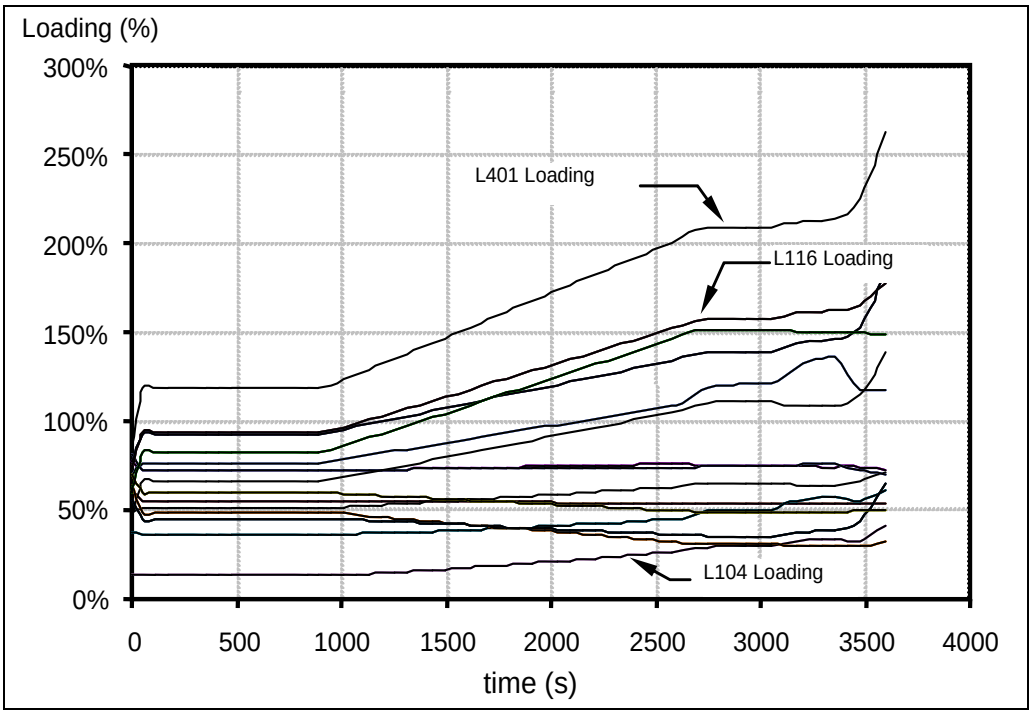

Fig. 40: Branch loading after loss of the largest generator

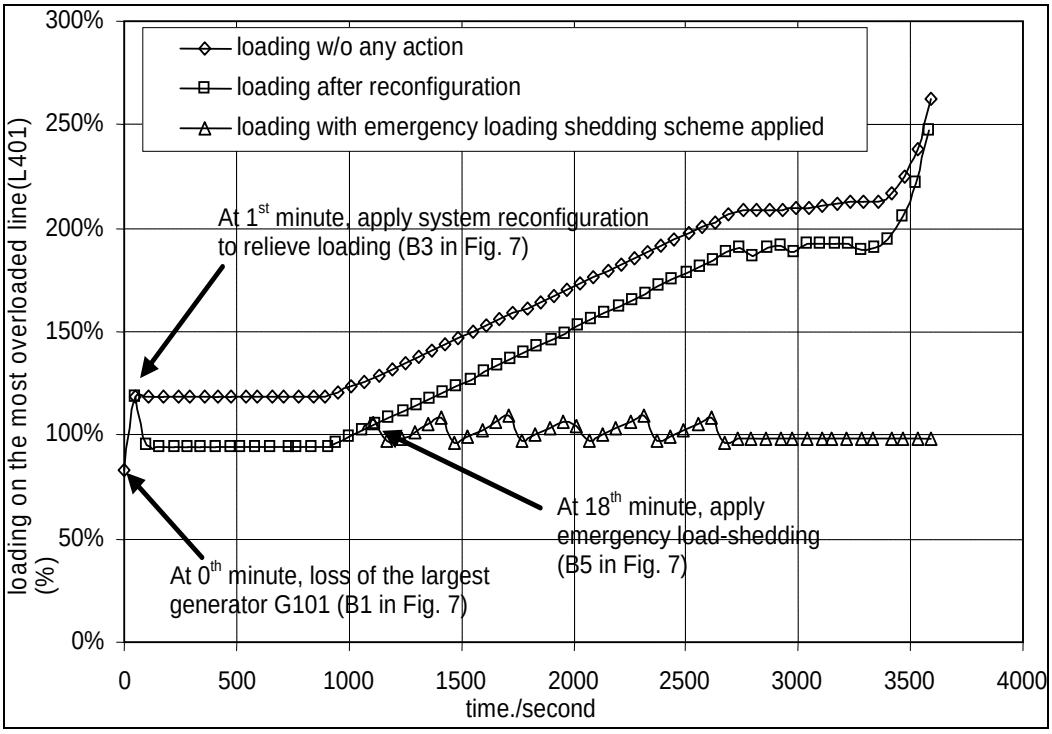

Fig. 41: Line flow response after the loss of the largest generator

Since our DET engine has the capability of slow dynamic simulation, we can also observe the voltage variation in the test system. We find that, even through the DET engine for the test system is designed to solve the overload problems only, the action

taken by the DET engine solves the voltage problems as well. Of the 312 stable, but unacceptable contingencies, 29 exhibited low voltages in the southern part of the system that were corrected by either the first (redispatch) or second (load interruption) actions taken. Fig. 42 illustrates a representative contingency, resulting in overloading and low voltage, via the flow on the most severely overloaded line after loss of lines L106 followed by the inadvertent tripping of L116. Fig. 43 shows the voltage of the most severely depressed bus following the same contingency. The contingency, decisions, and system behaviors of Fig. 42 and Fig. 43 are mapped to the branches and nodes of the DET in Fig. 38. The voltage collapses after 1800 seconds (point E in Fig. 43) if the operator does not take any action. Following the system reconfiguration (a redispatch) at 1 minute (point A in Fig. 43), the system behaves well until point D, where a low voltage problem shows up. If the secondary action at point B is applied, the system will avoid both the overloading and the voltage problems.

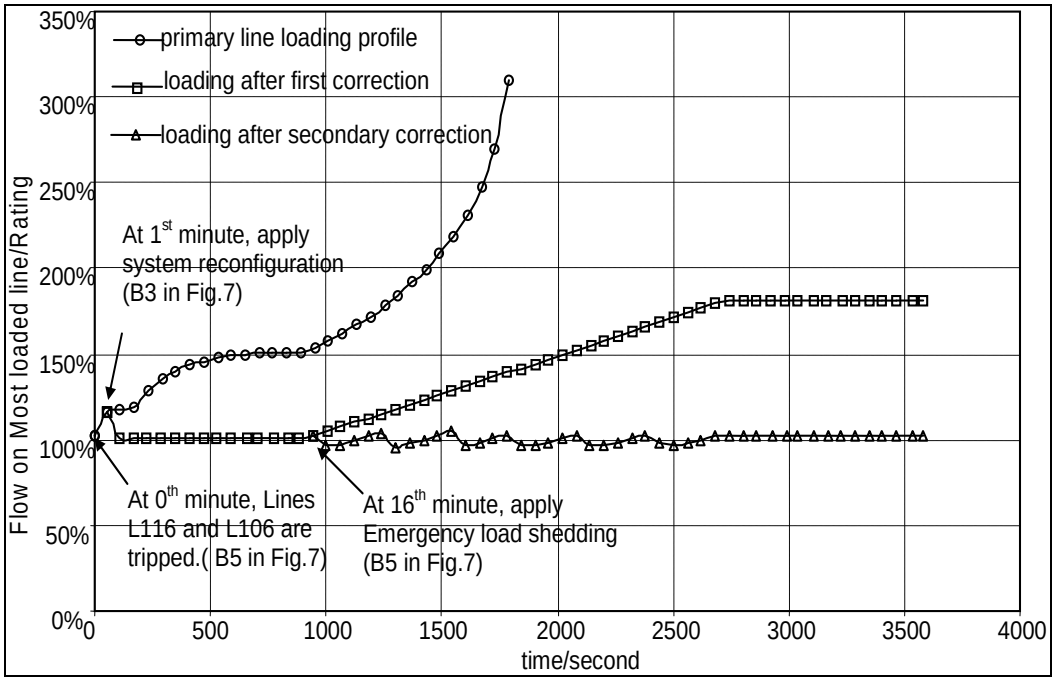

Fig. 42: The DET scheme for the tripping of lines L106 & L116 (most severely overloaded circuit)

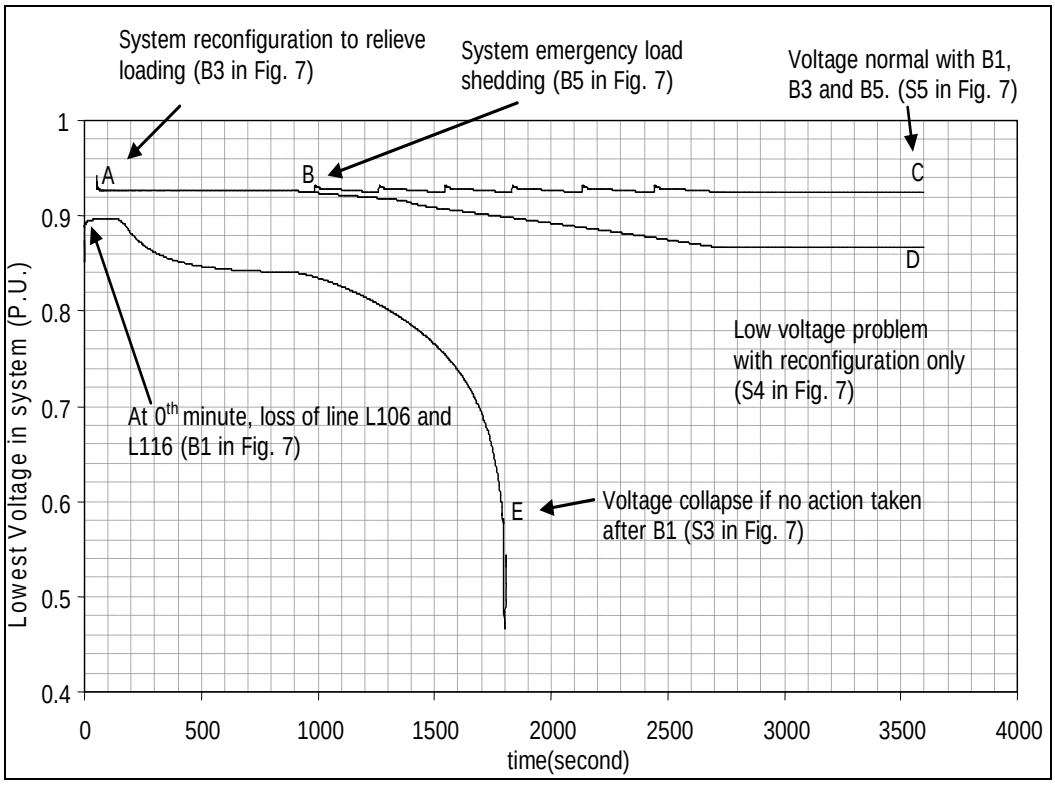

Fig. 43: Voltage response after the loss of L106 and L116

5.3.2 With Generation Protection

In this section we present the simulation results with the generator protection embedded into the simulator. A Depth First Search (DFS) based algorithm is implemented to detect island formation after any contingency and a recursive algorithm is implemented to continue dynamic simulation on each of the islands. The DFS algorithm is employed to simulate cascading under stressed condition of 20% load ramping from 900 seconds to 2700 seconds. The results presented are for the DET test system in Appendix D. Fig. 44 below shows the sequence of events that led to cascading when the system was under very stressed condition of heavy loading and one of relays, namely the overexcitation relay of the generator protecting the generator G101 was set lower than its actual setting, a classic case of setting errors. Therefore when there was a fault in line L215 at t= 300 seconds the generator G101 tripped and further stressed the system and thus causing the other generators to be overexcited and a sequence of events happened due to proper generator protection and generators G102 and G201 tripped in the next 15 minutes leading a major load generation imbalance and the system collapsed. Fig. 45 below show s the simulation result for the described cascading scenario. It shows the most loaded line flow on the system with and without the generator flow. In Fig. 45, the first line from below show the most loaded line flow without generator protection and we identify the point at which generator G101 would trip if the generator protection were in service. The next line simulates the flow with generator G101 tripped and identifies the point at which the next generator would trip if the relay is functional. This is simulated in the next line where the next generator G102 is tripped at t= 925.37s and identifies the

next generator trip at t = 1260.17s where the generator G202 trips and blacks out the system. Fig. 46 shows the lowest system voltage for the same cascading scenario and it corresponds to the maximum line flow graph in Fig. 45 with respect to the sequence of events.

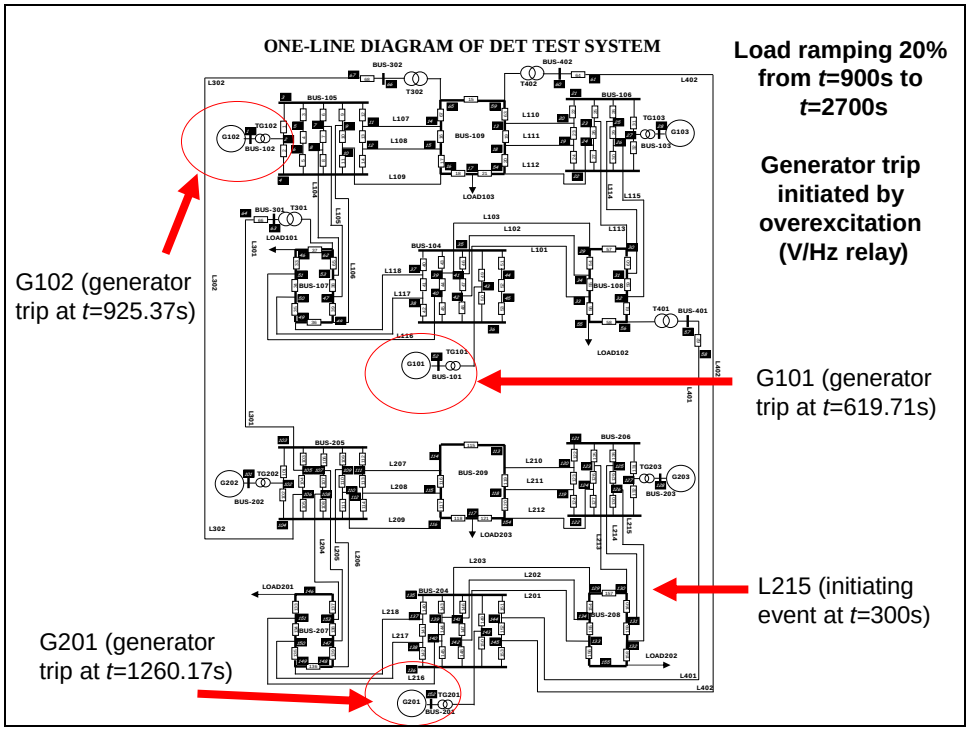

Fig. 44: Sequence of events leading to cascading

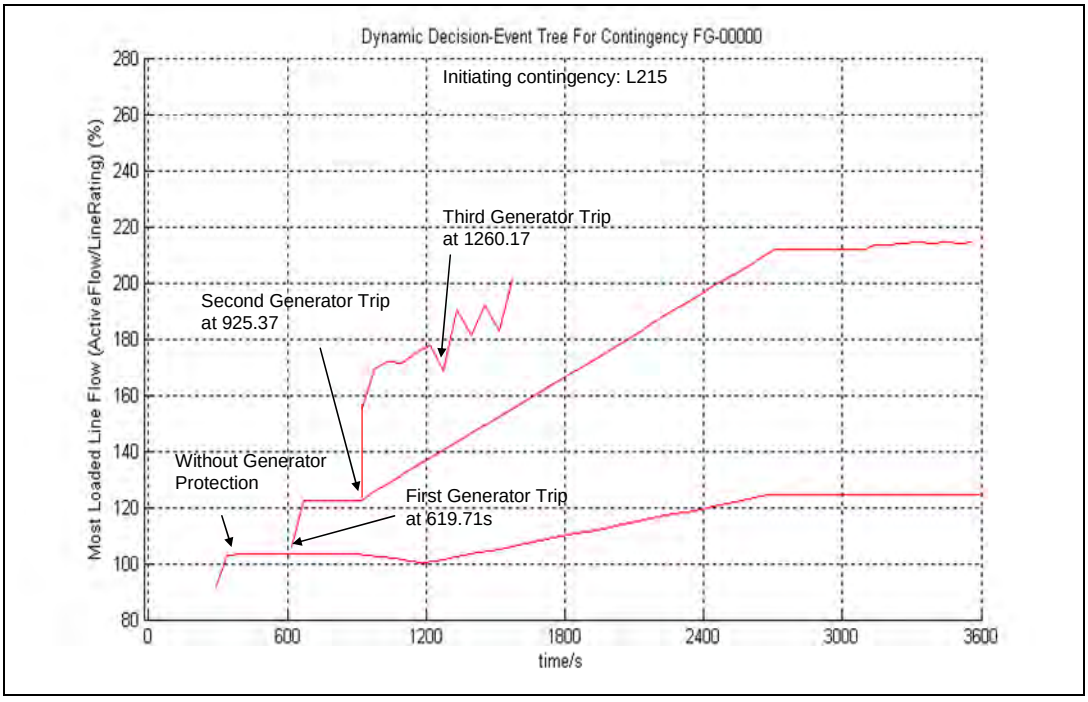

Fig. 45: Maximum line flow in a cascading scenario

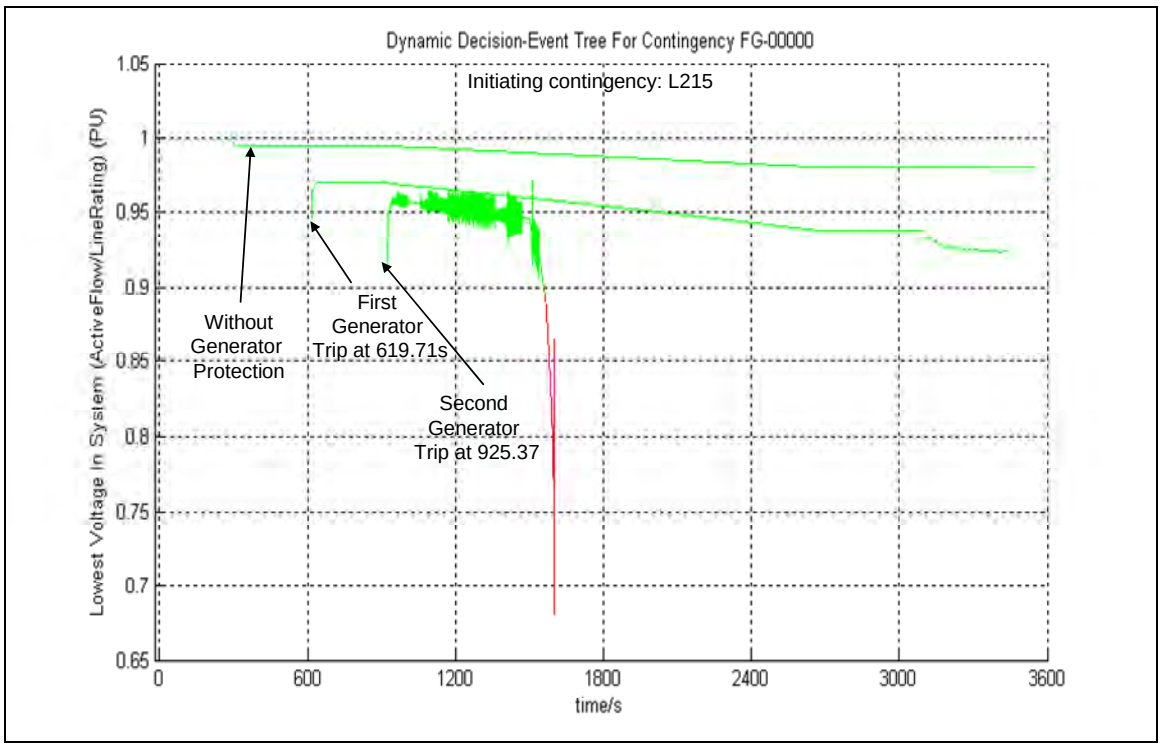

Fig. 46: Lowest voltage in the system for a cascading scenario

Fig. 47 shows a different system scenario with the sequence of events that led to islanding with the same initiating event as in Fig. 44, *i.e.*, L215. In this case also, the system response was simulated under stress condition of heavy loading, and the relay setting of generator G101 set below the calculated value. After the initiating event, the generator G101, and the four tie-lines L301, L302, L401, and L402 tripped separating the system into two islands - with the top island having 2 generators and load with deficient generation and frequency excursion, and the bottom island with 3 generators and load with excess generation. The top island collapsed immediately due to successive generator trips within a few seconds. In the bottom island, the generator G201 tripped at t=945.27s, and subsequently, the system recovered by balancing the generation and load through governor and other control mechanisms, and was stabilized. Fig. 48 shows the two islands formed after initiating event followed by the tie-line trips. Fig. 49 and Fig. 50 show the maximum loaded line flow, and the lowest system voltage for the above scenario.

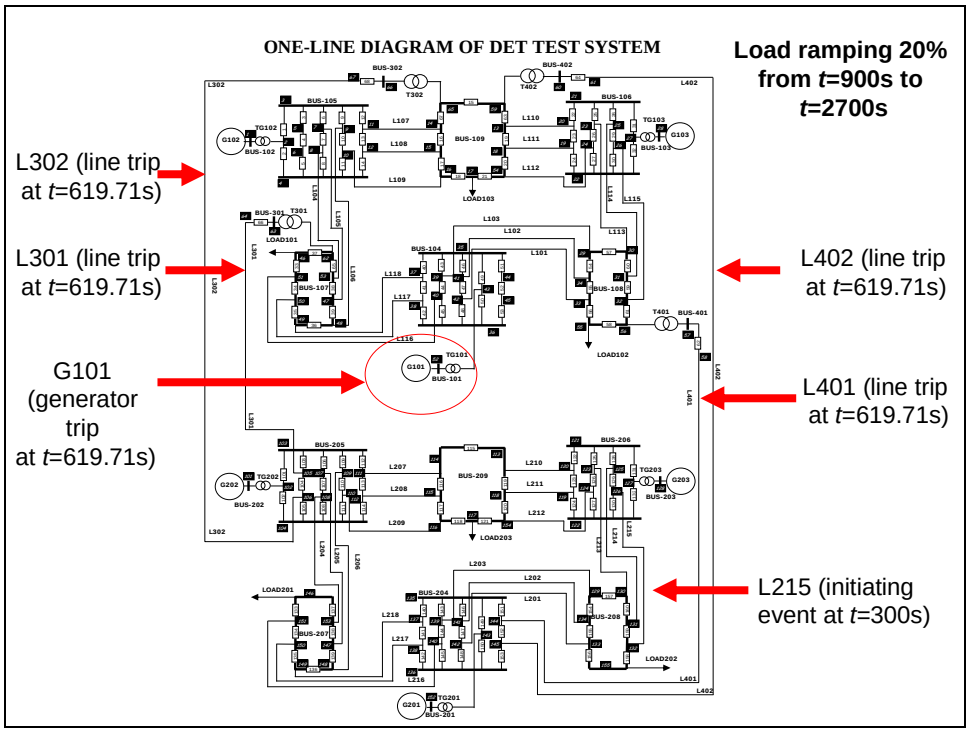

Fig. 47: Sequence of events leading to islanding

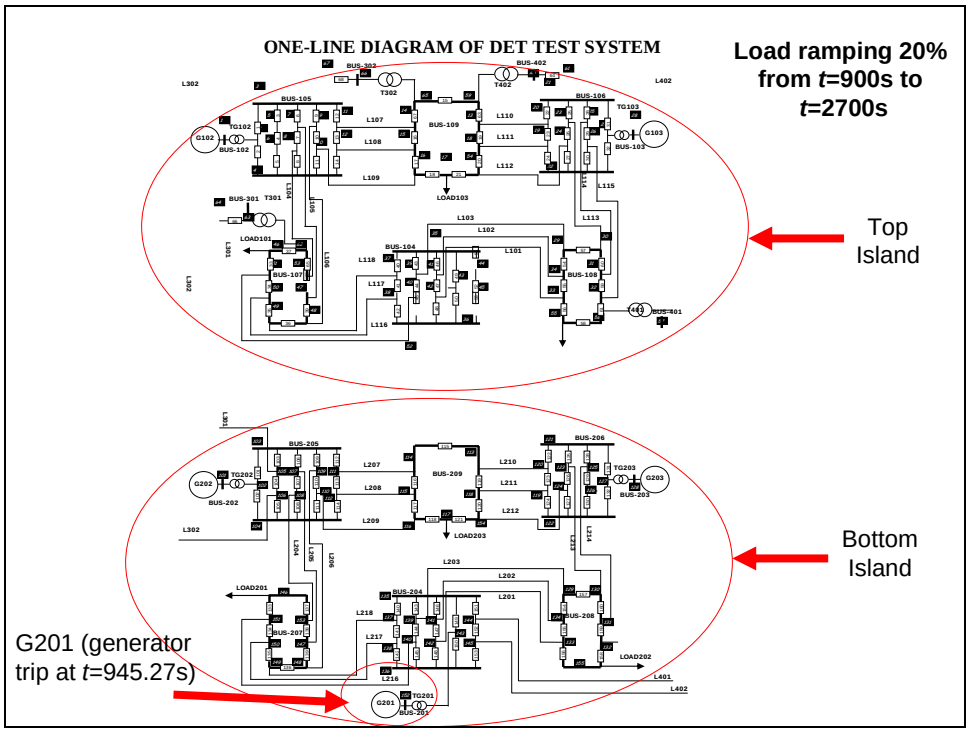

Fig. 48: The two islands resulting from the sequence of events in Fig. 47

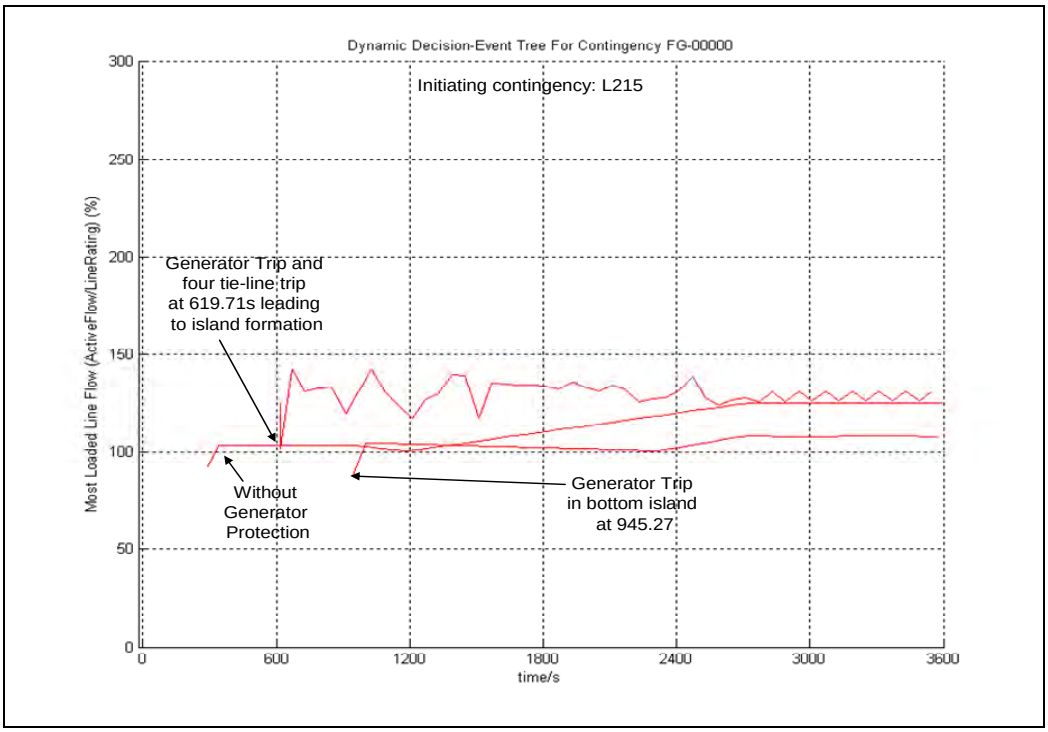

Fig. 49: Maximum line flow in an islanded scenario

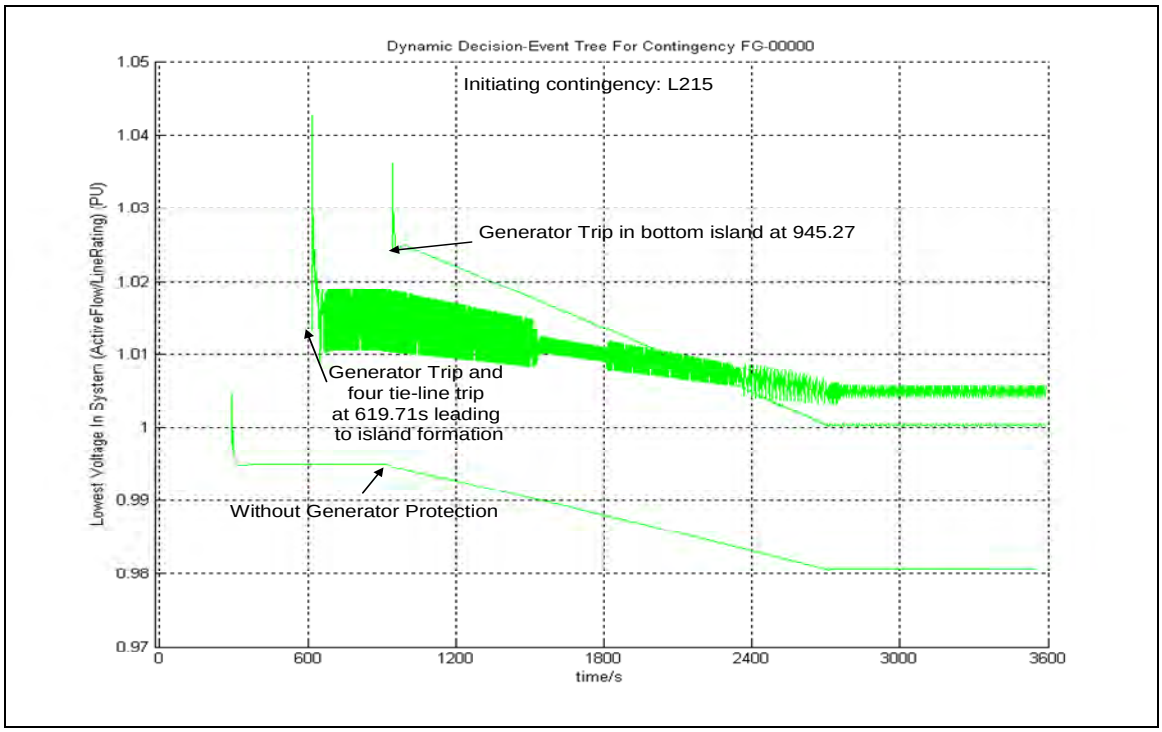

Fig. 50: Lowest voltage in the system in an islanded scenario

In both the scenarios described above - one leading to cascading, and the other leading to islanding, we observe that after the initiating event, there is a period of slow progression of trip events, which is followed by a fast succession of events, leading to high consequence events – like total system blackout, or unstable island formation, which ultimately culminates in cascading. This gives a chance to the operator to take corrective actions during the slow progression period to avoid the disaster, if he is aware of the complex unfolding of the future events.

In the next example shown in Fig. 51, the initiating event is a generator trip. In this case as well, the system is highly stressed, and the simulation results indicate that it would lead to cascading. However, if proper control actions are taken at the right time, the long term stability of the system can be ensured. Fig. 52 shows the simulation results with the corrective actions taken by the operator at t=608.74 and t=904.60. The first corrective action taken at t=608.74 brings the maximum line flow within the desired limits, and the system becomes stable after the initiating event and the transients. However, due to load ramping, the system again violates the operational constraints at a later time, as can be seen in Fig. 52. The second control action initiated at t=904.60, which involves multiple load shedding events at different points of time ensures system stability. Fig. 53 shows the lowest system voltage before and after the control actions following the initiating event.

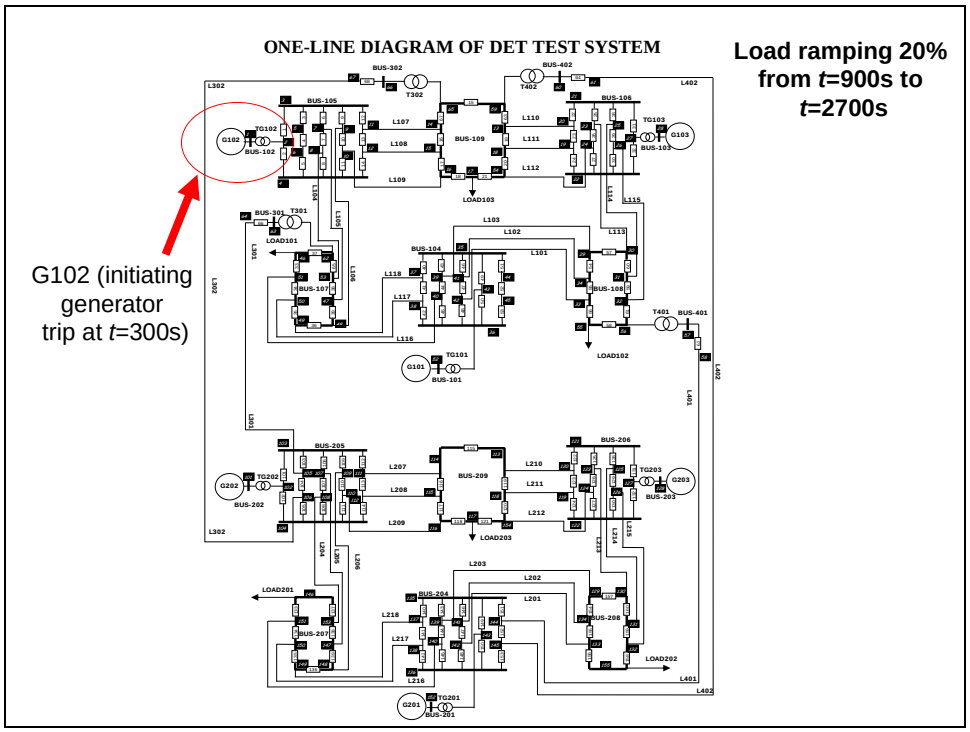

Fig. 51: A scenario with the initiating contingency as generator trip

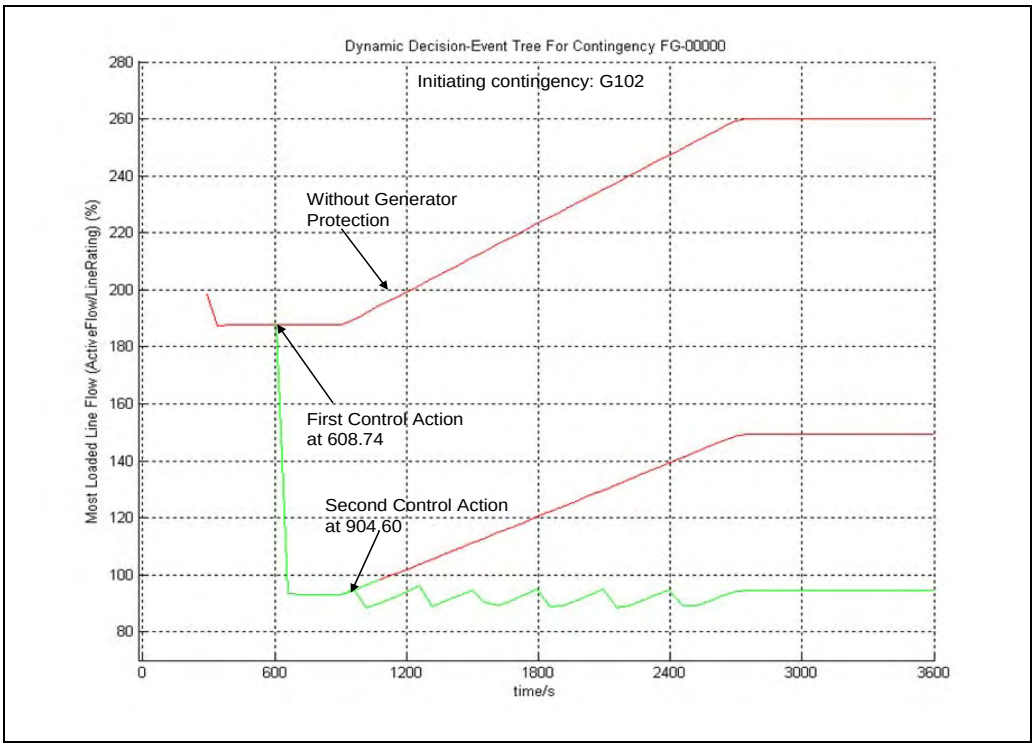

Fig. 52: Maximum line flow with corrective actions to prevent generator trip and relieve line overloading

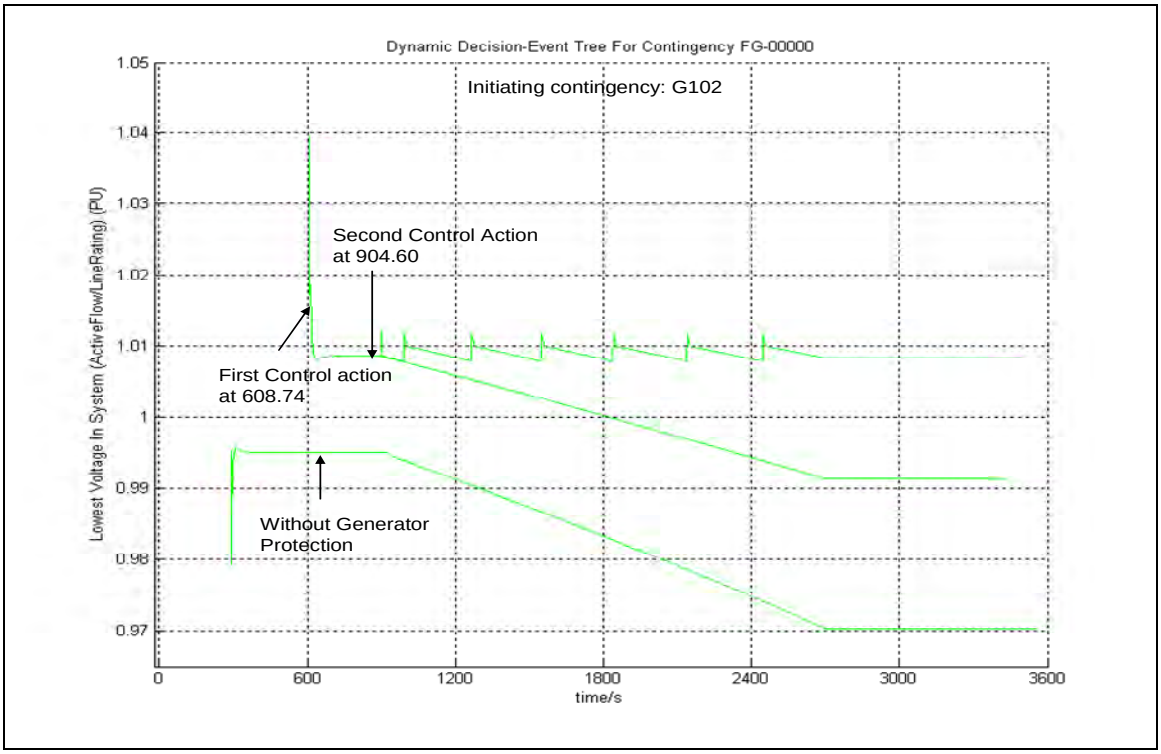

Fig. 53: Lowest voltage in the system with corrective actions to prevent generator trip and relieve line overloading

6 Conclusions

We have proposed a systematic way to identify power system initiating contingencies (including higher-order) for operational use. It is the first to use B-matrix to represent the connective of functional groups (also call protection control groups). It is the first to give the formula in matrix form to evaluate the probabilities of fault plus stuck breaker contingencies. The work extends the conventional contingency list by including a subset of high-order contingencies, which is identified through topology processing.

This work is the first to propose the use of dynamic event tree as an operational defense plan to cascading events in power systems. The DET can provide guidance for system operator to respond rapidly to the high-risk *N-k* contingencies. The idea significantly improves the readiness of system operators to possible cascadings.

We tested our DET concept on a small system, which proved the effectiveness of DET as a decision support tool for control room operator. The DET engine we designed is seamlessly integrated with system real time information such as topology and maintenance scheduling. Whenever the DET engine sees an overloading problem, it can suspend the on-going dynamic simulation process and does a static optimization (linear programming) to search for the redispatch to relieve the overloading. The contribution of this work can be summarized as the following bullets

- Proposed a systematic approach to strategically select *N-k* contingencies using system real-time topology information;
- Developed a method for contingency selection with an algorithm to calculate event probability as well;
- Designed a long-term dynamic simulation tool that
    - Integrates with system topology data in EMS;
    - Performs static optimization in a search for operator decision;
    - Accurately models generation protection systems
    - Is computationally enhanced via implementation of intelligent Jacobian updating and multifrontal linear solvers
- Proposed the use of the dynamic event tree (DET) to model and store possible cascading sequences;

Although it is unreasonable to claim that blackouts can be completely prevented, we can nonetheless reduce the frequency and impact of such high consequence events. This requires a comprehensive effort which includes innovations in tools, and training in those tools to build confidence in the individuals responsible for decision making. Blackouts typically result from low probability events. Corrective control is the operational solution to blackouts. It is event-based with actions determined on-line via anticipatory computing as decision support for the operator. This research addresses the need of an on-line tracking and blackout avoidance decision support tool. A follow-on project has just begun which will deploy the simulator developed in this work as a testing platform to explore the extent to which we may increase its computational efficiency via parallel implementation of numerical integration methods on an IBM Blue Gene/L Supercomputer.

7 Future Recommendations Based on Discussion with the Industry

1) Numerical analysis:
    a. Adaptively varying theta at every time step of simulation to minimize the local error and integrating with a different integration solver at every time step to study computational savings.
2) Field Trial and Testing
    a. Doing field trials: this would require system model from the EMS with associated dynamic data and development of an interface with the software with its associated data format.
    b. Test the developed software with large systems.
3) Out-of-Step Relaying across cutplanes [119,120]
    a. Well designed controlled system separation schemes, using special protection systems and/or Out-of-Step (OST) and power swing blocking (PSB) functions provide a safety net to lessen the consequences of major system disturbances.
    b. OST schemes for large steam turbo generators should be coordinated with the system OST schemes.
    c. Implementation of OST schemes for interregional cutplanes. Examples of cutplanes are the California- Oregon flow, or the east-of-river flow into southern California.
    d. Development of systematic methodology of quantified blackout risk assessment for types of cascades producing OST in stability studies. Assessment of probability of cascades leading to the OST conditions along these cutplanes

APPENDIX A: Rare Event Approximation

Suppose $p_1, p_2, \ldots, p_n$ are the individual probabilities of a group of independent events $E_1, E_2, \ldots E_3$. The probability of a compound event, i.e., a combination of events $E_1, E_2, \ldots, E_n$, can always be expressed as a polynomial of $p_1, p_2, \ldots, p_n$. For example, the probability of the event $(E_1 \cap E_2) \cup E_3$ is $p_3+p_1p_2-p_1p_2p_3$ Further suppose that $p_1, p_2, \ldots, p_n$ are all of approximately the same order of magnitude, then the order of magnitude of each product term in the polynomial will depend on how many terms are in the product. We call the number of terms in the product the *probability order*. Thus, the probability of $(E_1 \cap E_2) \cup E_3$ is composed of three different terms p_3 (probability *order 1*), p_1p_2 (probability *order 2*), and $p_1p_2p_3$ (probability *order 3*). ***In many decision problems, knowledge of the "probability orders" of the significant events is sufficient to distinguish between alternatives.***

The basic idea of rare event approximation is that, if the individual probabilities of a group of independent events are very small, we can always simplify the calculation by omitting the higher order terms of the polynomial without much loss of precision [18]. In the given example, if we knew that p_1, p_2, and p_3 were very small, then the probability of $(E1 \cap E2) \cup E3$ could be approximated as $p_3+p_1p_2$, or even as p_3.

Often, the failure probability of an individual component is very small for a well-managed system such as a power system. The fault probability of a power system component is usually at the magnitude of 10^{-6} per hour (or <1% per year) [121]. Suppose the fault probability of a line is p_1 per hour and the failure probability of a breaker is p_2/hour. Obviously, they are not exclusive events. The probability of a fault (p_1), breaker in a failed state (p_2), or both can be expressed as $p_1+p_2-p_1p_2$, assuming the two events are independent. Considering the small nature of p_1 and p_2, if we ignore the probability component of simultaneous occurrence of the two events, the error is only about 10^{-12}.

The implication is that when dealing with rare events, the probability of a compound event is dominated by the lowest *order* terms, and thus the probability *order* is a reasonable measure of event's probability. Based on this idea, we focus on the high order events with higher probability first, then lower probability, since, as the order of contingency increases, the probability of its occurrence decreases sharply to infinitesimal. A complete discussion of rare event systems can be found in [18].

APPENDIX B: Pseudo Code for Graph Search Algorithm for Functional Group Decomposition

This is a Breath-first search algorithm.

1. *Beginning of decomposition;*
2. *Label all components (bus section, non switching components (lines, capacitors, generators, transformers etc),switching components (switches, breakers etc) as unvisited;*
3. *Arbitrarily choose one unvisited vertex (bus section) as a starting component;*
4. *Initialize functional group and bus indices;*
5. *Establish a new empty functional group object without any component in it;*
6. *Add the chosen bus section to the functional group object as its first component;*
7. *Starting from this vertex, merge the functional group's immediate neighboring components (lines, capacitors, generators, transformers and other non switching components) into the group and label them as visited;*
8. *The step 2 continues until the group expands to its border, where the bordering components are all switching components (breakers and open switches);*
9. *If all components in the power system are visited, stop searching and go to the last step; else choose another unvisited bus section and return to step 2 all over again;*
10. *End of decomposition.*

APPENDIX C: Pseudo Code for Graph Search Algorithm for Inadvertent Tripping Contingency

1. *Graph Search Algorithm outlined in Appendix B finds all the Functional Group;*
2. *For each Functional Group we find the interfacing elements (breakers and switches) and the components in the Functional Group ;*
3. *For a failure/fault in the Functional Group extract the interfacing elements and the Functional Group connected to them (step 2);*
4. *Check if any of the Functional Groups extracted above have components other than a Bus section; then the one with component/components other than only Bus section can suffer inadvertent tripping;*
5. *If the Functional Groups connected the to faulted/failed Functional Group contain only Bus section as their components then we go for second tier of search;*
    a) *Identify the interfacing circuit breaker and Functional Group that connect the Bus section and take the union to form the set of Functional Groups excluding the failed/faulted Functional Group;*
    b) *If only one of the remaining Functional Groups has a component other than Bus section then only that Functional Group can trip (SB-TB) and stop.*
    c) *Else if there are more than one Functional Group with component other than Bus section then go for the third tier of search;*
6. *End of decomposition*

APPENDIX D: One-Line Diagram of Test System

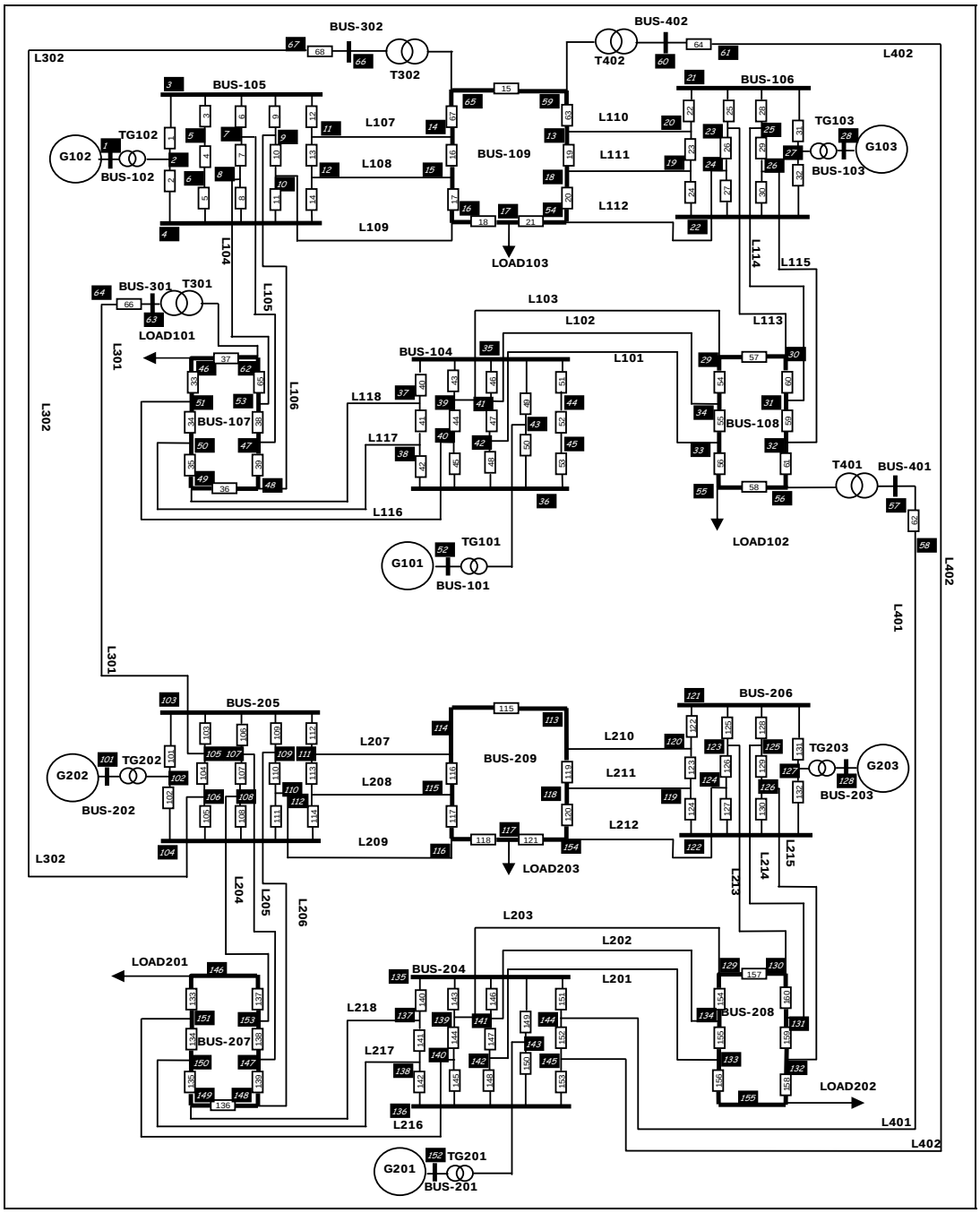

Fig. 54: One line diagram of a DET test system

APPENDIX E: Test System Data

Table 17: The bus-breaker connection data

fb	to	name	No	fb	to	name	No	fb	to	name	No	fb	to	name
2	3	BUS-7	33	46	51	BUS-5	67	18	65	BUS-8	131	127	121	BUS-9
2	4	BUS-7	34	51	50	BUS-5	68	66	67	BUS-8	132	122	127	BUS-9
5	3	BUS-7	35	50	49	BUS-5	101	102	103	BUS-7	133	146	151	BUS-5
5	6	BUS-7	36	49	48	BUS-5	102	102	104	BUS-7	134	151	150	BUS-5
6	4	BUS-7	37	46	62	BUS-5	103	105	103	BUS-7	135	150	149	BUS-5
7	3	BUS-7	38	53	47	BUS-5	104	105	106	BUS-7	136	149	148	BUS-5
8	7	BUS-7	39	47	48	BUS-5	105	106	104	BUS-7	137	146	153	BUS-5
8	4	BUS-7	40	37	35	BUS-4	106	107	103	BUS-7	138	153	147	BUS-5
9	3	BUS-7	41	37	38	BUS-4	107	108	107	BUS-7	139	147	148	BUS-5
9	10	BUS-7	42	38	36	BUS-4	108	108	104	BUS-7	140	137	135	BUS-4
10	4	BUS-7	43	39	35	BUS-4	109	109	103	BUS-7	141	137	138	BUS-4
3	11	BUS-7	44	39	40	BUS-4	110	109	110	BUS-7	142	138	136	BUS-4
11	12	BUS-7	45	40	36	BUS-4	111	110	104	BUS-7	143	139	135	BUS-4
12	4	BUS-7	46	41	35	BUS-4	112	103	111	BUS-7	144	139	140	BUS-4
13	14	BUS-8	47	42	41	BUS-4	113	111	112	BUS-7	145	140	136	BUS-4
14	15	BUS-8	48	42	36	BUS-4	114	112	104	BUS-7	146	141	135	BUS-4
15	16	BUS-8	49	43	35	BUS-4	115	113	114	BUS-8	147	142	141	BUS-4
16	17	BUS-8	50	43	36	BUS-4	116	114	115	BUS-8	148	142	136	BUS-4
13	18	BUS-8	51	44	35	BUS-4	117	115	116	BUS-8	149	143	135	BUS-4
65	54	BUS-8	52	45	44	BUS-4	118	116	117	BUS-8	150	143	136	BUS-4
17	54	BUS-8	53	45	36	BUS-4	119	113	118	BUS-8	151	144	135	BUS-4
20	21	BUS-9	54	34	29	BUS-6	120	118	154	BUS-8	152	145	144	BUS-4
20	19	BUS-9	55	34	33	BUS-6	121	117	154	BUS-8	153	145	136	BUS-4
19	22	BUS-9	56	33	55	BUS-6	122	120	121	BUS-9	154	134	129	BUS-6
21	23	BUS-9	57	29	30	BUS-6	123	120	119	BUS-9	155	134	133	BUS-6
23	24	BUS-9	58	55	56	BUS-6	124	119	122	BUS-9	156	133	155	BUS-6
24	22	BUS-9	59	31	32	BUS-6	125	121	123	BUS-9	157	129	130	BUS-6
25	21	BUS-9	60	30	31	BUS-6	126	123	124	BUS-9	158	155	132	BUS-6
25	26	BUS-9	61	56	32	BUS-6	127	124	122	BUS-9	159	131	132	BUS-6
26	22	BUS-9	62	57	58	BUS-6	128	125	121	BUS-9	160	130	131	BUS-6
27	21	BUS-9	65	53	62	BUS-5	129	125	126	BUS-9	-	-	-	-
22	27	BUS-9	66	63	64	BUS-5	130	126	122	BUS-9	-	-	-	-

Table 18: Line data for the test system

NAME	F-BUS	T-BUS
L1	42	33
L2	41	34
L3	39	29
L4	53	8
L5	47	7
L6	48	9
L7	11	14
L8	12	15
L9	10	16
L10	13	20
L11	18	19
L12	54	24
L13	30	23
L14	31	25
L15	32	26
L16	40	51
L17	38	50
L18	37	49
L101	142	133
L102	141	134
L103	139	129
L104	153	108
L105	147	107
L106	148	109
L107	111	114
L108	112	115
L109	110	116
L110	113	120
L111	118	119
L112	154	124
L113	130	123
L114	131	125
L115	132	126
L116	140	151
L117	138	150
L118	137	149
L301	105	64
L302	106	67
L401	144	58

APPENDIX F: IEEE-RTS 24 Bus Test System

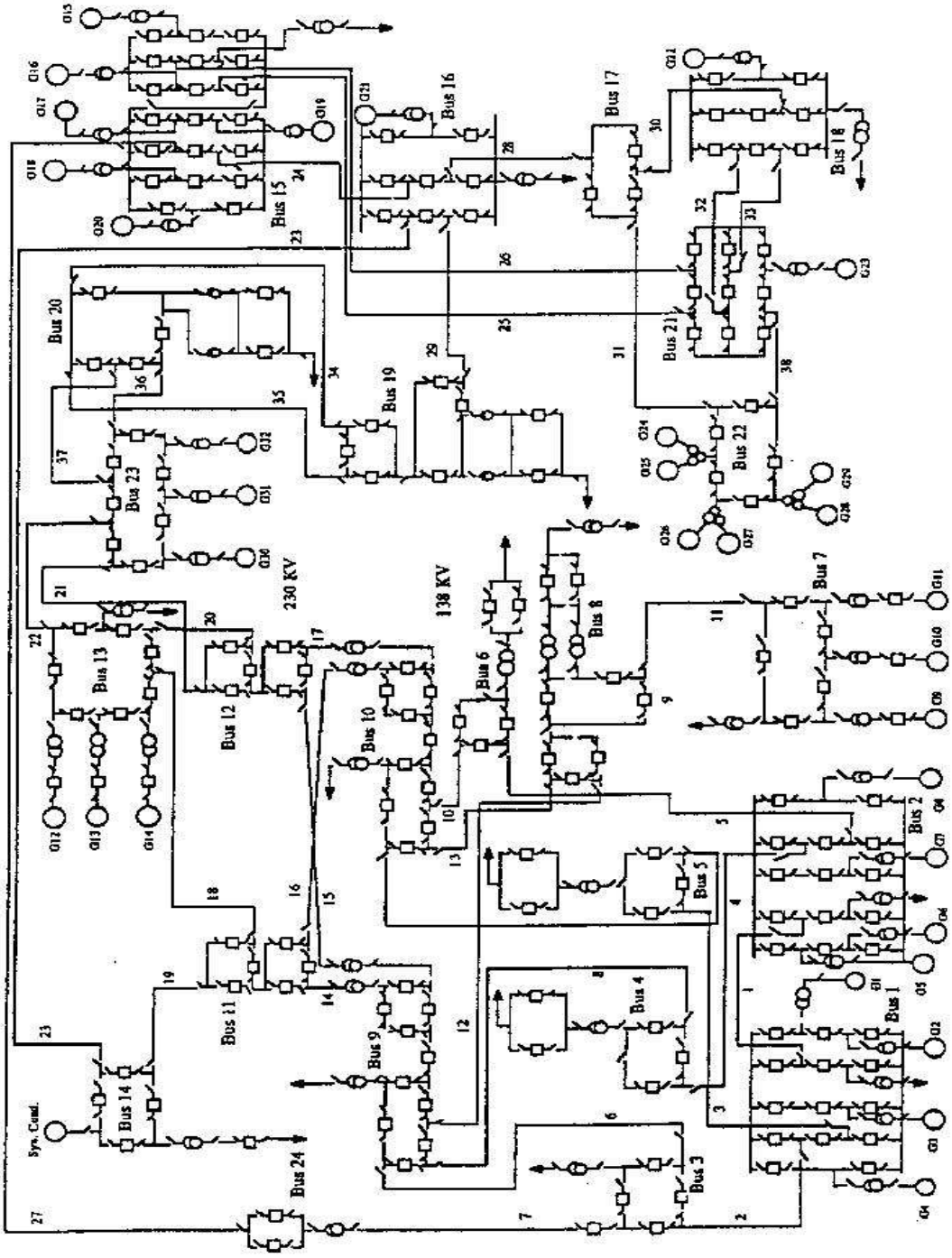

Fig. 55: IEEE RTS-24 bus test system substation diagram

APPENDIX G: Optimization Code for Redispatch and Load Shedding

Since branch loading is a slow process and each line usually has its emergency rating in addition to its normal rating to allow overloaded for a short time period, a system operator has the time needed to perform redispatch so that the power flow of related line is adjusted to its nominal limit. Load-shedding happens only if it is impossible to bring the power flow in each line back to its long-term rating using some other means. In order to simulate the action of system operator, we use the follow linear program problem to model what a system operator will do to avoid overloading.

Objective:

$$Max \sum_{i\in\{1,\ ...\ N\}} \alpha_i \times P_{D_i} \qquad \text{G.1}$$

Constraint:

$P_{D_i}^{\max} \geq P_{D_i} \geq 0, \quad i \in \{1,\ ...\ N_D\}$, The served load at bus i should be less than the total demand $P^{\max}$ at bus i;

$P_{G_i}^{\max} \geq P_{G_i} \geq 0, \quad i \in \{1,\ ...\ N\}$, Each generator generates between $0MW$ to $P_{\max}$;

$\gamma_i P_{B_i}^{\max} \geq P_{B_i} \geq -\gamma_i P_{B_i}^{\max}, \quad i \in \{1,\ ...\ N_B\}$, The power flow in each branch (line or transformer) is limited by its rating

$B' \times \theta = P^{inject} = (P_G - P_D)$, DC power flow equations;

$(D_B \times A) \times \theta - P_B = 0$, Branch flow equations;

where

N_D is the total number of load buses;

N_B is the total number of branches;

N_G is the total number of generating buses;

P_{D_i} is the load demand at bus i;

α_i is the price factor to shed one unit MW load at bus i;

L_i is the total load (MW) served at bus i;

P_{G_i} is the real power generation at bus i;

$P_{G_i}^{\max}$ is the maximum real power generation at bus i, it is the summation of rating of all generators connected to bus i;

P_{B_i} is the real power flow in branch i;

$P_{B_i}^{\max}$ is the short term rating (MVA) of branch i;

γ_i is the constant factor to account for the power factor of the power flow in branch i and $1 \geq \gamma_i \geq 0$;

$B^{'}$ is the $N \times N$ B-matrix used in DC power flow and N is the number of buses;

A is the $\mathrm{M} \times N$ adjacency (or incidence) matrix

D_B is the $M \times M$ diagonal matrix where the i^{th} diagonal element is the admittance of the i^{th} branch.

θ is the $N \times 1$ vector representing the voltage angles in radius at each bus;

P^{inject} is the $N \times 1$ vector representing the net power injection for each bus, and its element P_i can be calculated by $P_i = P_{g_i} - L_i$.

Not all the buses are both generator bus and load bus. It is observed that some buses are load bus only, some others are generation bus only, and some others may have no load or generator connected to them. If bus i has no generator connected to it, then we let $P_{G_i}^{\max}$ to be zero so that inequality $P_{G_i}^{\max} \geq P_{G_i} \geq 0$ will force the generation at bus i to be zero. We do the same thing for those buses without load connected to them.

In order to solve the above linear programming problem, we need to standardize the above inequalities and equalities so that we can use the standard LP subroutine in Matlab. We are going to take some time to elaborate our approach since we will use this approach again for our DET generating process later in this dissertation. We will change the object function and the constraint to the following standard format:

Objective:

$$\max f^T \cdot x \qquad \text{G.2}$$

Constraints:

$$A_{eq} \cdot x = b_{eq} \qquad \text{G.3}$$

$$lb \leq x \leq ub \qquad \text{G.4}$$

We define

$$P_G = \begin{pmatrix} P_{G_1} \\ P_{G_2} \\ \vdots \\ P_{G_{N_G}} \end{pmatrix}_{(N \times 1)} \quad ; \quad P_D = \begin{pmatrix} P_{D_1} \\ P_{D_2} \\ \vdots \\ P_{D_N} \end{pmatrix}_{(N \times 1)} \quad ; \quad P_B = \begin{pmatrix} P_{B_1} \\ P_{B_2} \\ \vdots \\ P_{B_M} \end{pmatrix}_{(M \times 1)} \quad ; \quad \theta = \begin{pmatrix} \theta_1 \\ \theta_2 \\ \vdots \\ \theta_N \end{pmatrix}_{(N \times 1)} \qquad \text{G.5}$$

$$P_G^{\max} = \begin{pmatrix} P_{G_1}^{\max} \\ P_{G_2}^{\max} \\ \vdots \\ P_{G_N}^{\max} \end{pmatrix}_{(N \times 1)} \quad ; \quad P_D^{\max} = \begin{pmatrix} P_{D_1}^{\max} \\ P_{D_2}^{\max} \\ \vdots \\ P_{D_N}^{\max} \end{pmatrix}_{(N \times 1)} \quad ; \quad P_B^{\max} = \begin{pmatrix} \gamma_1 P_{B_1}^{\max} \\ \gamma_2 P_{B_2}^{\max} \\ \vdots \\ \gamma_M P_{B_M}^{\max} \end{pmatrix}_{(M \times 1)} \quad ; \quad \theta^{\max} = \begin{pmatrix} \pi \\ \pi \\ \vdots \\ \pi \end{pmatrix}_{(N \times 1)} \qquad \text{G.6}$$

$$P_G^{\min} = \begin{pmatrix} 0 \\ 0 \\ \vdots \\ 0 \end{pmatrix}_{(N\times 1)} \quad ; \quad P_D^{\min} = \begin{pmatrix} 0 \\ 0 \\ \vdots \\ 0 \end{pmatrix}_{(N\times 1)} \quad ; \quad P_B^{\min} = \begin{pmatrix} -\gamma_1 P_{B_1}^{\max} \\ -\gamma_2 P_{B_2}^{\max} \\ \vdots \\ -\gamma_M P_{B_M}^{\max} \end{pmatrix}_{(M\times 1)} \quad ; \quad \theta^{\min} = \begin{pmatrix} -\pi \\ -\pi \\ \vdots \\ -\pi \end{pmatrix}_{(N\times 1)} \qquad \text{G.7}$$

$$\alpha_G = \begin{pmatrix} 0 \\ 0 \\ \vdots \\ 0 \end{pmatrix}_{(N\times 1)} \quad ; \quad \alpha_D = \begin{pmatrix} \alpha_1 \\ \alpha_2 \\ \vdots \\ \alpha_N \end{pmatrix}_{(N\times 1)} \quad ; \quad \alpha_B = \begin{pmatrix} 0 \\ 0 \\ \vdots \\ 0 \end{pmatrix}_{(M\times 1)} \quad ; \quad \alpha_\theta = \begin{pmatrix} 0 \\ 0 \\ \vdots \\ 0 \end{pmatrix}_{(N\times 1)} \qquad \text{G.8}$$

$$x = \begin{pmatrix} P_G^{\mathrm{T}} & \mathrm{P}_{\mathrm{D}}^{\mathrm{T}} & P_B^T & \theta^T \end{pmatrix}^{\mathrm{T}} \qquad \text{G.9}$$

$$f = \begin{pmatrix} \alpha_G^T & \alpha_D^T & \alpha_B^T & \alpha_\theta^T \end{pmatrix} \qquad \text{G.10}$$

$$\text{where } A_{eq} = \begin{pmatrix} 0 & 0 & I_{M\times M} & -D_{M\times M} \times A_{M\times N} \\ I_{N\times N} & -I_{N\times N} & 0 & -B'_{N\times N} \end{pmatrix}_{(M+N)\times(N+N+M+N)} \qquad \text{G.11}$$

where the submatrix A, D and B inside A_{eq} are what we have defined at the beginning of this section, and I is the identity matrix. A_{eq}, ub and lb are defined as follows

$$B_{eq} = \begin{pmatrix} 0 \\ \vdots \\ 0 \end{pmatrix}_{(M+N)\times 1} \qquad ub = \begin{pmatrix} P_G^{\max} \\ P_D^{\max} \\ P_B^{\max} \\ \theta^{\max} \end{pmatrix} \qquad lb = \begin{pmatrix} P_G^{\min} \\ P_D^{\min} \\ -P_B^{\max} \\ \theta^{\min} \end{pmatrix} \qquad \text{G.12}$$

After solving the LP to obtain a feasible solution for x, we get a new system profile that has no overloading problem. The total forced load shedding can be obtained through the following formula:

$$\sum_{i\in\{1,2,\cdots,N\}} (P_{D_i}^{\max} - P_{D_i}) \qquad \text{G.13}$$

We use a simple example to show our method. The following diagram shows a 2-generator 3-bus system taken from [7]. For this system, we assume each load is of the same importance such that the cost to shed 1.0 p.u. of load is uniformly one. The fact device can adjust the flow on each line so that power flow factor for each line is 0.8, i.e. $\gamma_i = 0.8$ for $i = 1,\ 2,\ 3$. Since we need the adjacency matrix of the graphic representation of this system, which model the topology of the power system as a directed graph, we label each line with an arrow showing the reference direction of the active power flow in the line. There is not generator at BUS-2 and there is no load at BUS-1 and BUS-3. The constraints in the LP problem formulation will force the generation at BUS-2 and the load at BUS-1 and BUS-3 to be zero.

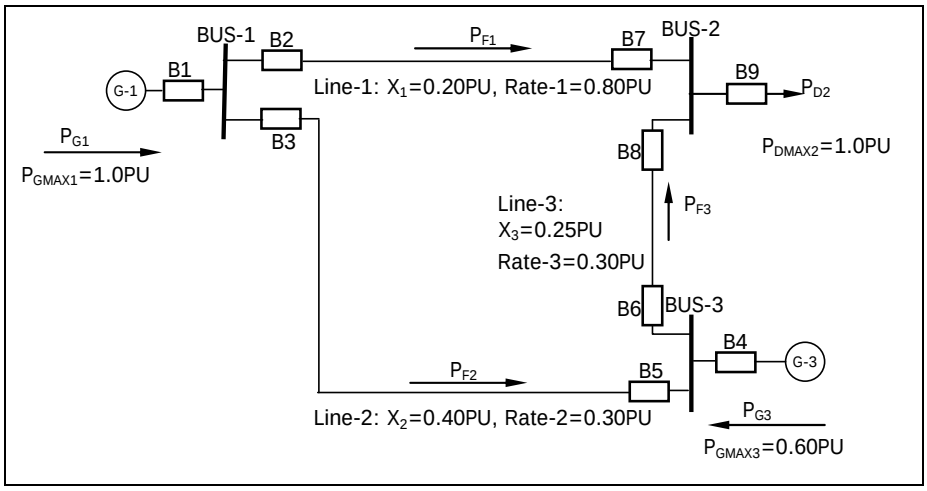

Fig. 56: Example system for linear programming illustration

Objective:

$$\max f^T \cdot x =$$
$$(0,\ 0,\ 0,\ 1,\ 1,\ 1,\ 0,\ 0,\ 0,\ 0,\ 0,\ 0)\times \qquad \text{G.14}$$
$$(P_{G_1},\ P_{G_2},\ P_{G_3},\ P_{D_1},\ P_{D_2},\ P_{D_3},\ P_{B_1},\ P_{B_2},\ P_{B_3},\ \theta_1,\ \theta_2,\ \theta_3,)^T$$

Constraints:

$$\begin{pmatrix} 0 & 0 & 0 & 0 & 0 & 0 & 1 & 0 & 0 & 5.0 & -5.0 & 0 \\ 0 & 0 & 0 & 0 & 0 & 0 & 0 & 1 & 0 & 2.5 & 0 & -2.5 \\ 0 & 0 & 0 & 0 & 0 & 0 & 0 & 0 & 1 & 0 & -4.0 & 4.0 \\ 1 & 0 & 0 & -1 & 0 & 0 & 0 & 0 & 0 & 7.5 & -5.0 & -2.5 \\ 0 & 1 & 0 & 0 & -1 & 0 & 0 & 0 & 0 & -5.0 & 9.0 & -4.0 \\ 0 & 0 & 1 & 0 & 0 & -1 & 0 & 0 & 0 & -2.5 & -4.0 & 6.5 \end{pmatrix} \times \begin{pmatrix} P_{G1} \\ P_{G2} \\ P_{G3} \\ P_{D1} \\ P_{D2} \\ P_{D3} \\ P_{B1} \\ P_{B2} \\ P_{B3} \\ \theta_1 \\ \theta_2 \\ \theta_3 \end{pmatrix} = 0 \qquad \text{G.15}$$

$$\begin{pmatrix} 0 \\ 0 \\ 0 \\ 0 \\ 0 \\ 0 \\ -0.8\times 0.80 \\ -0.8\times 0.30 \\ -0.8\times 0.30 \\ -\pi \\ -\pi \\ -\pi \end{pmatrix} \leq \begin{pmatrix} P_{G1} \\ P_{G2} \\ P_{G3} \\ P_{D1} \\ P_{D2} \\ P_{D3} \\ P_{B1} \\ P_{B2} \\ P_{B3} \\ \theta_1 \\ \theta_2 \\ \theta_3 \end{pmatrix} \leq \begin{pmatrix} 1.0 \\ 0 \\ 0.6 \\ 0 \\ 1.0 \\ 0 \\ 0.8\times 0.80 \\ 0.8\times 0.30 \\ 0.8\times 0.30 \\ \pi \\ \pi \\ \pi \end{pmatrix} \qquad \text{G.16}$$

Table 19: The solution for the above linear programming problem is listed in Fig. 56

P_{G1}	P_{G2}	P_{G3}	P_{D1}	P_{D2}	P_{D3}	P_{B1}	P_{B2}	P_{B3}	θ_1	θ_2	θ_3
0.81	0	0.07	0	0.88	0	0.64	0.17	0.24	-0.065	0.063	0.0027

Substitute the solution of the parameters in Table 19, we find the max load the system can serve is 88 MW (0.88 p.u.).

References

[1] N.B. Bhatt, " August 14, 2003 U.S. – Canada blackout," presented at the IEEE PES General meeting, Denver, CO, 2004

[2] W.R. Lachs - "Controlling Grid Integrity After Power System Emergencies," IEEE Transactions in Power Systems PWRS No.17 No.2 May 2002

[3] W.R. Lachs – "A New Horizon for System Protection Schemes," IEEE Transactions in Power Systems PWRS No.18 No. 1 – February 2003 pp.334-338

[4] Qiming Chen, "The probability, identification and prevention of rare events in power system," PhD Thesis, ECE, Iowa State University, 2004

[5] J. McCalley, "Transmission Security: Rules, Risks, and Blackouts," Midwest ISO's System Operator Training Short Course, April 24-28, 2006.

[6] P. Jian, J. McCalley, "On-line analysis of high-order contingencies," in Proc. North Amer. Power Symp., Oct. 15-16, 2001, pp. 297-302.

[7] Allen J. Wood, Bruce F. Wollenberg, "Power generation, operation and control," John Wiley & Sons, Inc., 1996

[8] A. O. Ekwue, "A review of automatic contingency selection algorithms for online security analysis," The Third International Conference on Power System Monitoring and Control, pp 152-155, June 26-28, 1991

[9] R. N. Allan, A. N. Adraktas, "Terminal effects and protection system failures in composite system reliability evaluation," IEEE Transactions on Power Apparatus and Systems, Vol. PAS-101, No. 12, pp 4557-4562, Dec. 1982

[10] R. Billinton, T. K. P. Medicherla, "Station originated multiple outages in the reliability analysis of a composite and transmission system," IEEE Transactions on Power Apparatus and Systems, Vol. PAS-100, No. 8, pp 3870-3878, Dec. 1982

[11] R. Billinton, P. K. Vohra, Sudhir Kumar, "Effect of Station originated outages in a composite system – adequate evaluation of the IEEE reliability test system," IEEE Transactions on Power Apparatus and Systems, Vol. PAS-104, No. 10, pp 2649-2656, Oct. 1985

[12] A. G. Phadke, J.S. Thorp, "Expose hidden failures to prevent cascading outages in power systems," IEEE Comput. Appl. Power, vol. 9, no. 3, pp. 20-23, Jul. 1996.

[13] D. C. Elizondo, J. de La Ree, A. G. Phadke, S. Horowitz, "Hidden failures in protection systems and their impact on wide area disturbances," in Proc. IEEE power Eng. Soc. Winter Meeting, vol. 2, 28 Feb. 2001, pp. 710-714

[14] Qiming Chen, "The probability, identification and prevention of rare events in power system" PhD Thesis, ECE, Iowa State University, 2004

[15] McCalley, J.D.; Vittal, V.; Abi-Samra, N., “An overview of risk based security assessment,” IEEE Power Engineering Society Summer Meeting, Vol. 1 ,pp 173-178, 1999

[16] Mohammad Modarres, Mark Kaminskiy, Vasiliy Krivtsov, “Reliability Engineering and Risk Analysis,” Marcel Dekker, Inc., 1999

[17] Arnljot Hoyland, Marvin Rausand, “System Reliability Theory Models and Statistical Methods,” John Wiley & Sons, Inc., 1994

[18] W.A. Thompson, Jr., “Point Process Models with Applications to Safety and Reliability,” Chapman and Hall, 1988

[19] J. Lewis Blackburn, “Protective relaying, principles and applications,” Marcel Dekker, Inc., 1987

[20] NERC (North American Reliability Council) Disturbance Analysis Working Group Database, “http://www.nerc.com/~dawg/database.html,” 1984-2001

[21] Xiumu Li, “Introduction to Graph Theory”, Publishing House of Huazhong Institute of Technology, China, 1986

[22] Harary, F., Graph Theory. Reading, MA: Addison-Wesley, 1994

[23] Sanchez-Gasca, J.J.; D'Aquila, R.; Price, W.W.; Paserba, J.J.; “Variable time step, implicit integration for extended-term power system dynamic simulation,” IEEE Conference Proceedings of Power Industry Computer Application Conference, pp 183-189, May 7-12, 1995

[24] Astic, J.Y.; Bihain, A.; Jerosolimski, M.; “The mixed Adams-BDF variable step size algorithm to simulate transient and long-term phenomena in power systems,” IEEE Transactions on Power Systems, Vol. 9, Issue 2, pp 929-935, May 1994

[25] Paul M. Anderson, A. A. Fouad, Power system control and stability, the Institute of Electrical and Electronic Engineers, Inc., 1994

[26] Brenan K.E., Campbell S.L.Petzold L.R, Numerical Solution of Initial-Value Problems in Differential-Algebraic Equations, SIAM,1996

[27] M. Berzins, R.M. Furzeland, “An Adaptive Theta Method for the Solution of Stiff and Non-Stiff Differential Equations,” App. Num. Math., Vol. 9, pp 1.19, 1992.

[28] F.L. Alvarado, R.H. Lasseter, J.J. Sanchez, “Testing of Trapezoidal Integration with Damping for the Solution of Power Transient Problems,” IEEE Trans. on Power App. and Syst., Vol. PAS-102, No. 12, pp. 3783-3790, 1983.

[29] T. Orfanogianni, R. Bacher. Using Automatic Code Differentiation in Power Flow Algorithms. IEEE Transactions on Power Systems, Vol. 14, No. 1, February 1999.

[30] J. Johnson, P. Vachranukunkiet, S. Tiwari, P. Nagvajara, C. Nwankpa, “Performance Analysis of Loadflow Computation Using FPGA,” Proc. of 15th Power Systems Computation Conference 2005.

[31] Davis, T. A. and Duff, I. S, “A combined unifrontal/multifrontal method for unsymmetric sparse matrices,” ACM Trans. Math. Software, Vol. 25, Issue 1, pp. 1–19, 1999.

[32] Davis, T. A., “Algorithm 832: UMFPACK - An unsymmetric-pattern multifrontal method,” ACM Trans. Math. Software, Vol. 30, Issue 2, pp. 196-199, 2004.

[33] Davis, T. A. ‘A column pre-ordering strategy for the unsymmetric-pattern multi-frontal method’, ACM Trans. Math. Software, Vol. 30, Issue 2, pp. 165-195, 2004.

[34] Davis, T. A., Amestoy, P. R. and Duff, I. S. ‘Algorithm 837: AMD, an approximate minimum degree ordering algorithm’, ACM Trans. Math. Software, Vol. 30, Issue 3, pp. 381-388, 2004.

[35] Davis, T. A., Gilbert, J. R. and Larimore, E. ‘Algorithm 836: COLAMD, an approximate column minimum degree ordering algorithm’, ACM Trans. Math. Software, Vol. 30, Issue 3, pp. 377-380, 2004.

[36] Irons, B.M. ‘A frontal solution scheme for finite element analysis’, Numer. Meth. Engg, Vol. 2, pp. 5-32.1970.

[37] P. Hood. Frontal solution program for unsymmetric matrices. Int. J. Numer. Meth. Engng. 10, 379-400, 1976.

[38] I.S. Duff, MA32 - A package for solving sparse unsymmetric systems using the frontal method. Technical Report AERE R11009, Her Majesty's Stationery Office, London, 1981

[39] Dongarra J. J., J. Du Croz and S. Hammarling, A set of level 3 basic linear algebra subprograms. ACM -Trans. Math. Sofiw. 16, 1-17 (1990).

[40] K. V. Camarda, M. A. Stadtherr. Frontal solvers for process engineering: local row ordering strategies. Computers in Chemical Engineering, 22, 333-341, 1998.

[41] Zitney S. E., Sparse matrix methods for chemical process separation calculations on supercomputers. In Proceedings of Supercomputing ‘92, pp. 414-423, IEEE Computer Society Press, Los Alamitos, CA (1992).

[42] Zitney S. E. and M. A. Stadtherr, Frontal algorithms for equation-based chemical process flow sheeting on vector and parallel computers. -Computers them. Engng ?c= 319-338, 1993.

[43] Zitney S. E: and fi. A. Stadtherr, Supercomputing strategies for the design and analysis of complex separation systems. Znd. Ennnn them. Res. 32. 604-612 1993.

[44] Zitney S. E., R. J. kmarger and P. Winter, The‘impact.of supercomputing on dynamic simulation using the SPEEDUP system., Presented at AIChE National Meeting, New Orleans, March 1992.

[45] Zitney S. E., L. Brilll, L. Lang and R. Zeller, Plant wide dynamic simulation on supercomputers: modeling a Bayer distillation process. Presented at Foundations of Computer Aided Process Design, Snowmass Village, Colorado, July 1994.

[46] Zitney S. E., K. V. Camarda and M. A. Stadtherr, Impact of supercomputing in simulation and optimization of process operations. In Proc. Second Int. Conf. on Foundations of Computer-Aided Process Operations (Edited by Rippen D. W. T., J. C. Hale and J. F. Davis), pp. 463-468. CACHE Corp., Austin, TX (1994b)

[47] I. S. Duff. A review of frontal methods for solving linear systems. Computer Physics Communications 97, 45-52, 1996.

[48] I. S. Duff, J.A. Scott. A comparison of frontal software with other sparse direct solvers. Technical Report RAL-TR-96-102 (Revised), Rutherford Appleton Laboratory, 1996a.

[49] I. S. Duff, J.A. Scott. The design of a new frontal code for solving sparse unsymmetric systems. ACM

Trans. Mathematical Software, 22(1), 30-45, 1996b.

[50] I. S. Duff, J.A. Scott. MA42 - a new frontal code for solving sparse unsymmetric systems. Technical Report RAL-93-064, Rutherford Appleton Laboratory, 1993.

[51] I. S. Duff, J.K. Reid. The multifrontal solution of indefinite sparse symmetric linear systems. ACM Trans. Math. Softw. 9, 302-325, 1983.

[52] I. S. Duff, J.A. Scott. The use of multiple fronts in Gaussian elimination. in J. Lewis, ed., 'Proceedings of the Fifth SIAM Conference Applied Linear Algebra', pp. 567 571. SIAM, 1994b.

[53] I. S. Duff, J.K. Reid. The multifrontal solution of unsymmetric sets of linear systems. SIAM J. Sci. Stat. Comput. 5, 633-641, 1984.

[54] I. S. Duff, J.K. Reid. The design of MA48, a code for the direct solution of sparse unsymmetric linear systems of equations. ACM Trans. Mathematical Software, 22, 187-226, 1996.

[55] C. C. Ashcraft, R. Grimes. The influence of relaxed supernode partitions on the multifrontal method. ACM Trans. Math. Softw. 15, 4, 291-309, 1989.

[56] M. T. Heath, P. Raghavan. A Cartesian parallel nested dissection algorithm. SIAM J. Matrix Anal. Applic. 16, 1, 235-253, 1995.

[57] A. Gupta, F. Gustavson, M. Joshi, G. Karypis, V. Kumar. PSPASES: an efficient and parallel sparse direct solver. In Kluwer Intl. Series in Engineering and Science, T. Yang, Ed. Vol. 515. Kluwer, 1999.

[58] J. W. H. Liu. The multifrontal method for sparse matrix solution: Theory and practice. SIAM Rev. 34, 1, 82-109, 1992.

[59] I. S. Duff, J. K. Reid. MA27 - a set of Fortran subroutines for solving sparse symmetric sets of linear equations. Tech. Rep. AERE-R-10533, AERE Harwell Laboratory, United Kingdom Atomic Energy Authority, 1982.

[60] I. S. Duff. A new code for the solution of sparse symmetric definite and indefinite systems. Tech. Rep. TR-2002-024, Rutherford Appleton Laboratory, 2002.

[61] P. R. Amestoy, I. S. Duff. Vectorization of a multiprocessor multifrontal code. Intl. J. Supercomputer Appl. 3, 3, 41–59, 1989.

[62] P. R. Amestoy, I. S. Duff, J.-Y. L'Excellent, J. Koster. A fully asynchronous multifrontal solver using distributed dynamic scheduling. SIAM J. Matrix Anal. Applic. 23, 1, 15–41, 2001a.

[63] I. S. Duff. The solution of nearly symmetric sparse linear systems. In Computing methods in applied sciences and engineering, VI, R. Glowinski and J.-L. Lions, Eds. North Holland, Amsterdam New York and London, 57–74, 1984.

[64] I. S. Duff, J. K. Reid. A note on the work involved in no-fill sparse matrix factorization. SIAM J. Num. Anal. 3, 37–40, 1983b.

[65] P. R. Amestoy, C. Puglisi. An unsymmetrized multifrontal LU factorization. SIAM J.Matrix Anal. Applic. 24, 553–569, 2002.

[66] T. A. Davis, I. S. Duff. An unsymmetric-pattern multifrontal method for sparse LU factorization. SIAM J. Matrix Anal. Applic. 18, 1, 140–158. 1997.

[67] A. Gupta. Improved symbolic and numerical factorization algorithms for unsymmetric sparse matrices. SIAM J. Matrix Anal. Applic. 24, 529–552, 2002.

[68] S. M. Hadfield. On the LU factorization of sequences of identically structured sparse matrices within a distributed memory environment. Ph.D. thesis, University of Florida, Gainesville, FL, 1994.

[69] S. M. Hadfield, T. A. Davis. The use of graph theory in a parallel multifrontal method for sequences of unsymmetric pattern sparse matrices. Cong. Numer. 108, 43–52, 1995.

[70] P. R. Amestoy, I. S. Duff, C. Puglisi. Multifrontal QR factorization in a multiprocessor environment. Numer. Linear Algebra Appl. 3, 4, 275–300, 1996a.

[71] P. Matstoms. Sparse QR factorization in MATLAB. ACM Trans. Math. Softw. 20, 1, 136–159, 1994.

[72] X. Li, Direct Solvers for Sparse Matrices, September 2006, http://crd.lbl.gov/~xiaoye/SuperLU/SparseDirectSurvey.pdf.

[73] Y. Chen, T. A. Davis, W. W. Hager, and S. Rajamanickam, Algorithm 8xx: CHOLMOD, supernodal sparse Cholesky factorization and update/downdate. Technical Report TR-2006-005, University of Florida, 2006. (http://www.cise.ufl.edu/research/sparse/cholmod/).

[74] I.S Duff and J. K. Reid. MA47, a Fortran code for direct solution of indefinite sparse symmetric linear systems. Technical Report RAL-95-001, Rutherford Appleton Laboratory, 1995

[75] F. Dobrian and A. Pothen. Oblio: a sparse direct solver library for serial and parallel computations. Technical report, Old Dominion University, 2000

[76] Kenneth Kundert. Sparse matrix techniques. In Albert Ruehli, editor, Circuit Analysis, Simulation and Design. North-Holland, 1986. (http://www.netlib.org/sparse)

[77] A. George and J. Liu. Computer Solution of Large Sparse Positive Definite Systems. Prentice-Hall Inc., Englewood Cliffs, New Jersey, 1981. (jageorge@sparse1.uwaterloo.ca).

[78] C. Ashcraft and R. Grimes. SPOOLES: An object-oriented sparse matrix library. In Proceedings of the Ninth SIAM Conference on Parallel Processing, 1999. (http://www.netlib.org/linalg/spooles).

[79] Esmond G. Ng and Barry W. Peyton. Block sparse Cholesky algorithms on advanced uniprocessor computers. SIAM J. Sci. Comput., 14(5):1034–1056, September 1993. (egng@lbl.gov).

[80] James W. Demmel, Stanley C. Eisenstat, John R. Gilbert, Xiaoye S. Li, and Joseph W. H. Liu. A supernodal approach to sparse partial pivoting. SIAM J. Matrix Anal. Appl., 20(3):720–755, 1999. (http://crd.lbl.gov/xiaoye/SuperLU).

[81] T. A. Davis. Algorithm 832: UMFPACK V4.3, an unsymmetric-pattern multifrontal method with a column pre-ordering strategy. ACM Trans. Mathematical Software, 30(2):196–199, June 2004. (http://www.cise.ufl.edu/research/sparse/umfpack/).

[82] Patel et al. “Performance of generator protection during major system disturbances, IEEE Transactions on power delivery”, Vol.19, Issue 4, October 2004.

[83] IEEE Task Force Report, Blackout Experiences and Lessons, Best Practices for System Dynamic Performance, and the Role of New Technologies, Final report May 2007

[84] G. S. Vassell, “Northeast Blackout of 1965,” IEEE Power Engineering Review, Jan. 1991

[85] G. D. Friedlander, “The Northeast power failure – a blanket of darkness,” IEEE Spectrum, Vol. 3, No. 2, Feb. 1966

[86] [Online]. Available http://blackout.gmu.edu/events/tl1965.html

[87] [Online]. Available http://www.cmpco.com/about/system/blackout.html

[88] [Online]. Available http://www.ceet.niu.edu/faculty/vanmeer/outage.htm

[89] [Online]. Available http://www.answers.com/topic/new-york-city-blackout-of-1977

[90] Feinstein, Jack. "Learning from Experiences: Case Study 1, 1977 Con Edison Blackout."

[91] Corwin, Jane L. and William T. Miles, "Impact Assessment of the 1977 New York City Blackout." Palo Alto: Systems Control Inc., Prepared for Lester H. Fink, Div. of Electric Energy Systems, U.S. Department of Energy, July 1978.

[92] A. Kurita, T. Sakurai, “The power system failure on July 23, 1987 in Tokyo,” Proc. 27th conf. on Decision and Control, Austin, Texas, pp. 2093-2097, 1988.

[93] C.W.Taylor and D.C.Erickson, “Recording and analyzing the July 2 cascading outage,” IEEE Comput. Appl. Power , vol 10, no. 4, pp. 40-44, Oct. 1997.

[94] The Electric Power Outages in the Western United States, July 2-3, 1996. Report to the President of the United States by the Secretary of Energy, August 2, 1996

[95] D. N. Kosterev, C. W. Taylor, and W. A. Mittelstadt, "Model Validation For The August 10, 1996 WSCC System Outage," IEEE Trans. Power Systems, vol. 14, no. 3, pp. 967-979, August 1999

[96] A Survey of the Implications to California of the August 10, 1996 Western States Power Outage. Report of the California Energy Commission, June 1997. Available on the Internet at http://www.energy.ca.gov/electricity/index.html#reliability

[97] U.S.-Canada Power System Outage Task Force, Final Report on the August 14, 2003 Blackout in the United States and Canada: Causes and Recommendations, April 2004.

[98] Office of Gas and Electricity Markets, Preliminary Report into the Recent Electricity Transmission Faults Affecting South London and East Birmingham, UK, September 2003.

[99] Elkraft System, Power failure in Eastern Denmark and Southern Sweden on 23 September 2003, Final report on the course of events, Nov. 2003.

[100] Svenska Kraftnat, The black-out in southern Sweden and eastern Denmark, 23 September, 2003 Preliminary report, Oct. 2003.

[101] Union for the Co-ordination of Transmission of Electricity, Interim Report of the Investigation Committee on the 28 September 2003 Blackout in Italy, UCTE Report, 27 October, 2003.

[102] AEEG and CRE: “Report on the events of September 28th, 2003 culminating in the separation of the Italian power system from the other UCTE networks”, available at http://www.autorita.energia.it/docs/04/061-04all.pdf

[103] S. Corsi and C. Sabelli, “General Blackout in Italy: Sunday September 28, 2003, h. 03:28:00”, Proceedings of IEEE-PES General Meeting, PSSS Panel on Recent blackouts, Denver 2004.

[104] A.Berizzi: “The Italian 2003 blackout”. 2004 IEEE PES General Meeting, PSSS Panel on Recent

Blackouts, Denver, June 2004.

[105] C. D. Vournas, V. C. Nikolaidis and A. Tassoulis, "Experience from the Athens Blackout of July12, 2004", IEEE Power Tech, St. Petersburg, June 2005.

[106] NEMMCO report "Power System Incident Report – Friday 13 August 2004", 28 January, 2005, http://www.nemmco.com.au/marketandsystemevents/232-0022.pdf

[107] IEEE Guide for AC Generator Protection, 1995, IEEE Standard C37.102-1995.

[108] IEEE Guide for AC Generator Protection, 1995, IEEE Standard C37.102-2006.

[109] D. Reimert, Protective Relaying for Power Generation Systems. Boca Raton: CRC Press, 2006.

[110] J.L. Blackburn, Protective Relaying Principles and Applications 2nd Edition New York Basel Marcel Dekker, Inc, 1998.

[111] P. Kundur, Power System Stability and Control. New York: McGraw-Hill, 1994.

[112] P. M. Anderson, Power System Protection, New York, IEEE Press/McGraw-Hill 1999.

[113] Requirements for Cylindrical Rotor Synchronous Generators, 1989 ANSI Std C50.13-1989

[114] Standard for Requirements for Salient-Pole Synchronous Generators and Generator/Motors for Hydraulic Turbine Applications, 1982. ANSI

[115] IEEE Guide for Abnormal Frequency Protection for Power Generating Plants, C37.106–1987, IEEE, New York, 1987.

[116] Crenshaw, M. L. and Temoshok, M., Protection of large steam turbine generators during abnormal operations, Pennsylvania Electric Association Relay Committee Meeting, October 21–22, 1971, Reading, PA.

[117] Baily, F. G., Bardwick, H. A., and Fenton, R. E. Operating and maintaining steam turbine generators–Operating at off-normal conditions, Power, August 1976, The McGraw-Hill Companies.

[118] Berdy, J., Brown, P. G., and Goff, L. E., Protection of Steam Turbine Generators During Abnormal Frequency Conditions, General Electric Company, Schenectady, New York.

[119] Gerasimov, A., and Koshcheev, L., Main principles of automatic counter-emergency control in UPS of Russia, IEEE PowerTech Conference, St.Petersburg, Russia, 2005.

[120] Madani, V., Taylor, E., Erwin, D., Meklin, A., Adamiak, M, High-Speed Control Scheme to Prevent Instability of A Large Multi-Unit Power Plant, 60th Annual Conference for Protective Relay Engineers, pp. 271-282, 2007.

[121] Probabilistic Methods Work Group, WSCC Reliability Subcommittee, "Probabilistic based reliability criteria Phase 1: Event probability development and implementation plan", June 25, 1998.

Risk of Cascading Outages

Part B:

Estimating Failure Propagation and the Distribution of Blackout Size and Evaluating the Long-Term Risk of the N-1 Criterion in an Evolving Power System

Part B Authors

Ian Dobson
Kevin R. Wierzbicki
Janghoon Kim
Hui Ren
University of Wisconsin-Madison

Information about Part B

For information about part B contact:

Ian Dobson
University of Wisconsin-Madison
Electrical and Computer Engineering Dept.
Madison WI 53706
Phone 608-262-2661
Email: dobson@engr.wisc.edu

Power Systems Engineering Research Center

This is a project report from the Power Systems Engineering Research Center (PSERC). PSERC is a multi-university Center conducting research on challenges facing the electric power industry and educating the next generation of power engineers. More information about PSERC can be found at the Center's website: http://www.pserc.org.

For additional information, contact:

Power Systems Engineering Research Center
Arizona State University
577 Engineering Research Center
Box 878606
Tempe, AZ 85287-8606
Phone: 480-965-1643
FAX: 480-965-0745

Notice concerning copyright material

Contents

1 Introduction

This is the final report for the part of the 2005-2007 PSerc project on Risk of Cascading Outages (S-26) performed at the University of Wisconsin-Madison. The main objective of this part of the project is to develop methods and tools for cascading failure.

1.1 Main accomplishments

The main accomplishments of the UW-Madison part of the project are

1. We developed a statistical estimator to measure the extent to which transmission line outages propagate in cascading failures. This has been tested on cascading line outage simulation data and initially tested on some industry line outage data.

   (a) *Testing on simulation data.* The estimator was tested on outage data generated by the OPA simulation[1] [5] of cascading overloads and outages. This is a step towards the goal of monitoring line outages to estimate the blackout risk. This work is documented in the conference papers [17, 23] and in section 2 of this report. We also discovered an improved variant of the estimator.

   (b) *Testing on industry data.* We studied cascading line outages recorded over nine years in an electric power system with approximately 200 lines. The average amount of propagation of the line outages is estimated from the industry data. The distribution of the total number of line outages is predicted from the propagation and the initial outages using a branching process model of cascading. This work starts to explore one way to apply our methods to industry data and is summarized in section 2.3 of this report. The method, once fully tested and established, would not be burdensome to implement.

2. We have extended the OPA simulation [7] to roughly estimate the effect of the n-1 criterion on the distribution of sizes of cascading outages and the efficiency of network utilization. The idea is to compare the effect of upgrading the network to satisfy the n-1 criterion with upgrading the network directly in response to the cascading outages.

[1] **OPA** stands for **O**ak Ridge National Laboratory, **P**ower Systems Engineering Research Center at the University of Wisconsin, University of **A**laska to indicate the institutions collaborating to devise the simulation.

Very simple models of cascading failure and network upgrade are assumed and the simulation reaches a complex systems steady state in the long-term. This work evaluates highly simplified versions of industry practice with new ideas of complex systems.

3. We have made considerable progress in quantifying how well a branching process model approximates a probabilistic model of cascading failure. We have obtained useful bounds on the ratio and difference of the probabilities from these two models. This work helps to justify the use branching processes in the project to quantify cascading failure. This work is not described in this report, but the math will be checked and polished for a journal paper.

4. We have, in collaboration with Professor Daniel Kirschen and Dr. Dusko Nedic of the University of Manchester, verified the criticality of blackout risk in an AC blackout model that represents many of the interactions that occur in cascading failure. A realistic case of a 1000 bus network was used and loading was gradually increased until a critical loading was found. At the critical loading there is a sharp rise (change of gradient) in the mean blackout size and a power law probability distribution of blackout size that indicates a phase change in the risk of large blackouts. This work was documented in a conference and journal paper [35]. The work is not described in this report, but [35] is available on the PSerc web site.

5. We put effort into papers and talks to communicate our results and respond to questions. We wrote a tutorial paper [22] for the IEEE PES General Meeting super session reviewing the emerging approaches to quantifying the overall risk of blackout due to cascading failure and determining the corresponding safe limits for power system design and operation. We wrote an overview paper [21] summarizing and explaining much of our last decade of work on blackout risk. We contributed material on blackout risk to IEEE and CIGRE reports [27, 12]. We were invited to give a plenary talks at a SIAM applied math conference and two complex network symposia.

1.2 Students and publications

We summarize the student education supported and the papers and talks produced.

The project helped to support the following education at the University of Wisconsin-Madison:

- MS degree for Kevin Wierzbicki, "Statistical estimation of cascading blackout size and propagation with branching processes" [49]
- MS degree of Janghoon Kim (ongoing)
- visit of visiting scholar Hui Ren

The conference papers produced are:

- D.P. Nedic, I. Dobson, D.S. Kirschen, B.A. Carreras, V.E. Lynch, Criticality in a cascading failure blackout model, Fifteenth Power Systems Computation Conference, Liege Belgium, August 2005.
- I. Dobson, K.R. Wierzbicki, B.A. Carreras, V.E. Lynch, D.E. Newman, An estimator of propagation of cascading failure, 39th Hawaii International Conference on System Sciences, January 2006, Kauai, Hawaii.
- K.R. Wierzbicki, I. Dobson, An approach to statistical estimation of cascading failure propagation in blackouts, CRIS, Third International Conference on Critical Infrastructures, Alexandria, Virginia, September 2006.
- I. Dobson, Where is the edge for cascading failure?: challenges and opportunities for quantifying blackout risk, IEEE Power Engineering Society General Meeting, Tampa FL USA, June 2007
- I. Dobson, K.R. Wierzbicki, J. Kim, H. Ren, Towards quantifying cascading blackout risk, Bulk Power System Dynamics and Control-VII, Charleston SC USA, August 2007.

The journal papers that are published to date are the following (other journal papers, including [38, 39], are in progress):

- D.P. Nedic, I. Dobson, D.S. Kirschen, B.A. Carreras, V.E. Lynch, Criticality in a cascading failure blackout model, International Journal of Electrical Power and Energy Systems, vol. 28, 2006, pp. 627-633.
- I. Dobson, B.A. Carreras, V.E. Lynch, D.E. Newman, Complex systems analysis of series of blackouts: cascading failure, critical points, and self-organization, Chaos, vol. 17, no. 2, June 2007.

All these papers, including this final report, are available on the PSerc web site www.pserc.org.

The following report sections were written for CIGRE and IEEE:

- Defense plans against extreme contingencies, CIGRE Task Force C2.02.24 report, and a paper summarizing the report in Electra no. 231, April 2007. (I. Dobson drafted a section "Complex systems analysis of series of blackouts".)

- Blackout Experience and Lessons, Best Practices for System Dynamic Performance, and the Role of New Technologies, Special Publication 07TP190, prepared by the IEEE PES Task Force on Blackout Experience, Mitigation, and Role of New Technologies of the Power System Dynamic Performance Committee of the IEEE Power Engineering Society, July 2007. (I. Dobson drafted a section "NERC historical data on blackouts and overall blackout risk".)

In addition to the presentation of the conference papers listed above, the following presentations were made:

- Cascading Phenomena, lecture in Power system blackouts course, University of Wisconsin Engineering and Professional Development, Madison, Wisconsin, May 2005

- Plenary talk: Cascading Failure and Complex Dynamics in Large Blackouts, at SIAM Conference on Applications of Dynamical Systems, Snowbird UT, May 2005.

- Overall blackout risk and cascading failure, presentation as panelist in panel session Technical and Economic Metrics of Reliability, IEEE Power Engineering Society General Meeting, San Francisco, CA June 2005.

- Monitoring risk of cascading failure blackouts, Presentation at Oak Ridge National Lab to representatives from Nuclear Regulatory Commission, Federal Energy Regulatory Commission, and North American Electric Reliability Council, July 2005

- Cascading failure in electric power system blackouts, Talk at Brunel University, Uxbridge England, September 2005.

- Monitoring risk of cascading failure blackouts, Invited presentation at NSF/EPRI workshop, Denver CO October 2005.

- Towards estimating the risk of cascading failure blackouts, ETH, Zurich, Switzerland, February 2006.
- Towards Estimating the Risk of Cascading Failure Blackouts, Northwestern University, Evanston IL, April 2006
- Plenary Talk: Criticality, Self-organization and Cascading Failure in Blackouts of Evolving Electric Power Networks, Sixth Understanding Complex Networks Symposium, University of Illinois at Urbana-Champaign, May 2006.
- Plenary Talk: Cascading Failure and Complex Dynamics in Large Blackouts, Los Alamos National Laboratory Center for Nonlinear Studies Workshop on Optimization in Complex Networks, June 2006.
- Panelist, California Energy Commission PIER TRP Policy Advisory Committee Meeting, San Ramon, CA June 2006.
- Criticality, Self-organization and Cascading Failure in Electric Power System Blackouts, University of California-Davis, June 2006
- Can we estimate the overall risk of cascading blackouts?, PSerc summer workshop, Ashland WI, August 2006.
- Risk of Large Cascading Blackouts, EUCI Transmission Reliability Conference, Washington DC, October 2006.
- Criticality, Self-organization and Cascading Failure in Electric Power System Blackouts, Rice University, October 2006.
- NSF workshop, Monitoring and Controlling the Nations Critical Infrastructure, Washington DC, November 2006.

2 Towards Branching Process Methods for Quantifying Cascading Blackout Risk

It would be very useful to be able to efficiently quantify overall blackout risk from simulated or real power system data. Established analytic methods of power system risk analysis can model the detail of some likely and foreseen combinations of failures and estimate their risk. This is very useful in finding and mitigating likely failures, but it does not address quantifying the overall risk of large cascading blackouts, in which there is combinatorial explosion of potential rare, unforeseen, and interacting events ranging from diverse power system physical effects through software failures to deficiencies in planning, operation, organization, and maintenance. Here the term "failure" includes outages in which the component or process is intact but temporarily unavailable to transmit power or function properly as well as outages in which the component or process is damaged or impaired.

Studying the intricate details of particular blackouts [44], in addition to quickly reinforcing the case for the complexity of these events, also provides a useful method for finding and mitigating weaknesses in the power system. However, larger blackouts are infrequent events in developed economies, and, after a large blackout, it is difficult to ascertain whether the blackout should be attributed to bad practice or bad luck, especially with everyone's attention riveted on only one sample from the huge number of potential blackouts. A detailed analysis of the chain of events after the blackout is useful in suggesting specific weaknesses that can be rectified, but gives little guidance on the overall problem of whether society is rationally balancing the blackout risks with the costs of investing in increased reliability. Quantifying the overall blackout risk would allow this balancing by putting an approximate value on reliability.

The most straightforward way to estimate the probabilities of various sizes of blackouts is simply to wait a long time to observe enough blackouts to get good estimates of blackout probabilities. But in practice the wait is too long for most purposes because the large blackouts occur too rarely. (Observed blackouts in several countries have power law regions in the distribution of blackout size [21] and empirical estimation of these distributions requires many samples.) Moreover, the power system upgrades over time so that the observed statistics represent the average over a considerable time of an evolving system. Therefore, we aim for efficient methods of estimating blackout risk that could work in a time scale of about one year. While there are certainly challenges in estimating the direct and indirect

costs of blackouts and both cost and probability of blackouts are needed to estimate blackout risk, this report focusses on estimating the probability of blackouts, or, more precisely, the probability distribution of blackout size. The probability distribution of blackout size can be combined with the cost as a function of blackout size to yield the distribution of blackout risk as a function of blackout size. We maintain that problem of blackout risk is better framed in terms of the distribution of risk of various sizes of blackouts rather than the risk of blackouts in general [21].

We suggest that any practical approach to efficient estimation of blackout probabilities must be a bulk "top-down" statistical approach that incorporates a verified understanding of cascading failures in power systems. This is a departure from methods of risk analysis that rely on detailed analysis of enumerated interactions, but it is complementary to these detailed analyses. The purpose of this report is to review progress in developing and testing a bulk statistical method to estimate the probability of cascading blackouts.

Specialized simulations can sample a subset of the intricacies of large cascading blackouts [2, 5, 9, 25, 31, 33, 34, 35, 41, 45] and, while they may never be able to capture all the interactions in blackouts, simulations are vital in testing statistical methods for monitoring the power system. Moreover, efficient estimation of blackout probabilities from data produced by cascading failure simulations makes efficient use and leverages understanding of the simulation results. In particular, reducing the number of simulation runs would enable the effects of proposed reliability upgrades to be quickly assessed.

Our top-down modeling views cascading as a random initial disturbance followed by a random propagation of failures. The outcome of each cascade is probabilistic, but its statistics are governed by the size of the initial disturbance and the average tendency for the failures to propagate. A simple way to capture this mathematically is to use a branching process model.

Why consider a branching process model?

1. Branching processes are a standard model for cascades in many other subjects, including genealogy, cosmic rays, and epidemics [26, 3]. This makes branching processes an obvious first choice for modeling cascading failures.

2. Observed [8, 21] and simulated [5, 9, 35, 32] power system data shows qualitative features such as distributions of blackout sizes with near power law regions and criticality that can be produced by branching processes as illustrated in section 2.1.1 and [16].

3. The CASCADE model [19] is another high-level probabilistic model of cascading failure. CASCADE is well approximated by Galton-Watson branching process models in suitable parameter ranges [16].

4. Branching processes are simple and tractable models and it is good to test simple models first. In particular, branching process models can be tested against real and simulated power system data as described in this report.

If branching processes are useful models of cascading processes, this would open up several opportunities. In addition to providing the essential understanding of the overall features of cascading, the probability distribution of blackout size could be quantified more efficiently from much smaller samples of cascades. One reason is that estimating the parameters of a branching process model and then computing the distribution of blackout size using the model requires much smaller samples than directly estimating the distribution of blackout size exhaustively, especially since large cascading blackouts are rare events. The smaller number of samples is important when observing cascades in the power system because smaller samples enable a shorter observation time that can make the approach practical. The smaller number of samples is similarly important when simulating cascading failure because smaller samples enable shorter run times.

However, we still need to exhaustively determine the distribution of blackout size by simulation and observation in order to test whether branching process models are valid and applicable. This report shows how to test branching process models on observed or simulated power system data. A large number of cascades are observed or simulated in order to exhaustively determine the distribution of blackout size. Then the same data is used to estimate the branching process model parameters and compute the distribution of blackout size with the branching process model and see how well this matches the empirical distribution. If the match is acceptable, then the branching process model is useful for determining the distribution of blackout size.

Throughout the report there are two measures of blackout size of interest to monitor the progress and outcome of the cascade; namely, number of transmission lines failed and the load shed. The lines failed are more easily tracked and analyzed and are of internal interest to the utilities and system operators. Moreover, lines may fail in "precursor" events with no load power shed. On the other hand, load power shed matters to the utilities, society, industry and government.

Section 2.1 reviews and explains several branching process models and the statistical estimation of their parameters. Section 2.2 tests branching process models on data from a power systems simulation and section 2.3 tests a branching process model on observed power system cascades. Section 2.4 examines issues and challenges in further work towards quantifying cascading failure risk in power systems. Section 2.5 concludes the chapter.

2.1 Branching processes

Branching processes have long been used in a variety of applications to model cascading processes [26, 3], but their application to the risk of cascading failure is novel [16, 17]. The branching processes of primary interest produce failures in stages starting from some initial distribution of failures. There are several types of branching processes that we describe below: A Galton-Watson process has discrete numbers of failures such as numbers of transmission lines failed. A continuous-state branching process has a continuously varying amount of failure in each stage such as load power shed in each stage. Other branching processes evolve in continuous time.

2.1.1 Galton-Watson branching process

The Galton-Watson branching process gives a probabilistic model of the number of failures. There are a random number of initial failures that then propagate randomly to produce subsequent failures in stages. The mean number of initial failures is θ. The subsequent failures are produced in stages or generations starting from the initial failures. Each failure in each stage (a "parent" failure) independently produces a random number 0,1,2,3,... of failures ("child" failures) in the next stage as illustrated in Figure 1. The children failures then become parents to produce the next generation and so on. If the number of failures in a stage becomes zero, the cascade stops. The mean number of child failures for each parent is the parameter λ. λ quantifies the average tendency for the cascade to propagate. The intent of the modeling is not that each parent failure in some sense "causes" its children failures; the branching process simply produces random numbers of failures in each stage that can statistically match the outcome of cascading processes.

The branching process theory gives analytic formulas for the probability distribution of the total number of failures. For example, when the number of initial failures is a Poisson distribution of mean θ and the number of children failures for each parent failure is a Poisson distribution of mean λ,

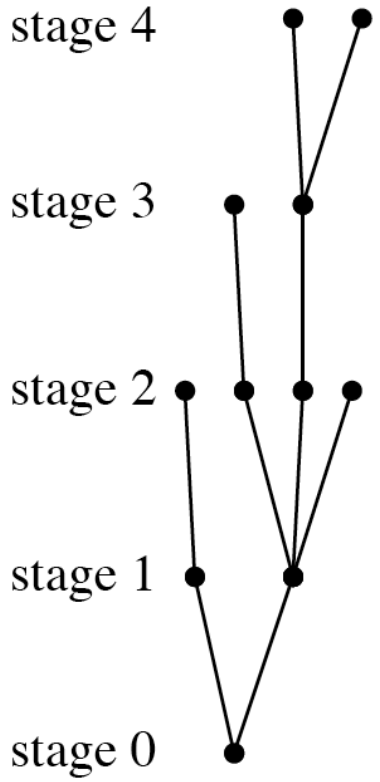

Figure 1: Example of failures produced in stages by a Galton-Watson branching process. Each "parent" failure independently has a random number of "child" failures in the next stage.

the total number of failure follows a generalized Poisson distribution that is parameterized by θ and λ [13, 14, 16]. There are general arguments supporting the choice of Poisson distributions [13, 14]. The Poisson distribution is a good approximation when each failure propagates to a large number of components so that each parent failure has a small, fairly uniform probability of independently causing child failures in a large number of other components. This assumption seems reasonable for cascades in power systems, especially in the initial portions of the cascade when there are many unfailed components that are stressed by the failed components.

There are assumed to be N transmission lines and there are Z_0 initial failures. Line failures occur in stages with Z_n the number of failures in stage n and Y_n the total number of failures up to and including stage n.

$$Y_n = Z_0 + Z_1 + Z_2 + ... + Z_n \tag{1}$$

The process saturates when $S \leq N$ lines fail. Each of the Z_n failures in stage n independently causes a further number of failures in stage $n+1$ according to a Poisson distribution with mean λ, except that if the total number of failures exceeds S, then the total number of failures is limited to S. That is, the jth failure in stage n causes $Z_{n+1}^{[j]}$ failures in stage $n+1$ according to the Poisson distribution and the total number of failures in stage $n+1$ is

$$Z_{n+1} = \min\left\{Z_{n+1}^{[1]} + Z_{n+1}^{[2]} + \cdots + Z_{n+1}^{[Z_n]},\ S - Y_n\right\}, \tag{2}$$

where $Z_{n+1}^{[1]}, Z_{n+1}^{[2]}, \cdots, Z_{n+1}^{[Z_n]}$ are independent. (A different form of saturation is described in [16, 20].)

The modeling of saturation is essential for λ near or exceeding 1 because then there is a significant probability of cascading to all N lines of the system failing (total blackout). That is, practical application of the branching process requires an upper limit $S \leq N$ of components failing for λ near or exceeding 1. Moreover there may be saturation effects encountered before all N components fail and then S can be chosen less than N, either because the number failures tend to bunch at S or because the modeling is uncertain or variable after S components fail. These saturation effects are not well understood and it remains to be seen how or whether saturation effects are significant for cascading failure in practical systems.

There are several variants of analytic formulas for the distribution of the total number of failures Y [17], depending on the assumed distribution of initial failures Z_0, whether saturation is assumed, and whether the distribution of Y is conditioned on Y being nonzero. If the initial failures Z_0

are distributed according to a Poisson distribution with mean θ and saturation S is assumed, then the total number of failures conditioned on Y being nonzero is distributed according to a saturating generalized Poisson distribution:

$$P[Y = r \mid Y > 0] = \begin{cases} \theta(r\lambda + \theta)^{r-1} \frac{e^{-r\lambda-\theta}}{r!(1-e^{-\theta})}; & 1 \leq r < S \\ 1 - \sum_{s=1}^{S-1} P[Y = s]; & r = S \end{cases} \tag{3}$$

Some qualitative features of the saturating generalized Poisson distribution (3) are shown in Figure 2. For small propagation $\lambda = 0.1$, the distribution drops off sharply and there is negligible probability of a large number of line failures. As λ increases, the distribution extends towards a large number of line failures until at $\lambda = 1$, there is a power law region of slope approximately -1.5. Moreover, a graph of average blackout size as a function of λ (not shown here) shows a change in gradient at $\lambda = 1$, indicating criticality at $\lambda = 1$. The example in Figure 2 assumes saturation at $S = 1000$ lines. If an unsaturating branching process would have proceeded beyond 1000 lines failures, then the saturating branching process records that event as 1000 lines failures. The probability of 1000 lines failing increases as the system becomes more stressed. At $\lambda = 1$ the probability of 1000 lines failed is 0.025 and this increases to 0.797 at $\lambda = 2$. The very low probability of an intermediate number of failures at $\lambda = 2$ is due to almost all the cascades that have an intermediate number of failures continuing to grow until there are 1000 lines failed.

If there is an arbitrary distribution of nonzero initial failures $P[Z_0 = z_0]$ for $z_0 = 1, 2, 3, ...$, and no saturation, then the total number of failures is distributed according to a mixture of Borel-Tanner distributions:

$$P[Y = r] = \sum_{z_0=1}^{r} P[Z_0 = z_0] z_0 \lambda (r\lambda)^{r-z_0-1} \frac{e^{-r\lambda}}{(r - z_0)!} \tag{4}$$

The neglect of saturation implies that (4) is only valid for subcritical $\lambda < 1$.

The simulation is run or data are observed K times to produce K independent realizations of the cascade. Since a cascades with $Z_0 = 0$ are discarded, all cascades have $Z_0 > 0$ and all statistics are conditioned on the nontrivial start of a cascade. The failures in the kth run are written as $Z_0^{(k)}$,

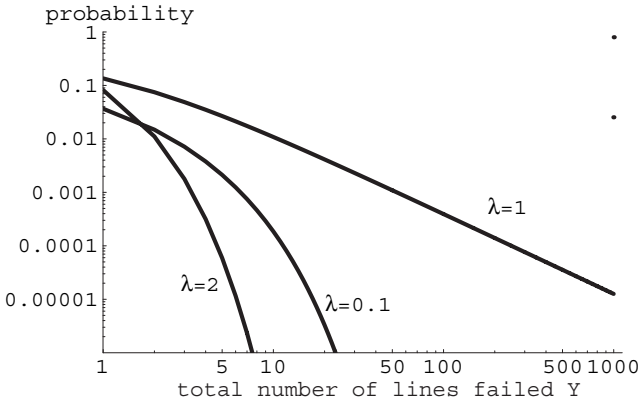

Figure 2: Probability distributions of total number of line failures Y according to the generalized Poisson distribution with saturation at $S = 1000$ lines for three values of propagation λ. The distribution has an approximate power law region at criticality when $\lambda = 1$. The probability of 1000 lines failing is 0.025 for $\lambda = 1$, and 0.797 for the supercritical case $\lambda = 2$.

$Z_1^{(k)}$, $Z_2^{(k)}$, $Z_3^{(k)}$,... . The data can be tabulated as follows:

$$\begin{array}{cccccc} & \text{stage 0} & \text{stage 1} & \text{stage 2} & \text{stage 3} & \cdots \\ \text{run 1} & Z_0^{(1)} & Z_1^{(1)} & Z_2^{(1)} & Z_3^{(1)} & \cdots \\ \text{run 2} & Z_0^{(2)} & Z_1^{(2)} & Z_2^{(2)} & Z_3^{(2)} & \cdots \\ \text{run 3} & Z_0^{(3)} & Z_1^{(3)} & Z_2^{(3)} & Z_3^{(3)} & \cdots \\ . & . & . & . & . & \\ . & . & . & . & . & \\ \text{run } K & Z_0^{(K)} & Z_1^{(K)} & Z_2^{(K)} & Z_3^{(K)} & \cdots \end{array} \tag{5}$$

Define the cumulative number of failures in run k up to and including stage n as

$$Y_n^{(k)} = Z_0^{(k)} + Z_1^{(k)} + Z_2^{(k)} + ... + Z_n^{(k)} \tag{6}$$

Each run has a stage at which the number of failures is zero and remains zero for all subsequent stages, either because the cascade dies out, or the cascade has saturated. The number of failures at which saturation occurs is $S \leq N$. Define

$$s(k, S) = \max\{\, n \mid Y_n^{(k)} < S \ \text{ and } \ Z_{n-1}^{(k)} > 0 \,\} \tag{7}$$

That is, $s(k, S)$ is either the first stage at which there are zero failures or the last stage before a total of S failures.

We define an estimator of λ as

$$\widehat{\lambda} = \frac{\sum_{k=1}^{K}\left(Z_1^{(k)} + Z_2^{(k)} + ... + Z_{s(k,S)}^{(k)}\right)}{\sum_{k=1}^{K}\left(Z_0^{(k)} + Z_1^{(k)} + ... + Z_{s(k,S-1)-1}^{(k)}\right)} = \frac{\sum_{k=1}^{K}\left(Y_{s(k,S)}^{(k)} - Z_0^{(k)}\right)}{\sum_{k=1}^{K} Y_{s(k,S-1)-1}^{(k)}} \tag{8}$$

The estimator $\widehat{\lambda}$ is asymptotically unbiased as $K \to \infty$ if the offspring distribution is Poisson. This asymptotic unbiasedness property shows that the estimator $\widehat{\lambda}$ is an improved variant of the estimator of λ proposed in [18].

We determined the bias and variance of $\widehat{\lambda}_s$ numerically for a saturating branching process with one initial failure by computing $\widehat{\lambda}$ 1000 times and computing the sample mean $\mu(\widehat{\lambda})$ and standard deviation $\sigma(\widehat{\lambda})$ of $\widehat{\lambda}$.

For saturation $S = 20$, $0 < \lambda < 2$, and number of runs $10 \leq K \leq 1000$, $|\mu(\widehat{\lambda}) - \lambda| \leq 0.05$ and

$$\sigma(\widehat{\lambda}) \leq \frac{0.81}{\sqrt{K}}. \tag{9}$$

For saturation $S = 100$, $0 < \lambda < 2$, and number of runs $10 \leq K \leq 150$, $|\mu(\widehat{\lambda}) - \lambda| \leq 0.07$ and

$$\sigma(\widehat{\lambda}) \leq \frac{0.51}{\sqrt{K}}. \tag{10}$$

For example, $K = 25$ runs gives $\sigma(\widehat{\lambda}) \leq 0.1$.

When significant saturation effects are encountered, it is essential to use the estimator (8) to avoid underestimating λ [18]. However, when the branching process is subcritical ($\lambda < 1$) and there is no saturation or negligible saturation ($S = \infty$), $\widehat{\lambda}$ reduces to the standard Harris estimator for λ [26, 51, 15, 24]:

$$\widehat{\lambda} = \frac{\sum_{k=1}^{K}\left(Z_1^{(k)} + Z_2^{(k)} + ...\right)}{\sum_{k=1}^{K}\left(Z_0^{(k)} + Z_1^{(k)} + ...\right)} = \frac{\sum_{k=1}^{K}\left(Y_{\infty}^{(k)} - Z_0^{(k)}\right)}{\sum_{k=1}^{K} Y_{\infty}^{(k)}} \tag{11}$$

The Harris estimator (11) is an asymptotically unbiased maximum likelihood estimator [26, 51]. The asymptotic standard deviation of the Harris estimator can be worked out using the methods of [51], in the case of Poisson offspring distribution with one initial failure, to be

$$\sigma(\widehat{\lambda}) \sim \frac{\sqrt{\lambda(1-\lambda)}}{\sqrt{K}} \leq \frac{0.5}{\sqrt{K}} \tag{12}$$

The Harris estimator (11) is intuitive: Think of "parent" failures in each generation giving rise to "child" failures in the next generation. The child failures then become parents to produce the next generation and so on. Then λ is the average family size; that is, the average number of child failures for each parent. Since $Z_0, Z_1, ...$ are all parent failures and $Z_1, Z_2, ...$ are all child failures, the Harris estimator (11) is simply the total number of children in all the cascades divided by the total number of parents in all the cascades.

If the initial failures Z_0 are approximated by a Poisson distribution conditioned on a nonzero number of failures, then an estimate of the mean initial failures $\widehat{\theta}$ can be obtained by solving

$$\frac{\widehat{\theta}}{1-e^{-\widehat{\theta}}} = \frac{1}{K}\sum_{k=1}^{K} Z_0^{(k)}. \tag{13}$$

It is straightforward to derive (13) by maximum likelihood methods or the method of moments.

2.1.2 Continuous state branching process

We summarize the application of continuous state branching processes to model the cascading of load shed in [50]. Continuous state branching processes have a similar theory to Galton-Watson branching processes, but the computations of the distribution of the total load shed are more difficult. See [28, 42] for systematic accounts of continuous state branching processes. Throughout this subsection, we assume the subcritical case $\lambda < 1$ and no saturation.

There is an initial amount of load shed Z_0 in stage 0 that is given by a probability density function (pdf) $G(z)$ and the load shed amounts Z_1, Z_2, ... in stages 1, 2, ... are produced using an offspring distribution $H(z)$. $H(z)$ is defined to be the pdf of load shed in any stage if the load shed in the preceding stage is 1. We write Z for a random variable with pdf $H(z)$. The expected value of Z is λ.

For the subsequent stages $n = 1, 2, 3...$, the load Z_n shed in stage n has pdf that is the convolution of $H(z)$ with itself Z_{n-1} times, or, equivalently, the pdf of the sum of Z_{n-1} independent copies of Z. These pdfs are computed in the frequency domain using their cumulant generating functions (cgf's). The cgf $h(s)$ of the offspring distribution is the negative logarithm of the Laplace transform of $H(z)$:

$$h(s) = -\ln \int_0^\infty e^{-sz} H(z) dz = -\ln E e^{-sZ}.$$

and, since we choose $H(z)$ to be a gamma distribution, $h(s)$ has the form

$$h(s) = \frac{\lambda^2}{\sigma_{\text{off}}^2} \ln \left(1 + s \frac{\sigma_{\text{off}}^2}{\lambda} \right). \tag{14}$$

The distribution of the total load shed Y can be computed from the offspring distribution as follows [50]. Computer algebra is used to perform the symbolic operations. Let Z_0 have a cgf of the form

$$m(s) = \frac{\theta^2}{\sigma_{\text{init}}^2} \ln \left(1 + s \frac{\sigma_{\text{init}}^2}{\theta} \right) \tag{15}$$

so that Z_0 also has a gamma distribution. Then the cgf of Y is

$$k(s) = m(k_\bullet(s)) \tag{16}$$

where $k_\bullet(s)$ satisfies

$$k_\bullet(s) = s + h(k_\bullet(s)). \tag{17}$$

The implicit equation (17) can be solved for $k_\bullet(s)$ by the Lagrange inversion method [47] and then the pdf $K(x)$ of the total load shed Y can obtained as the inverse Laplace transform of $e^{-k(s)}$ using the Post-Widder method [48].

Some cascades may have negligible or zero load shed in initial stages. These initial stages are discarded from the data so that all nontrivial cascades start with $Z_0 > 0$. (Trivial cascades with no load shed are also discarded.) Then the estimator $\widehat{\lambda}$ is the same as (8) except that saturation is neglected ($S = \infty$), and we impose a maximum of 10 stages so that (7) becomes

$$s(k, S) = \max\{\, n \mid n \le 10 \ \text{ and } \ Z_{n-1}^{(k)} > 0 \,\} \tag{18}$$

The condition on $Z_{n-1}^{(k)}$ may be omitted without changing the value of $\widehat{\lambda}$ in (8).

2.1.3 Continuous time branching process

There are many interesting generalizations of basic Galton-Watson and continuous state branching process, notably those that evolve in continuous time instead of stages and those with variable propagation. In this report we focus on basic Galton-Watson and continuous state branching processes because of their simplicity and their basic approach to the timing of failures.

Many of the current cascading failure simulations do not model the detailed timing of failures (exceptions include [2] and the sequences of discrete events simulated in voltage collapse simulations [46]) and naturally compute failures in stages. Observed failure data can be grouped into stages by simple methods such as grouping together failures occurring closely in time as explained in section 2.3. The stages occur in a discrete time that advances by one unit with each successive stage but has no correspondence with the real time of the failures. These simple approaches avoid explicitly modeling the time evolution of the failures. However, it remains a possibility to model the time evolution of the failures in a branching process. For example, a continuous time Markov branching process is used in [17] to try to fit the time evolution of failures in large blackouts.

2.2 Estimating λ and blackout size distribution from simulations

We test branching process models using simulated power system cascades as follows:

1. Run the power system simulation a large number of times to produce cascading failure data in stages and the blackout size.

2. Estimate the empirical distribution of the blackout size. This is a brute force evaluation that relies on the large number of runs in step 1.

3. Use the cascading failure data in stages to estimate the parameters of the branching process, such as the average propagation λ. (The large number of runs will produce accurate parameter estimates, so that we do not have to address in this testing of the branching process model the tradeoff that will arise in practice when the branching process model is applied to a much smaller number of runs and some parameter inaccuracy is tolerated.)

4. Use the estimated branching process parameters and the branching process theory to predict the distribution of blackout size.

5. Compare the empirical blackout size distribution obtained by brute force with the blackout size distribution obtained via the branching process. The extent that these distributions match indicates the success of the branching process model in capturing the overall features of the cascading process in the power system simulation.

2.2.1 OPA cascading failure simulation

The OPA model produces cascading failures in stages resulting from a random initial set of line failures [5, 21]. The power transmission system is modeled using DC load flow and LP generator dispatch, and cascading line overloads and failures are represented. Each cascade produces a number of lines failed and the load shed in each stage of the cascade. The power system is assumed to be fixed with no transmission line upgrade process.

For each case considered, OPA was run so as to produce 5000 cascades with a nonzero number of line failures. These 5000 runs yield both line failure data and load shed data in the form (5). All our statistics are conditioned on a nonzero number of line failures.

2.2.2 Estimating line outage probability distribution

This subsection tests whether the line outages produced by the OPA simulation are governed by a Galton-Watson branching process with Poisson offspring distribution. The results are very similar to those in [18], but here we use the improved estimator $\widehat{\lambda}$ in (8). The parameters are the mean of the initial distribution of failures θ and the mean of the offspring distribution λ. The parameter estimators $\widehat{\lambda}$ and $\widehat{\theta}$ were obtained using equations (8) and (13) with saturation $S = 100$. According to (10), the number of runs $K = 5000$ gives a negligible standard deviation of $\sigma(\widehat{\lambda}) < 0.01$. For each case, the probability distribution of line failures was predicted using the estimates $\widehat{\lambda}$ and $\widehat{\theta}$ in the saturating generalized Poisson distribution formula (3). This tests the validity of the branching process model underlying (3) and the estimates $\widehat{\lambda}$ and $\widehat{\theta}$.

The first three cases used the IEEE 118 bus system at average load levels of 0.9, 1.0, and 1.3 times the base case loading. (The OPA parameters (explained in [5]) are $\gamma = 1.67$, $p_0 = 0.0001$ and $p_1 = 1$.) The estimated parameters are shown in Table 1. Good matches between the empirical and estimated distributions are shown in Figures 3-5.

The last two cases used the 190 bus tree-like test system [5] at average load levels of 1.0 and 1.2 times the base case loading. (The OPA param-

eters are $\gamma = 1.94$, $p_0 = 0.005$ and $p_1 = 0.15$.) The estimated parameters are shown in Table 1. The matches between the empirical and estimated distributions are shown in Figures 6 and 7. The match is not as good for the 190 bus system for 1.2 times the base case loading. The branching process captures the general trend of the empirical distribution, but does not capture the peaks at 15 and 30 lines. It is conceivable that the peaks are caused by saturation effects or by nonuniformity in the (artificially regular) design of the 190 bus tree-like test system.

The results suggest that good predictions of the probability distributions of the number of line failures can be obtained as long as saturation effects are not significant. We do not understand how to accurately model the saturation effects at present. The ability to predict the probability distribution of the number of line failures in non saturating cases supports the applicability of branching models to cascading failure before saturation is reached and the usefulness of the estimate $\widehat{\lambda}$ of failure propagation. $\widehat{\lambda}$ can be obtained much more efficiently than empirical probability distributions of line failures obtained by brute force.

Table 1: Estimators for line failure data produced by OPA

power system	loading factor	$\widehat{\theta}$	$\widehat{\lambda}_s$
IEEE 118 bus	0.9	1.10	0.19
IEEE 118 bus	1	1.66	0.41
IEEE 118 bus	1.3	12.20	0.44
tree-like 190 bus	1.0	1.49	0.53
tree-like 190 bus	1.2	6.21	0.62

2.2.3 Estimating load shed pdf

This subsection summarizes testing in [50] that tests whether the load shed produced by the OPA simulation is governed by a continuous state branching process with a gamma initial distribution and a gamma offspring distribution. The load shed is measured as a fraction of the total load so that the maximum load shed possible is 1, or total blackout.

The estimated propagation $\widehat{\lambda}$ and other parameters of the gamma distributions are estimated for the OPA data. The estimated propagation $\widehat{\lambda}$ at each load level is shown in the second column of Table 2. As expected,

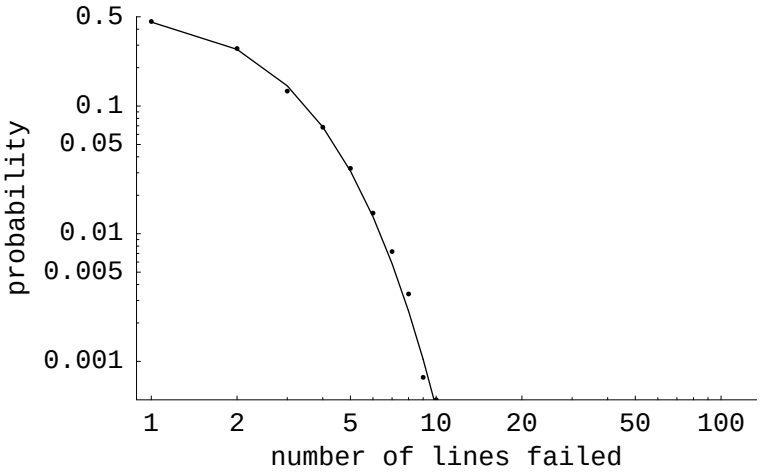

Figure 3: IEEE 118 bus system with loading factor 0.9. Distribution of line outages estimated with branching process (solid line) compared with OPA empirical distribution (dots). Note the log-log scales.

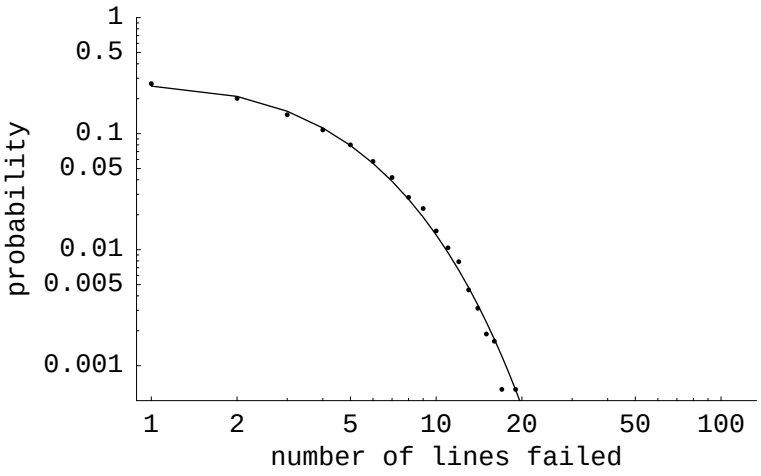

Figure 4: IEEE 118 bus system with loading factor 1.0. Distribution of line outages estimated with branching process (solid line) compared with OPA empirical distribution (dots).

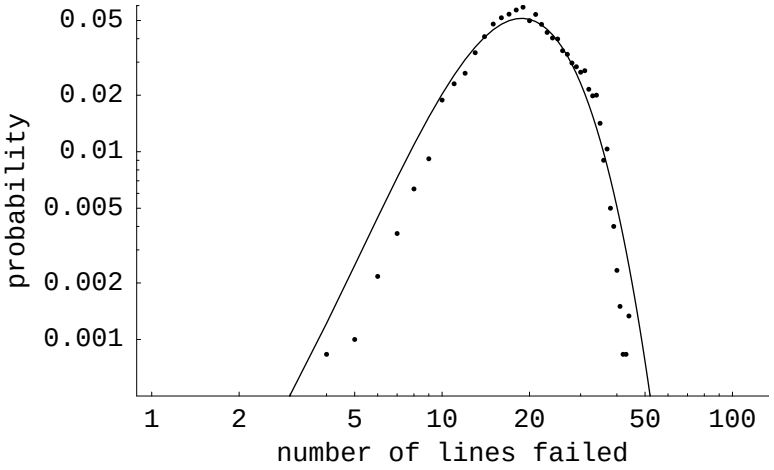

Figure 5: IEEE 118 bus system with loading factor 1.3. Distribution of line outages estimated with branching process (solid line) compared with OPA empirical distribution (dots).

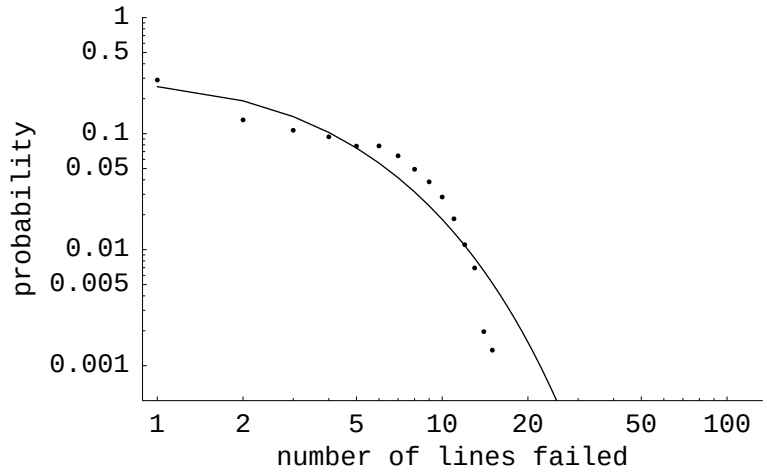

Figure 6: Tree-like 190 bus system with loading factor 1.0. Distribution of line outages estimated with branching process (solid line) compared with OPA empirical distribution (dots).

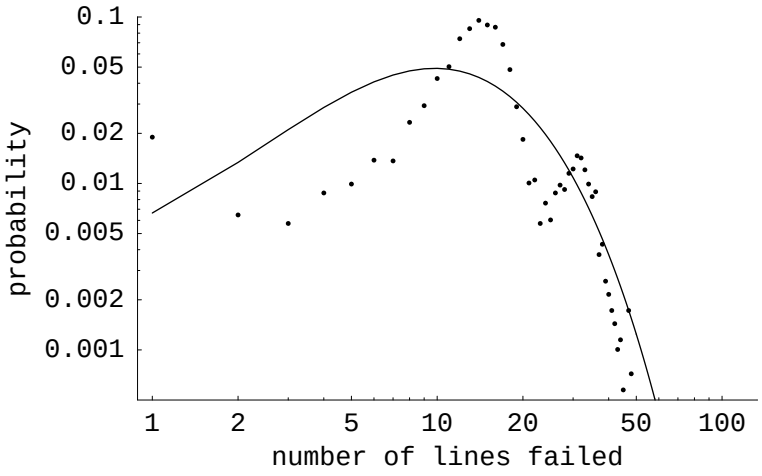

Figure 7: Tree-like 190 bus system with loading factor 1.2. Distribution of line outages estimated with branching process (solid line) compared with OPA empirical distribution (dots).

$\widehat{\lambda}$ increases with loading. All cases considered are subcritical ($\lambda < 1$) as required in subsection 2.1.2.

Figure 8 compares the empirical and estimated PDFs for loading factor 0.85, and Figure 9 compares the empirical and estimated PDFs for loading factor 1.0. The blackout size is plotted on a log scale over two decades, from a small blackout $Y = .01$ (shedding of 1% of total load) to $Y = 1$ (shedding of 100% of total load and total blackout).

2.2.4 Comparing λ estimated from line and load shed data

There are several ways to think of the cascading processes that are occur during a blackout, but one possible way is to think of a single cascading process that is monitored by two different measurements, lines failed and load shed. From this point of view, it would be natural for the propagation λ of the cascade measured by line failures to be the same as the propagation λ of the cascade measured by the load shed. (Note that since λ is a ratio of similar quantities, it is dimensionless and λ estimates using different quantities can be directly compared.) Using the same OPA cascades, Table 2 compares $\widehat{\lambda}$ computed from the load shed with $\widehat{\lambda}$ computed from the lines failed. The $\widehat{\lambda}$ for load shed matches well with the $\widehat{\lambda}$ for line failures. This result is consistent with the lines failed and the load shed reflecting a

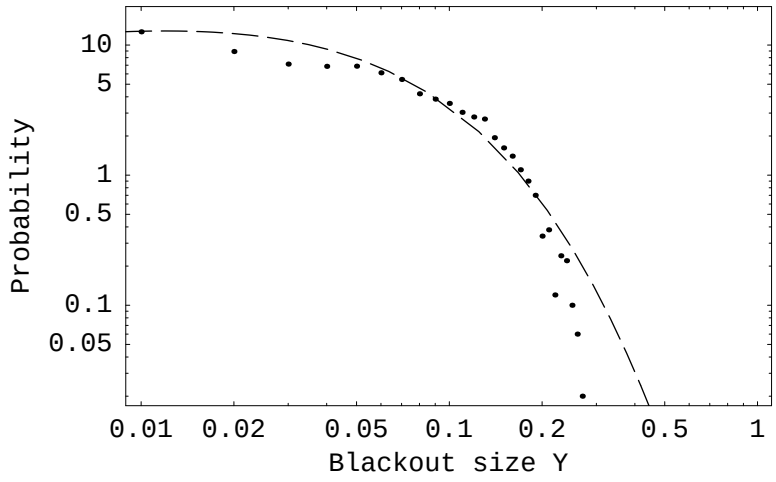

Figure 8: IEEE 118 bus system with loading factor 0.85. Probability density function of fraction of load shed Y. PDF estimated from branching process (dashed line) compared with empirical PDF from OPA simulation (dots).

common cascading process.

This result that the propagation of line failures and load shed agree is obtained here for only a few cases, but if the result is repeated for other simulations and cases, it would be useful because then one could use the monitoring of the propagation of line failures to predict the propagation of load shed.

Table 2: Estimated propagation $\hat{\lambda}$ from load shed and line failure data produced by OPA on IEEE 118 bus system

loading factor	load shed $\hat{\lambda}$	line failures $\hat{\lambda}$
0.85	0.128	0.115
0.9	0.159	0.188
0.95	0.264	0.288
1.0	0.429	0.430

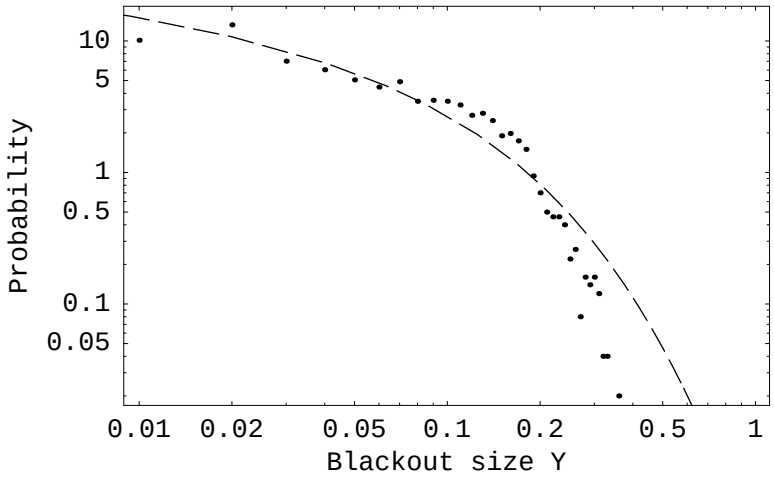

Figure 9: IEEE 118 bus system with loading factor 1.0. Probability density function of fraction of load shed Y. PDF estimated from branching process (dashed line) compared with empirical PDF from OPA simulation (dots).

2.3 Estimating line outage distribution from observed data

This section shows how to test branching process models on observed line outage data. Further work and and an enhanced write-up are in progress [38].

2.3.1 Observed line outage data

We processed approximately nine years of transmission line fault data from a regional electric power system with approximately 100 buses and 200 high voltage lines. The voltage levels considered are 220 kV and 500 kV; outages at lower voltage levels are not considered because of the potential number of unrecorded cases. There are several types of line outages in the data, including three phase and single phase and outages with successful or unsuccessful auto-reclosing. In this initial work processing the data, both voltage levels and all types of line outages are regarded as the same and the detailed causes of the line outages (line fault, busbar fault, or other fault or operations) are neglected. This is consistent with an initial, "top-down" analysis of the overall cascading process. Large flashover events in the data with approximately 260 outages over two days are neglected because they lack time tags. The data for each transmission line outage include the time (to the nearest minute), voltage level, and the auto-recloser's action.

2.3.2 Grouping outages into cascades and stages

We group the line outages first into different cascades, and then into different stages within each cascade using a simple method based on the time of the outages. Since operator actions are usually completed within one hour, we assume that successive outages separated in time by more than one hour belong to different cascades; since transients or auto-recloser actions are completed within one minute, we assume that successive outages in a given cascade separated in time by more than one minute are in different stages within that cascade.

Table 3: Total number of outages in each stage

stage	0	1	2	3	4	5	6	7	8	9	10	11	12	13	14	15
outages	296	45	18	14	10	3	1	1	1	1	1	1	2	1	1	0

Table 3 is obtained by summing over all the 226 cascades the number of outages in each stage. The initial outages are the 296 outages in stage

0. The probability distribution of the number of initial outages is shown in Fig.10a. The distribution in Fig.10a has a peak at 6 outages that prevents it being well fit by a Poisson distribution. One reason for the peak is that some cascades are initiated by a bus outage, and the relay trips off all transmission lines connected to that bus simultaneously at the start of the cascade.

2.3.3 Estimating λ and the distribution of outages

Assuming a Galton-Watson branching process model with no saturation, we use (11) to estimate λ based on the data in table 3:

$$\widehat{\lambda} = \frac{45+18+14+10+3+1+1+1+1+1+1+2+1+1+0}{296+45+18+14+10+3+1+1+1+1+1+1+2+1+1} = 0.25$$

That is, each outage produces an average of $\lambda = 0.25$ outages in the next stage. This result is insensitive to the grouping of outages into stages (re-defining the minimum time between successive outages in different stages to be 2 minutes and recomputing λ yields $\lambda = 0.24$).

To test how well the branching process model describes the data, we use the branching process with $\lambda = 0.25$ and the empirical distribution of initial outages to predict the distribution of the total number of outages Y using (4), and compare this with the distribution of the total number of outages directly obtained from the data. The comparison is shown in Figs. 10b and 11. A chi-squared goodness-of-fit test shows that the distributions are consistent at the 5% confidence level (the test groups together 5 or more outages). A heavy tail in the distribution of the total number of line outages is also observed in North American data in [11, 1], but our data has a heavier tail than [11, 1].

Observing outages for one year in this power system would yield an average of 25 cascades. To show how accurately λ could be estimated from one year of data, we took 9 non-overlapping random samples of 25 cascades and estimated λ for each sample of 25 cascades. A typical result is that the estimated λ has a standard deviation of 0.14. That is, assuming normality, an estimate of λ from one year of data lies within 0.14 of the true value about 68% of the time. This accuracy can be improved by collecting data over a longer time or over a larger region.

To summarize, the line failures are grouped into cascades and stages according to the failure times and we estimate the distribution of the initial number of failures and the propagation λ of the failures and hence estimate the distribution of the total number of line failures using a Galton-Watson

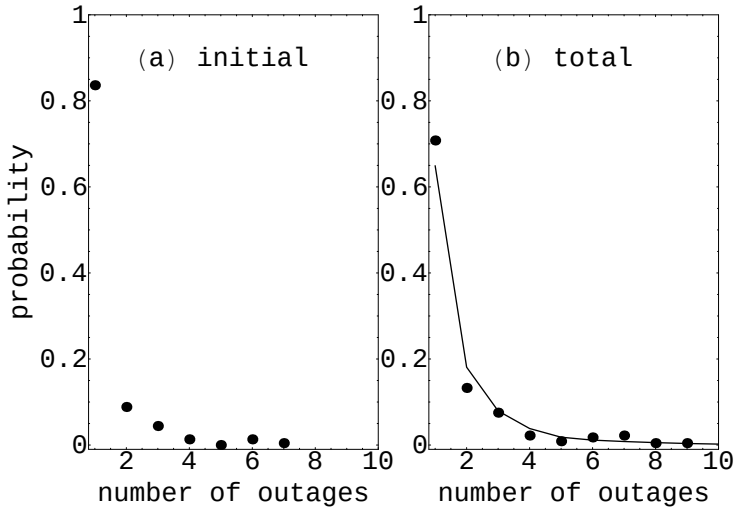

Figure 10: Probability distributions of number of outages. (a) Initial outages from data; (b) Total number of outages estimated using branching process (line) and from empirical observed data (dots).

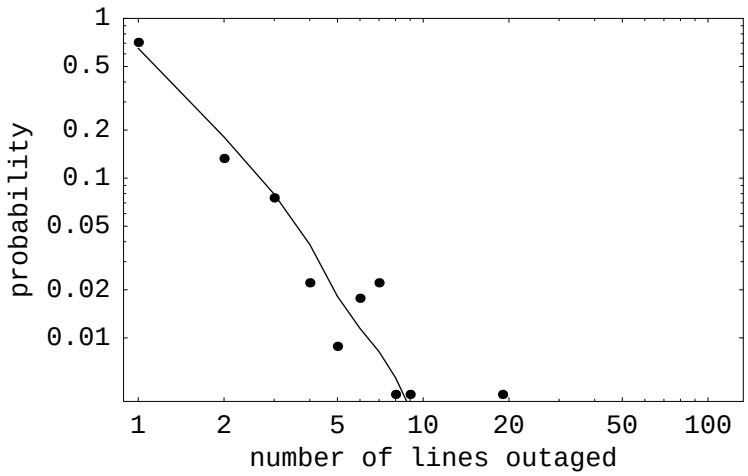

Figure 11: Distribution of total number of line outages estimated using branching process (line) and from empirical observed data (dots); this log-log plot shows a heavy tail.

branching process model. For this observed data, the empirical distribution of the total number of line outages is well approximated by the initial line outages propagating according to a branching process with parameter λ. Estimating λ requires significantly less data than estimating the heavy tail of the empirical distribution so that the distribution of blackout size may be efficiently estimated from data observed over a much shorter time. The efficiency of this estimation opens up possibilities of practical monitoring of power system reliability based on direct observations.

2.4 Discussion and future directions

This section considers some challenges to be addressed in modeling cascading failure with branching processes and future work.

2.4.1 Efficiency

Methods for quantifying cascading failure become practical when they require a modest number of cascades in a sample. There is a tradeoff between an efficiently small number of cascades in a sample and the accuracies of the estimated branching process parameters and the blackout size distribution based on these estimates.

Formula (12) for the asymptotic standard deviation of the estimator $\widehat{\lambda}$ suggests that a standard deviation in $\widehat{\lambda}$ of 0.1 requires about 25 cascades in the sample if there is one initial failure. The line outages observed in the 200 line power system of section 2.3 occur at about 25 cascades per year and each year of data yields a standard deviation in $\widehat{\lambda}$ of 0.14. Halving the standard deviation would require quadrupling the number of cascades in the sample to 100, either by observing data over four years or by monitoring the line outages over a larger portion of the power system with 800 lines. That is, improving the accuracy of $\widehat{\lambda}$ requires either waiting longer and having less time resolution or gathering statistics over a wider area with a loss of spatial resolution. It is inherent in the method that the estimated value $\widehat{\lambda}$ is averaged over the time period and spatial extent over which the cascades were observed.

Describing these temporal and spatial limitations in quantifying cascading failure requires further experience, especially with observed data, before firm conclusions can be drawn. However, it is seems that the branching process estimation methods will offer substantial improvements in efficiency over estimating blackout probability distributions exhaustively. If estimates of the size of the initial disturbance are known accurately, we can hope for

at least order of magnitude reductions in the number of cascades to be simulated or observed in order to predict the frequency of larger cascades. In particular, in North America, the largest blackouts occur on a time scale of decades and waiting to accumulate enough statistical data on these blackouts is much slower than using branching process models that could give approximate results on a time scale of about one year.

2.4.2 Elaborations in modeling and data processing

In this report, we start with the simplest branching process models and estimate a few model parameters without distinction between types of outages and averaged over the duration of the cascade, the portion of the network studied, and the sample of cascades. Parsimony in parameters and simplicity of modeling are desirable, but it is not clear whether the branching process models require elaboration, or what is the best processing of data before the branching process model is applied. For example, it is not clear in processing line outage data whether a higher voltage line outage should be given more weight than a lower voltage line outage. Another example is that if the power system stress varies over the day, it might be desirable to accumulate data for high stress and low stress periods separately. Experimenting with the processing is needed.

We are applying a model of random propagation that is uniform over the duration of the cascade with parameters estimated by data averaged over the cascade. There could be changes in the cascading phenomenon as the cascade proceeds. For example, it is conceivable that λ could decrease over the duration of the cascade as blackout inhibition or saturation effects start to apply. The current calculations for the Galton-Watson branching process do allow for estimation of λ before a saturation limit of S is reached, but we do not yet have a good understanding of possible saturation effects or whether or how they impact the computations of cascading failure risk. Saturation effects have been observed as peaks in some simulations of smaller power systems of the order of 100 buses [20], but it is unknown whether saturation effects are important in large power systems. It seems likely that any model of cascading could be expected to break down or become inaccurate at some extreme level of network disconnection, but simulations on smaller test systems do not provide data to address this question and the rarity of the largest possible blackouts of entire interconnections limits the applicability of observations.

The current initial approach for processing the observed cascades combines together all the observed cascades so that the computed propagation

λ is averaged over all the system conditions. This should be a meaningful measure of the average cascading conditions, but it is not representative, for example, of the cascading under high stress conditions. The results so far on simple cascading models show that lambda increases with system loading. So one way to get a more refined picture would be to divide the cascades into those occurring under high load and low load conditions and compute a high load and low load lambda. If there was enough data, one could also consider multiple load levels.

Considerations of method efficiency and applicability typically depend on the range of λ considered. For example, lower values of λ make saturation unimportant, the standard deviation of the estimator $\widehat{\lambda}$ depends on λ, and the continuous state branching process methods presented in this report assume that $\lambda < 1$. Further work with realistic simulations and especially with observed data can determine the range of λ that we are trying to measure.

While there are reasonable arguments for choosing Poisson offspring distributions for the Galton-Watson branching processes, a good choice of the offspring distribution for continuous state branching processes is an open question. Directly estimating the offspring distribution from data could be difficult.

The role of time in the branching processes is one area of possible elaboration of the processing and the modeling, both in the possibility of modeling the time at which the failures occur and improving the methods of grouping failures into stages.

2.4.3 Further testing

This report initially tests branching process models on cascading line failures in systems of the order of 100 buses with line outage data observed over one decade and data simulated by the OPA model of cascading line failures. The results are promising and further testing on other cases and larger systems is indicated. It would be particularly useful to test the results on cascading failure simulations with more modeling detail such as the Manchester model [41, 35] and TRELSS [45, 25] and any real data summarizing cascading that can be made available for research. If there is some universality to the gross features of cascading failure in power system blackouts, then many cases need to be tested to gain confidence in this universality.

The speculation that the propagation λ of line failures is the same as the propagation λ of load shed that is supported by the cases considered in section 2.2.4 should be tested further.

2.5 Conclusions

We have shown how to test branching process models on observed and simulated power system cascading failure data. The observed data is grouped into stages according to the failure times and the simulated data is naturally produced in stages by the OPA model of cascading line overloads. Then the propagation λ and other parameters of the branching process model are estimated and used to compute the probability distribution of blackout size. The estimator for λ has less bias than the estimator proposed in [18] when there are saturation effects. Both the number of line failures and the load shed can be used as measures of blackout size. The models corresponding to these measures are a Galton-Watson branching process with saturation and a continuous state branching process respectively. In the case of the observed outages, the method amounts to predicting from industry data the statistics of the size of cascading line outages when the initial line outage distribution is specified.

For the cases examined, which include cascading line overloads on the IEEE 118 bus test system and observations of line failures on a power system with approximately 100 buses, the probability of blackout size obtained via the branching process compares well with the probability of blackout size obtained by observing the power system for a long time or by exhaustive simulation. Quantifying cascading failure by first estimating branching process parameters requires significantly fewer cascades to be observed or simulated. This efficiency is key to practical application to monitoring the risk of cascading failure or using simulations to efficiently quantify the reliability benefits of proposed upgrades.

The initial results in this report are promising and further testing of branching process models is warranted using other cascading failure simulations and other observations of cascading failures. The bulk statistical analysis of cascading failure using branching process models is developed here for blackouts, but could also be tested on data for cascading failure in or between other infrastructures.

3 Long-term effect of the n-1 criterion on cascading line outages with complex system upgrade

How does one assess the long-term effect of planning and operational policies on power transmission system reliability? This is a challenging question because as the power system upgrades, the power flows and patterns of use of the power system are not static. That is, a change in policy not only has an immediate effect on reliability, but eventually the patterns of power flows react to both the effects of the policy and the upgrade. It is the combined effects of the policy and the evolving grid that produce the long-term reliability.[2] For example, according to the convincing examples by both Kirschen[30] and Reppen[40], an upgrade in power system equipment or procedures that is made for the purpose of reliability may soon be exploited to increase the economic rewards from power system transactions. The long-term effect of the upgrade on reliability may be small or even negative.

In this chapter we suggest a way to assess by simulation the long-term effects of a policy on the reliability of an evolving power grid with respect to cascading line overloads. Further work on an enhanced write-up is in progress [39]. The grid evolves and upgrades in response to a slow load increase and the reliability policy. We consider two policies. The first policy is a standard n-1 criterion. That is, upgrade of the transmission lines is done to satisfy the requirement that any single contingency in a contingency list does not overload any other line. The second policy responds to directly to blackouts by upgrading the lines involved after each blackout.

We assess and compare the long-term effect of these policies on the probability distribution of blackout size and the grid utilization. The probability distribution of blackout size describes the frequency of small, medium and large blackouts and can be combined with blackout cost to yield estimates of the risk of various sizes of blackouts. The grid utilization is related to the average line loading or the average line rating relative to the total power supplied. Higher grid utilization extracts more value from the grid investment.

Previous simulation tools to assess power system planning or operational rules regard the power system and its pattern of use in a more static context [5, 9, 31, 29, 35, 45, 25] and evaluate the effect of different policies by showing, for example, that a particular security problem or a particular blackout

[2] An analogous question in transportation asks whether widening a road will reduce accidents due to traffic congestion. It is clear that widening a road will reduce congestion if traffic flows stay the same, but it is routine for traffic flows to eventually exploit the increased capacity and congest the road again.

would have been avoided if the policy had been different. This type of analysis is very useful in identifying weak points in power system policies, operations, or the grid itself. Indeed, these analyses are used to guide the upgrade of the grid. Moreover, the simulation tools can be sophisticated in their modeling of the detail of the power system and a variety of different security and adequacy concerns can be addressed. From the point of view of this chapter, in this type of analysis, the short-term or immediate effect of the policy is assessed and the power system is assumed to be static in the sense that there is no dynamic evolution of the grid or its pattern of use.

There are several models of cascading overloads of transmission lines representing the power grid at the level of DC load flow and LP dispatch of generation [5, 7, 9, 31, 2]. Examples of special capabilities of these models are that our OPA model represents the slow evolution of grid as it upgrades [7] and the model developed by Chen and Thorp represents hidden failures of the protection system [9]. The state of the art in terms of detailed modeling of a static power grid is to use an AC load flow and approximately represent protection, operator actions and voltage collapse as in the Manchester model [29, 35] and TRELSS [45, 25]. The Manchester model has been run on a 1000 bus industrial case and the cascading mode of TRELSS is used by industry to identify cascading failure problems in large power systems.

The idea of modeling the evolving grid is first suggested in [4, 8] and the OPA model[3] of an evolving grid is described in [7] and applied in [6]. For an overview, see [21]. Newman et al. [36] use the OPA model to evaluate the effect of component reliability, operational margins, and redundancy on long-term blackout risk. A result in [36] that illustrates the importance of modeling the evolving grid is that while increasing the reliability of components decreases the probability of small blackouts, it can actually increase the probability of large blackouts in the long term as the patterns of power flow change to take advantage of the increased component reliability. This chapter is also based on the OPA model and has a similar overall approach to [36] but is different from [36] in that in this chapter we extend the OPA model to implement the n-1 criterion.

Anghel et al. [2] develop a model of an evolving grid using the PSA suite at Los Alamos National Laboratory. In addition to modeling the grid at the level of DC load flow and LP dispatch, they represent the timing of blackout events and grid restoration and repair. Operator actions are represented and

[3] **OPA** stands for **O**ak Ridge National Laboratory, **P**ower Systems Engineering Research Center at the University of Wisconsin, University of **A**laska to indicate the institutions collaborating to devise the simulation.

the tradeoff between load shedding and cascading outages is optimized to minimize the cost of cascades in a 100 bus power system.

There are interesting discussions of the n-1 criterion and its probabilistic generalizations in the literature. Zima and Andersson [52] assume a loading-dependent probability of line trip and redispatch generation to minimize the risk of subsequent line trips for any contingency. They compare this policy with the n-1 criterion and find that it slightly reduces the probability of medium size blackouts due to cascading line outages. Nippert [37] generalizes and alters the n-1 criterion to a probabilistic criterion that bounds the expected energy unserved based on observed failure statistics. He illustrates this approach in planning the maximum load of a 110/10 kV transformer station. Chen and McCalley [10] discuss the combinatorial difficulties of systematic treatment of higher order n-k contingencies and select higher order contingencies based on their risk computed from their probability and from their impact assessed by evaluating dependencies caused by switching actions.

3.1 Modeling cascading and the evolving grid

This section summarizes the OPA model of the evolving grid [5, 7] and describes its extension to represent the n-1 criterion. The strengths and weaknesses of modeling the evolution of the grid are discussed. In particular, it should be noted that the blackouts we are studying with the OPA model are only due to cascading line outages and overloads; many other mechanisms involved in real blackouts are neglected.

3.1.1 Cascading overloads

The OPA model represents probabilistic cascading line overloads and outages in a power grid and is used to produce blackout statistics. Each trial of the model starts from a solved DC load flow. Some of the trials produce cascading line outages and/or load shed in blackouts. To obtain diversity in the trials, the system loads at the start of each trial are varied randomly about their mean values. After the initial solved DC load flow, transmission lines outage probabilistically and the consequent redistribution of power flows is calculated using the DC load flow and a standard LP dispatch of generation [43]. The LP dispatch can shed load, but the cost function is weighted to ensure that load shedding is avoided where possible. Lines that are overloaded in the redistribution of power flow are assumed to be the lines vulnerable to further outage and each of these lines outages with a

given probability. If none of these vulnerable lines fail, the cascade stops. If some of these vulnerable lines fail, the load flow and redispatch is solved again and further vulnerable lines may fail. The cascade of line outages continues in this manner until no further lines fail. For each trial, the lines that have outaged (if any), the total amount of load shed (can be zero), and diagnostic data are recorded. A blackout is defined to occur when the load shed is not negligible. (Negligible load shed is defined to be less than 10^{-5} times the total load.)

3.1.2 Grid evolution

The grid evolves in time by slowly upgrading system capacity to satisfy the gradual growth in load. The gradual growth in load is modeled by multiplying the average load by 1.00005 before every trial. If each trial of the model is thought of as one day of operation, then this amount of gradual load growth corresponds to an annual load growth of 1.8%. However, although time in the model advances with each successive trial, we do not insist that the time in the model be strictly interpreted as one trial per day. One reason is that the chance of a blackout is not constant in time and there could be several or no times during a day when a blackout is likely. Another reason is that the real power system is upgraded not only in response to actual blackouts but also to simulated blackouts or potential blackouts under contingency conditions. There can be a variable number of simulations to detect potential blackout conditions in one day of power system operation.

The slow average load growth gradually makes the system more stressed and some reliability criterion finally can not be satisfied. Then system capacity has to be upgraded. The transmission lines are upgraded by increasing their maximum power flow limits. (There are number of ways of implementing an upgrade that have the effect of increasing a line maximum flow limit such as reconductoring, upgrade elsewhere that relaxes an operational limit on the line, vegetation control, load voltage support to decrease reactive power flows, and upgrade of protection or operating procedures.) The choice of which transmission lines to upgrade and by how much is the upgrade policy described in the next subsection. Of course, to satisfy adequacy, the generation also has to be upgraded. The generation upgrade is done as needed to maintain coordination with the transmission line upgrades. In particular, the generation is increased at randomly selected generators subject to coordination with the limits of nearby lines when the generator capacity margin falls below a threshold [7].

The upgrade process starts from some assumed initial grid and there is a transient before the upgrading grid settles down to a "steady state". In this steady state, the load is slowly increasing and the grid is correspondingly slowly upgrading, but the blackout statistics are stationary. To obtain statistics for the blackouts in the steady state, the blackouts during the initial transient are discarded. Studying the steady state distribution of blackouts ensures that the method examines the long-term effects of the upgrade policy. It is not yet known to what extent the nation's power grids are near such a steady state, but studying the steady state is the obvious starting point for the study of the complex upgrading power grid.

3.1.3 Upgrade policies

The transmission line upgrade policy determines how and when to increase the maximum line flow limits of the transmission lines. In this chapter we compare the following two upgrade methods:

1. At the beginning of each trial, test whether the system satisfies the n-1 criterion given the initial pattern of loading and the assumed contingency list. Any line that overloads in the test of the n-1 criterion is upgraded until it no longer overloads.[4] No lines are upgraded if the n-1 criterion is satisfied.

2. Upgrade the line flow limit when that line was tripped in a blackout in the previous trial [7]. This upgrade method directly responds to each blackout immediately after it occurs.

The n-1 criterion and directly responding to blackouts are both used in practical power system design and operation. Here we test idealized forms of each method applied exclusively.

We interpret the n-1 criterion as requiring the transmission system to allow any single outage of a line in a contingency list without overload of any other line (we do not consider generator outages). For each initial pattern of loading, including the load variation assumed for that case, we check the n-1 criterion and, if it is not satisfied, upgrade all the lines that were overloaded before simulating the cascading outages in the usual way.

The contingency list of length k was determined as follows. We ranked the lines of the transmission system according to their impact on other lines using line outage distribution factors and then selected the first k highest impact lines to be in the contingency list.

[4] Generation is redispatched if the contingency islands the power system.

3.1.4 Discussion of the modeling

The OPA model is "top-down" and represents the processes in greatly simplified forms, although the interactions between these processes still yield complex and complicated behaviors. The simple representation of the processes is desirable both to initially study only the main interactions governing the complex system and for pragmatic reasons of model tractability and simulation run time. (There is some tradeoff between modeling the upgrade process and how much detail can be included in modeling the cascading.) The modeling of the cascading overloads neglects the timing of events and does not consider the many other ways that disturbances can propagate in blackouts, such as protection system failures, dynamics, and human factors. However the cascading overloads are consistent with power system modeling at the level of DC load flow and LP dispatch. The modeling of the grid evolution captures some simplified basic elements of the upgrade process and policy.

The modeling of the cascading overloads and the grid evolution is simple, but modeling both processes together is a significant innovation that allows the slow, complex dynamics of the interaction of the power system reliability and upgrade to be studied. One can think of the upgrade process as a feedback that adjusts the reliability of the power system. If the grid has too little capacity, there will be more blackouts or security violations and the feedback will cause more upgrade. If the grid has excess capacity, there will be fewer blackouts or security violations and the feedback will reduce the upgrades until load growth erodes the excess capacity. It is routine in control systems that system behavior is dominated by the feedback and is insensitive to the details of the "plant" being controlled. That is, a good, approximate model of the control system should represent the feedback and can use a simplified model of the plant. This analogy with control systems suggests that a basic model of power system reliability should represent the upgrade process and can use a simplified model of the failure mechanisms. In this regard, it is encouraging that the OPA model can approximately reproduce the form of the observed statistics of distribution of blackout sizes in North America [7].

Another, more traditional way to model reliability is to consider a fixed power system that does not upgrade, but is representative of a realistic power system that has already undergone the upgrade process. Simulating such a power system with a different upgrade policy evaluates the short-term effect of the policy. This is definitely useful, but it does not account for the way in which the power system may evolve over the long term in response

to the different upgrade policy. We suggest that our initial modeling with OPA shows how to evaluate the long-term effect of the policy and explore a complementary aspect of reliability.

3.2 Results

All results use the IEEE 118 bus system on the OPA model with upgrade controlled either by the n-1 criterion or by responding directly to blackouts by upgrading the lines involved in the blackout.[5] Each case simulated 50,000 trials of the model and the last 30,000 trials are used to generate the steady state blackout statistics and grid utilization measures.

3.2.1 Grid evolving with n-1 criterion with 10 contingencies

We show the OPA results for the n-1 criterion reliability policy with a contingency list of length 10. Fig. 12 shows the exponentially increasing average load growth and the random variability about that average load that is assumed by the model. It follows that the blackout size measured by load power shed has an exponentially increasing trend as shown in Fig. 13. The fractional blackout size measured by the fractional load power shed in each trial of the model is the load shed divided by the load supplied at the end of each trial and this becomes stationary as the grid evolves as shown in Fig. 14. The enlargement in Fig. 15 shows that in many trials there is no load shed. Indeed the overall frequency of blackouts (some load shed) is 0.114.

Blackout size can be measured by the fraction of load that is shed. Figs. 16 and 17 show the probability distribution of blackout size as measured by fractional load shed in two ways. Fig. 16 plots the probability that a trial of the model has a blackout exceeding a given blackout size. In particular, the probability that a trial has blackout size greater than zero is the probability that a trial has a blackout and Fig. 16 shows this probability as 0.114. That is, 11.4% of trials shed load. Fig. 17 shows the distribution of blackout size as a probability density function (pdf). The maximum likely blackout is about 20% of the total load. If we define risk as probability times cost and assume that blackout cost is proportional to blackout size, then we obtain Figure 18 which shows the distribution of risk of blackouts of various sizes.[6]

[5]The OPA parameters are explained in [5, 7] and the values used are: 50 trials with no output, 50000 trials written to output, $\lambda = 1.00005$, $\gamma = 1.67$, $\mu = 1.07$, $p_0 = 0.001$, $p_1 = 0.15$, $\Delta P/P = 0.3$, $\kappa = 0.04$, delay to upgrade generators = 1.

[6]There are many uncertainties in determining direct and indirect blackout costs, particularly for large blackouts, and the assumption of blackout cost proportional to blackout size is crude. Despite this considerable uncertainty in determining costs, it is still worth-

Fig. 18 shows that the larger blackouts have more than double the risk of the smaller blackouts.

The fractional loading of a line is the line power flow divided by the maximum line power flow and is measured at the beginning of each trial. One measure of grid utilization is the fractional line loading averaged over all the lines. This measure indicates the average fraction of the grid capacity that is used in operation of the grid. Fig. 19 shows how the average fractional line loading changes as the grid evolves from its initial condition. The average value of the fractional line loading in the steady state is 0.229 as shown in Table 4.

As the grid evolves, the average maximum flow limit of the lines has an exponentially increasing trend that follows the exponentially increasing system load. We can see this from the average maximum flow limit averaged over the lines divided by load served, which becomes stationary as shown in Fig. 20. The time average of this quantity in the steady state indicates the average line flow limit per MW served to the load and is another measure of grid utilization shown in Table 4. Since the grid investment is related to the maximum line flow limits and the societal benefit is related to the power served, the average line flow limit per MW served is one way to indicate the ratio of societal benefit to the grid investment.

3.2.2 Comparing direct response to blackouts with n-1 criterion

The effect of changing the reliability policy from the n-1 criterion with 10 contingencies to the direct response to the blackouts is examined. Figs. 21 and 22 compare the probability distribution of blackouts. The two cases have almost the same probability distribution except that there are more small blackouts with the direct response to blackouts.

The grid utilization of the n-1 case and direct response to blackouts is compared in Table 4. The average line loading for the n-1 criterion with 10 contingencies is about 41% smaller than with direct response to blackouts. It appears that the n-1 criterion gives a smaller average line loading because the network is upgraded unevenly, with line flows ranging from 10% of the flow limit to 95% of the flow limit. The average line flow limit per MW served for the n-1 criterion is about 4 times the line flow limit per MW served for the direct response to blackouts.

---

while to illustrate a sample risk calculation with an assumption about costs.

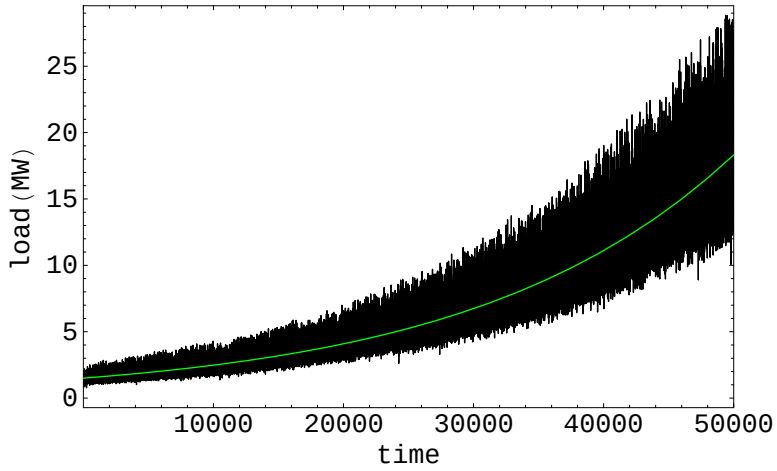

Figure 12: Average load growth and the random variation about the average load. The time shown is number of model trials. The average load growth is exponential because the average load is multiplied by 1.00005 before each trial.

3.2.3 The effect of length of contingency list

We examine the n-1 criterion with contingency lists of length 1, 10 and 50. 10 and 50 contingencies yield almost the same distribution of blackout size, while 1 contingency has many more small blackouts as shown in Fig. 24. The frequencies of blackouts with various numbers of contingencies are compared in Table 4. The longer contingency lists have lower blackout frequencies and less grid utilization as shown by the lower average line loading and higher line flow limit per MW served.

Table 4: Grid utilization and blackout frequency

	direct response	n-1 list of 1	n-1 list of 10	n-1 list of 50
Average line loading	0.387	0.277	0.229	0.176
Average line flow limit per MW served	0.017	0.031	0.074	0.085
Blackout frequency	0.139	0.723	0.114	0.107

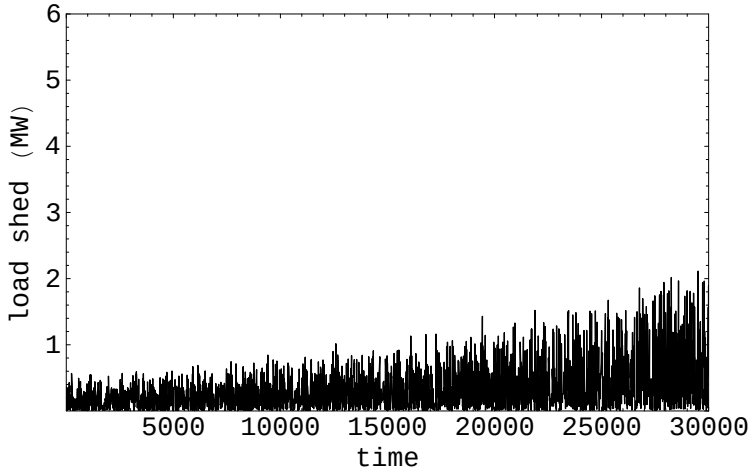

Figure 13: Load shed. n-1 criterion with 10 contingencies on IEEE 118 bus test system.

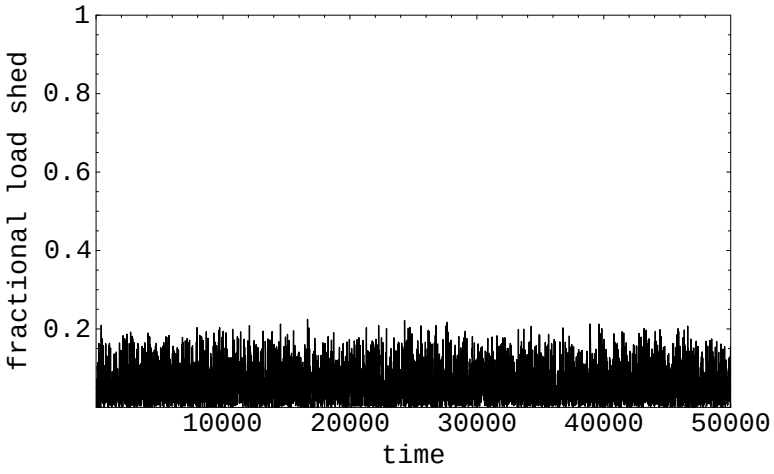

Figure 14: Fractional load shed. n-1 criterion with 10 contingencies.

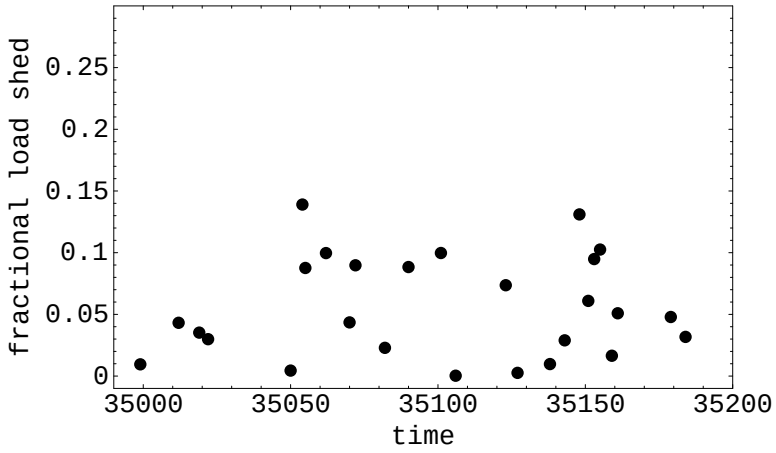

Figure 15: Fractional load shed for a sample of 200 trials to show detail. n-1 criterion with 10 contingencies.

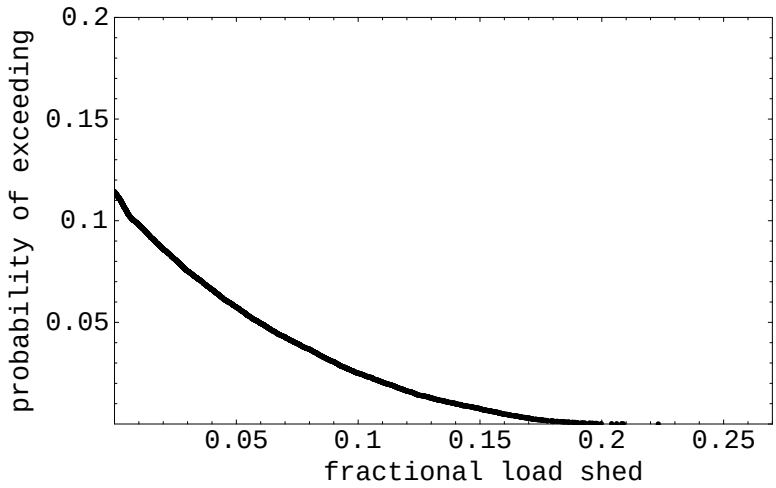

Figure 16: Probability of blackout exceeding a blackout size. Blackout size is measured in fractional load power shed. n-1 criterion with 10 contingencies.

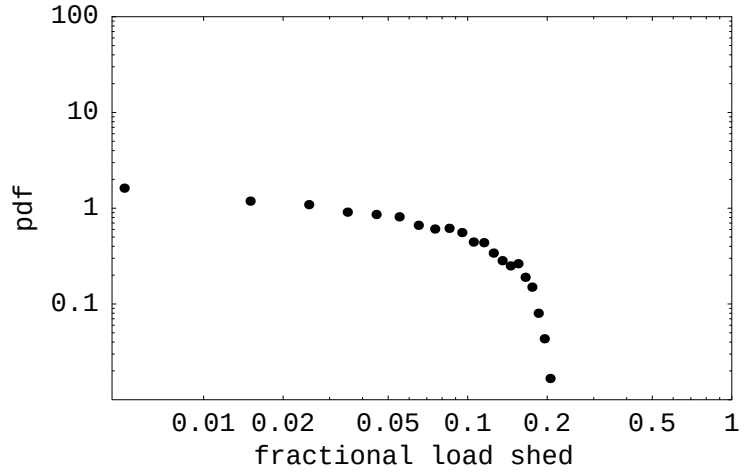

Figure 17: pdf of blackout size measured in fractional load shed. n-1 criterion with 10 contingencies.

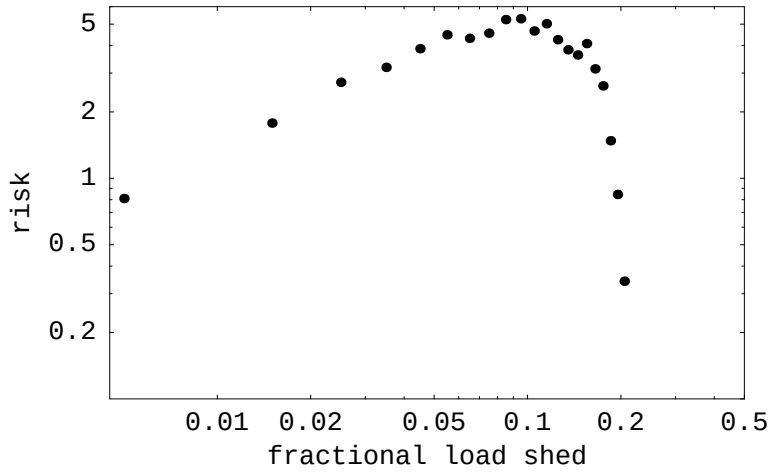

Figure 18: Distribution of blackout risk. n-1 criterion with 10 contingencies.

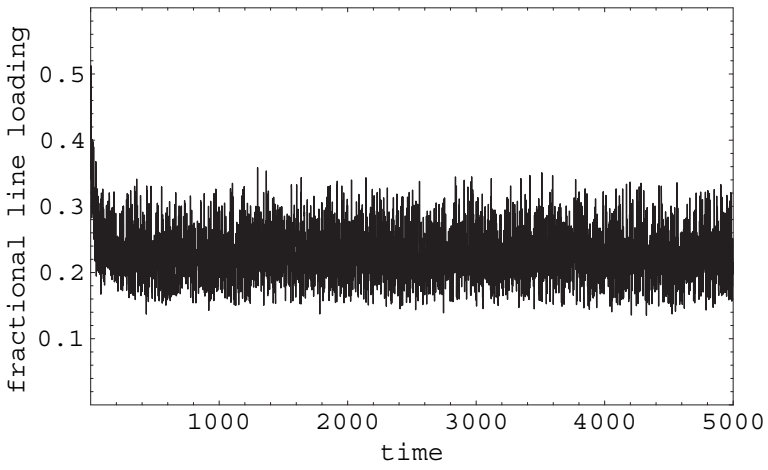

Figure 19: Average fractional line loading. n-1 criterion with 10 contingencies for the first 5000 trials.

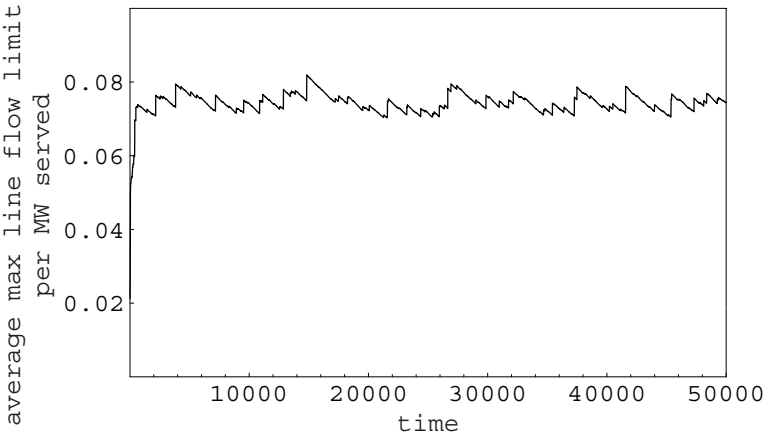

Figure 20: Average maximum line flow limit per MW served. n-1 criterion with 10 contingencies.

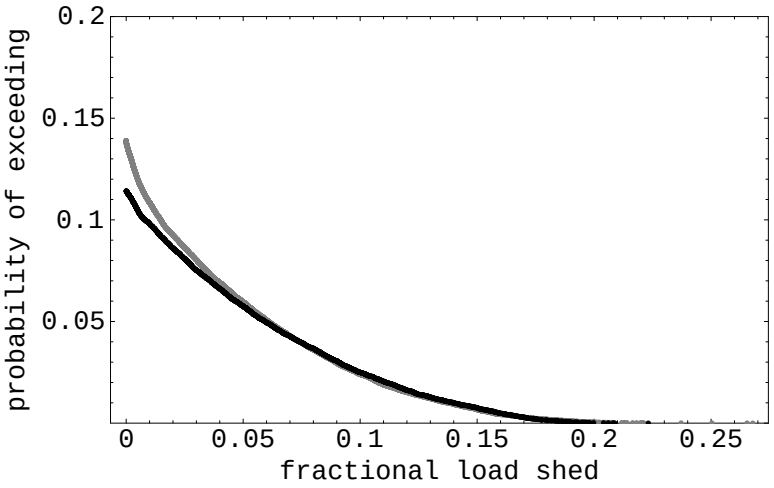

Figure 21: Probabilities of blackout exceeding a blackout size. Blackout size is measured in fractional load power shed. Black line is n-1 criterion with 10 contingencies. Gray line is direct response to blackouts.

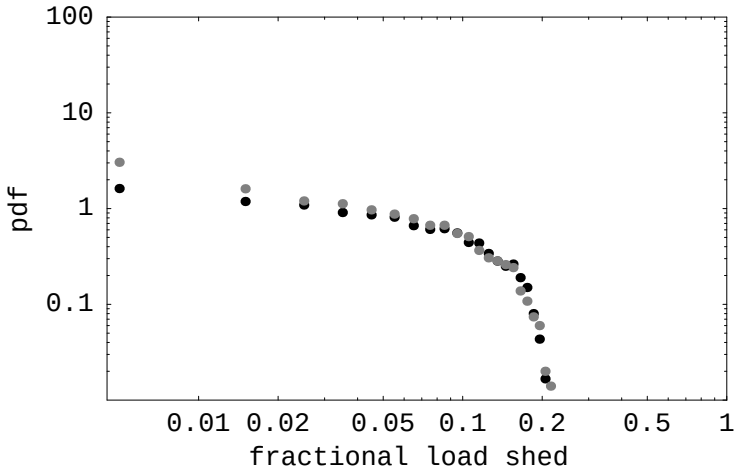

Figure 22: Log-log plot of pdfs of blackout size. Blackout size is measured in fractional load power shed. Black dots are n-1 criterion with 10 contingencies. Gray dots are direct response to blackouts.

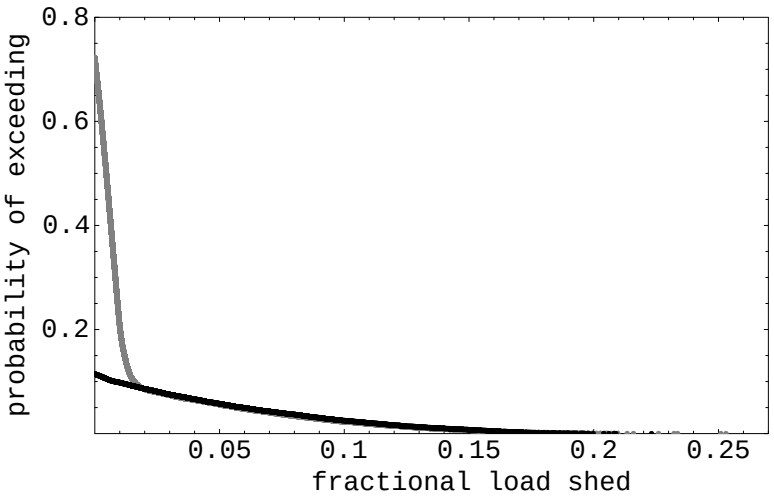

Figure 23: Probabilities of blackout exceeding a blackout size. Black line is n-1 criterion with 10 contingencies. Gray line is n-1 criterion with 1 contingency.

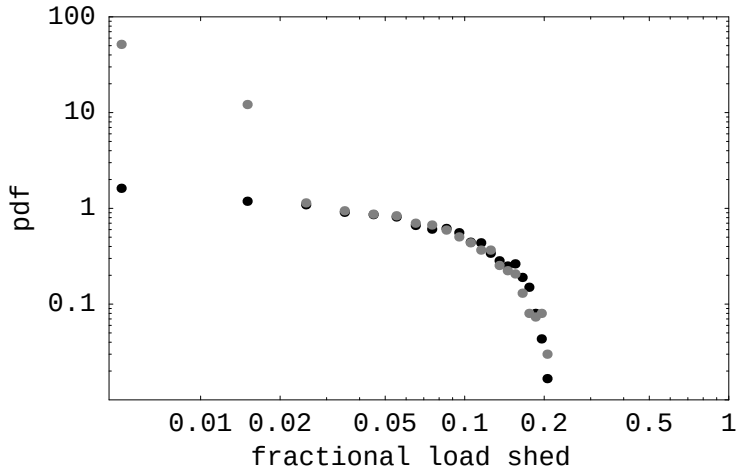

Figure 24: Log-log plot of pdfs of blackout size. Black dots are n-1 criterion with 10 contingencies. Gray dots are n-1 criterion with 1 contingency.

3.3 Conclusions

We consider the n-1 criterion and another reliability policy that responds directly to blackouts by upgrading the lines that outaged in the blackout. We show how to assess the effect of these policies on the blackout probability distribution that describes the long-term steady state frequency of small, medium and large blackouts due to cascading line outages. As the load slowly grows, the grid upgrades to maintain the reliability policy and the patterns of power flows in the network evolve. Eventually this evolving grid settles down to a "steady state" in which, although there remains variability in the blackouts, the blackout statistics and the grid utilization are stationary. We simulate this evolving grid together with the cascading line overloads to compute these long-term blackout statistics and the grid utilization. Although each part of this complex system is represented simply, accounting for the joint evolution of the grid and the patterns of power flow gives a new type of reliability calculation that is complementary to reliability calculations that assess the short-term effect of policies on reliability assuming that the grid remains fixed.

To illustrate the approach, we compute the long-term effect of the n-1 criterion with 10 contingencies on the reliability of the IEEE 118 bus test system. The long-term probability distribution of blackout size and measures of average grid utilization are computed. If it is assumed that blackout cost is proportional to power shed, then the risk of larger blackouts exceeds the risk of smaller blackouts.

To show how reliability policies can be compared, we study the effect of varying the length of the contingency list and of changing the policy to a direct response to blackouts that upgrades the lines involved after each blackout. Reducing the contingency list from 10 contingencies to a single contingency greatly increases the frequency of small blackouts and increases the grid utilization. Changing the n-1 criterion policy with 10 contingencies to the direct response to blackouts increases the frequency of small blackouts somewhat and increases the grid utilization.

Although it is obvious that power grids are continually evolving to meet the demands of supplying an increasing load and maintaining reliability, it is exciting to suggest a way to describe the complex interactions between these processes and to take an initial step towards quantifying the impact of reliability policies on the long-term reliability.

References

[1] R. Adler, S. Daniel, C. Heising, M. Lauby, R. Ludorf, T. White, An IEEE survey of US and Canadian overhead transmission outages at 230 kV and above, IEEE Transactions Power Delivery, vol. 9, no. 1, Jan. 1994, pp. 21-39.

[2] M. Anghel, K. A. Werley, A. E. Motter, Stochastic Model for Power Grid Dynamics, 40th Hawaii International Conference on System Sciences, Hawaii, January 2007.

[3] K.B. Athreya, P.E. Ney, *Branching Processes*, Dover NY 2004 (reprint of Springer-verlag Berlin 1972).

[4] B.A. Carreras, D. E. Newman, I. Dobson, A. B. Poole, Initial evidence for self-organized criticality in electric power blackouts, 33rd Hawaii International Conference on System Sciences, Maui, Hawaii, January 2000.

[5] B.A. Carreras, V.E. Lynch, I. Dobson, D.E. Newman, Critical points and transitions in an electric power transmission model for cascading failure blackouts, Chaos, vol. 12, no. 4, December 2002, pp. 985-994.

[6] B.A. Carreras, V.E. Lynch, D.E. Newman, I. Dobson, Blackout mitigation assessment in power transmission systems, 36th Hawaii International Conference on System Sciences, Hawaii, 2003.

[7] B.A. Carreras, V.E. Lynch, I. Dobson, D.E. Newman, Complex dynamics of blackouts in power transmission systems, Chaos, vol. 14, no. 3, September 2004, pp. 643-652.

[8] B.A. Carreras, D.E. Newman, I. Dobson, A.B. Poole, Evidence for self organized criticality in a time series of electric power system blackouts, IEEE Transactions on Circuits and Systems I, vol. 51, no. 9, September 2004, pp. 1733-1740.

[9] J. Chen, J.S. Thorp, I. Dobson, Cascading dynamics and mitigation assessment in power system disturbances via a hidden failure model, International Journal of Electrical Power and Energy Systems, vol. 27, no. 4, May 2005, pp. 318-326.

[10] Q. Chen, J.D. McCalley, Identifying high risk n-k contingencies for online security assessment, IEEE Transactions on Power Systems, vol. 20, no. 2, May 2005, pp. 823-834.

[11] Q. Chen, C. Jiang, W. Qiu, J.D. McCalley, Probability models for estimating the probabilities of cascading outages in high-voltage transmission network, IEEE Trans. Power Systems, vol. 21, no. 3, August 2006, pp. 1423-1431.

[12] Defense plans against extreme contingencies, CIGRE Task Force C2.02.24 report, and a paper summarizing the report in Electra no. 231, April 2007.

[13] P.C. Consul, M.M. Shoukri, Some chance mechanisms related to a generalized Poisson probability model, American Journal of Mathematical and Management Sciences, vol. 8, nos. 1 and 2, pp. 181-202, 1988.

[14] P.C. Consul, *Generalized Poisson Distributions*, Dekker, NY 1989.

[15] J.-P. Dion, N. Keiding, Statistical inference in branching processes, in *Branching Processes*, editors A. Joffe, P. Ney, Marcel Dekker, New York 1978, pp. 105-140.

[16] I. Dobson, B.A. Carreras, D.E. Newman, A branching process approximation to cascading load-dependent system failure, 37th Hawaii International Conference on System Sciences, Hawaii, 2004.

[17] I. Dobson, B.A. Carreras, D.E. Newman, Branching process models for the exponentially increasing portions of cascading failure blackouts, 38th Hawaii International Conference on System Sciences, January 2005, Hawaii.

[18] I. Dobson, K.R. Wierzbicki, B.A. Carreras, V.E. Lynch, D.E. Newman, An estimator of propagation of cascading failure, 39th Hawaii International Conference on System Sciences, January 2006, Kauai, Hawaii.

[19] I. Dobson, B.A. Carreras, D.E. Newman, A loading-dependent model of probabilistic cascading failure, Probability in the Engineering and Informational Sciences, vol. 19, no. 1, 2005.

[20] I. Dobson, B.A. Carreras, V.E. Lynch, B. Nkei, D.E. Newman, Estimating failure propagation in models of cascading blackouts, Probability in the Engineering and Informational Sciences, vol. 19, no. 4, October 2005, pp 475-488.

[21] I. Dobson, B.A. Carreras, V.E. Lynch, D.E. Newman, Complex systems analysis of series of blackouts: cascading failure, critical points, and self-organization, Chaos, vol. 17, no. 2, June 2007.

[22] I. Dobson, Where is the edge for cascading failure?: challenges and opportunities for quantifying blackout risk, IEEE Power Engineering Society General Meeting, Tampa FL USA, June 2007

[23] I. Dobson, K.R. Wierzbicki, J. Kim, H. Ren, Towards quantifying cascading blackout risk, Bulk Power System Dynamics and Control-VII, Charleston SC USA, August 2007.

[24] P. Guttorp, *Statistical inference for branching processes*, Wiley, NY, 1991

[25] R.C. Hardiman, M.T. Kumbale, Y.V. Makarov, An advanced tool for analyzing multiple cascading failures, Eighth International Conference on Probability Methods Applied to Power Systems, Ames Iowa, September 2004.

[26] T.E. Harris, *Theory of branching processes*, Dover NY 1989.

[27] Blackout Experience and Lessons, Best Practices for System Dynamic Performance, and the Role of New Technologies, IEEE Special Publication 07TP190, prepared by the IEEE PES Task Force on Blackout Experience, Mitigation, and Role of New Technologies of the Power System Dynamic Performance Committee of the IEEE Power Engineering Society, July 2007.

[28] P.J.M. Kallenburg, *Branching processes with continuous state space*, Mathematical Centre Tracts 117, ISBN 90 6196 188 2, Amsterdam 1979.

[29] D.S. Kirschen, D. Jawayeera, D.P. Nedic, R.N. Allan, A probabilistic indicator of system stress, IEEE Transactions on Power Systems, vol. 19, no. 3, 2004, pp. 1650-1657.

[30] D.S. Kirschen, Do investments prevent blackouts?, IEEE Power Engineering Society General Meeting, Tampa FL USA, June 2007.

[31] H. Liao, J. Apt, S. Talukdar, Phase transitions in the probability of cascading failures, Electricity Transmission in Deregulated Markets, conference at Carnegie Mellon University, Pittsburgh PA USA Dec. 2004.

[32] S. Mei, Yadana, X. Weng, A. Xue, Blackout model based on OPF and its self-organized criticality, Proceedings of the 25th Chinese Control Conference, Harbin, Heilongjiang, China, August 2006.

[33] L. Mili, Q. Qui, A.G. Phadke, Risk assessment of catastrophic failures in electric power systems, International Journal of Critical Infrastructures, vol. 1, no. 1, pp.3863, 2004.

[34] D.P. Nedic, D.S. Kirschen, Discovering mechanisms of disturbance development, IREP Conference on Bulk Power System Dynamics and Control VI, Cortina D'Ampezzo, Italy, August 2004.

[35] D.P. Nedic, I. Dobson, D.S. Kirschen, B.A. Carreras, V.E. Lynch, Criticality in a cascading failure blackout model, International Journal of Electrical Power and Energy Systems, vol. 28, 2006, pp. 627-633. (journal publication of conference paper in Fifteenth Power Systems Computation Conference, Liege Belgium, August 2005)

[36] D.E. Newman, B.A. Carreras, V.E. Lynch, I. Dobson, The impact of various upgrade strategies on the long-term dynamics and robustness of the transmission grid, Electricity Transmission in Deregulated Markets, conference at Carnegie-Mellon University, Pittsburgh PA USA, December 2004.

[37] T. Nippert, Improvement of the (n-1) criterion introducing a probabilistic failure-related reliability criterion, CIRED97, 14th International Conference and Exhibition on Electricity Distribution, vol. 6, IEE Conf. Publ. No. 438, Birmingham, UK, 1997, pp. 37/1-37/6.

[38] H. Ren, I. Dobson, Using transmission line outage data to estimate cascading failure propagation in an electric power system, to appear in IEEE Transactions on Circuits and Systems Part II, in 2008.

[39] H. Ren, I. Dobson, B.A. Carreras, Long-term effect of the n-1 criterion on cascading line outages in an evolving power transmission grid, to appear in IEEE Transactions on Power Systems, accepted April 2008.

[40] N.D. Reppen, Increasing utilization of the transmission grid requires new reliability criteria and comprehensive reliability assessment, Eighth International Conference on Probabilistic Methods Applied to Power Systems, Ames, Iowa USA September 2004.

[41] M.A. Rios, D.S. Kirschen, D. Jayaweera, D.P. Nedic, R.N. Allan, Value of security: modeling time-dependent phenomena and weather conditions. IEEE Transactions on Power Systems, vol. 17, no. 3, pp. 543-8, 2002.

[42] E. Seneta, D. Vere-Jones, On the asymptotic behaviour of subcritical branching processes with continuous state space, Zeitschrift fur Wahrscheinlichkeitstheorie und verwandte Gebiete, vol. 10, pp. 212-225, 1968.

[43] B. Stott, E. Hobson, Power system security control calculations using linear programming, Part I and Part II, IEEE Transactions on Power Apparatus and Systems, vol. PAS-97, no. 5, Sept/Oct 1978, pp. 1713-1731.

[44] U.S.-Canada Power System Outage Task Force, Final Report on the August 14th blackout in the United States and Canada. United States Department of Energy and National Resources Canada, April 2004.

[45] Transmission reliability evaluation for large-scale systems (TRELSS): version 6.0 User's manual, EPRI, Palo Alto, CA: 2000. 1001035

[46] T. Van Cutsem, Voltage instability: phenomena, countermeasures, and analysis methods, Proceedings of the IEEE, vol. 88, no. 2, Feb 2000, pp. 208-227.

[47] E.T. Whittaker, G.N. Watson, *A Course of Modern Analysis*, Cambridge University Press, Cambridge, UK, 1948.

[48] D.V. Widder, *The Laplace Transform*, Princeton University Press, Princeton, NJ, 1946.

[49] K. R. Wierzbicki, Statistical estimation of cascading blackout size and propagation with branching processes, MS thesis, ECE department, University of Wisconsin-Madison, 2006.

[50] K.R. Wierzbicki, I. Dobson, An approach to statistical estimation of cascading failure propagation in blackouts, CRIS, Third International Conference on Critical Infrastructures, Alexandria, Virginia, September 2006.

[51] N.M. Yanev, On the statistics of branching processes, Theory of Probability and its Applications, vol. 20, 1975, pp. 612-622.

[52] M. Zima, G. Andersson, On security criteria in power systems operation, Power Engineering Society General Meeting, vol. 3, San Francisco CA USA 2005, pp. 3089- 3093.